THE UNIVERSITY OF QUEENSLAND

SCHOOL OF CIVIL ENGINEERING

REPORT CH99/15

TURBULENCE AND MIXING IN THE ENVIRONMENT: MULTI-DEVICE STUDY IN A SUB-TROPICAL ESTUARY

AUTHORS: Kabir SUARA, Richard BROWN
and Hubert CHANSON

HYDRAULIC MODEL REPORTS

This report is published by the School of Civil Engineering at the University of Queensland. Lists of recently-published titles of this series and of other publications are provided at the end of this report. Requests for copies of any of these documents should be addressed to the Civil Engineering Secretary.

School of Civil Engineering
The University of Queensland
Brisbane QLD 4072
AUSTRALIA

Telephone: (61 7) 3365 4163
Fax: (61 7) 3365 4599

URL: http://www.civil.uq.edu.au/

First published in 2015 by
School of Civil Engineering
The University of Queensland, Brisbane QLD 4072, Australia

ISBN No. 978 1 74272 138 5

The University of Queensland, St Lucia QLD, Australia

Turbulence and Mixing in the Environment: Multi-Device Study in a Sub-tropical Estuary

by

Kabir SUARA

PhD Candidate, Queensland University of Technology, Science and Engineering Faculty, Brisbane QLD 4000, Australia, Email: k.suara@qut.edu.au

Richard BROWN

Associate Professor, Queensland University of Technology, Science and Engineering Faculty, Brisbane QLD 4000, Australia, Email: richard.brown@qut.edu.au

and

Hubert CHANSON

Professor, The University of Queensland, School of Civil Engineering, Brisbane QLD 4072, Australia, Email: h.chanson@uq.edu.au

REPORT No. CH99/15

ISBN 978 1 74272 138 5

School of Civil Engineering, The University of Queensland

June 2015

Sampling site at Eprapah Creek (QLD, Australia) on 30 September 2013 at mid-ebb tide, looking from the left bank – Note the tripod holding the ADV units and the surface probe to the left, and GPS-tracked drifters at centre of the channel

ABSTRACT

In an estuary, mixing and dispersion result from a combination of large-scale advection and small-scale turbulence, which are complex to estimate. The predictions of scalar transport and mixing are often inferred and rarely accurate, due to inadequate understanding of the contributions of these difference scales to estuarine recirculation. A multi-device field study was conducted in a small sub-tropical estuary under neap tide conditions with near-zero fresh water discharge for about 48 hours. During the study, acoustic Doppler velocimeters (ADV) were sampled at high frequency (50 Hz), while an acoustic Doppler current profiler (ADCP) and global positioning system (GPS) tracked drifters were used to obtain some lower frequency spatial distribution of the flow parameters within the estuary. The velocity measurements were complemented with some continuous measurement of water depth, conductivity, temperature and some other physiochemical parameters. Thorough quality control was carried out by implementation of relevant error removal filters on the individual data set to intercept spurious data. A triple decomposition (TD) technique was introduced to access the contributions of tides, resonance and 'true' turbulence in the flow field. The time series of mean flow measurements for both the ADCP and drifter were consistent with those of the mean ADV data when sampled within a similar spatial domain. The tidal scale fluctuation of velocity and water level were used to examine the response of the estuary to tidal inertial current. The channel exhibited a mixed type wave with a typical phase-lag between 0.035π–0.116π. A striking feature of the ADV velocity data was the slow fluctuations, which exhibited large amplitudes of up to 50% of the tidal amplitude, particularly in slack waters. Such slow fluctuations were simultaneously observed in a number of physiochemical properties of the channel. The ensuing turbulence field showed some degree of anisotropy. For all ADV units, the horizontal turbulence ratio ranged between 0.4 and 0.9, and decreased towards the bed, while the vertical turbulence ratio was on average unity at $z = 0.32$ m and approximately 0.5 for the upper ADV ($z = 0.55$ m). The result of the statistical analysis suggested that the ebb phase turbulence field was dominated by eddies that evolved from ejection type process, while that of the flood phase contained mixed eddies with significant amount related to sweep type process. Over 65% of the skewness values fell within the range expected of a finite Gaussian distribution and the bulk of the excess kurtosis values (over 70%) fell within the range of -0.5 and +2. The TD technique described herein allowed the characterisation of a broader temporal scale of fluctuations of the high frequency data sampled within the durations of a few tidal cycles. The study provides characterisation of the ranges of fluctuation required for an accurate modelling of shallow water dispersion and mixing in a sub-tropical estuary.

Keywords: Turbulence, acoustic Doppler velocimetry (ADV), acoustic Doppler current profiler (ADCP), GPS tracked drifter, triple decomposition technique, Reynolds stress tensor, vertical profiling, turbulence statistics, flow measurements, tidal current, resonance, frequency domain filtering.

TABLE OF CONTENTS

LIST OF SYMBOLS

The following symbols are used in this report:

a	convergence length;
A	cross sectional area;
A_o	cross sectional area at the mouth;
d	water depth (m);
F_{cl}	lower cut-off frequency (Hz);
F_{cu}	upper cut-off frequency (Hz);
g	gravity acceleration (m/s^2);
h	height;
H	water elevation (m AHD);
H_p	adjusted water elevation using pressure sensor (m);
l	wavelength (m);
P_{fluc}	period of longest slow fluctuation (s);
P_{min}	period of shortest tidal cycle (s);
R	normalised correlation coefficient;
R_{ij}	correlation coefficient of Reynolds stress obtained as a normalised product of turbulence velocities: $R_{ij} = \frac{\overline{v_i v_j}}{(v_i' v_j')}$ where i, j = x, y, z;
t	time (s);
T_E	Eulerian integral time scale (s);
T_{Ex}	Eulerian integral time scale of streamwise velocity (s);
T_{Ey}	Eulerian integral time scale of transverse velocity (s);
T_{Ez}	Eulerian integral time scale of vertical velocity (s);
T_{res}	resonance period: $T_{res} = \frac{2 \text{ x } l}{\sqrt{g \text{ x } d}}$ where l = wavelength (m) and g = acceleration due to gravity (m/s^2) and d = water depth (m);
U_{slip}	wind slip velocity (m/s);
U_{wind}	wind speed (m/s);
V	instantaneous velocity (m/s);

V_H horizontal velocity (m/s);

V_x instantaneous streamwise velocity (m/s);

V_y instantaneous transverse velocity (m/s);

V_z tidal component of streamwise velocity (m/s) - low-pass filtered data;

$<V_y>$ tidal component of transverse velocity (m/s) - low-pass filtered data;

$<V_z>$ tidal component of vertical velocity (m/s) - low-pass filtered data;

$[V_x]$ slow fluctuating of component of streamwise velocity (m/s) - band-pass data;

$[V_y]$ slow fluctuating of transverse velocity (m/s) - band-pass data;

$[V_z]$ slow fluctuating of vertical velocity (m/s) - band-pass data;

$[Vi]'$ standard deviation slow fluctuating of velocity component (m/s) - band-pass data;

$[V_x]'$ standard deviation of slow fluctuating of streamwise velocity (m/s);

$[V_y]'$ standard deviation of slow fluctuating of transverse velocity (m/s);

$[V_z]'$ standard deviation of slow fluctuating of vertical velocity (m/s);

v_x streamwise turbulent velocity (m/s)- high-pass filtered data;

v_y transverse turbulent velocity (m/s) - high-pass filtered data;

v_z vertical turbulent velocity (m/s) - high-pass filtered data;

v_i' standard deviation of velocity component (m/s);

x longitudinal distance from the mouth;

z elevation of instrument from the bed;

δ small change;

ε wind effect '*Leeway*' [-]

$\rho v_i v_j$ instantaneous Reynolds stress (Pa), with i = x, y or z and j = x, y or z;

τ time lag (s);

τ_E Eulerian dissipation time scale (s);

τ_{Ex} Eulerian dissipation time scale of streamwise velocity (s);

τ_{Ey} Eulerian dissipation time scale of transverse velocity (s);

τ_{Ez} Eulerian integral time scale of vertical velocity (s);

ø diameter;

ζ_{ij} Reynolds stress tensor

Subscript

c critical flow conditions;

cl lower cut-off;

cu upper cut-off;

DS downstream flow conditions;

fluc	fluctuation;
i	i = x, y or z;
j	j = x, y or z;
min	minimum ;
slip	slip;
US	upstream flow conditions;

Abbreviations

ADCP	acoustic Doppler current profiler;
ADV	acoustic Doppler velocimeter;
AHD	Australian height datum;
AMTD	adopted middle thread distance, measured upstream from the river mouth;
AWW	assigned wrist watch;
C	Celsius;
DD	double decomposition;
DO	dissolved oxygen content;
DSITIA	Queensland Department of Science, Information Technology, Innovation and Arts;
ENU	local East, North, Up coordinates;
GPS	global positioning system;
HT	high tide;
HWS	high water slack;
hr	hour;
Ku	kurtosis;
LT	low tide;
LWS	low water slack;
min	minute;
N	number;
PSD	power spectral density;
QLD	Queensland, Australia;
s	seconds;
Sk	skewness;
Std	standard deviation;
STP	sewage treatment plant;
TD	triple decomposition;
T	period;

TKE	turbulence kinetic energy.

1. INTRODUCTION

1.1 PRESENTATION

Mixing and dispersion in estuaries are complex phenomena due to the transition and strong competition between ocean and river processes. The circulation is driven by tidal flows, river discharge, energetic turbulence and rough bathymetry among other factors (Chen and Sanford, 2009). In an estuary, mixing has been identified to result from the combination of small scale turbulence diffusion and large scale advection in the mean flow (Fischer, 1976, Fischer et al., 1979). The predictions of scalar transport and mixing are often inferred and rarely accurate due to inadequate understanding of these factors in natural estuaries. A few studies have been carried out in small estuaries, for example Kawanisi (2004), Voulgaris and Meyer (2004), Chanson et al. (2005); most were limited in spatio-temporal resolution and could not give insight into the inherent fine-scale turbulence. A number of studies were performed for longer durations with high temporal resolution (Trevethan et al., 2006a, Trevethan et al., 2007a) and the results provided useful insights into the turbulence phenomenon of shallow waters. However, further extensive study is required to span multiple combinations of driving factors. Traditional double decomposition of turbulent flows, which was used in those studies, only separate the mean and fluctuating components from the instantaneous measurements by assuming a constant mean flow field for a fixed time period. However, flow fields in tidal shallow waters are periodic. Previous studies (Trevethan et al., 2008a, Chanson and Trevethan, 2010) reported fluctuations that related to the periodic tidal circulation, periodic reflection from landmarks (resonance) and 'true turbulence', but were not categorically separated. Thus, new analyses would require application of triple decomposition (TD) analysis, to separate the flow field into its three components based on their periodicity.

The present work details a multi-device field study conducted in Eprapah Creek – a small subtropical estuary with a semidiurnal tidal pattern – for about 48 hours. In the mid-estuarine zone, three acoustic Doppler velocimeters (ADV) were sampled simultaneously at a frequency of 50 Hz located at different heights above the channel bed. An acoustic Doppler current profiler (ADCP) was deployed to sample the vertical velocity distribution during the study, while global positioning system (GPS)-tracked drifters were used to quantify the horizontal velocity distribution in the estuary during some part of the study. A bathymetric survey of the channel was conducted; physiochemical properties were sampled and local weather information was collected. A new triple decomposition technique was introduced into the data analysis, to take into consideration the periodicity of the large-scale tidal circulation and resonance for separating the flow field into its constituents. The results provide new useful sets of information about the contributions of slow and fast fluctuating components and their variations through tidal cycles.

1.2 STRUCTURE OF THE REPORT

In the present study, new field measurements were conducted at the mid-estuarine zone of Eprapah Creek, Australia, where a number of previous studies were carried out. The study was conducted under neap tide conditions with near-zero freshwater discharge ([1]). The multi-device measurements of turbulent velocity were performed continuously for 48 hours. ADV were sampled at high frequency (50 Hz) while an acoustic ADCP and GPS-tracked drifter were used to obtain some lower frequency spatial distribution of the flow parameters within the estuary. The velocity measurements were complemented with some continuous measurement of water depth, conductivity, temperature and some other physiochemical parameters. This research report documents the details of the field study, post-processing and analysis of the turbulence data. The field investigation and instrumentation are described in Section 2. General observations regarding the physiochemical data are provided in Section 3. Section 4 compares the observations between the different flow measurement instruments deployed during the field study while some spatial distribution of velocity across the channel is also provided. Sections 5 and 6 present the main results from analysis of high frequency ADV data. Appendix A lists the fieldwork participants. Appendix B shows some photographs of the field study. Appendix C provides the physiochemical data. Appendices D and E document the post-processing and results of the analysis of the ADV data sets.

[1] The freshwater discharge was checked at the Cleveland-Redland Bay Road bridge.

2. FIELD INVESTIGATION, INSTRUMENTATION AND SAMPLING SITE

2.1 FIELD INVESTIGATION AND SITE

A field study was conducted in the estuary of Eprapah Creek (Longitude 153.30º East, Latitude 27.567º South) - a subtropical creek located in eastern Australia (Chanson et al., 2005, 2012) between September 29 and October 1, 2013. Eprapah Creek catchment is about 39 km^2 with a length of up to 52 km within the catchment consisting of a main channel and two other tributary channels[2]. The estuarine zone is about 3.8 km long with a typical semi-diurnal tidal pattern that flows into Moreton Bay adjacent to the Pacific Ocean at Victoria point (Trevethan et al., 2008) (Fig. 2-1). The estuarine zone is nourished by saline water and bordered by mangrove trees, which protect the surface water and boundaries from direct wind erosion. The estuarine zone (Fig. 2-2) is comprised of a combination of straight channels (near boat yards) and meandering channels.

Several studies were carried out in Eprapah Creek including during king tidal conditions (Table 2.1 study E11) (Chanson et al., 2012) and the neap tide after a moderate rainfall (Table 2.1 study E10) (Trevethan et al., 2008). Table 2.1 summarises conditions for the key studies previously carried out at Eprapah Creek (E1 –E11). The results showed that small estuaries exhibit turbulence parameters contrasting with those of larger estuaries and distinct behaviour of turbulence properties in response to spring tidal forcing (Trevethan and Chanson, 2009). The diffusivity, usually assumed constant in modelling water quality of estuaries (large and small) was found to increase by three orders of magnitude during a tidal cycle at Eprapah Creek (Trevethan and Chanson, 2009). In addition, long-term oscillations were previously observed, with periods smaller than tidal time scales, and were believed to affect significantly turbulent mixing particularly during neap tides (Chanson et al., 2012).

The field study was conducted during neap tidal conditions between the 29th September and the 1st October 2013 with no prior rain for 7 days. The creek had a maximum depth of 2 to 3.5 m within the upper estuary at high tide, a free-surface width of about 50 m at site 1 close to the channel mouth and 10 m at site 3 (3.1 km AMTD). The bulk of the field data was collected at site 2B, located 2.1 km upstream the mouth of the channel (Fig. 2-2). The average tidal range during the field study was 1.2 m, while the local water depth at the sampling location (site 2B) at high tides was between 2.5 m at high tide and 0.9 m at low tides (Fig. 2-3). The total rainfall for September 2013 was between 17–23 mm at weather stations within a 20 km radius of the catchment and the

[2]Eprapah Creek catchment:
http://www.redland.qld.gov.au/EnvironmentWaste/Water/Waterways/Pages/OurCatchmentsEprapahCreek.aspx

cumulative rainfall for the last 7 days immediately prior to the field study was nil ([3]).

Fig. 2-1 - Aerial view of the estuarine zone of Eprapah Creek catchment taken at high tide on September 25, 2013; "Eprapah Creek" 153.30^{o}E and -27.567^{o}S. Nearmap (2013).

[3] Australian Bureau of Meteorology (ABM) (2013): http://www.bom.gov.au/climate/data/index.shtml?bookmark=200.

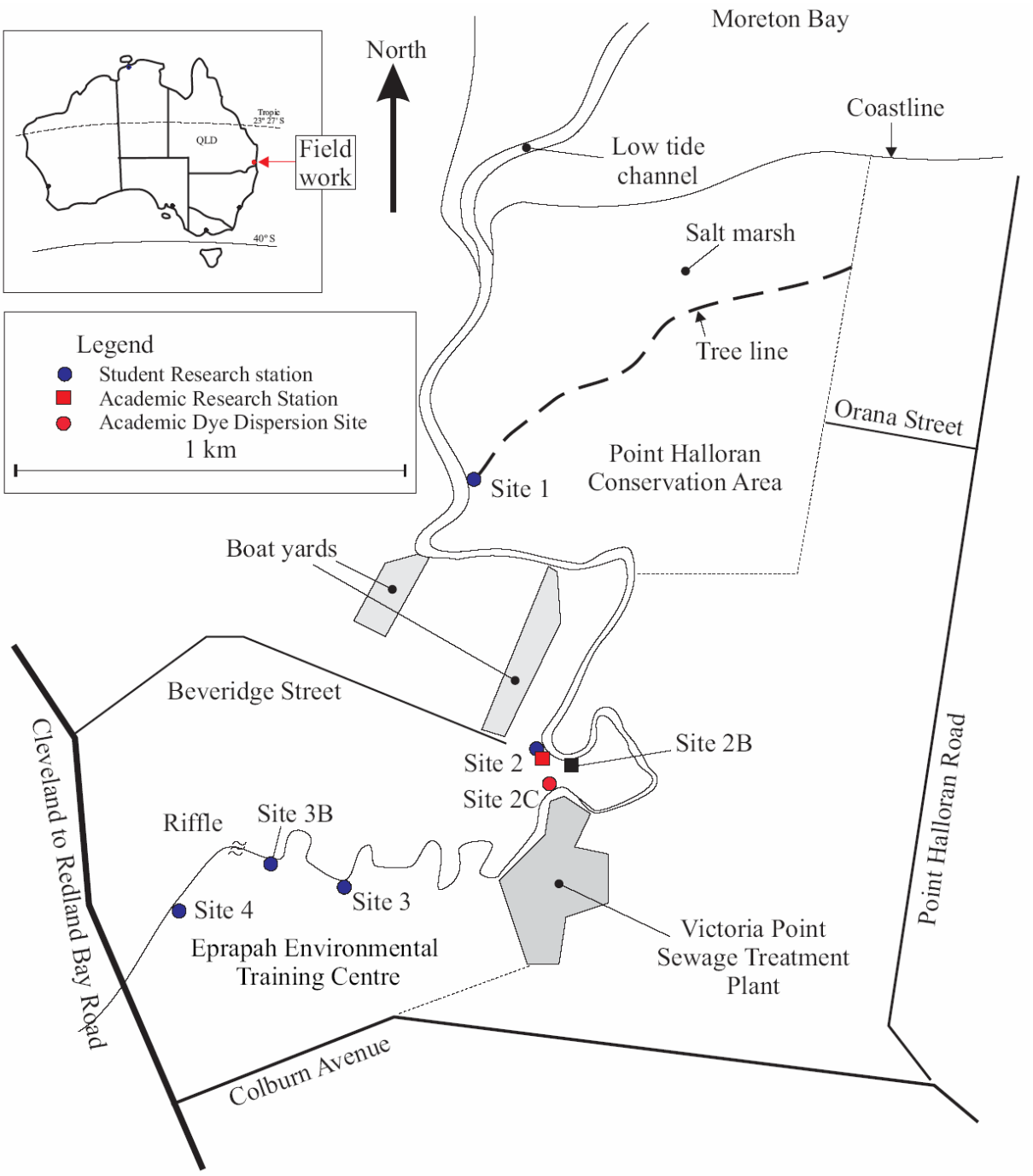

Fig. 2-2 - Map and sketch of Eprapah Creek estuarine zone showing the study site and the location of previous studies. Several studies ranging from velocity sampling, water quality and fish sampling dye dispersion analysis were carried out at site 1, site 2, site 2B, sites 3 and site 4 (blue circles) (Chanson, 2008; Chanson et al., 2005,2012; Trevethan et al., 2007a,b,2008a,b; Trevethan and Chanson, 2009). Dye dispersion experiments were carried out at site 2C (Situ and Brown, 2013) (red circle). ADVs were deployed during the present field study E14 at site 2B (black square).

Table 2-1 - Turbulence field measurements at Eprapah Creek, Queensland, Australia

Study (1)	Dates (2)	Tidal range (m) (3)	ADV system (MHz) (4)	Sampling rate (Hz) (5)	Sampling duration (6)	Sampling volume location(s) (7)
E1	4/04/2003	1.84	10	25	9 x 25 min	AMTD ([4]) 2.1 km, 14.2 m from left bank ([5]), 0.5 m below surface.
E2	17/07/2003	2.03	10	28	8 hr	AMTD 2.0 km, 7.7 m from left bank, 0.5 m below surface
E3	24/11/2003	2.53	10	25	7 hr	AMTD 2.1 km, 10.7 m from left bank, 0.5 m above bed
E4	2/09/2004	1.81	10	25	6 & 3 hr	AMTD 2.1 km, 10.7 m from left bank, 0.052 m above bed.
E5	8/03/2005 to 9/03/2005	2.37	10	25	25 hr	AMTD 2.1 km, 10.7 m from left bank, 0.095 m above bed
E6	16/05/2005 to 18/05/2005	1.36	10 &16	25	49 hr	AMTD 2.1 km, 10.7 m from left bank, 0.2 & 0.4 m above bed
E7	5/06/2006 to 7/06/2006	1.58	10 & 16	25 & 50	50 hr	AMTD 3.1 km, 4.2 m from right bank, 0.2 & 0.4 m above bed
E8	28/08/2006	2.10	--	--	--	AMTD 1.0, 2.1 & 3.1 km
E10	6/07/2007 to 8/07/2007	1.76	16	50	50 hr	AMTD 2.1 km, 10.7 m from left bank, 0.13 & 0.38 m above bed
E11	31/01/2010 to 3/02/2010	2.78	16	50	60 hr	AMTD 2.1 km, 10.75 m from left bank, 0.12 & 0.32 m above bed; AMTD 3.1 km, 3.85 m from right bank, 0.235 m above bed
E14	29/09/2013 to 1/10/2013	1.20	16	50	48 hr	AMTD 2.1 km, 11.05 m from left bank, 0.32 , 0.42 & 0.55 m above bed

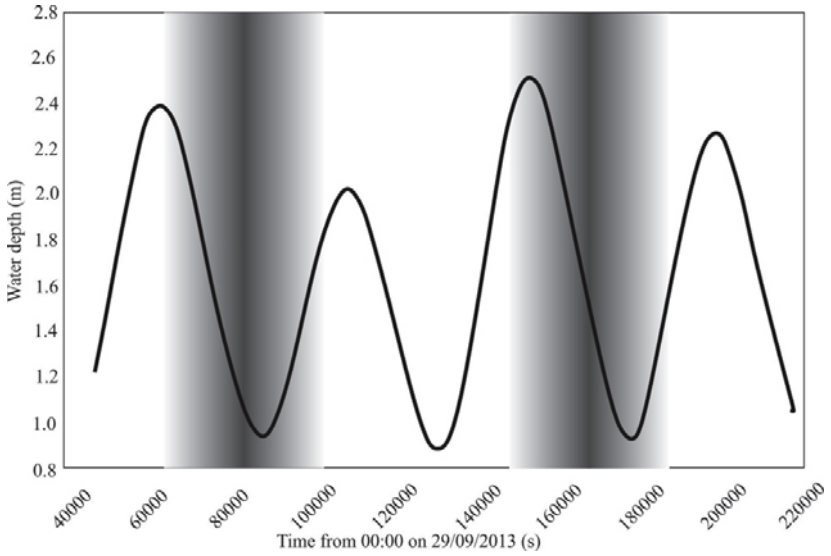

Fig. 2-3 - Local water depths at the sampling location as a function of time during the field study E14; greyed portions indicate time between sunset and sunrise.

[4] AMTD stands for adopted middle thread distance measured upstream from the river mouth

[5] The left bank is on the left when looking downstream.

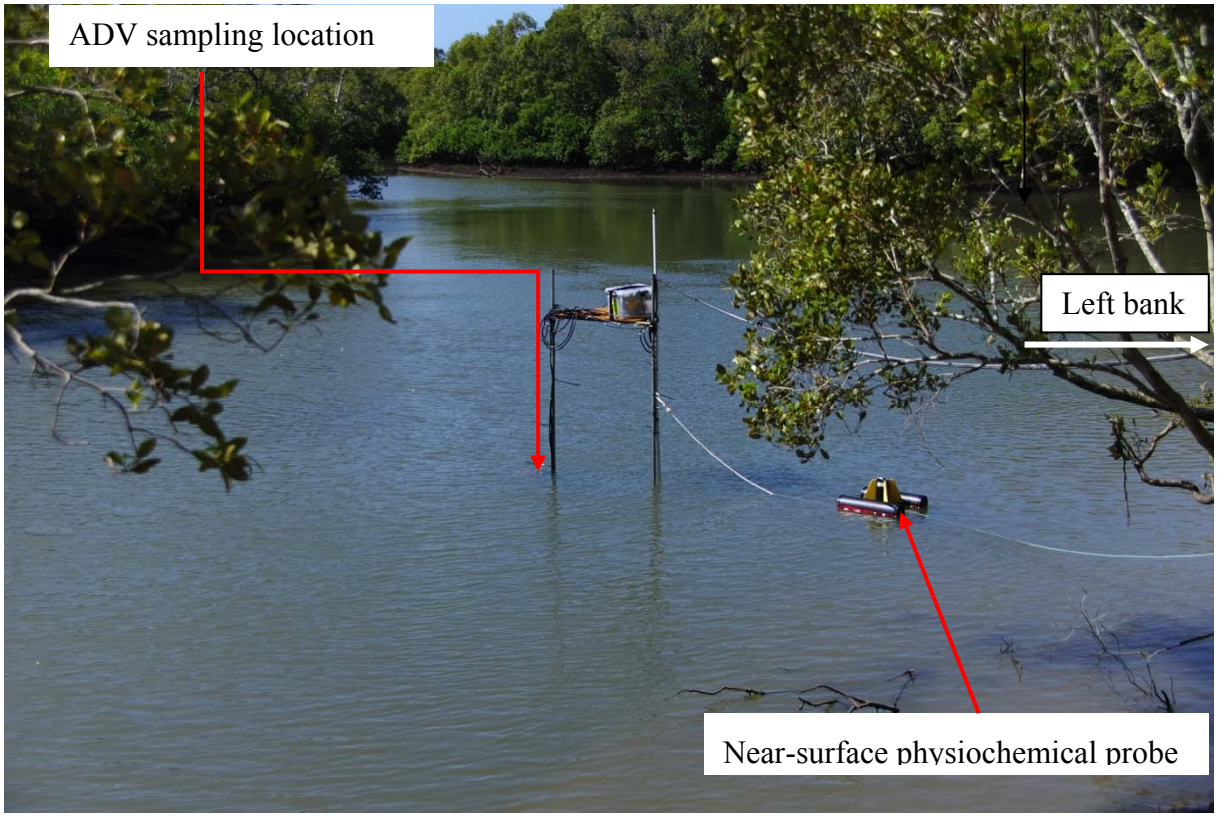

Fig. 2-4 - Sampling location downstream on September 29, 2013 at mid-tide showing a stretch of mangrove swamps elongated throughout the estuarine zone. ADV sampling location 11.05 m from the left bank (Photograph by H. Chanson).

2.2 BATHYMETRIC SURVEY

Bathymetric surveys were conducted on the 29 and 30th September 2013 at AMTD 0.3 km (site 1), AMTD 2.0 km (downstream site 2B), AMTD 2.1 km (site 2B) and AMTD 3.0 km (site 3). Figure 2-4 shows the profile of the five transects. The cross-sections were asymmetrical, deeper towards the right bank and widen toward the mouth. The bed composition at site 2B changed from muddy fine silt at the banks to relatively large gravels and rocks in the middle. This changed the bed roughness friction rapidly and could alter the properties within the turbulent boundary layer. Between the mouth and the upper estuary, the channel depth varied from 1 to 3.5 m below the mean sea level. The bathymetric survey revealed a reduction in cross-sections from the mouth through the upper estuary. The cross-section area A decays exponentially along the length from the river mouth:

$$A = A_o \exp\left(-\frac{x}{a}\right) \quad (2\text{-}1)$$

where A_o is the cross-sectional area at the mouth, x is the longitudinal distance from the mouth and a is the convergence length (Savenije, 2006, Chanson, 2008) The detailed analysis of the survey

data alongside 4 other transects ([6]) obtained between AMTD 1 to 2 km on 31st August 2013 yielded A_o = 106.44 m^2 and a = 1.4 km at mean sea level (Kelly, 2014). These estimates were consistent with value A_o = 109.2 m^2 and a = 0.655 km reported in Chanson (2008) and Chanson et. al (2012).

It is worth noting that the large rocks present in the cross-section at site 2B, where some previous field studies were carried out, appeared to have been gradually removed (Fig. 2-5). This change could cause a change in the local turbulent properties close to the bed across the cross-section when compared with previous studies because of the change in bathymetry.

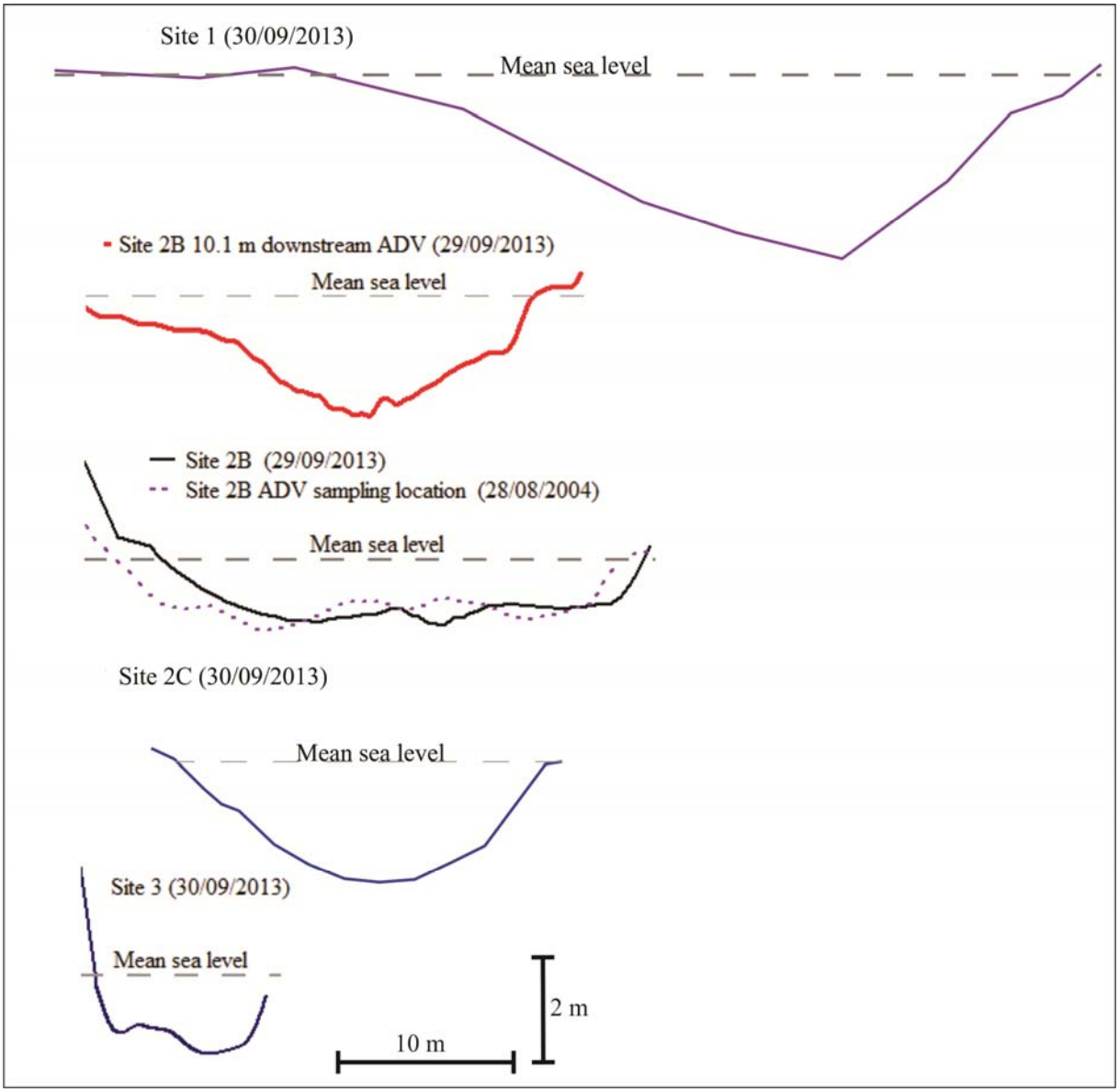

Fig. 2-5 - Surveyed cross-sections of Eprapah Creek estuarine zone at sites 1, 2B, 2C and 3, looking downstream. Legend indicate the location and survey dates in brackets. Site 2B: comparison of surveyed cross-section (29/09/2013) with a previous survey (28/08/2004).

[6] Survey data provided by Dr. Adrian McCallum of University of the Sunshine Coast.

2.3 ATMOSPHERIC AND WEATHER CONDITIONS

During the field study, a Vintage Pro 6150C weather station was deployed on the left bank, about 11 m downstream of site 2B. The wind speed and direction were sampled at an interval of 1 min. The vane was located about 3.5 m above the ground. The wind speeds were corrected to the standard height of 10 m above the ground using the logarithmic profile (Eqn. 2-2):

$$U_{10} = U_{3.5}\left(\frac{\ln\left(10/z_o\right)}{\ln\left(3.5/z_o\right)}\right) \qquad (2\text{-}2)$$

where U_{10} is the wind speed at 10 m from the ground and $U_{3.5}$ is the wind speed at 3.5 m. The sampling location contained few trees and mangrove branches; therefore a roughness height of the terrain, z_o = 0.25 m was employed (Manwell et al., 2009). Figure 2-6 shows the wind rose during the 48 hr study. The daylight hours were partly sunny with a few clouds, the temperature reaching a peak of 30 C and wind speed of up to 3 m/s from the northeast at 10 m above ground level. The night time was still with air temperature dropping to 14 C (Time from 00:00 on 29/09/2013, t = 108,000 s) and 18°C (t = 190,000s). 8.00 am – 5:00 pm had an average humidity of 51%, while 6.00 pm – 5:00 am had an average humidity of 93% with 5.00 am – 8:00 am had a saturated humidity. The total September rainfall was 18.2 mm with the maximum of 17.4 mm recorded on 17th September (2 weeks prior to the field trip).

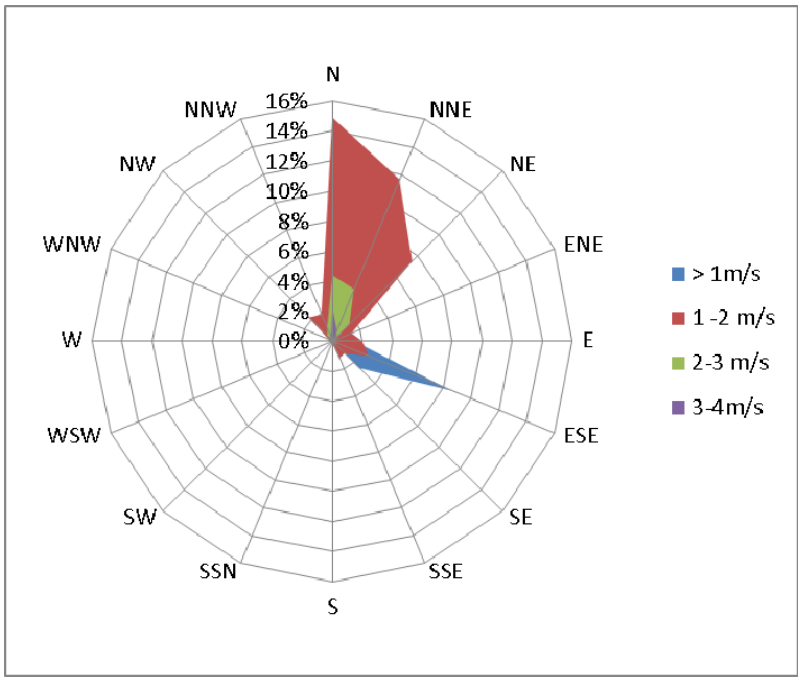

Fig. 2-6 - Wind rose of Eprapah Creek wind speeds at 10 m above the ground. Estimates deduced from Vintage Pro weather station data placed at site 2. 48 hours of data between 29/09/2013 and 30/10/2013.

2.4 INSTRUMENTATION

Turbulent velocities were measured with three ADV Sontek™ microADV. The ADV1 was a 3D side-looking probe micro-ADV (16 MHz), the ADV2 was a 2D side-looking probe micro-ADV (16 MHz) and the ADV3 was a 3D down-looking probe micro-ADV (16 MHz). The ADVs were mounted on a bracket held outside of structural poles whose wakes did not affect the sampling volumes, as observed visually. Figure 2-7 shows the installation of the ADV mounting system. The ADVs were sampled continuously at 50 Hz with the sampling volumes located vertically above each other at 0.32 m, 0.42 m and 0.55 m above the bed (Fig. 2-8B). Figure 2-8B presents the dimensioned position of the instrument control volumes. Vertical velocity profiles were obtained using a Teledyne RD Instruments™ Workhorse ADCP. The self-logging ADCP was installed on the sediment-water interface in an upward looking configuration. The ADCP was located 10.1 m downstream of the ADVs and approximately 12.6 m from the left bank. It used a 0.05 m vertical bin size resulting in 55 bins. The ADCP ping-rate was 5.56 Hz and produced averaged data over an 854 second interval. The first bin of the ADCP was 0.85 m from the bed at its sampling location.

Table 2-2 - Sampling and location information for instruments deployed at site 2B

Instrument code (1)	Instrument description (2)	Sample location (3)	Sampling frequency (4)
ADV1	Sontek 3D-sidelooking microADV A813F (16MHz)	0.32 m above the bed 11.06 m from the left bank	50 Hz
ADV2	Sontek 2D-sidelooking microADV A641F (16MHz)	0.42 m above the bed 11.04 m from the left bank	50 Hz
ADV3	Sontek 3D-downlooking microADV A843F (16 MHz)	0.55 m above the bed 11.05 m from the left bank	50 Hz
ADCP	Teledyne RDI Workhorse (1200kHz)	12.06 m from the left bank. 10.1 m from ADV1	Every 854s (averaged data)
GPS-D[7]	GPS-tracked drifters in differential mode	Sub-surface with pseudo-Lagrangian motion	10 Hz
YSIB	YSI 6600 multi-parameter probe	0.45 m above the bed 10.87 m from the left bank	0.1 Hz
YSIF	YSI 6600 multi-parameter probe	0.05 m from the free surface	0.1 Hz
MW6	MW600 Dissolved oxygen meter	Manual sampling	Every 15 min
HI9	HI 98130 HANNA pH/Conductivity/TDS Tester	Manual sampling	Every 15 min

[7] Three high resolution GPS-trackers were deployed, one capsule had its waterproofing destroyed while the other had a connection error

Fig. 2-7 - Research team preparing the sampling site and installing ADV mounts. In parallel, the cross-sectional survey was conducted at ADVs sampling location. View from the left bank at 12:10pm on the 29th September 2013.

Some Lagrangian estimate of horizontal velocity was collected using high resolution drifters sampled at a frequency of 10 Hz. The GPS-tracked drifters were designed and manufactured at Queensland University of Technology (QUT) to sample the subsurface current with minimal direct wind drag. The drifters used a Novatel™ dual frequency receiver for resolving GPS positions. The high precision of the receivers was coupled with real time kinematic solution in differential mode, leading to errors associated with position estimates limited to < 1 cm. Because of the sinuosity and small width of the channel, the drifter deployment was limited to only a few periods during the field experiments.

The physiochemical properties were obtained using two multi-parameter water quality probes (YSI 6600) deployed close to the bed and the free surface respectively. Both probes were sampled at 0.1 Hz. The probes measured conductivity, salinity, temperature, pH, dissolved oxygen, chlorophyll A and turbidity. In addition, some data were collected manually every 15 minutes using alcohol thermometers for temperature, Milwaukee™ MW600 DO metre for dissolved oxygen and HANNA HI 98130 for pH and conductivity measurements. The manual samples were obtained from the left bank at site 2B. At each instance, a bucket was used to collect 2 – 3 litres of water before the relevant probes were used. The manual conductivity data were obtained by diluting the estuary water with fresh water. The local water elevation was read manually every 15 minutes, from a survey staff attached to the ADV mounts while the ADV1 unit also provided local pressure

measurement at 50 Hz.

A summary of all the devices is provided in Table 2-2. The arrangement of the devices across the channel cross-section (site 2B) relative to the channel bed is shown in Figure 2-8.

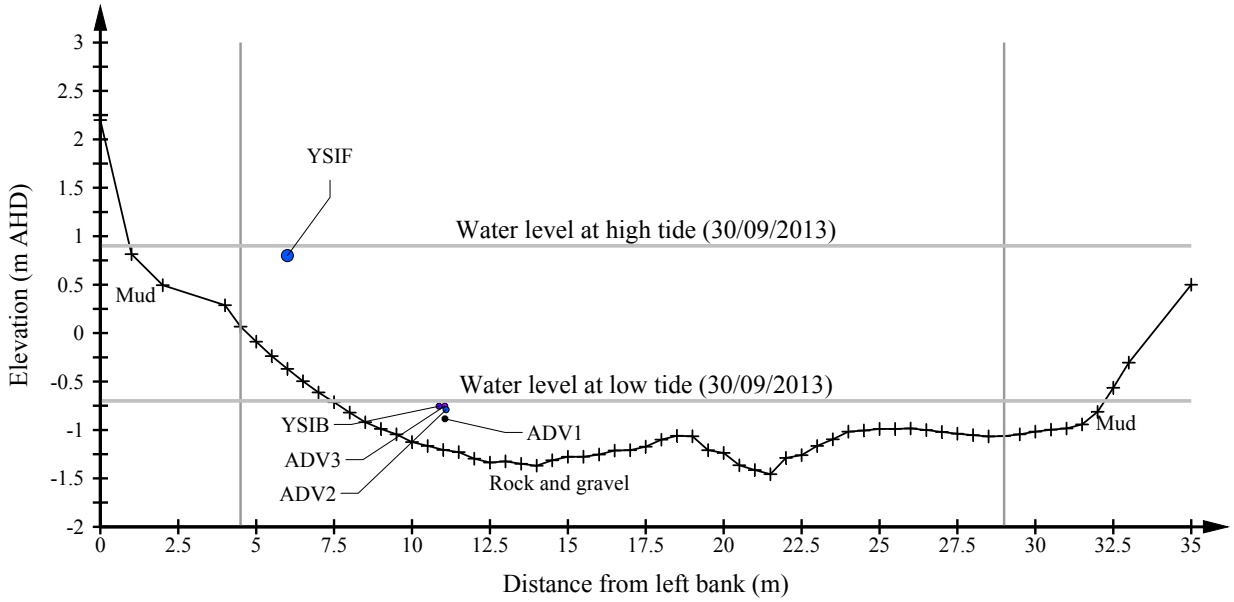

(A) Surveyed cross-section looking downstream; for the ADV measurements, +ve x-axis points into to screen while +ve y-axis is towards the left bank and +ve z-axis points downward; the distance of the ADV sampling volumes, O, from the channel bed for each instrument is shown in (B)

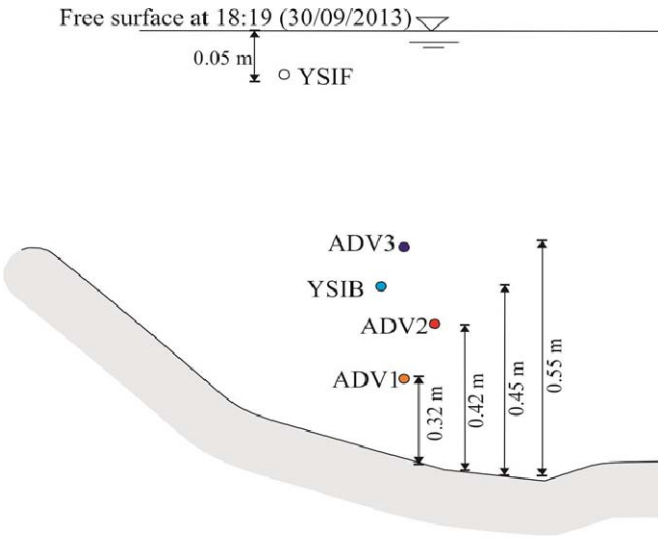

(B) Dimensioned sketch showing arrangement of sampling volumes of instruments relative to the channel bed and free surface at 18:19 on 30 September 2013

Fig. 2-8 - Eprapah Creek cross-section at site 2B in September 2013

2.5 DATA PROCESSING AND QUALITY CONTROL

Raw ADV velocity data contains some noise, spikes and less correlated outputs, which are spurious and should not be mistaken for physical processes especially in high-turbulence environmental flows. Because these erroneous data points are not a true representation of any physical process, ADV data cannot be used without post-processing (Chanson et al., 2008). Quality control measures for isolating this erroneous data evolved from previous field studies (Chanson et al., 2005, Trevethan et al., 2007b & Trevethan et al., 2008a). The ADV data sets were post-processed by removal of communication errors, data with correlation less than 60% and signal-noise-ratio less than 5 dB (Brown and Chanson, 2012). The data sets were also de-spiked using the phase-spaced thresholding technique (Goring and Nikora, 2002). Less than 5% of all the ADV data were removed after the processing. The ADV data quality control was performed using WinADV32 version 2.029 software. A MATLAB algorithm was developed to fill gaps with last of the valid data points for further analysis.

The ADCP data were quality controlled by removing the bins ([8]) located in the air as a result of the periodic oscillation of the water level above the bed, using the water depth measured by the ADCP pressure sensor. Furthermore, the ADCP data sets were post-processed following Symonds (2006) by removal of bins with (1) vertical velocities > $0.2V_{max}$ ([9]), (2) horizontal velocities > $2V_{max}$ (3) SerPG4 < 60% ([10]) and (4) correlation values < 60%.

Quality control of GPS-tracked drifter raw data included the removal of paths associated with disturbances, proximity to obstacles/banks of the channel and cluster influence during group deployment based on event records of field studies. Spikes that resulted from poor GPS-fixing were removed based on fixed accelerations values. GPS device white noise was estimated from stationary measurement and was found to have the same energy level as the true signal at frequencies higher than 1.5 Hz. Therefore position estimates from the GPS-drifter were passed through a low-pass filter with a cut-off frequency of 1.5 Hz to remove high frequency noise. From an ENU ([11]) coordinate system, the time series was transformed to a river-based local x-y coordinates using the method described in Legleiter and Kyriakidis (2006) with errors limited to a few centimetres. The x-coordinate was the streamwise component and the y-coordinate was across-shore component.

---

[8] Bins are cells locations from the beam of the ADCP

[9] V_{max} is the maximum velocity value set for the ADVs: herein, 0.3 m/s

[10] SerPG4: Percentage of good points from 4-beam solutions passing the low correlation and fish detection threshold

[11] Local East, North, Up (ENU) coordinates.

2.6 TIME SYNCHRONISATION

A previous field study using 3 ADV units (Trevethan et al., 2007a) revealed variations in ADV computer clocks, which resulted in a drift of up to 1 s (50 samples at 50 Hz) over a period of 50 hours between ADVs. This time drift could have implications on the interpretation of high frequency events thus the time synchronisation of devices was carefully conducted. Side-to-side screen shots of ADV computers at the beginning and at the end of the data acquisition were used to estimate the time drifts over the sampling period. The ADVs and other devices (GPS and ADCP) were synchronised within a second against an assigned wrist watch (AWW) selected as the reference device and assigned to timing the manual data collection.

ADV1 and ADV2 drifted by 0.48 s and 1.36 s over the sampling duration compared to the ADV3. Therefore, 24 and 68 artificial sample points were introduced to ADV1 and ADV2 data sets, respectively. The added points were spread linearly across the data sets, similar to the concept described by Trevethan et al. (2007). These points were simulated as the mean of the two end points and were flagged. To ensure that the number of data points in the three ADV units corresponded to the duration of the sample taken by the AWW that had a second resolution, the number of samples at the first second (computer start time) on each ADV unit was analysed. The initial times of the ADVs were corrected to the next second by removing the incomplete data in the first 1 s of sampling (Table 2-3).

Table 2-3 - Computer start time correction using number of samples in the first second

ADV unit	ADV computer start time	Number of data in 1st min	Start time forward-corrected to nearest s	Nos. samples removed	Start time based on AWW*
(1)	(2)	(3)	(4)	(5)	(9)
ADV 1	13:29:00	2974	13:29:01	24	13:29:21
ADV2	13:39:43	550	13:39:49	0	13:34:03
ADV 3	13:14:31	1407	13:14:32	7	13:15:20

Note: * Assigned wrist watch.

3. WATER QUALITY OBSERVATIONS

3.1 WATER ELEVATION

During the field study E14, water depth and physio chemical data collection started about mid-flood tide and were carried out over four subsequent high-tides. The water levels and pressure measurements were dominated by the semi-diurnal tidal fluctuation and some resonance fluctuations with periods of about 3,000 s were observed particularly at high-tides (Fig. 3-1). The runoff from the catchment and the diurnal discharge from the sewage treatment plant (STP) had negligible effect on the water level.

Figure 3-1 shows the adjusted instantaneous pressure at site 2B. The pressure sensor was located at 0.7 m from the velocity sampling volume of ADV1, which was 0.32 m above the channel bed. This resulted in constant air pressure values during the low-tides and periods when the local water depth went below 1.02 m for example between 88,000 and 91,000 s.

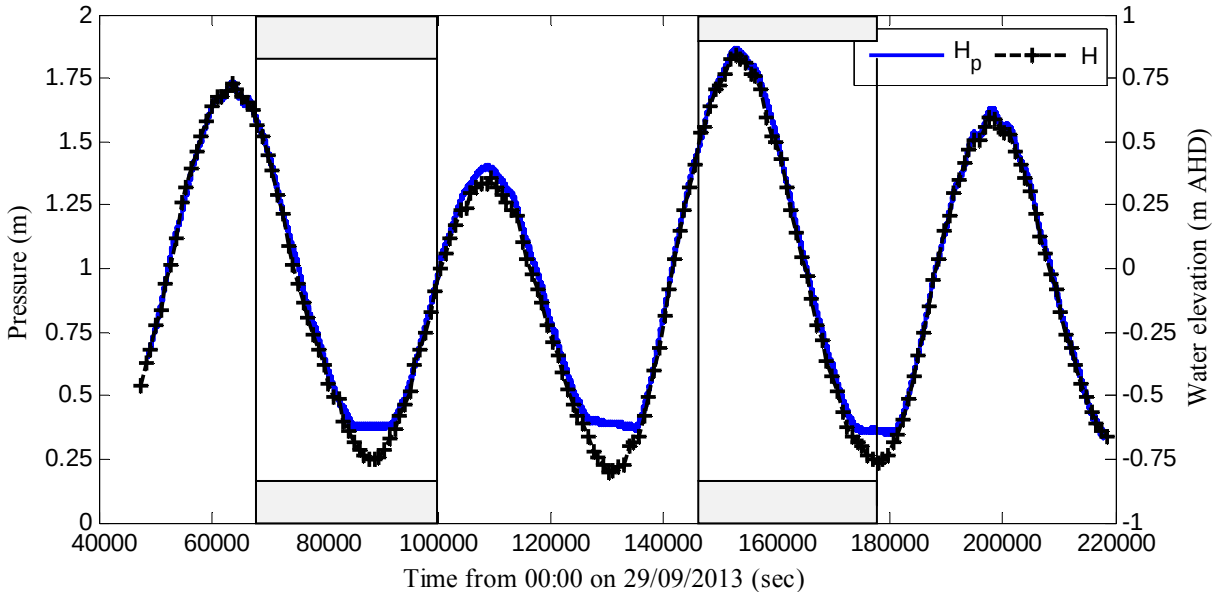

Fig. 3-1 - Water elevation H (m AHD) and adjusted pressure H_p (m) measured with ADV1 pressure sensor as functions of time. Enclosed portions show periods between sunset and sunrise.

3.2 FIXED INSTANTANEOUS MEASUREMENTS USING YSI6600 PROBES

The YSI probes continuously collected data at both a point next to the channel bed and close to the free surface. The sampling included specific conductivity, temperature, pH, dissolved oxygen, salinity, chlorophyll A and turbidity. Most properties showed a clear tidal trend with maximum values at high-tide, except the turbidity and chlorophyll A, which appeared to correlate with the longitudinal velocity. In addition, the chlorophyll A data showed a diurnal trend with peaks just

before sunset as the algal growth declined in the absence of sunlight (Appendix C).

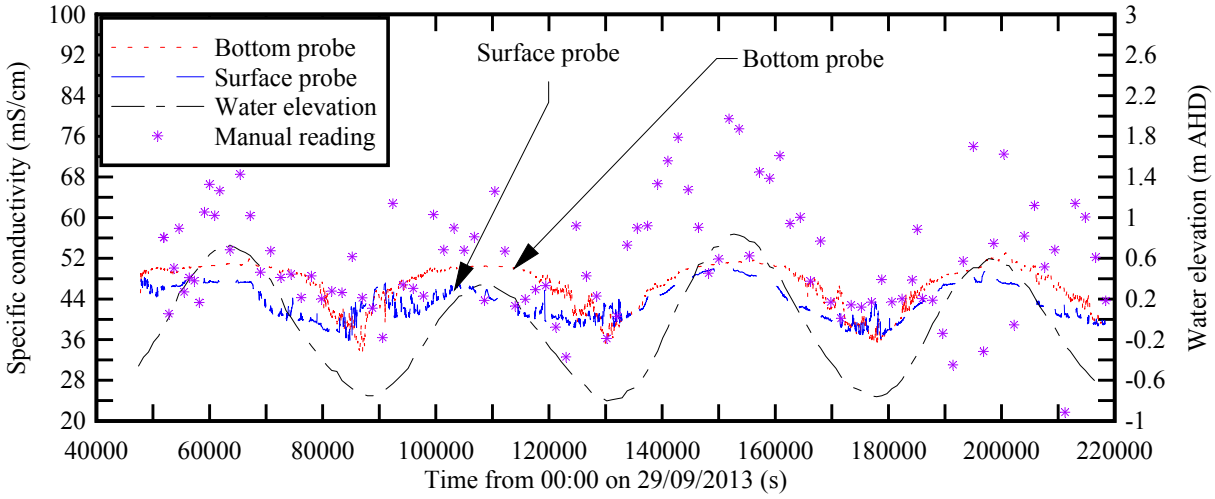

(A) Specific conductivity (mS/cm)

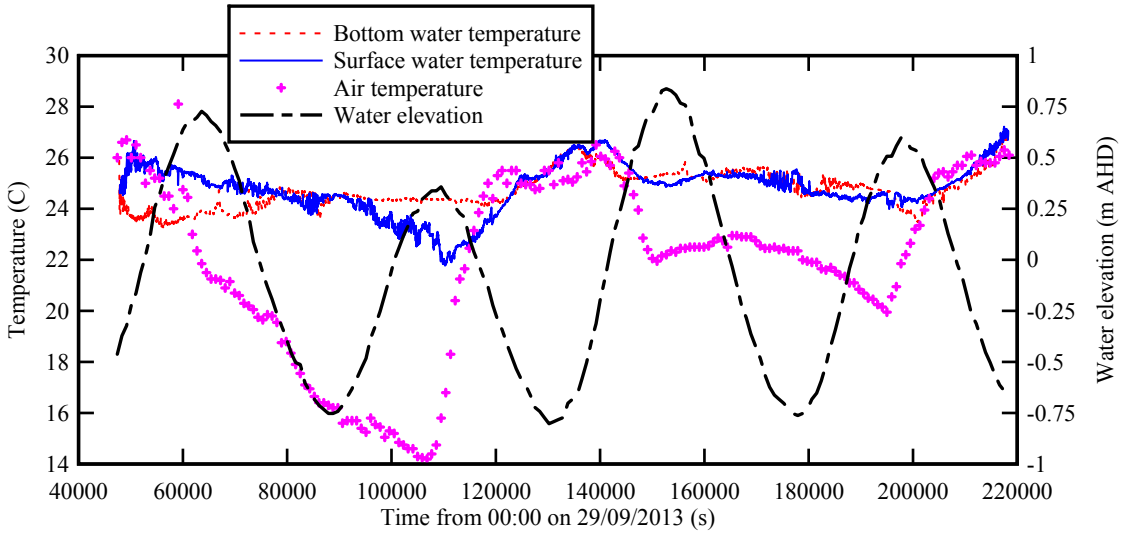

(B) Temperature (C)

Fig. 3-2 - Time variation of water depth, conductivity, temperature and turbidity - data collected by the YSI6600 units at site 2B in Eprapah Creek during the study

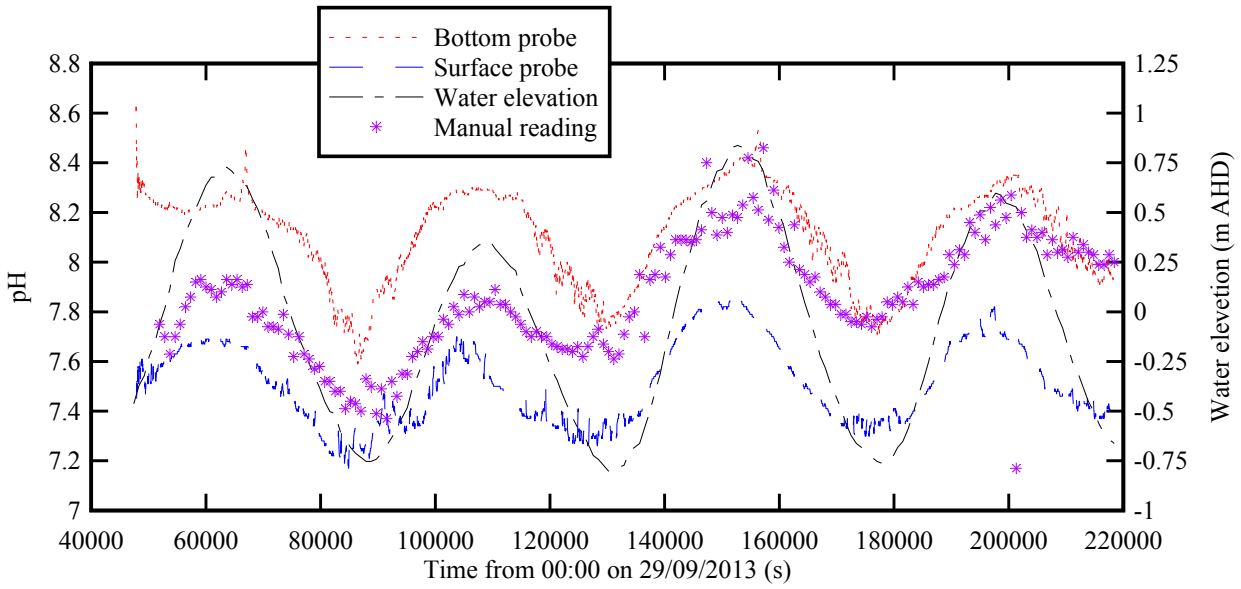

(C) pH level

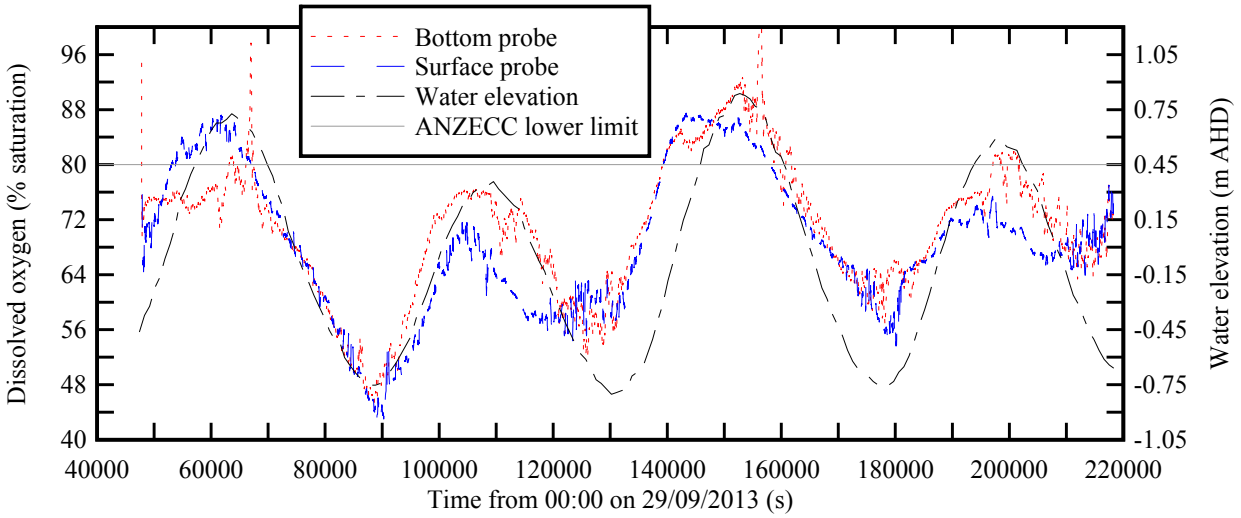

(D) Dissolved oxygen (% saturation). Comparison with recommended ANZECC lower limit (ANZECC, 2000) (solid line).

Fig. 3-2 - Time variation of water depth, conductivity, temperature and turbidity - data collected by the YSI6600 units at site 2B in Eprapah Creek during the study

The specific conductivity was dominated by tidal influence during the study period, with an average of 47 mS/cm and 43.7 mS/cm next to the surface and next to the bed, respectively. These values were higher compared to an average conductivity of 19 mS/cm obtained during study E8 (Table 2-1) on the 28th August 2006 with significant fresh water runoff. The specific conductivity range was consistent with water conductivity of 49 mS/cm obtained on the 2nd September 2004, during a drought period. The temperature difference across the water column was up to 3 C around the first two high-tides (t = 55,000 – 60,000 s and t = 110,000 – 112,000 s). This might be caused by the increased air-water interface heat exchange rates associated with the high day-to-night temperature

range (about 12 C) observed within these periods. The lower surface temperature partly contributed to lower specific conductivity of the surface probe at these periods. The ebb tides also exhibited well-mixed conditions with occasions of denser water being advected over the less dense water (e.g. at t =128,000 – 132,000 s).

The pH (Fig. 3-2C), dissolved oxygen (Fig. 3-2D) and chlorophyll (Appendix C) showed some marked oscillation with a period of about t = 3,000 s. Fluctuations with a similar period were observed with velocity and water elevation data. These oscillations occurred throughout the tidal study but were more pronounced during high-tide with an approximately 15 km wavelength. The wavelength was obtained based on the first mode of natural resonance having a period T_{res} = 3,000 s assuming an average depth of 10 m at high tide. This large wavelength was significantly larger than the 2.1 km, the distance of site 2B from the channel mouth. Therefore these fluctuations were possibly linked with resonance from outside the channel (Trevethan et al., 2008). The data also showed some discernable oscillations in the chlorophyll and dissolved oxygen (at high-tide) with periods of about 6000 s and 10,000 s respectively. Further investigation is required to identify the processes controlling the variation of these parameters in Eprapah Creek.

The manually sampled data of specific conductivity showed a clear tidal trend with the maximum values obtained during the third high-tide. The large disparity between the conductivities obtained from manual sampling and continuous sampling (YSI probes), were associated with a difference in instrument sensitivities and calibration. In addition, some difference was associated with the different sampling locations and human error during the dilution process. However, the manually sampled pH data showed results that were in agreement with the YSI probe data, possibly because the pH values were measured without dilution. The small disparity in the manual pH data was likely indicative of the difference in sampling locations.

Table 3-1 shows a summary of average physiochemical properties for the study. The results indicated that the pH level was within the range of 7 - 8.5, which is the standard range set for fresh and marine waters by Australian and New Zealand guidelines (ANZECC, 2000). However, the dissolved oxygen level was generally lower (Fig. 3-2C) than the standard level of 80 - 110% saturation, expected of fresh and marine waters, except for t = 140,000 – 160,000 s. This period was within a major tidal cycle with the highest tidal range being 1.4 m occurring around sunset. Thus, the improved dissolved oxygen saturation could be linked to the concurrence of high salinity with active plant photosynthesis.

The near surface salinity and chlorophyll data were of the similar in magnitude as the respective readings next to the bed. This showed that the water column was well mixed and the river discharge was insignificant compared to the large gradient in physiochemical properties observed after rain (Trevethan et al., 2008). The peak in pH value coincided with the peak in dissolved oxygen

concentration. The physiochemistry of the system suggested that the water column was reasonably mixed in terms of conductivity, temperature, DO, turbidity and chlorophyll, while it was partly stratified in terms of pH.

Table 3-1- Average physiochemical conditions of Eprapah Creek site 2B (29/09/2013 to 1/10/2013)

Sample (1)	Air Temp. (C) (2)	Water Temp. (C) (3)	Conductivity (mS/cm) (4)	DO (mg/L) (5)	pH (6)	Turbidity (NTU) (7)	Salinity (ppt) (8)	Chlorophyll (ug/L) (9)
Manual	21.8	24.2	52.0	6.70	7.86	-	-	-
Bottom	21.8	24.7	46.9	4.93	8.11	9.1	30.5	2.92
Surface	21.8	24.8	43.7	4.84	7.51	7.79	28.2	2.87

3.3 VERTICAL PROFILES OF PHYSIO-CHEMISTRY MEASUREMENTS WITH THE YSI6920 PROBE

The health of Eprapah Creek has been closely monitored by the water quality monitoring group, Queensland Department of Science, Information Technology, Innovation and Arts (DSITIA). During a scheduled monitoring, vertical profiles of water quality parameters were recorded at several longitudinal locations from the upper estuary to the mouth of the channel on the 11th October 2013 ([12]). The measurements were conducted at the beginning of ebb tide in neap tidal conditions. The tidal range was 1.5 m compared to the average tidal range of 1.2 m during the E14 study. The rainfall recorded in the weather station within 10 km of the catchment between the field study, E14 and the 11th October was nil ([13]). Therefore, the river discharge was expected to be insignificant. Fig. 3-3 shows some typical results in terms of water conductivity, dissolved oxygen and pH. The vertical profiles suggested that the system was well mixed from the river mouth to site 2. However, the fresh water discharge from the STP might induce some gradient in physiochemical properties across the adjacent water column. This was observed with some partial stratification in terms of the conductivity, dissolved oxygen and pH at STP and site 3. The vertical profiles of the physiochemical parameters suggested that the water column was reasonably well mixed in terms of specific conductivity and dissolved oxygen, but it was weakly stratified in terms of temperature, chlorophyll and pH. It is worth noting that the dissolved oxygen level at site 3 was about 60%, well below the standards recommended by ANZECC. Additional physiochemical

[12] Data provided by Water Quality Monitoring Group, QLD DSITIA, Brisbane.

[13] Australian Bureau of Meteorology (ABM) 2013: http://www.bom.gov.au/climate/data/index.shtml?bookmark=200.

properties are presented in Appendix C.

3.3 REMARKS

In general, the observed water quality data suggested that the channel was reasonably mixed during study E14 and the field observations by DSITIA, both carried out under neap tidal conditions with insignificant fresh water runoff. This supported the stratification of the upper estuary being primarily governed by the volume of runoff from the river and tributaries. Thus Eprapah Creek is expected to have a fairly well mixed water column during periods of insignificant runoff from tributary and river discharge.

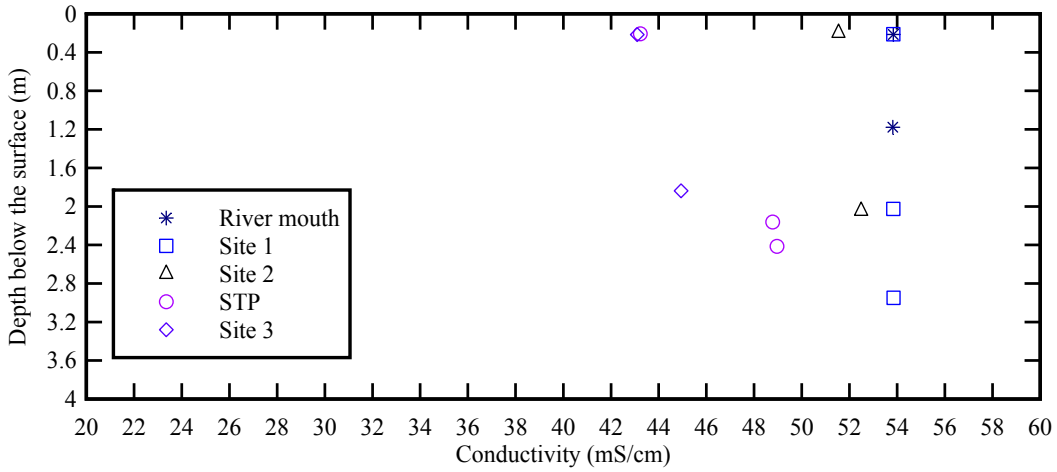

(A) Conductivity (mS/cm)

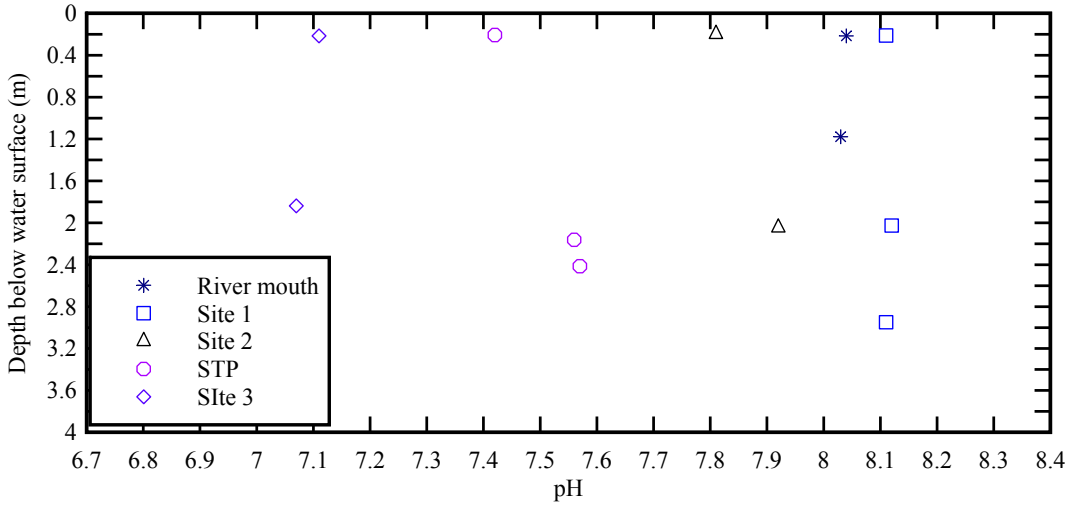

(B) pH

Fig. 3-3 - Vertical profiles of water properties along Eprapah Creek channel by DSTIA on the 11th of October 2013 at the beginning of the ebb tide. First reading was taken at 14:42 (at the river mouth) and the last reading was taken at 15:09 (at site 3)

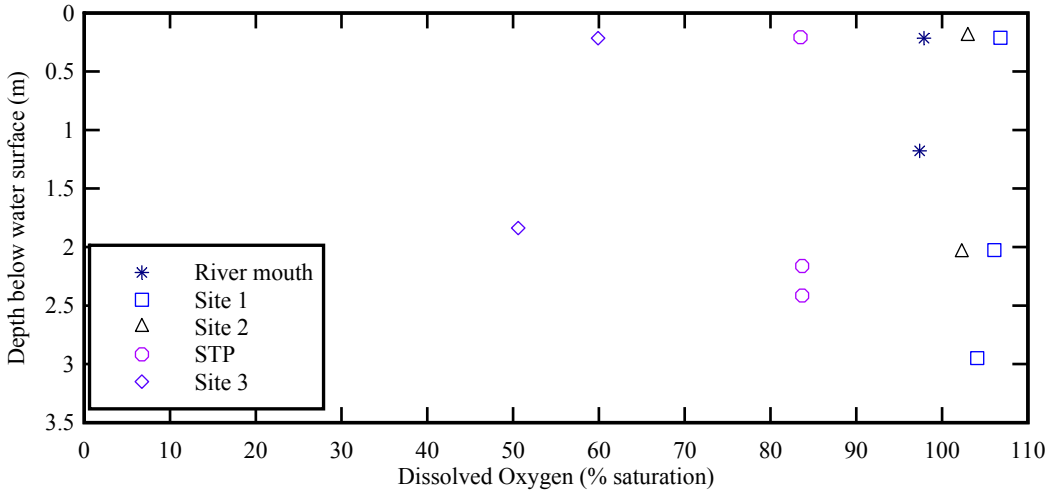

(C) Dissolved oxygen (% saturation)

Fig. 3-3 - Vertical profiles of water properties along Eprapah Creek channel by DSTIA on the 11th of October 2013 at the beginning of the ebb tide. First reading was taken at 14:42 (at the river mouth) and the last reading was taken at 15:09 (at site 3)

4. MULTI-DEVICE FLOW MEASUREMENTS EVALUATION

4.1 PRESENTATION

In previous field studies (E1 to E11) at Eprapah Creek, ADVs were deployed and rigorous quality control procedures, data analysis, and overall capability of the instrumentation to shallow water turbulence measurements were established and documented (Chanson et al., 2005, Chanson et al., 2007, Chanson et al., 2008 & Trevethan et al., 2008a). Potential devices for further understanding the spatio-temporal variation of the flow field in Eprapah Creek include the ADCP and GPS-tracked drifters. While stationary deployment of ADCP permits vertical and transverse profiling of velocities, free floating GPS-tracked drifters can provide the 2 dimensional description of the near-surface flow field. Applicability of ADCP and GPS-tracked drifters to shallow water flow field measurement is investigated. This section reports the comparison of mean velocities of ADCP, GPS-tracked drifters and ADV. The vertical velocities of the ADCP and some GPS-tracked drifter spatial velocity is also reported.

4.2 COMPARISON OF ADV, ADCP AND DRIFTER DATA

4.2.1 ADCP and ADV comparison

During the field study E14 at Eprapah Creek, three ADVs were sampled at site 2B, while an ADCP was sampled at a cross-section location 10.1 m downstream of site 2B. The drifter experiments were carried out on the 30th September 2013 with some deployment made upstream from site B during the ebb tide (around t = 118,000 s) and other deployments between the mouth of the Creek, back to site 2B during the subsequent flood tide. The ADV system has a 3D cylindrical sampling volume (diameter ø = 0.4 cm and height h = 0.45 cm) at the location described in section 2. The ADCP velocity sampling volumes occupy a cone with a diameter joining the centres of the four beams, which increases proportionally with the distance from the ADCP due to beam divergence (20^{o} for the ADCP model deployed) (Gunawan et al., 2011). The sampling volume was estimated from ø = 44 cm, h = 5 cm for Bin 1 and ø =104 cm, h = 5 cm for Bin 44.

The location of the sampling volumes of ADVs and ADCP in relation to their respective sampling location is described in Figure 4-1. The last bins were Bin 47 and Bin 15 at the largest high-tide and smallest low-tide, respectively. Figure 4-2 shows the variation of the relative heights of the sampling volumes of ADVs and ADCP bins with time throughout the study period. The relative heights varied significantly between high and low tides. The ADVs were sampled relatively close to the bed compared to the ADCP, except a few points at low-tide (Fig. 4-2). Therefore a direct correlation between the ADV and ADCP velocity data was not physically meaningful. ADV3 was

the closest to the ADCP bin and was used for the comparison.

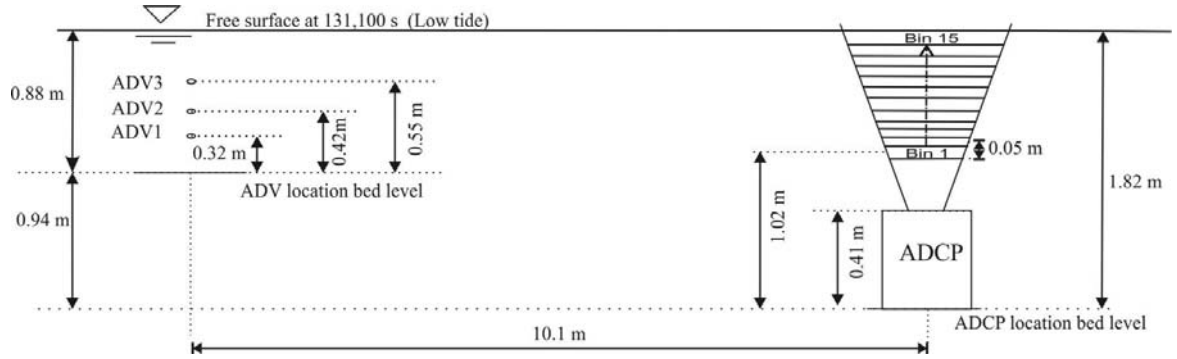

(A) Instrument arrangement at low-tide

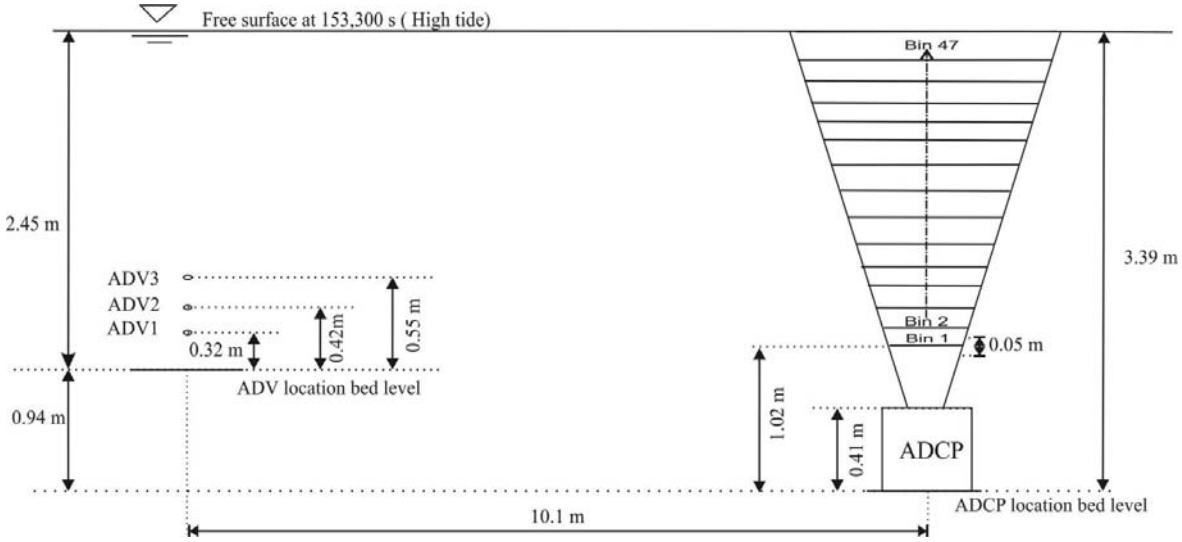

(B) Instrument arrangement at high-tide

Fig. 4-1 - Schematic diagrams of the sampling volumes of the ADVs and ADCP relative to the channel bottom (site 2B and 10.1 m downstream)

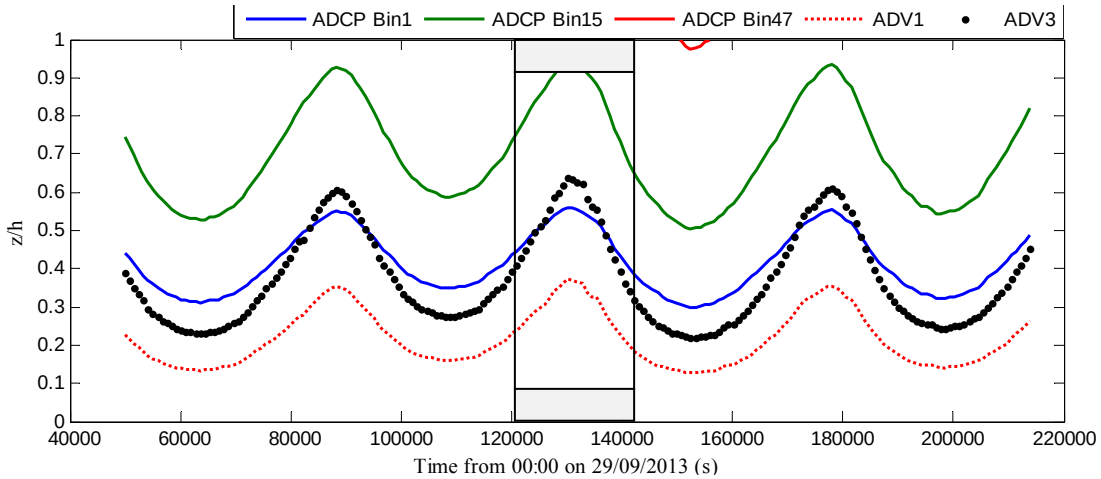

Fig. 4-2 - Time variation of relative height z from the channel bed normalized by water depth h; box shows portion where drifter deployments were carried out

In comparing the ADV and the ADCP, the ADV data were averaged over an interval of 854 s, equivalent to the sampling interval for the ADCP. Because of differences in sampling location, the horizontal velocity V_H was calculated as:

$$V_H = \frac{|V_x|}{V_x}\left(\sqrt{V_x^2 + V_y^2}\right) \tag{4-1}$$

where V_x is the streamwise velocity (+ve downstream), V_y is the transverse velocity. Figure 4-3 shows the time variation of V_H for ADV3 and ADCP Bins 1 and 15.

The horizontal velocities fluctuated throughout the study period. Both instruments recorded very slow oscillations in velocity with the period of about T_{res} = 3,000 s . These long-period fluctuations was believed to be linked to external resonance in the Moreton Bay:, namely between the river mouth and nearby landmarks about 15 km away (assuming an average water depth of 10 m). The ADCP measurements showed a tidal trend similar to that of the ADV data, while the ebb and flood tide velocity maxima occurred before and after low slack water respectively. The ADCP Bin 1 and Bin 15 horizontal velocity magnitudes were consistent with those of the ADV3 except at peak flows. The velocity maxima occurred around low-tide, where ADV3 was closer to the free surface than ADCP Bin 1 (e.g. 123,000 – 135,000 s). The free surface wind and subsurface velocity shear therefore contributed to the larger velocity ADV3 when compared with ADCP Bin 1.

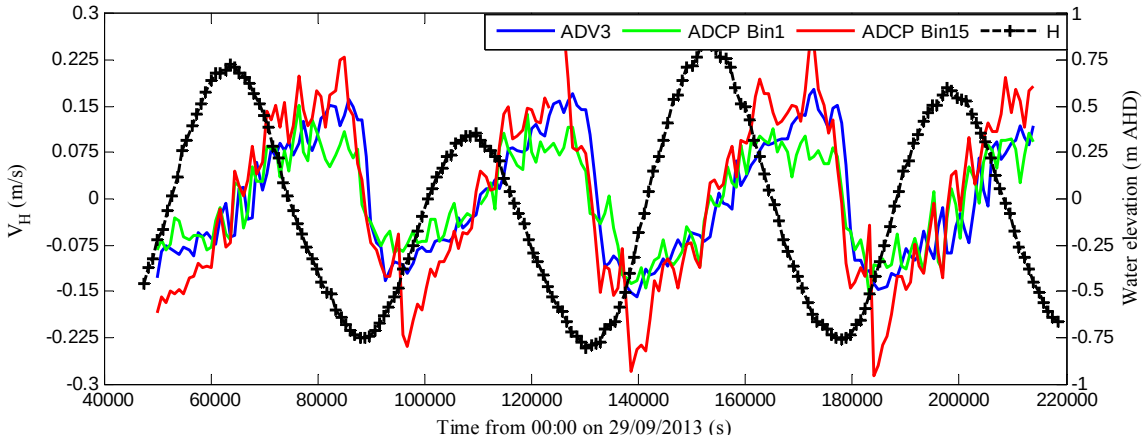

Fig. 4-3 - Mean horizontal velocity as a function of time for ADV1, ADCP Bin 1 and Bin 15

The ADCP Bin 15 had velocity magnitude values significantly larger than those of Bin 1 and ADV3 around low-tide. In addition to the effect of free surface, this difference could be related to the location of the two instruments. The ADCP was placed at the outer bend of the meander at site 2B, which was expected to experience higher velocity magnitudes during peak flows. Despite the large sampling volumes of the ADCP, the results showed no significant deviations in the overall

tidal trend from the point measurements of the ADVs. This is because the length scales of the fluctuations observed in the mean velocity data were significantly larger than the ADCP bin sampling size. This suggested that proper quality-controlled ADCP data could be used to observe very large scale variation of flow parameters within the channel.

Table 4-1 - Summary of field deployments of the GPS-tracked drifter

Test (1)	Start time (s) (2)	Location (3)	Drifter trajectories (4)	Effective drift time (s) (5)	Mean flow speed (m/s) (6)	Average wind speed (m/s) (7)	Mean velocity of ADV3 at site 2B (m/s) (8)	U_{slip} (m/s) (9)
1	119,250	Across site 2B and 2BB (*)	4	4,800	0.14	1.18	-	0.0071
2	135,480	Site 1A (*)	1	2,160	0.24	1.42	0.13	0.0092
3	138,120	Site 1B (*)	1	2,400	0.20	1.34	0.14	0.0084
4	141,360	Site 2	1	3,000	0.15	1.01	0.11	0.0060

Notes: U_{slip}: drifter wind slip velocity due to wind drag in the same direction as the water flow (wind analysis provided in Appendix F); (*): See Figure 4-5 for location.

4.2.2 GPS, ADV and ADCP comparison

The GPS-tracked drifters have a diameter ø = 19.7 cm with a total height of 26 cm, submerged to height h = 23 cm, leaving 3 cm above the surface to reduce the direct wind drag ([14]). Drifter deployments were short (20 – 60 min) because of the presence of meanders and the limited width. Table 4-1 shows the summary of the deployment conditions. Test 1 was carried out during an ebb tide from upstream of site 2B so the drifters could sample subsurface flow within a few metres of the fixed ADVs and ADCP for comparison.

The time-averaged velocities of the drifter during the ebb tide were compared with those of the fixed ADV and ADCP. There were difficulties in validating the Lagrangian data with those of the Eulerian devices (ADV and ADCP) because these devices experienced similar velocity for short times. In addition, the combined effects of wind, tides, resonance and bathymetry induced high spatial variability of the velocity within the channel. Figure 4-4A shows the comparison of the horizontal velocity of the instruments when a drifter was within a 50 m radius of the ADV sampling

[14] The analysis of wind effect on the drifter is provided in Appendix F

location. The ADV and drifter velocities were averaged over 30 s to remove the high frequency fluctuations. The drifter velocities showed similar trends in time with those of the ADVs and were within the data range of the ADCP. The vertical profile of the horizontal velocity using the time series and the ADCP depth measurements at time centred at t = 119,100 s is also shown (Fig. 4-4B). Figure 4-4B shows the ADCP ensembled horizontal velocity at the centered time, t = 119,100 s and the average of the time series (ADV and GPS-drifter) shown in Figure 4-4A. The horizontal velocity increased with increasing deviation above the bed in a manner similar to steady wide-open channel flow with maximum velocity close to the surface as indicated by the drifter velocity and the ADCP bins next to the free surface. The scatter near the surface suggested some influence of the wind on the subsurface layer of the channel. The large values of the drifter velocity between 119,200 – 119,450 s were likely caused by some wind induced motion on the subsurface layer of the channel and some direct wind drag on the unsubmerged surface of the drifter ($U_{slip} \sim 0.007$ m/s). During this period, the average wind speed U_{wind} was about 1.2 m/s in the North-North-East direction.

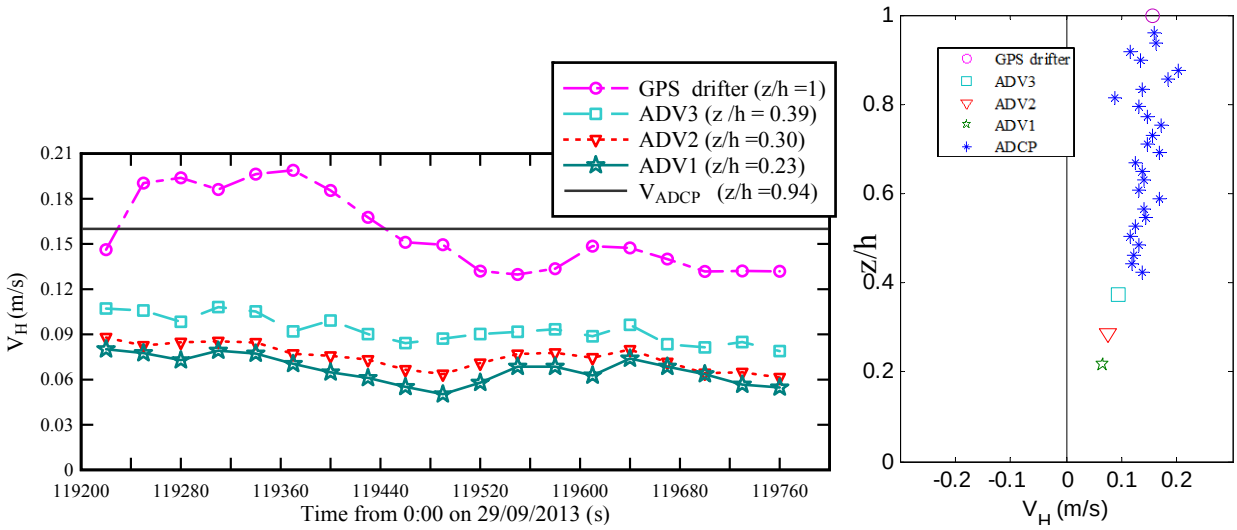

(A, Left) Average of 30 s data points when the drifters were within 50 m radius of the ADVs sampling location; two horizontal lines indicate the values of the ADCP (last bin) velocities
(B, Right) Averaged velocity of three ADVs and GPS time series in (Figure 4-4A) with depth variation of ADCP horizontal velocity data at time centred at t = 119,100 s
Fig. 4-4 - Comparison of the streamwise velocities of the drifter, ADCP and ADV

Slip is the horizontal motion of a drifter from the motion of currents (Lumpkin and Pazos 2007). The wind-induced velocity, U_{slip}, depends on both drifter drag area ratio and wind vectors in the vicinity of the measurements. The present drifter configuration has a drag area ratio of 8.5 – 13 and a velocity difference attributed to wind of less than 1% of wind speed (Suara et.al 2014b) using a

simple empirical model (Niiler and Paduan, 1995) and theoretical drag balance on the capsule (Table 4-1; Colum 8). The calculation of wind effect on the drifter is presented in Appendix F, where the wind effect ε of O[0.01] at a speed of 2 m/s could induce about 10% slippage at low current speed (O[0.1 m/s]) (section F.1). Increasing the submerged surface area, which could be done by attaching a window shade or parachute drogue types to the drifter capsule, could further reduce this direct wind effect on the drifter.

The average horizontal velocities of the drifter were sampled at several locations upstream of the mouth of the channel and the corresponding horizontal velocities obtained from ADV3 at site 2B are summarised in Table 4-1. The trajectories of the tests are also shown in Figure 4-5 with test 2 carried out about 100 m from the mouth of the channel. The drifter followed the main channel and was believed to be driven by strong tidal forces due to the meander before it got close to the bank. The average horizontal velocity V_H was 0.24 m/s for trajectory across site 1A (test 2), close to the channel mouth compared to 0.13 m/s at site 2B at the time. Similarly V_H was 0.13 m/s for a trajectory sampled from site 2 through to sites 2B and 2BB (test 4; Fig. 4-5); at the same time, V_H was 0.11 m/s at site 2B (ADV3). Therefore, drifter mean velocities between these two times and locations changed by 0.09 m/s while the ADV3 recorded a 0.02 m/s change in velocity at the same time. This suggested some spatial variation in the mean velocity distribution with distance away from the channel mouth. This might be the influence of strong tidal incursion at the beginning of the flood tides forcing the current to one side of the channel. This effect could not be experimentally verified because cross-sectional average velocity distribution was not obtained from the drifter's deployments. Further investigation is required with the use of multiple drifters and implementation of spatial binning to transform the pseudo-Lagrangian estimate of the drifter to an Eulerian distribution to establish the circulation pattern particularly close to the mouth of the channel.

Spectral analysis

Turbulent velocity fluctuations have some similarity with white noise in terms of statistical properties but both have different spectral structures ([15]). Therefore, it is important to verify that the velocity fluctuations measured by a turbulence measuring device have some structure associated with canonical turbulence (Rusello et al., 2011). The spectra of velocity measured using the ADV, ADCP and GPS-tracked drifters was examined against the slope predicted by Kolmogorov's second similarity hypothesis (Davidson, 2004). Figure 4-6 shows the power spectral densities (PSD) of the streamwise velocity for the ADV1, ADCP Bin 1 and a drifter trajectory. The ADV and ADCP data

[15] White noise signal has flat (constant) power spectral densities while the power spectral densities of turbulent velocity measurement vary with frequency

covered the full study period. The drifter data contained only a 50 minutes observation during a flood tide on the 30th September, 2013 at about 700 m downstream from the ADV sampling location to site 2B (AMTD 2.1 km).

The spectra densities showed slopes similar to -5/3 expected within the inertial sub-range, particularly at higher frequencies. The ADCP and ADV had power spectral densities of the same order of magnitude between the frequency range covered by the ADCP (frequency, F < 0.023 Hz). The distinctive peak in power spectral density at about 0.00004 Hz seemed related to the tidal fluctuation. The drifter also had similar spectrum densities as the ADV within F = 0.003 – 1 Hz, beyond which the GPS-drifter contained noise that was more than 10% of the true signal and was therefore, filtered-off during the post-processing stage. The peak in PSD of the drifter velocity at about 1 Hz was possibly related to bobbing and rocking of the capsule in response to surface waves.

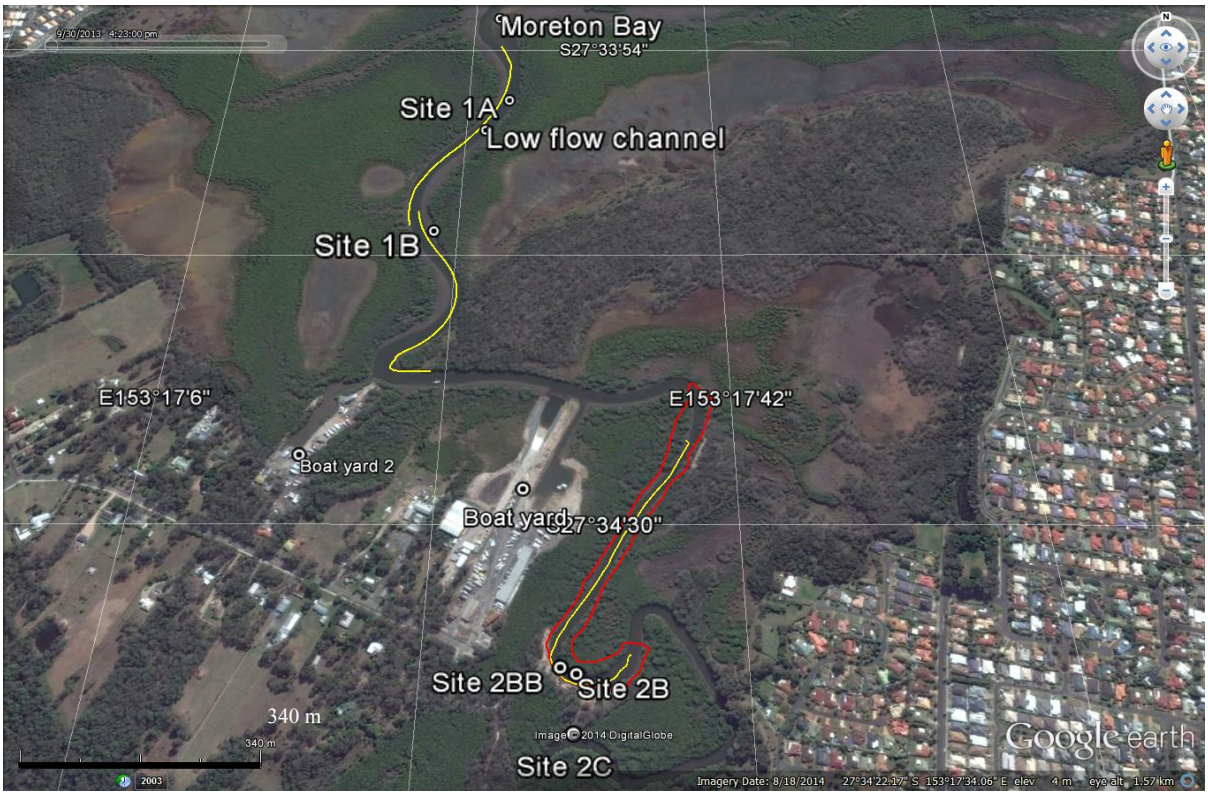

Fig. 4-5 - Google Earth vicinity map of Eprapah Creek; yellow lines show trajectories of a drifter. The scale is shown in the black thick line in the bottom left corner. "Eprapah Creek" 153.30°E and -27.567°S. Google Earth 7.1.2.2041. Google Inc. (2013).

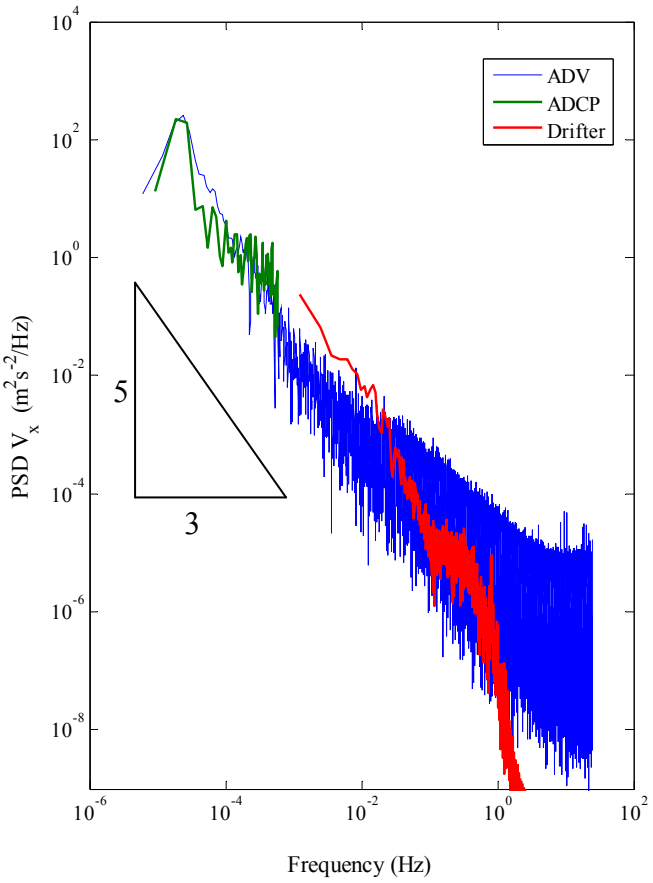

	ADV	ADCP	Drifter
Sampling/ cut-off frequency (Hz)	50/-	0.0012/-	10/1.5
Length of data set (s)	172,518	169,608	3,000

Fig. 4-6 - Spectral analysis of fluctuations of streamwise velocities V_x, for ADV1 measured at z = 0.32 m, ADCP Bin1 at z = 0.58 m and drifter (subsurface): solid black line is a -5/3 slope. Note that the PSD for instruments had different data length and frequency ranges as summarised in the table above.

4.3 VERTICAL PROFILE OF HORIZONTAL VELOCITY USING ADCP

The vertical distribution of mean velocity in a turbulent open channel flow is complex and three regions defined by a relative height from the bed are present (González et al., 1996). In an idealised turbulent open channel, the wall region ($z/h \leq 0.15$-0.2), sometimes referred to as the inner layer, is significantly affected by the bed conditions. In the free surface region ($0.6 \leq z/h \leq 1$), the velocity distribution is determined by the free surface conditions and wind induced shear. In the intermediate region, both the wall properties and free surface conditions have limited effects, and production and dissipation of turbulent energies are approximately equal. In such idealised water column, the vertical distribution of velocity may be approximated using logarithmic or power law distributions with a few measurement points placed at strategic locations within the channel. The vertical distributions of the horizontal velocities are examined herein to determine whether a unique pattern

of velocity could be identified.

Figure 4-7 shows the contour plot of the horizontal velocity, V_H of the ADCP during the field deployment. The contour levels are at an interval of 0.05 m/s. The horizontal velocity ranged between ±0.3 m/s throughout the field study. The variation in velocities with times was largely tidal dominated, due to fluctuations caused by resonance. A unique feature of the ADCP data set was the large velocity magnitudes observed near the free surface rather than the free surface itself. This could be caused by wind-induced instability in the subsurface layer of the channel. Unreliability of the free surface ADCP measurements due to interference in the acoustic signals from the boundary reflectance (González et al., 1996) could not be ruled-out ([16]).

The vertical profiles of the ADCP horizontal velocities were examined as functions of relative heights of the measuring points from the surface. Figure 4-8 shows the vertical velocities starting around low-tide, preceded by an ebb tide (t = 132,763 s) to a subsequent low tide (t = 172,904 s) within a semidiurnal tidal cycle. The profiles confirmed the flow instabilities were likely wind induced near the surface. Around low-tide (e.g. t = 132,763 and 138,742 s) the gradients of velocities across the water column were highest because of the shallow water depth.

The intermediate region was observed as the flood tide increased the relative water height (e.g. t = 148,136 s). Some reverse in surface current was observed in the horizontal velocities around high-tide; during the same periods, measurements in the intermediate region ($0.2 \leq z/h \leq 0.6$) showed nearly constant value of V_H close to zero (e.g. t = 152,406 and 155,823 s). The intermediate region was likely driven by the tidal flow inertia and depleted gradually as low-tide approached and the velocity gradient increased through the water column. In general, the shape of the velocity distribution varied with tidal phase throughout the field observation.

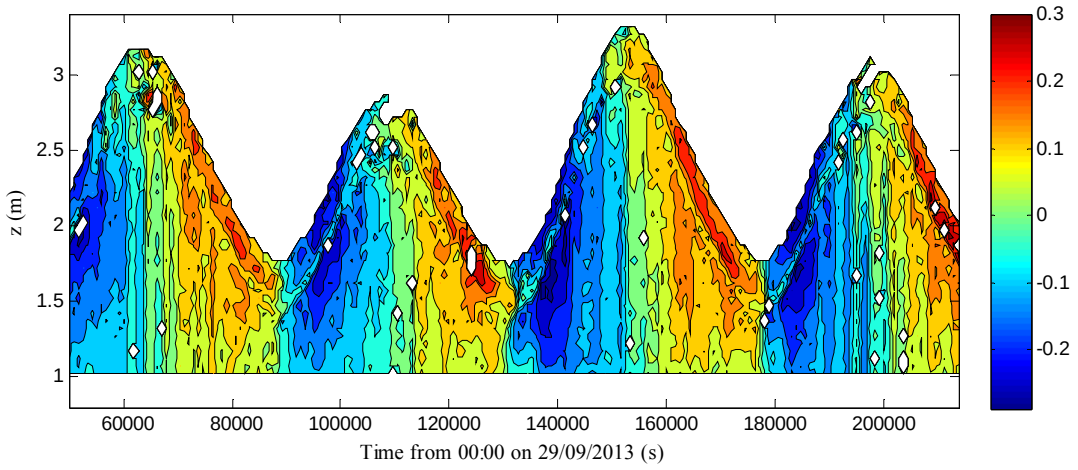

Fig. 4-7 - Mean horizontal velocity V_H (m/s) measured with ADCP during the deployment period.

[16] Possible reasons for unreliable velocities might be their magnitude close to the threshold limits.

Contour levels are every 0.05 m/s; +ve downstream of site 2B.

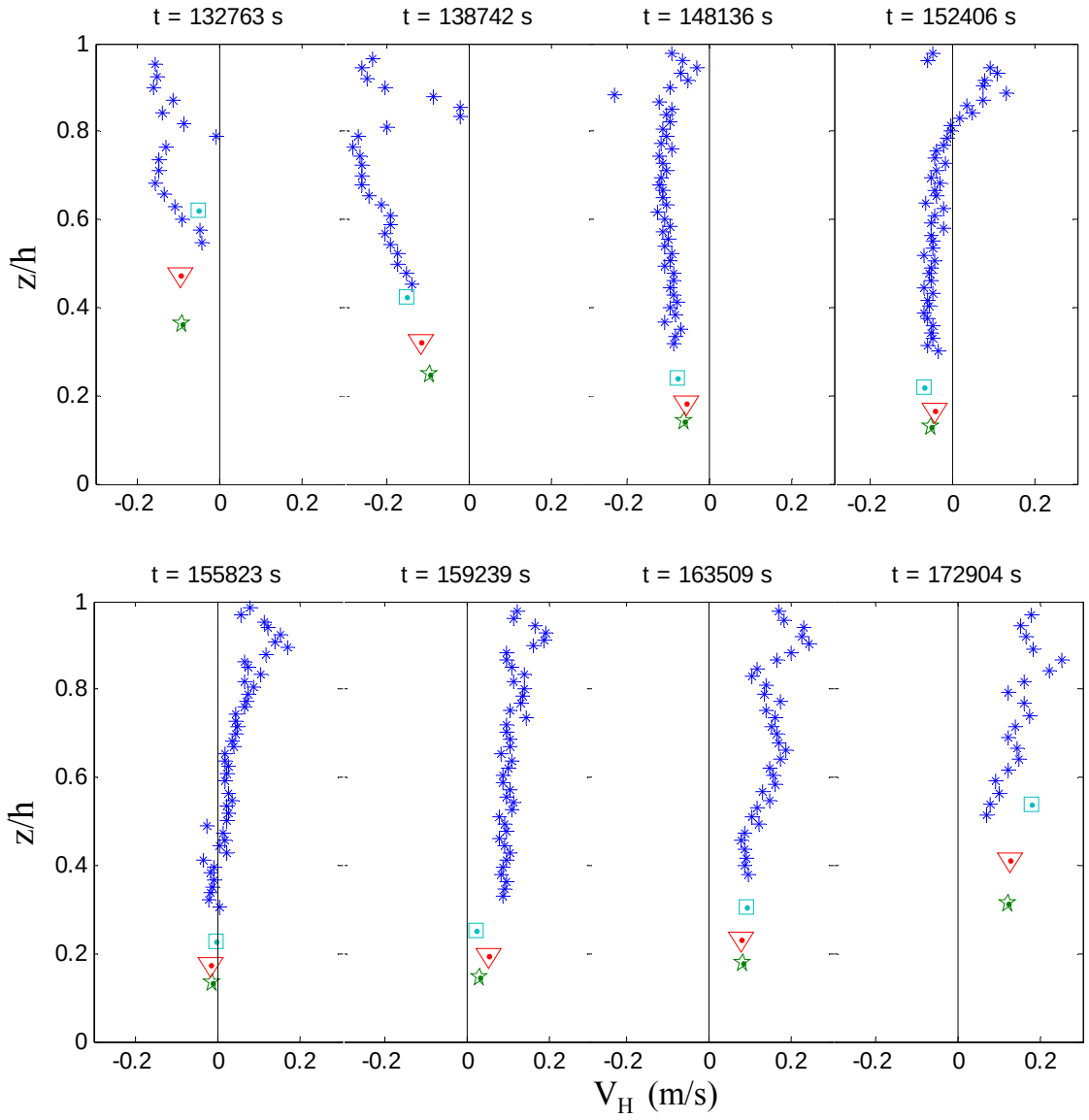

Fig. 4-8 - Vertical distributions of the mean horizontal velocity of ADCP at different phases of the tide within a complete semidiurnal tidal cycle.

4.4 REMARKS

Apart from the differences as a result of the relative locations of sampling volumes, the mean horizontal velocities of the ADCP showed little significant deviation in the overall tidal trend from the point measurements of the ADVs. This suggested that proper quality-controlled ADCP data could be used to observed large scale variation of flow parameters within the channel. However, accurate sampling of fine scale turbulent parmaters could be greatly impaired because of large sampling volumes of the ADCP. The results of the GPS-tracked drifter experiments showed that the drifters sampled the subsurface velocities well and also suggested some spatial variation in the

transverse velocity distributions within the channel. However unavoidable wind drag on the unsubmerged area of the drifter could modify the velocity measurements. The GPS-tracked drifter sampled a finer scale velocity than the ADCP because of higher sampling frequency and smaller sampling volumes.

The channel flow was non-uniform and highly unsteady, which caused the observable regions from an idealised open channel, to vary with time. In addition, various forcing factors including the tides and resonances, rough bathymetry, varying transverse shear, and wind affected the vertical distribution of velocity in the channel. Therefore, a unique profile describing the vertical distribution of velocity within the channel could not be identified from the study.

5. ADV DATA ANALYSIS

5.1 INSTANTANEOUS FLOW FIELD

The instantaneous fields of velocity and pressure are highly fluctuating in Eprapah Creek. Herein, the streamwise velocity, V_x is positive downstream (i.e. facing toward the mouth of the Creek), the transverse velocity, V_y is positive towards the left bank and the vertical velocity, V_z is positive upwards. The velocity and pressure data contained the superimposition of pseudo periodic fluctuations occurring at many different timescales. These fluctuations may be categorised into three groups: tidal, slow and fast fluctuations. The tidal scale fluctuations were governed by rise and fall of the tides, while the slow fluctuations were pseudo periodic, caused by the reflection of tidal force from certain geographical landmarks (Trevethan et al., 2006b). The fast fluctuations represented 'true' turbulent fluctuations. Turbulence was generated by both the fluid interface (internally generated) and the boundary layer (boundary generated) at the channel bed, resulting in various degrees of mixing and stratification (Dyer, 1997).

Figure 5-1 shows the three instantaneous velocity components and water depth as functions of time for the field study. The streamwise velocity showed strong tidal incursion when the water was low with maximum velocities around +0.19 m/s and -0.16 m/s during the late ebb and early flood tides, respectively. Similar flood and ebb tide maxima phases were observed in various locations in Eprapah Creek (Trevethan et al., 2006b, Trevethan et al., 2008a & Chanson et al., 2012). The velocity maxima of the ebb tides were larger than of those of the flood tides, contrary to previously observed at site 2B (Trevethan and Chanson, 2009). This difference could be linked to the change in the bathymetry of the sampling location. The transverse velocity showed some tidal influence with the maximum occurring when the water was low (Fig. 5-1b). Slow and fast fluctuations dominated both transverse and vertical velocities (see sections 5.5 and 5.6).

The streamwise velocity showed occasional distinctive long-period oscillations with periods of about 3,000 s and an amplitude of about 0.08 m/s. This was clearly shown by the flow reversals around the high water slacks, for example between 55,000 and 75,000 s (Fig. 5-1A). Similar observations of flow reversal were reported in Eprapah Creek (Trevethan et al., 2008b). These long period fluctuations were observed simultaneously in the transverse and vertical velocity components. The fluctuations were likely linked to the interaction of tidal forcing and external landmarks, which could affect the turbulence field because of their large amplitudes (Trevethan et al., 2006b). Some slow fluctuation was also observed in terms of the water pressure and local water elevation at high-tide – for example at the first and third high-tides. The slow fluctuations are discussed later in this section.

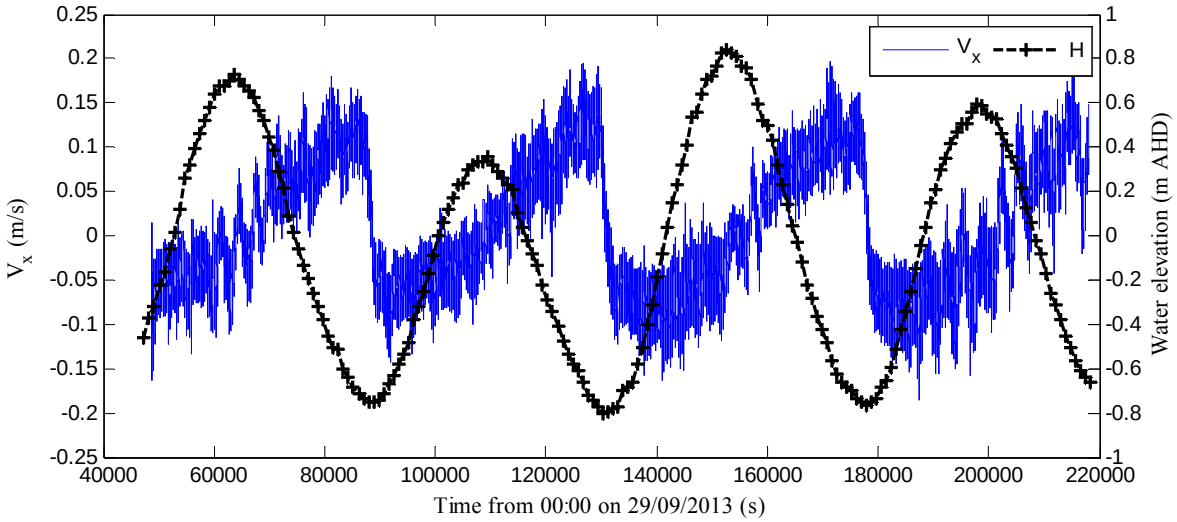

(A) Streamwise velocity, V_x (m/s)

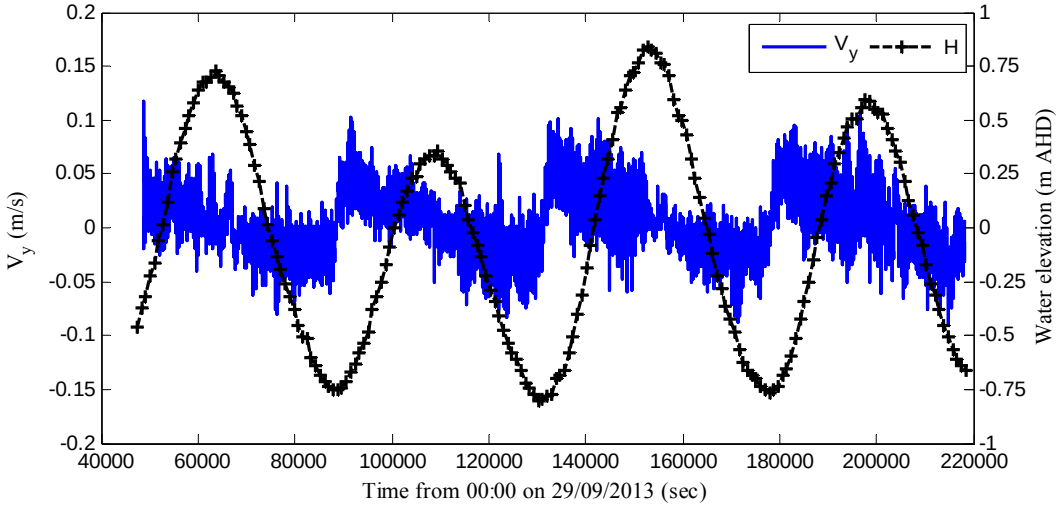

(B) Transverse velocity, V_y (m/s)

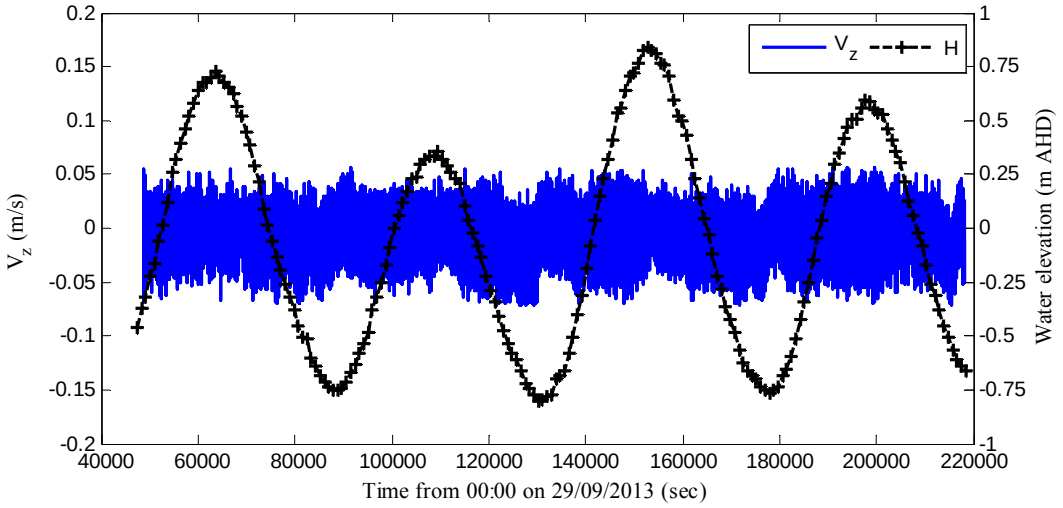

(C) Vertical velocity, V_z (m/s)

Fig. 5-1 - Instantaneous velocity components and water elevation as functions of time; ADV1 sampling volume location: 0.32 m above the bed and 11.056 m from the left bank

5.1.1 Remark

On average, the magnitude of the ebb velocity was greater than that of the flood. The ebb velocity maxima were approximately 15% larger than the flood velocity maxima. This was contrary to previous data from Eprapah Creek at site 2B, suggesting strong spatial variability in velocity along the cross-section of the channel. Further investigation is recommended to examine the transverse variation of velocity across the channel.

The fluctuation in the water level with a period around 3,000 s (50 minutes) was more pronounced around high-tide than other times. This fluctuation corresponded to the sloshing period between two landmarks separated by a length of about 15 km at average depth of 10 m, which is approximately the distance between the mouth of the creek and North Stradbroke Island, a neighbouring island delimiting Moreton Bay to the East.

5.2 CONCEPT OF TRIPLE DECOMPOSITION

The measured instantaneous flow fields contained several categories of fluctuation, which had to be decomposed in order to characterise their respective contributions to the physical processes occurring in the estuary. Successful techniques previously applied to both laboratory and environmental flows were the double and triple decompositions.

A standard means of separating the contributions of the instantaneous flow field is the *Reynolds decomposition* in which the mean and the fluctuating flow contributions are obtained through a form of time averaging (i.e. double decomposition). For example the instantaneous streamwise, V_x is decomposed into:

$$V_x = \overline{V_x} + v_x \tag{5-1}$$

where $\overline{V_x}$ is the mean streamwise velocity component and v_x is the fluctuation of streamwise velocity around the mean. This technique, also called Reynolds decomposition, is applicable to flows with a steady mean. The mean flow field (e.g. $\overline{V_x}$) is computed in a phase/time average, such that the average converges to a true mean value and is *ergodic* ([17]) (Tennekes and Lumley, 1972):

$$\overline{V_x} = \frac{1}{T}\int_{t_o}^{t_o+T} V_x(t)dt \tag{5-2}$$

where t_o is the start time of the averaging phase and T is the time period within which $\overline{V_x}$ could be assumed to be constant. A modification of the approach applicable to gradually varying flow is the use of $\overline{V_x}$ as a variable time average or running mean (low-pass filtered value) with step size less

[17] A variable is said to be ergodic when all quantities (e.g. integral scales) formed from it converge (Tennekes and Lumley, 1972)

than the cut-off period T (Trevethan et al., 2007b).

The effectiveness of the double decomposition method depends on the selection of the period T (Eqn. 5-2) and the cycle-to-cycle consistency of the organised motions. Cycle-to-cycle variation of the tidal flows and the large-scale pseudo periodic flow can lead to inaccurate turbulence estimates. The Reynolds decomposition was originally developed for laboratory applications and has been systematically and successfully applied to the study of turbulence and the mixing of environmental flows (Chanson and Trevethan, 2010 & Chanson et al., 2012). This approach requires a trade-off of tidal variation in the flow field within a selected time frame upon which the flow field could be assumed constant. In most cases when applied to tidal channels, some slow fluctuation is embedded in the turbulent components, distorting the statistics of the resulting turbulence field.

The triple decomposition (TD) technique involves the separation of a pseudo-periodic flow field into its three components based on their periodicity. In the triple decomposition technique, the instantaneous flow fields may be decomposed into a varying mean velocity component and the identified fluctuating fields. For a tidal flow, the high-frequency flow field fluctuations would correspond to random motions (small-scale, 'true' turbulence) and the low-frequency flow fluctuations to some resonance (large-scale fluctuations). The TD technique assumes implicitly that each occupies a different range in the energy spectrum. The TD was applied to a laboratory flow, characterised by superimposed periodic waves coupled with turbulent motions (Hussain and Reynolds, 1972). It was also applied systematically in an open channel flow motion (Fox et al., 2005) and to describe turbulence during a major flood in an urban environment (Brown and Chanson, 2012).

The triple decomposition theorem was applied to the instantaneous flows fields observed at Eprapah Creek. Herein, instantaneous velocities and pressure were decomposed using Eqn. 5-3:

$$V_i = \langle V_i \rangle + [V_i] + v_i \quad (5\text{-}3)$$

where $<V_i>$ is the tidal component, $[V_i]$ is the slow fluctuating component and v_i is the turbulent component. Figure 5-2 shows a hypothetical power spectrum of an instantaneous field in a tidal channel. The tidal fluctuation occupies the low frequency regime followed by the slow fluctuations occupying the regime between low and high frequency fluctuation vis-à-vis true turbulence. In applying the TD technique, a key issue is the determination of the characteristic frequencies (upper and lower cut-offs) for separating the organised and random turbulent motions from the instantaneous fields (Brown and Chanson, 2012, Suara et. al., 2014a). To isolate the large eddies within open channel flows, visual interpretation of moving averaged data could be used (Tamburrino and Gulliver, 1999) in combination with some turbulence statistics (Fox et al., 2005).

Frequency domain filtering recognises the existence of cycle to cycle variation of organised motions in unsteady flows and was applied to a pulsatile flow (Walburn et al., 1983) and an

environmental flow (Brown and Chanson, 2013). The frequency domain filtering techniques do not require a precise knowledge of the period of these motions (Brereton and Kodal, 1992). However for the present study, cut-off frequencies for the filter were chosen systematically through a sensitivity analysis. A digital filtering technique described in Bendat and Piersol (2011) was followed.

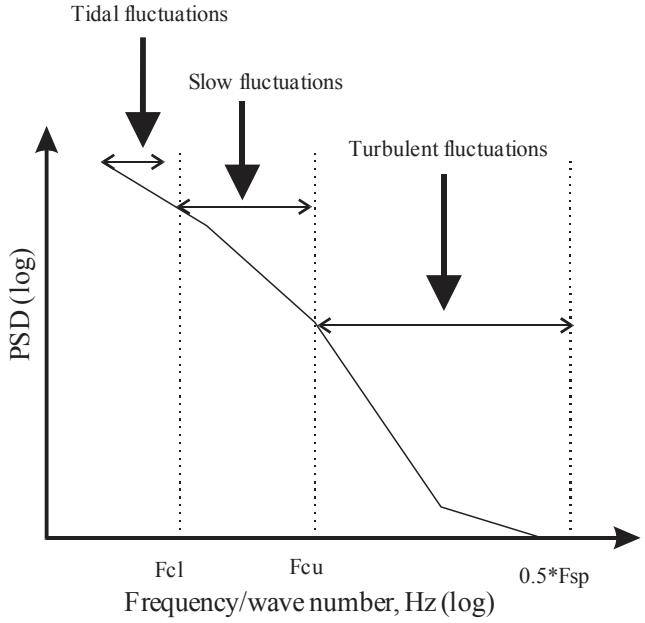

Fig. 5-2 - Hypothetical power spectral density of an instantaneous velocity field measured in a tidal channel. F_{cu} indicates the upper cut-off frequency, F_{cl} is the lower cut-off frequency, while F_{sp} is the sampling frequency of the instrument

5.3 SENSITIVITY ANALYSIS

The decomposition of the instantaneous flow field was performed based upon characteristic frequencies. These were identified by visual observations, power spectra analyses and celerity of water within the channel. Although the flow field in the channel was unsteady, the goal was to choose cut-off frequencies that provided appropriate isolation of the constituents of the decomposed flow fields.

5.3.1 Selection of lower cut-off frequency F_{cl}

The aim was to select a lower cut-off frequency that would produce the pure tidal constituent through a low-pass filter. In the present study, in addition to the tidal oscillation, the velocity data revealed some slow fluctuation; the largest with period of about 3,000 s through visual inspection of the time series. Distinctive fluctuations were also observed in the power spectra analyses of

instantaneous data for velocity and pressure (Fig. 5-3). Figure 5-3 shows the spectra of velocity and water pressure with smoothed curves highlighting distinctive peaks and troughs in the power spectrum of the instantaneous data (ADV1) at frequencies greater than 0.00004 Hz, which corresponds to about half of a semidiurnal tidal period. The peaks could not be confirmed in the smoothed data because of the limited number of data points at this very low frequency but seemed related to the tidal fluctuation. The succeeding peaks and troughs suggested some energetic event with frequency corresponding to the periods of the visually observed slow fluctuations. Similar peaks and troughs were also observed in the power spectra for the velocities of the other ADV units (see Appendix D). These observations suggested that a low-pass filter with a cut-off frequency between 0.00004 and 0.0002 Hz – about twice the period of dominant slow fluctuation – would remove all possible slow fluctuations from the instantaneous flow field to obtain the tidal component.

Further analysis was performed around $F_{cl.}$ = 0.0001 Hz. Figure 5-4 shows that a cut-off frequency higher than 0.0001 Hz introduced some signature of the slow fluctuations in the tidal velocity while using a lower frequency (e.g. $F_{cl.}$ = 0.00008 Hz) caused a phase shift around the slack water (highlighted box). Therefore $F_{cl.}$ = 0.0001 Hz was selected for obtaining the tidal flow fields from the instantaneous measurements.

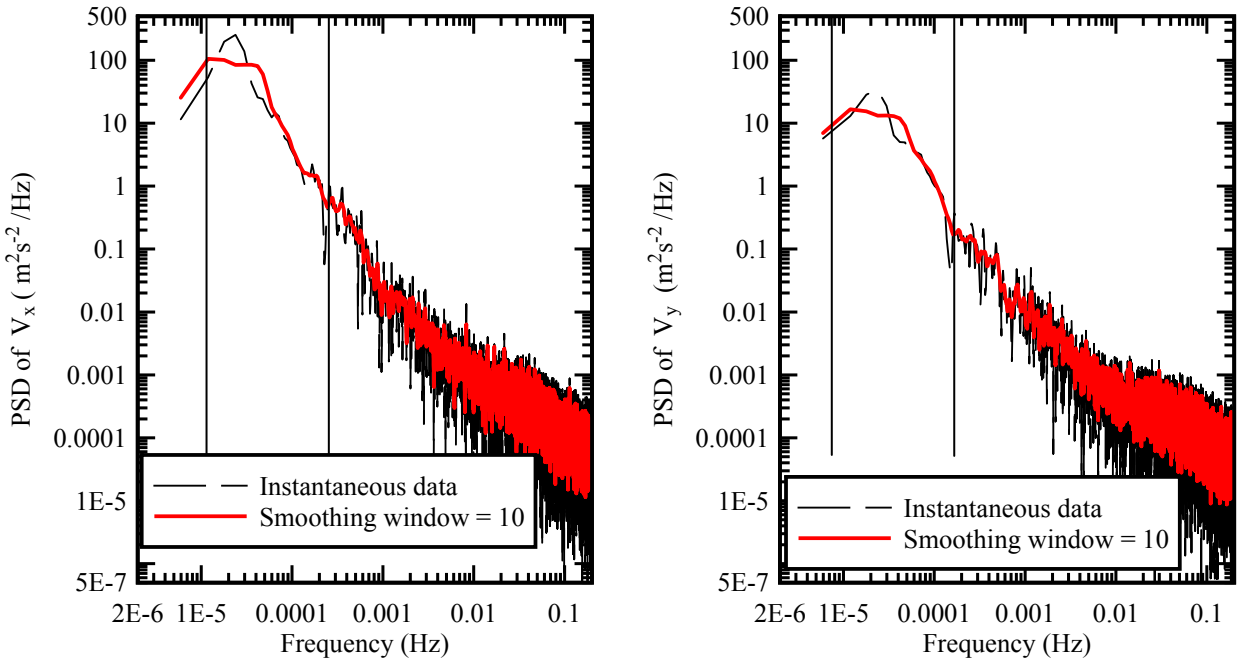

(A) PSD of $V_{x,}$ (m^2/s^2/Hz)

(B) PSD of $V_{y,}$ (m^2/s^2/Hz)

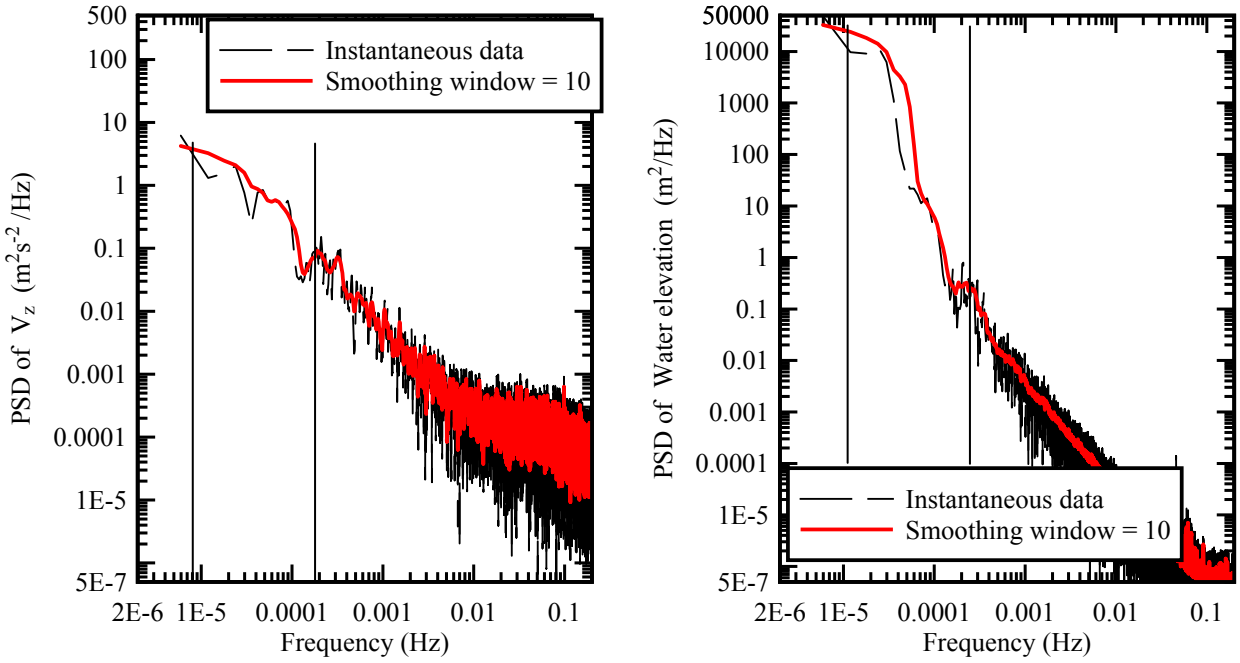

(C) PSD of V_z, (m^2/s^2/Hz) (D) PSD of water level, (m^2/Hz)

Fig. 5-3 - Spectral analysis of fluctuations of streamwise velocity V_x, transverse velocity V_y, vertical velocity V_z and water elevation measured using ADV1. Sampling volume location: 0.32 m above the bed, 11.056 m from left bank. Vertical lines indicate frequency range where F_{cl} could be located.

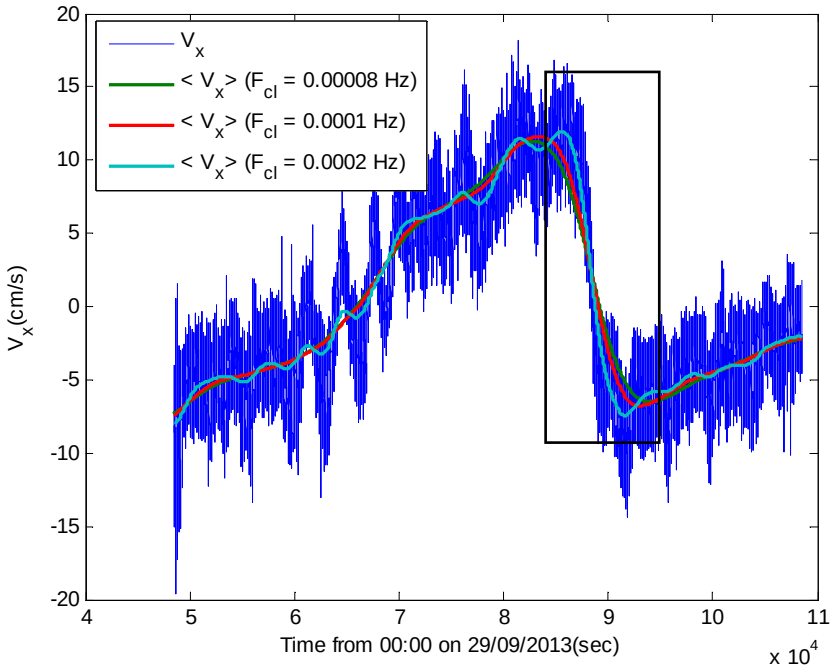

Fig. 5-4 - Sensitivity analyis on the effect of the upper cut-off frequency on the approximation of the tidal component of velocity. ADV1 Sampling volume location: 0.32 m above the bed, 11.056 m from left bank. Frame shows slack water phase shift discused in the text.

5.3.2 Selection of upper cut-off frequency F_{cu}

The aim here was to select an upper cut-off frequency to isolate the 'true' turbulence through a high-pass filter, by removal of the large-scale fluctuations. This was done by evaluating the effect of the upper cut-off frequency on the statistical properties and derivatives of the resulting turbulence flow field. The skewness Sk (Eqn. 5-4) is particularly considered an additional diagnostic for determining F_{cu} because of its relationship with fluid eddy physics (Grass, 1971, Fox et al., 2005).

$$Sk = \frac{\frac{1}{n}\sum_{n} v_x^3}{\left(\frac{1}{n}\sum_{n} v_x^2\right)^{3/2}} \quad (5\text{-}4)$$

where n is the sample size taken as 10,000 (200 s). The analyses of the effect of upper cut-off frequency of some turbulence paramater presented in Appendix D showed the difficulty of identifying a clear cut-off frequency. For example, the effect of the upper cut-off frequencies upon the skewness of the streamwsie turbulent velocity is illustated in Figure 5-5. The skewness converged to zero (the value for a normal distribution) as the upper frequency is increased. However the results showed that an increase in the upper cut-off frequency does not indicate a significant change in skewness within the investigated frequency range, except at end of flood tide. This suggested that a more intuitive way of fixing the upper cut-off frequency was required.

The resonance period T_{res} for water traveling between landmarks can be estimated in first approximation from the wave celerity:

$$T_{res} = \frac{2l}{\sqrt{gd}} \quad (5\text{-}5)$$

where l is the distance between landmarks, g is the gravitational acceleration and d is the water depth (Chanson, 2004). The slow fluctuations in Eprapah Creek channel were a result of resonance between landmarks which are either external or internal to the channel (Trevethan, 2008). The shortest was the width of the channel at the sampling location which was approximately 25 m at low tide (30/10/2013) and corresponded to $T_{res.} \approx 16$ s. The shortest slow fluctuation expected within the channel during the field study had therefore, a characteristic frequency around 0.063 Hz. Thus, an upper frequency of 0.1 Hz was used to separate the slow fluctuations from the instantaneous flow fields.

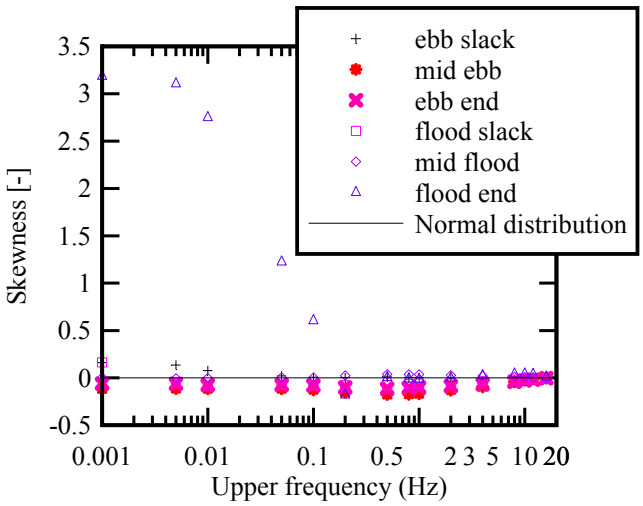

(A) ADV 1

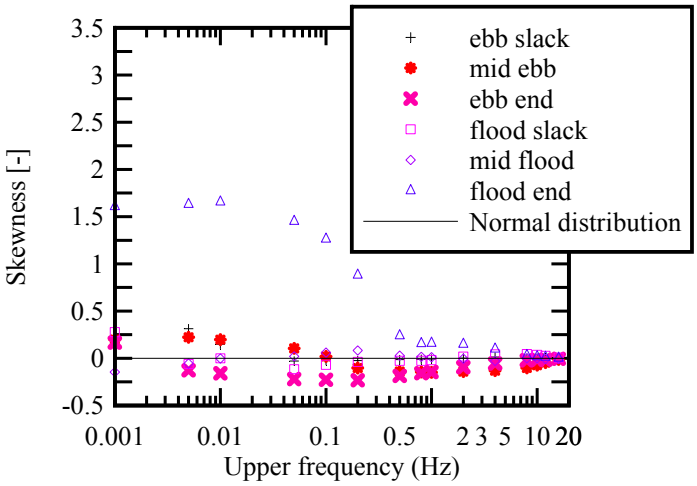

(B) ADV2

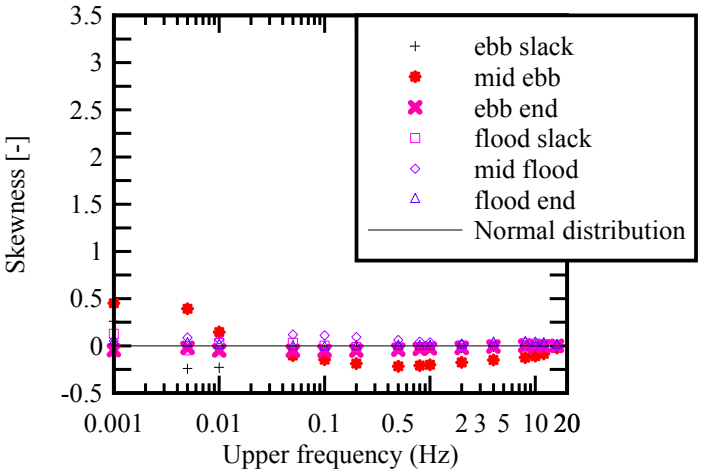

(C) ADV3

Fig. 5-5 - Sensitivity analyses on the effect of cut-off frequency on skewness of the streamwise turbulence velocity (highpass filtered data). (A) ADV1; Sampling volume location: 0.32 m above the bed, 11.056 m from left bank. (B) ADV2; Sampling volume location: 0.42 m above the bed, 11.042 m from left bank. (C) ADV3; Sampling volume location: 0.55 m above the bed, 11.05 m from left bank.

5.3.3 Remarks

The major harmonic constituents of a semidiurnal tide are the principal lunar M2 and the luni-solar constituents K2. The spring-neap cycle and tidal range are determined by the difference in speeds and amplitudes of these components and other constituents. In addition, wind and local bathymetry have some influence on the tides causing assymetry. Therefore, It is difficult to obtain a precise frequency for defining tidal constituent of the flow field from short period time series. However, the minor tide during the field experiment had a period of 42,660 s. Based on the sensitivity analysis of

the lower cut-off frequency for the Eprapah Creek field data and other field data obtained in a similar semidiurnal channel, Mayes Canal at the Sunshine Coast (data not presented), the lower cut-off frequency using the triple decomposition technique described herein could be generalised as:

$$\frac{4}{P_{min}} \leq F_{cl} < \frac{1}{P_{fluc}} \quad (5\text{-}6)$$

where $F_{cl.}$ is the lower cut-off frequency which fullfill the Nyquist condition, P_{min} (herein ~42,000 s) is the period of the shortest tidal cycle observed and P_{fluc} (herein ~3,000 s) is the period of the longest slow fluctuations.

The slow fluctuation (bandpass filtered data) was obtained by substracting the sum of the tidal components (lowpass filtered data) and the turbulent component (highpass filtered data) from the instantaneous flow fields. The upper and lower cut-off frequencies had thus some effect on the slow fluctuation estimate. It is worth noting that the tidal components and the turbulent components were obtained from direct filtering of the instantaneous flow field. Therefore the lower cut-off frequency had no effect on the resulting turbulence and the upper cut-off frequency had no effect on the tidal components. The same triple decomposition cutoff frequencies were applied to all velocity components and water level data.

5.4 TIDAL SCALE FLOW VARIATION

Figure 5-6 shows the time variation of the tidal-scale velocity components <V> for ADV1. The streamwise velocity $<V_x>$ data showed that the largest velocities with magnitude around 0.1 m/s for both the ebb and flood tides occur around low water. This is consistent with previous field experiments at various other locations within Eprapah Creek (Trevethan et al., 2006b, Trevethan et al., 2008a, Chanson et al., 2012) and the mean horizontal velocities examined in Section 4. Contrary to previous field data, the magnitude of the ebb tidal velocity was on average greater than that of the flood tide. This difference could be related to bathymetry change and transverse variability of the flow field within the channel as observed in the instantaneous velocity components. This suggests that the higher values of the ebb velocity maxima over the flood was tidal related. Detail of the ebb-flood velocity comparison is presented in Appendix B.

The transverse tidal velocity $<V_y>$ (Fig. 5-6B) had its largest velocity magnitude around low water with the direction variation with tidal phase. Positive values of $<V_y>$ indicated that flood tides forced the current across the channel toward the outer boundary while $<V_y>$ was predominantly negative during the ebbs. The magnitude of $<V_y>$ was larger on average during the flood tide than the ebb tide. The magnitude of the tidal vertical velocity $<V_z>$ was approximately zero during the flood tides while fairly significant negative values (downward flow) were observed during the ebb tides (Fig. 5-6C). These results were consistent with the free surface condition of negative pressure

gradient described by:

$$\left.\frac{\partial H}{\partial t}\right|_{z=h} = V_z|_h \qquad (5\text{-}7)$$

The sloping bottom in the cross section of the channel where the ADVs were deployed most likely contributed to the non-zero magnitudes of vertical mean velocities.

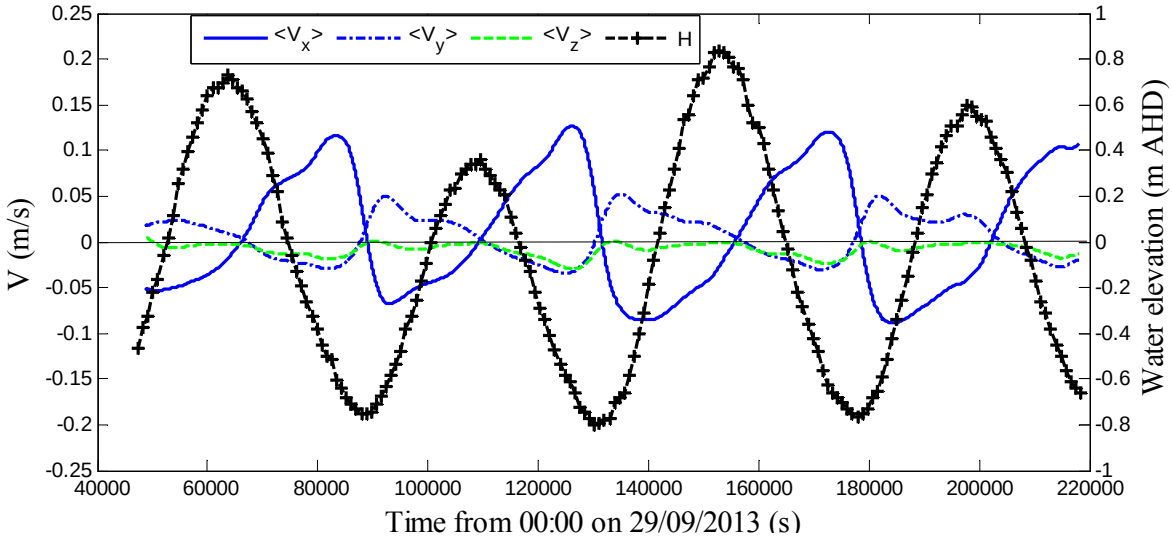

(A) ADV1; Sampling volume location: 0.32 m above the bed, 11.056 m from left bank

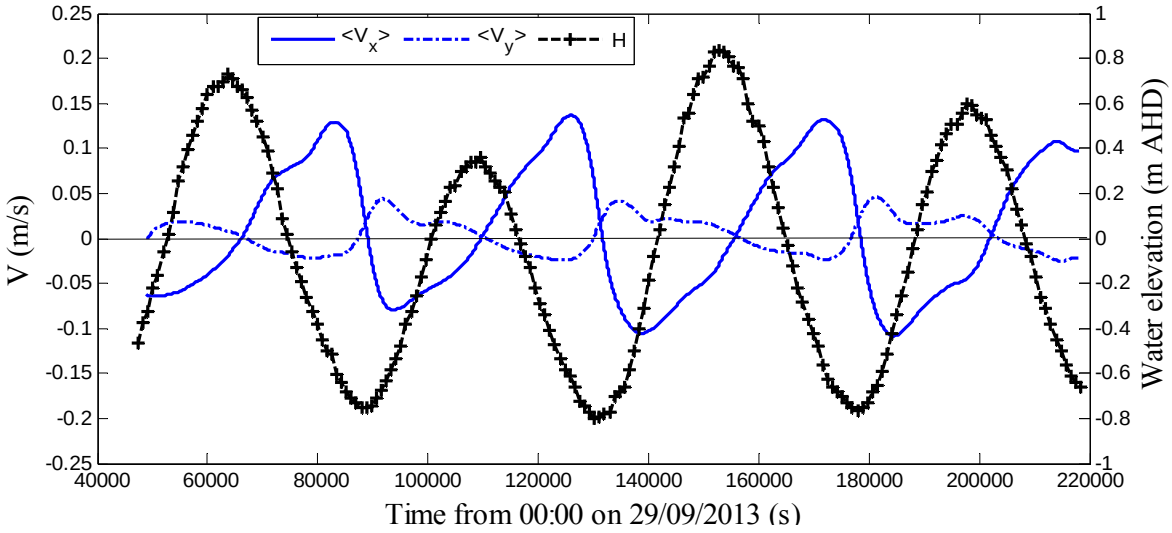

(B) ADV2; Sampling volume location: 0.42 m above the bed, 11.042 m from left bank

Fig. 5-6 - Tidal varying velocity components $<V_i>$ for the three ADV units obtained as low-pass filtered data of instantaneous velocity.

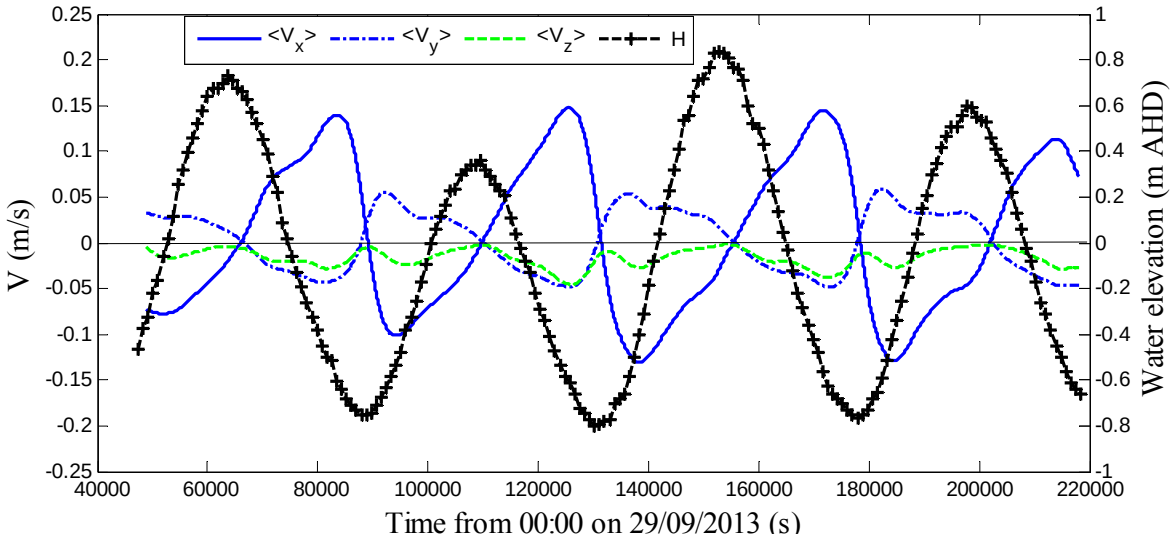

(C) ADV3; Sampling volume location: 0.55 m above the bed, 11.05 m from left bank

Fig. 5-6 - Tidal varying velocity components $<V_i>$ for the three ADV units obtained as low-pass filtered data of instantaneous velocity.

5.4.1 Tidal characteristics

Four high tides and three low tides were observed during the field study. The first and the last high tides had similar tidal amplitudes and periods. For comparative purposes, two tidal cycles –major and minor tidal cycles (Fig. 5-7) were analysed. Herein a semidiurnal tidal cycle starts from the beginning of a flood tide to the end of the subsequent ebb tide, for example, a cycle is between LT1 and LT2 or LT2 and LT3 (see Fig. 5-7 caption). The tidal range was the difference between the highest and lowest water levels while a period was taken from low tide to subsequent low tide. To compare flood and ebb tidal velocity maxima for these cycles, the flood velocity was considered from low tide slack ([18]), LWS to next high water slack, HWS, while the ebb conditions were considered conversely (Savenije, 2006) (see Appendix D). Note that tidal asymmetry was pronounced with these cycles.

Table 5-1 shows that the major tidal cycle had a higher amplitude and longer period than the minor tidal cycle. Both the major and minor tidal cycles showed ebb-dominance. The duration and maximum velocity of the ebb tides were larger than those of the flood tides. This behaviour was unexpected considering that the low tides showed no significant variation from cycle to cycle. This behaviour might require further investigation.

[18] Although there are several definitions for slack water. Herein for consistency with the low tide and high tides definitions, the low water slack (LWS) is defined as the time on zero tidal component of streamwise velocity succeeding a discharge from the channel while the HWS is zero tidal velocity after an inflow event. This is similar to the interpretation given by Savenije (2006).

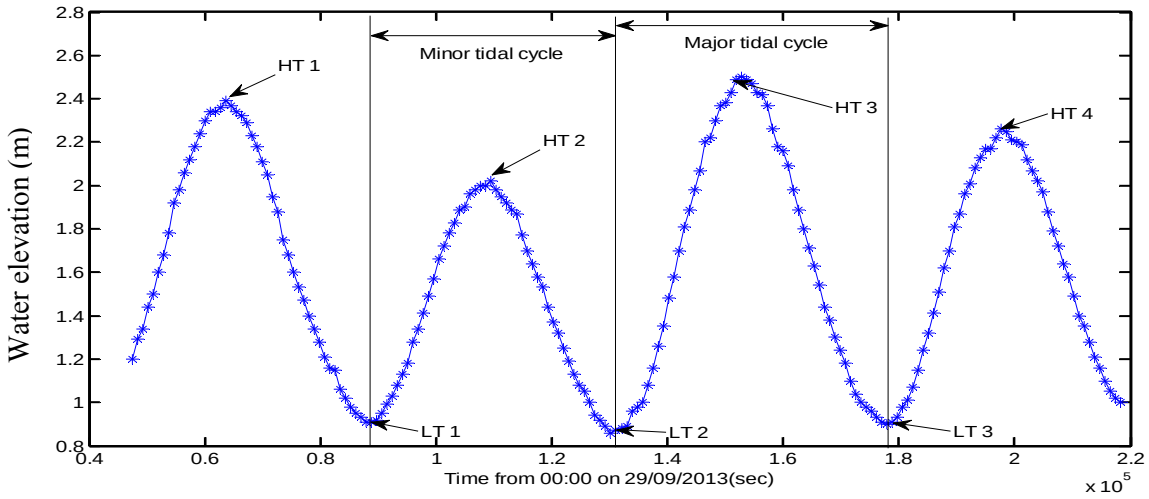

Fig. 5-7 - Time series of water elevation showing the amplitudes and periods of tides observed during the study; HT 1 – High tide 1; LT 1 – Low tide 1; HT 2 – High tide 2; LT 2 – Low tide 2; HT 3 – High tide 3; LT 3 – Low tide 3; HT 4 – High tide 4

Table 5-1 - Comparison of the tidal range properties of the major and minor tidal cycles

Cycle	Time LT – LT (s)	Period (s)			Tidal range (m)	Distance from bed (m)	Maximum tidal velocity (m/s)	
(1)	(2)	(3)			(4)	(5)	(6)	
		Flood	Ebb	Total			Flood	Ebb
Minor	88398 – 130949	20324	22227	42551	0.9	0.32	0.07	0.13
						0.42	0.08	0.14
						0.55	0.10	0.15
Major	130949 – 177698	22199	24550	46749	1.4	0.32	0.09	0.12
						0.42	0.11	0.13
						0.55	0.13	0.14

5.4.2 Lag and channel wave type

Tidal waves traveling through a natural channel could either be a standing, a progressive or a mixed type ([19]). The duration between the change in direction of tidal waves and a corresponding change

[19] An estuary is said to exhibit a purely standing wave when all reaches along the channel observe extreme water simultaneously. Also, the high tides, HT, coincide with the high water slack HWS, and low waters, LT, coincide with low water slack, LWS. The phase lag between the peak water and peak velocity would be π/2. An estuary is said to exhibit a purely progressive wave when extreme water levels coincides with the peak streamwise velocity magnitudes. That is, the water

in flow is defined as the lag. The lag of the streamwise velocity in a channel relative to tidal stage – channel water level relative to the mean sea level – depends on a combination of factors, which includes but is not limited to regional tidal dynamics and frictional response to tidal forcing (MacVean and Stacey, 2011). As the tides interact with a basin, the degree of reflection of the tidal wave determines whether the tides are standing waves or progressive waves. The tidal components of both the streamwise velocity and the water level were used to examine the lag and the wave type exhibited in Eprapah Creek.

Figure 5-8 shows the stage-velocity diagram for the minor and major tidal cycles observed during the field study. The graphs show that both the high water slacks and low water slacks occurred after high tides and low tides respectively. The stage-velocity at site 2B exhibited a mixed-type tidal wave. Previous observations of water level along various reaches along Eprapah Creek estuarine zone showed that the channel exhibited similar amplitude and phase particularly at high tides (Trevethan and Chanson, 2009, Chanson et al., 2012). This suggested that the same mixed-type wave could be exhibited throughout the estuarine zone. However the lag varied between tides. In addition, the effect of slow flow fluctuations on phase lag cannot be ruled-out.

The lags between velocity and water elevation were obtained for the high and low tides by subtracting the time when $<V_x>$ is equal to zero from the time for preceding peak water level. In general, the lag between change in flow direction and water gradient was larger during the ebb tides than for the flood tides. Table 5-3 summarises the lag observations. The high tides HT1 and HT3 occurred before high slacks by about 42 min while the low tides LT1 and LT2 occurred between 8.5 and 12.5 min before the change in flow direction. The lag on consecutive cycles showed some high to low pattern and was suspected to have some diurnal pattern for example; the slack phase lag for HT1 was about 42 min which has the same magnitude as slack water phase lag corresponding to HT3 where HWS lags HT2 by about 15 minutes. This pattern could be related to the modulation of the tidal constituents responsible for the neap-spring tidal variation.

---

level and velocity are in phase. A mixed wave system is exhibited in a channel when there phase lag varies between 0 and $\pi/2$. That is, both HWS and LWS occur after HT and LT respectively but before the mean tidal level (Savenije, 2006).

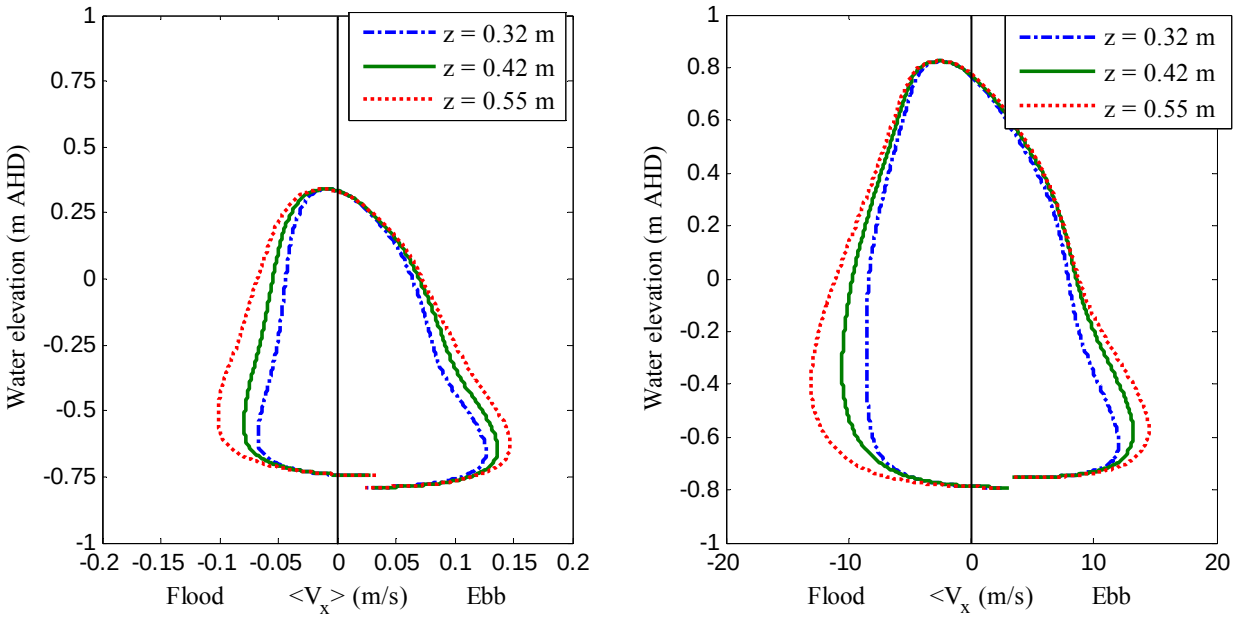

(A) Minor tide (LT1 – LT2) (B) Major tide (LT2 – LT3)

Fig. 5-8 - Stage-velocity plots of tidal components for the minor and major tidal types observed. Streamwise velocity $<V_x>$ is the low-pass filtered data and water elevation is the low-pass filtered data manual height readings.

Table 5-3 - Time lag between the change in direction of tidal component of the streamwise velocity and tidal stage

Type	Water height (m)	Lag (s)		
		z = 0.32 m	z = 0.42 m	z = 0.55 m
HT 1	2.40	2583	2584	2416
LT 1	0.91	645	713	755.
HT 2	2.02	775	875	1018
LT 2	0.89	648	742	511
HT 3	2.49	2483	2402	2223
LT 3	0.91	933	830	785

Notes: Low and high water evaluated based upon the low-pass filtered manual water level; Lag: time lag defined as $\text{Lag} = T|_{\text{high/low-water}} - T|_{\text{water-slack}}$

5.4.3 Remarks

The tidal variations in streamwise velocity showed remarkably strong ebb flow that was consistent with the instantaneous data and contrary to previous observations in Eprapah Creek. This was possibly linked with a local bathymetric change or a possibility of some hydraulic structure within

the boat yard suppressing the incoming tidal forcing. The stage-velocity graph for the period suggested that a mixed type with characteristic phase lag between 0 and π/2 (normalised). The phase lag between the HWS and HW ranges between 13 – 43 min. These corresponds to normalised phase lag of 0.035π – 0.116π (assuming π = 6 h and 12 min). Thus Eprapah Creek falls into the category of alluvial estuaries which are described with a typical phase lag 0.3 (0.096π) indicative of the ratio of bank convergence to tidal wavelength (Savenije, 2006).

5.5 SLOW FLUCTUATION AND RESONANCE

5.5.1 Spectral analyses of band-pass data

The velocity and water level data highlighted some slow fluctuation. The most pronounced fluctuations were observed around slack tides and high waters. These were observed in the form of episodic flow reversals and periodic rise and fall in water level. These observations were consistent with previous studies at Eprapah Creek (Chanson and Trevethan, 2010). The application of triple decomposition isolated the slow frequency fluctuations into the band-pass component of the instantaneous flow field i.e. $[V_i]$.

Figure 5-9 shows the spectral analysis of the band-pass horizontal velocity components and water elevation for ADV placed at z = 0.32 m above the bed. Similar spectra were observed for the other ADV units (Appendix D). The smoothed curves highlighted some prominent peak in spectral densities corresponding to energetic events. For example, a series of energetic events occurred at a frequency corresponding to period of about 3400 s. These were observed for both the streamwise velocity and the water level. This period was similar to that of large period fluctuations observed in the time series of the instantaneous data. Furthermore the spectral analysis of band-pass velocity components highlighted other characteristic slow fluctuations. These fluctuations were reported in previous studies (Trevethan et al. 2006,2008a, Trevethan and Chanson, 2009) and were associated with reflection of the tidal forcing between different landmarks and the corresponding lengths were calculated from the application of the wave equation described in Eqn. 5-1. For example, an event identified in the power spectral density of the water level and streamwise velocity with period of 21.5 s corresponded to a reflection between landmarks with length ~45 m around mid-tide. This was possibly linked with transverse wave resonance/ sloshing between the channel banks. Fluctuations with periods less than 1400 s were possibly generated by internal resonance between landmarks such as banks, meanders and the entire estuarine zone (~3.8 km long). The fluctuations with periods greater than 1400 s were likely associated with external resonance superimposed on the tidal forcing.

Figure 5-10 shows the slow fluctuation component of the streamwise velocity highlighting large

amplitude about high tide (between 55,000 and 75,000 s). The fluctuations had amplitude about 0.08 m/s, more than half of the tidal constituent of the streamwise velocity. A fluctuation of similar period was also observed in the measured physiochemical properties of the channel (See discussion provided in section 3). This suggested that mixing and dispersion with the channel was influenced by slow fluctuations, some of which have to be accounted for in the modelling of dispersion and mixing within the channel.

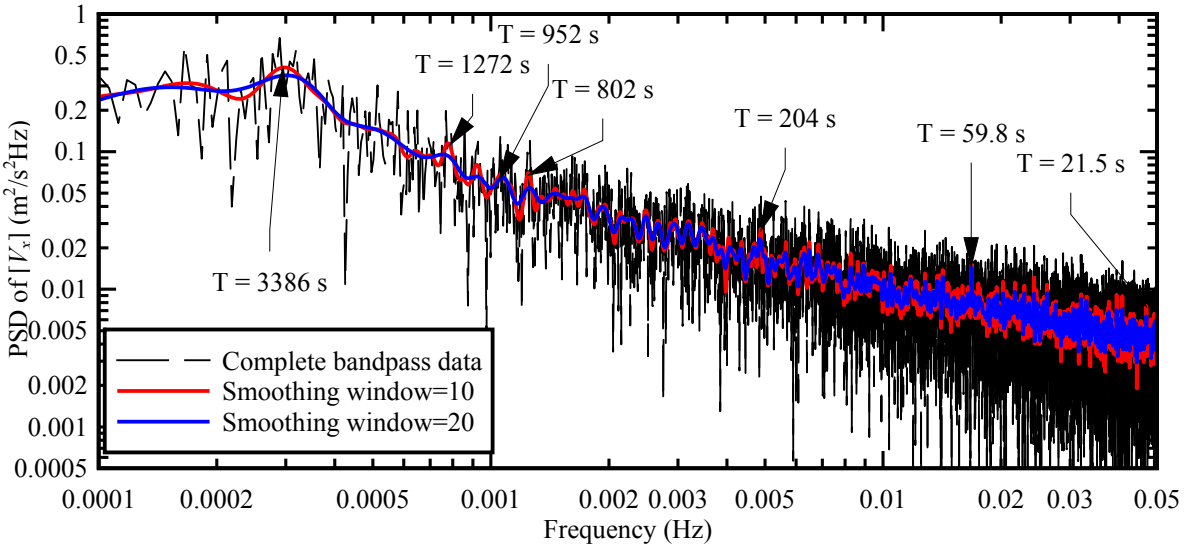

(A) Power spectral density of $[V_x]$ (m^2/s^2Hz)

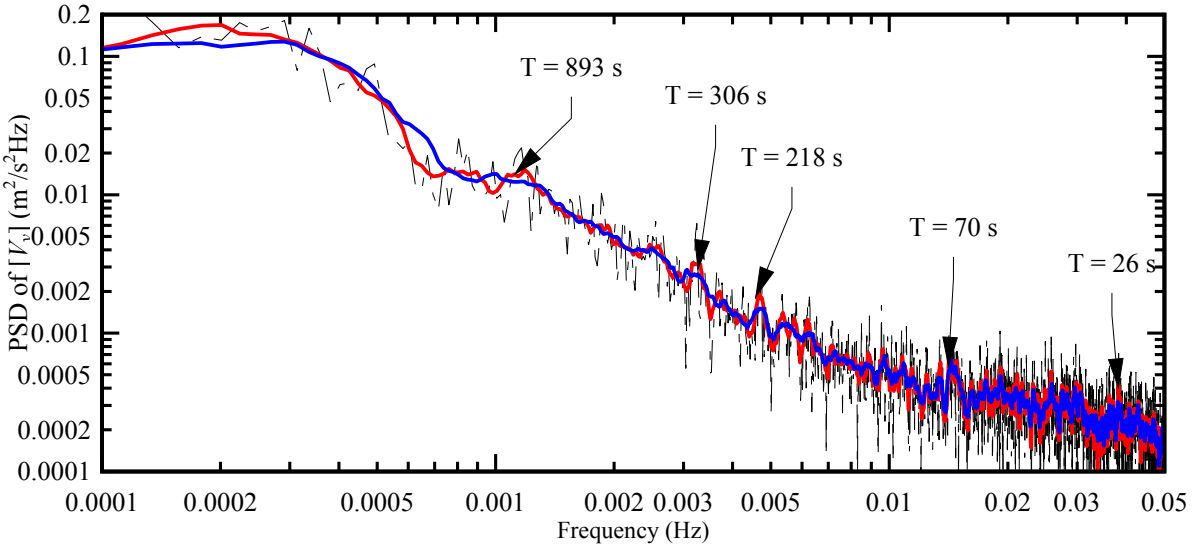

(B) Power spectral density of $[V_y]$ (m^2/s^2Hz)

Fig. 5-9 - Spectral analysis of fluctuations of streamwise velocity $[V_x]$, Water elevation measured using ADV1. Sampling volume location: 0.32 m above the bed, 11.056 m from left bank.

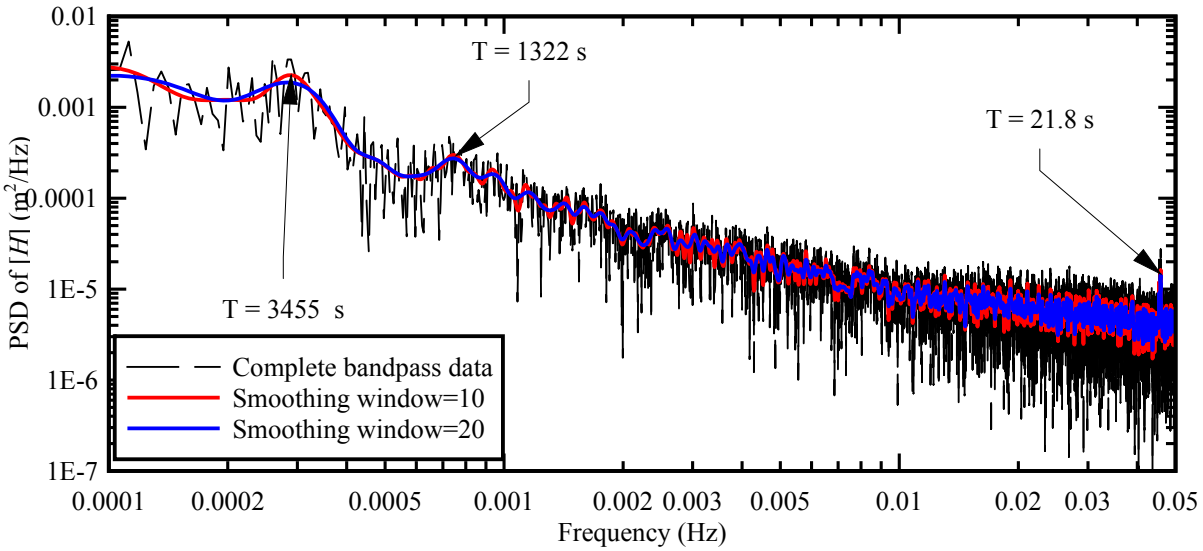

(C) Power spectral density of [Water level] (m^2/Hz)

Fig. 5-9 - Spectral analysis of fluctuations of streamwise velocity [V_x], Water elevation measured using ADV1. Sampling volume location: 0.32 m above the bed, 11.056 m from left bank.

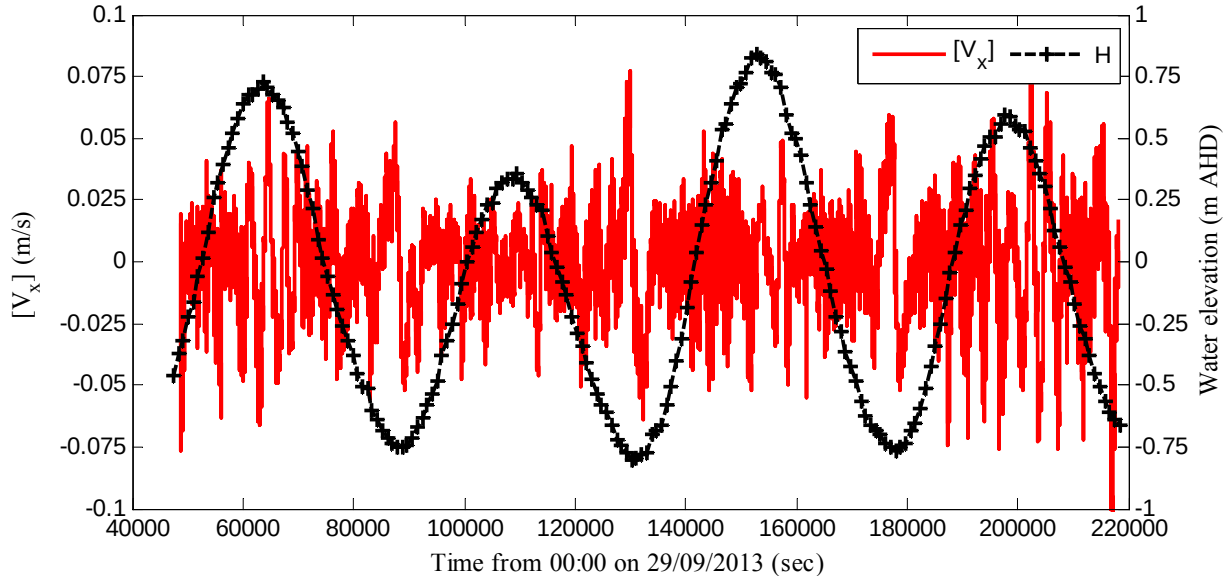

Fig. 5-10 - Slow fluctuation component of the streamwise velocity and water elevation as functions of time; using ADV1. Sampling volume location: 0.32 m above the bed, 11.056 m from left bank.

5.5.2 Standard deviation of slow fluctuations

The standard deviation of velocity is a measure of the magnitude of velocity fluctuations about the mean. The standard deviation and other statistical properties were calculated over a period of 200 s (10,000 data points) every 10 s interval for the entire data sets. Figure 5-11 shows the standard deviation of all components as a function of time, for the streamwise velocity component recorded

0.32 m above the bed. The standard deviations were generally large during the flood tides compared to those during the ebb tides. This was the result of strong tidal forcing coupled with resonance (slow fluctuation). The results showed that, on average, the standard deviation of the slow fluctuation had the same order of magnitude as that of the 'true' turbulence fluctuation. The standard deviations of slow fluctuation were higher during the flood tides than that of the ebb tides.

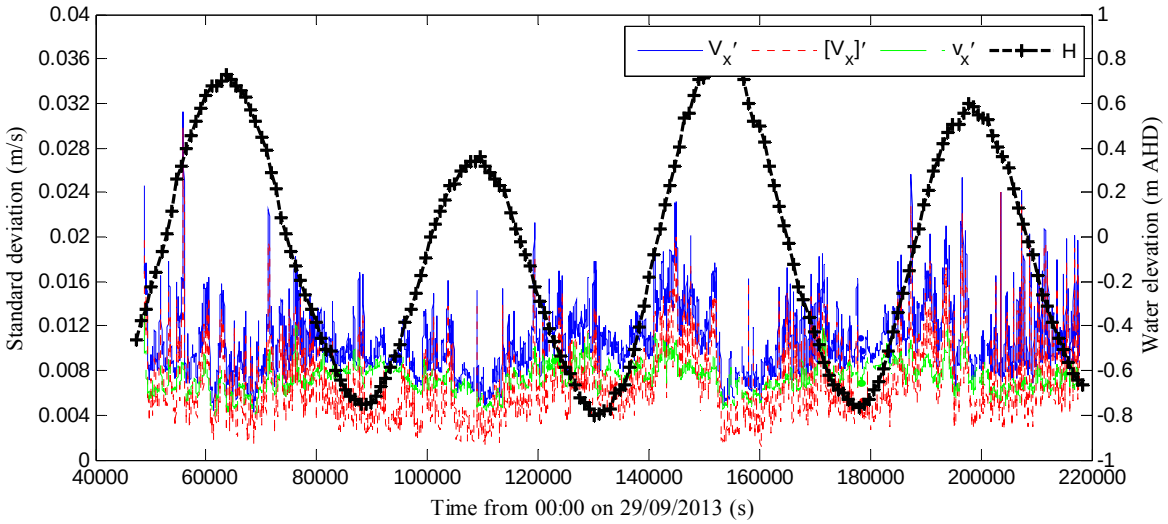

Fig. 5-11 - Standard deviation of the streamwise velocity and water elevation as functions of time; using ADV1; Sampling volume location: 0.32 m above the bed, 11.056 m from left bank; Data based on 10,000 samples (200 s) every 10 s along the entire data set

5.6 TURBULENCE DISSIPATION RATE AND ANISOTROPY

5.6.1 Turbulence power spectra density

The application of TD to the instantaneous data yielded the 'true' turbulence as the high-pass filtered component of the instantaneous flow field. The dissipation rate of turbulent kinetic energy, TKE is described as the proportionality constant of the energy spectrum and the wavenumber (Tennekes and Lumley, 1972). Figure 5-12 shows the power spectral density of the streamwise turbulence velocity of ADV1 placed at 0.32 m above the bed. The power spectral density followed the Kolmogorov model for energy distribution in the range of 0.2 to 2 Hz.

Comments

The instrument noise dominated the turbulence power spectral density at frequencies above 5 Hz. This limits the ADV's ability to resolve flow properties within the viscous and dissipation scales. A similar situation was reported in the evaluation of an ADV unit (Voulgaris and Throwbridge, 1998), although this does not significantly affect the measurement of turbulence intensities (Voulgaris and

Throwbridge, 1998) and thus, does not contaminate the turbulence statistics reported in this report. The energy containing eddies, where most of the variance was found, were at lower frequencies and those above 2 Hz are less than 1% of the energy on Figure 5-12. Detailed statistical analysis of the turbulence data is presented in Section 6.

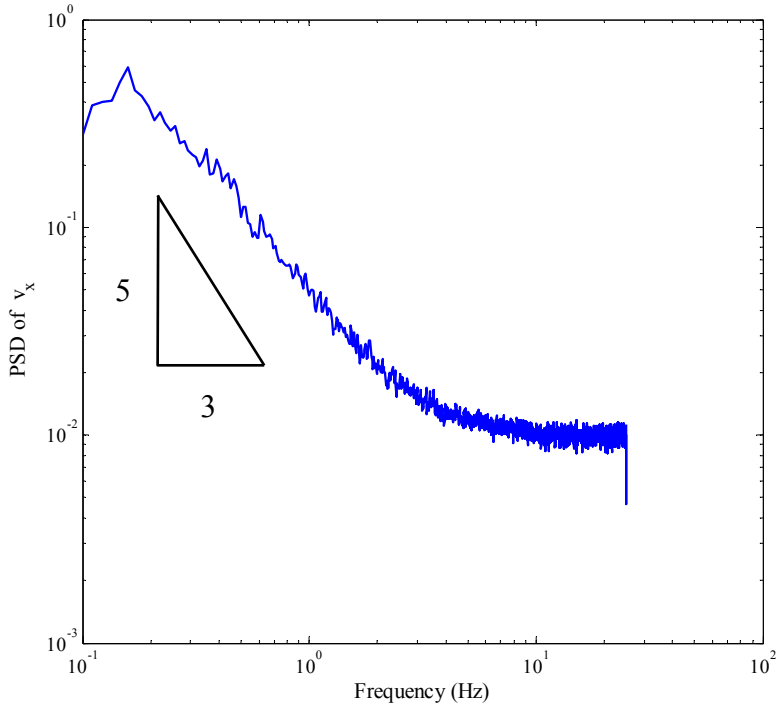

Fig. 5-12 - Turbulence power spectra of streamwise velocity fluctuation (high-pass filtered data); using ADV1 data: sampling volume location: 0.32 m above the bed, 11.056 m from left bank; PSD calculated as non-overlapping average of 100 realisations of 200 s length data.

5.6.2 Turbulence anisotropy

Anisotropy was studied to describe the directional structure of turbulence within the channel and the deviation of the 'true' turbulence from the ideal form of isotropic turbulence. The standard deviations of the transverse velocity v_y' and vertical velocity v_z' were normalised with the streamwise velocity component v_x'. The horizontal turbulence ratio v_y'/v_x' showed some tidal trend, increased with an increase with streamwise velocity and had peaks around slack waters. The horizontal turbulence ratios of the channel were on average higher during the flood tides than the ebb tides. Figure 5-13A shows that the horizontal turbulence ratio increased from the bed. For ADV units sampled at 0.32 m and 0.42 m, the horizontal turbulence ratio v_y'/v_x' mostly ([20]) ranged between 0.4 – 0.9. These values were similar to laboratory observations in straight prismatic rectangular channel $v_y'/v_x' = 0.5 – 0.7$ reported by Nezu and Nakagawa (1993) and smaller than values

[20] Within 90% prediction bound around the average value

previously observed in Eprapah Creek during a spring tide $v'_y/v'_x \sim 1$ (Trevethan et al., 2006b). The horizontal turbulence ratio $v'_y/v'_x = 0.8–1.2$ was mostly observed for the ADV sampled at 0.55 m above the bed. This difference was likely associated with differences in instruments used. As with the horizontal turbulence ratio, the vertical turbulence ratio v_z'/v_x' increased with increasing streamwise velocity. Peak values occurred at mid-water level.

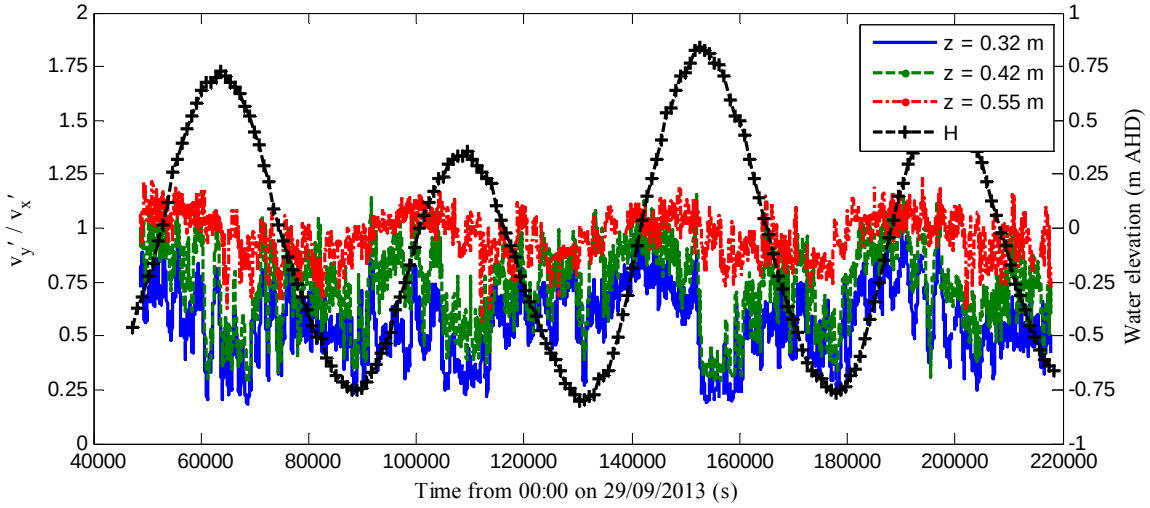

(A) Horizontal turbulence ratio

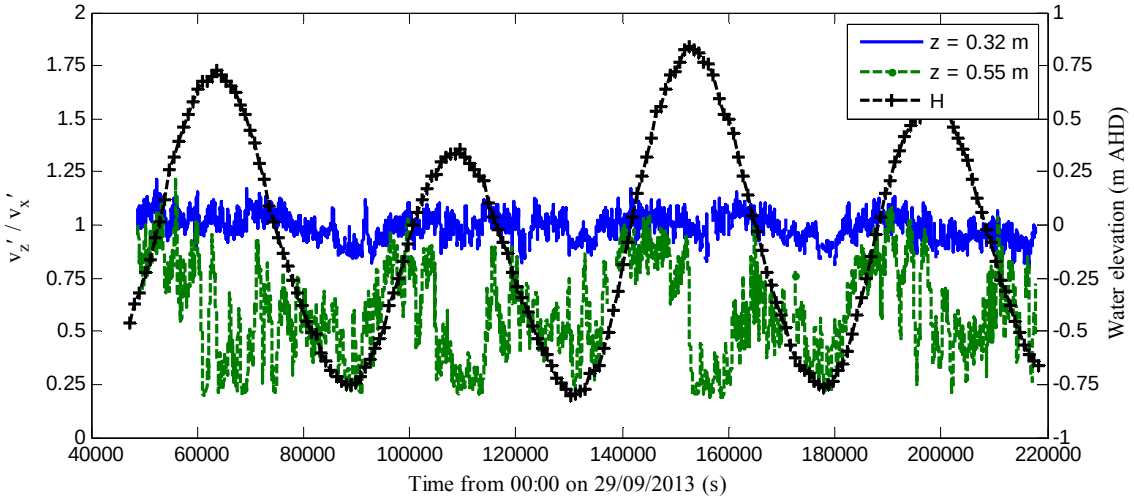

(B) Vertical turbulence ratio

Fig. 5-13 - Time variation of turbulence ratio at different distances from the bed. Standard deviation based on 10,000 samples (200 s) every 10 s along the entire data set.

Unlike the horizontal anisotropy, the vertical anisotropy was weaker close to the bed (Fig. 5-11B). The magnitude of the turbulence ratio v_z'/v_x' at 0.32 m was close to isotropic and double that at 0.55 m above the bed. This suggested that the channel experienced rigorous vertical mixing due to bed friction, particularly at low water during the neap tides. Overall, these results showed the variability

of the anisotropy of the turbulence field within the channel. In particular, the contrary behaviour of the horizontal and vertical anisotropy observed near the bed and reduced anisotropy as the mean velocity increased.

5.6.3 Resonance anisotropy

The directional preference for the slow fluctuation, resonance anisotropy defined as horizontal resonance ratio, $[V_y]'/[V_x]'$ and vertical resonance ratio $[V_z]'/[V_x]'$ was studied. Figure 5-14A shows that the horizontal resonance ratio $[V_y]'/[V_x]'$ had no clear tidal trend and was consistent at the three elevations. For the three ADV units, the horizontal resonance ratio mostly ranged between 0.2 – 1.4 and some occasional higher value was observed. On average, $[V_y]'/[V_x]'$ was slightly less than 1 which suggested that resonance was a little more pronounced in the streamwise direction than the transverse direction. For ADV1 located at 0.32 m above the bed, the vertical resonance ratio $[V_z]'/[V_x]'$ showed no discernible tidal trend and values were predominantly less than 1 (Fig. 5-14B). On the other hand, $[V_z]'/[V_x]'$ showed large values (up to 2) at slack water for the ADV3 located at 0.55 m above the bed. This observation suggested that vertical resonance structure varied across the water depth and the near bed vertical slow fluctuation was lower than that in the streamwise direction.

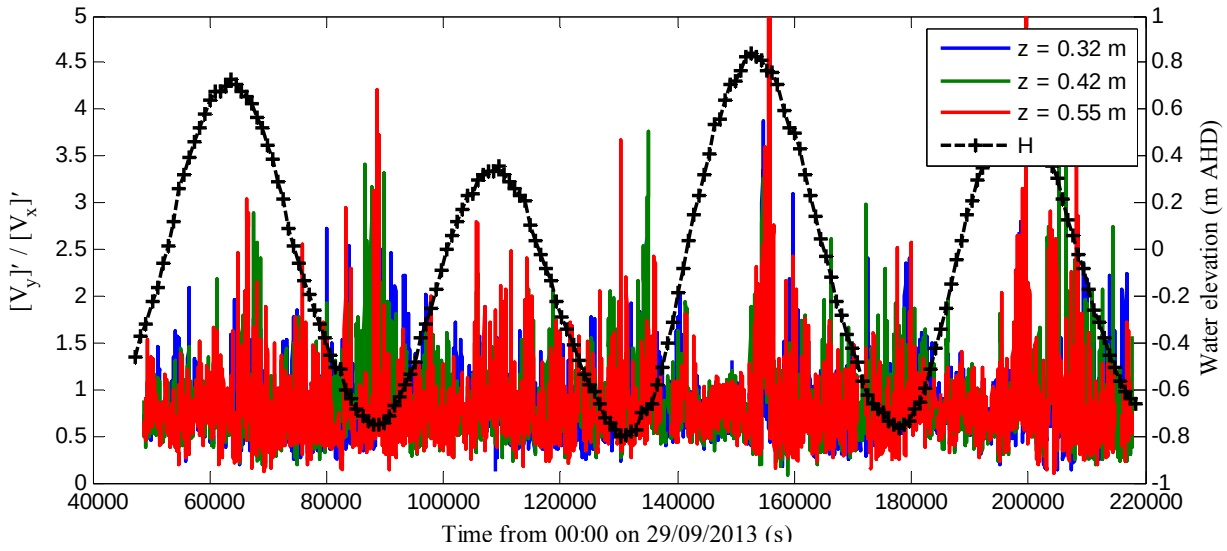

(A) Horizontal resonance ratio

Fig. 5-14 - Time variation of resonance ratio at different distances from the bed; Standard deviation based on 10,000 samples (200 s) every 10 s along the entire data set

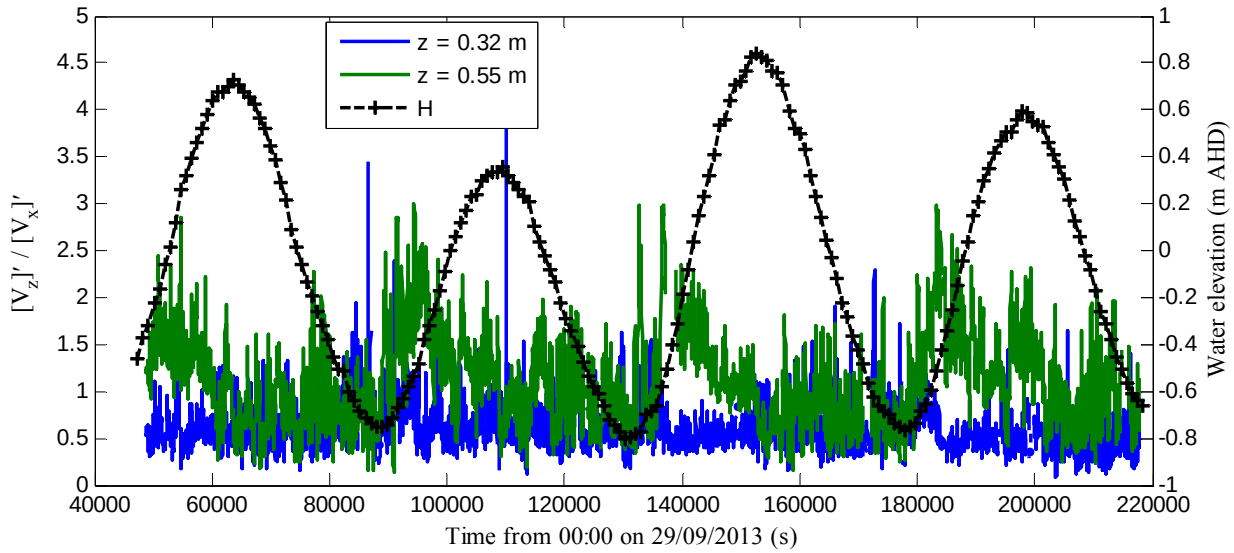

(B) Vertical resonance ratio

Fig. 5-14 - Time variation of resonance ratio at different distances from the bed; Standard deviation based on 10,000 samples (200 s) every 10 s along the entire data set

5.6.3 Summary

Parameters comparing the magnitude of the slow and fast fluctuations with their directional preferences for the data set are summarised in Table 5-4 below. The values reported are based on 90% prediction bound around the average values. The results showed that for the streamwise and transverse directions, on average, both slow and fast fluctuations were equal weighted while the vertical fluctuation at 0.32 m above the bed was predominantly 'true' turbulence related.

Table 5-4 - Slow and fast fluctuations ratio at three distances from the bed; Standard deviations are based on 10,000 samples (200 s) every 10 s along the entire data set; Data range (unshaded rows) is reported as 90% prediction bound around the average value (shaded rows)

ADV	z (m)	$v_x/[V_x]'$	$v_y/[V_y]'$	$v_z/[V_z]'$	$[V_y]'/[V_x]'$	$[V_z]'/[V_x]'$	v'_y/v'_x	v'_z/v'_x
(1)	(2)	(3)	(4)	(5)	(6)	(7)	(8)	(9)
1	0.32	0.5 – 2.5	0.4 – 1.4	1.1 – 3.1	0.3 – 1.4	0.3 – 1.0	0.3 – 0.8	0.9 – 1.1
		1.25	0.88	2.10	0.81	0.60	0.56	0.99
2	0.42	0.3 – 1.6	0.4 – 1.4	-	0.2 – 1.5	-	0.4 – 1.0	
		0.93	0.85		0.84		0.73	
3	0.55	0.3 – 1.8	0.5 – 2.2	0.3 – 1.8	0.1 – 1.5	0.3 – 1.8	0.8 – 1.2	0.2 – 1.0
		0.99	1.26	1.08	0.82	1.08	0.96	0.59

6. TURBULENCE AND REYNOLDS STRESSES

6.1 TURBULENT PARAMETERS

The application of the triple decomposition technique to the turbulent field data separated the turbulence into tidal scale, resonance and 'true' turbulence. The contribution of each component was described in Section 5. The turbulent velocities fluctuated significantly during the field studies with some form of anisotropy in the resonance and 'true' turbulence. The approach and results of the analysis on the 'true' turbulence are presented in this section.

Turbulence analysis was carried out on the high-pass filtered velocity v_x, v_y, and v_z. The analysis included the calculation of standard deviations, skewnesses, kurtoses, correlation coefficients, Reynolds stresses and time scales. All statistical data and time averaged properties were calculated based upon 200 s (10,000 sample points), following Trevethan and Chanson (2009). This period is larger than the time scale of the turbulence velocity fluctuation, smaller than the tidal velocity fluctuation and contains enough data points for statistical stability (Trevethan and Chanson, 2009). Herein, turbulent parameters were not calculated for the 200 s of data when more than 10% corrupted samples were found.

Statistical parameters

The first statistical moment of the turbulence velocities, v_x, v_y, and v_z was approximately zero. i.e. for example, $v_x' \sim 0$. The second moment, standard deviation of a discrete sampled data is:

$$v_x' = \frac{1}{n}\sum_n \sqrt{(v_x - \overline{v_x})^2} = \frac{1}{n}\sum_n \sqrt{(v_x)^2} = 0 \quad (6\text{-}1)$$

where over-bar signifies mean ([21]). The turbulence ratios (horizontal and vertical) were obtained by normalising v_y' and v_z' with the corresponding v_x' values. The skewness is the third statistical moment of the velocity. The skewness magnitude shows the extent to which the turbulence field deviates from a Gaussian distribution ([22]), and it retains sign information about the temporal asymmetry of the distribution (Buffin-Bélanger and Roy, 1998, Fox et al., 2005, Chanson, 2009). The kurtosis is the fourth statistical moment which determines the peakiness or flatness of the probability distribution function, PDF of the turbulence field. Herein, skewness and excess kurtosis are normalised by the standard deviation and are calculated respectively as:

[21] Over-bar signifies ensemble average/mean.

[22] A Gaussian or normal distribution has a skewness of zero.

$$Sk(v_x) = \frac{\frac{1}{n}\sum_n v_x^3}{\left(\frac{1}{n}\sum_n v_x^2\right)^{3/2}} \tag{6-2}$$

$$Ku(v_x) = \frac{\frac{1}{n}\sum_n v_x^4}{\left(\frac{1}{n}\sum_n v_x^2\right)^{2}} - 3 \tag{6-3}$$

Time scales

The characteristic time scales were calculated from the autocorrelation function of the turbulent velocities. The normalised autocorrelation function, R describes the evolution of the turbulence field with time. R describes how a turbulence velocity correlates with values at difference times. For example, R_{xx} is defined as:

$$R_{xx}(\tau) = \frac{\overline{v_x(t)v_x(t+\tau)}}{\overline{v_x^2}} \tag{6-4}$$

where τ is the time lag. Figure 6-1 shows a sample autocorrelation.

The integral time scale is a measure of the correlation time between turbulent velocities. The integral length scale, e.g. T_{Ex} is the integral of the autocorrelation function which is obtained herein by numerical integration performed only up to the time of the first zero crossing using a maximum time lag of 10 s.

The dissipation time scale, also known as Taylor's micro scale is a measure of the most rapid changes that occur in the turbulence velocity. The dissipation time scale, e.g. τ_{Ex} may be estimated from the curvature of the autocorrelation function in the neighbourhood of $\tau = 0$ (Hinze, 1975). For data sampled every time interval δt, $\tau_{Ex}^{(\delta t)}$ may be described based upon sampling interval δt:

$$\tau_{Ex}^{(\delta t)} = \sqrt{2 \times \frac{\overline{v_x^2}}{\overline{\left(\frac{\delta v_x}{\delta t}\right)^2}}} \tag{6-5}$$

The calculation of $\tau_{Ex}^{(\delta t)}$ is repeated for several sampling intervals and may be approximated by a quadratic function (Eqn. 5-7) (Fransson et al., 2005, Chanson, 2009):

$$\tau_{Ex}^{(\delta t)} = \tau_{Ex} + a(\delta t) + b(\delta t^2) \tag{6-6}$$

That is, τ_{Ex} is the limit of $\tau_{Ex}^{(\delta t)}$ when δt tends to zero.

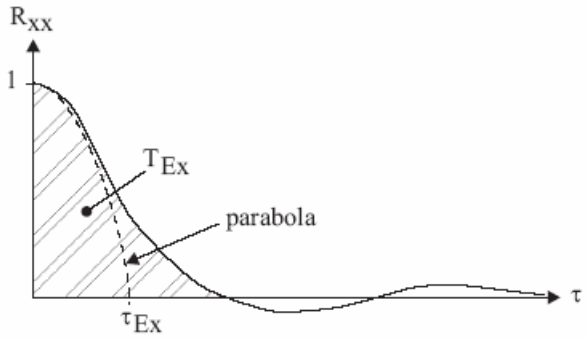

Fig. 6-1 - Sketch of typical autocorrelation function of a fluctuating sample as a function of τ (after Chanson, 2009).

Reynolds stresses and correlation coefficients

The Reynolds stress tensor, ζ_{ij} includes the normal stresses and the tangential stresses. The normal stress is the correlation between turbulent velocity components along the principal plane (i.e. i = j) and describes the kinetic energy of the turbulence field. The tangential stress is the correlation between velocity components in adjacent planes (i.e. i ≠ j). The instantaneous Reynolds stresses were calculated from direct products of the water density and relevant turbulent velocity components at each data point (for example, $\rho v_x v_y$).

The correlation coefficient describes the degree of connections between turbulent velocities. The correlation coefficient is the dimensionless covariance, normalised with the standard deviation of the relevant turbulent velocity component. The correlation coefficient ranges from -1 to 1 with the magnitude indicating strength, its sign reflecting the directional structure. The correlation coefficients were calculated using:

$$R_{ij} = \frac{\overline{v_i' v_j'}}{(v_i' v_j')} \tag{6-8}$$

where the subscript i,j represent the x,y, and z directions. Herein, the correlation coefficients between velocity components from the same ADV and different ADV units were studied ([23]).

6.2 TURBULENCE PROPERTIES

Using a sample size of 10,000 data points (200 s), the time-average of the turbulent velocities (high-pass filtered data) had a maximum magnitude about 0.00015 m/s and were on average zero. The standard deviation showed some variation with tidal phase. The turbulence ratios which are the

[23] Note that the three ADV units were synchronised within 0.02 s.

standard deviations normalised by the standard deviation of the streamwise component were presented in Section 5.6. The overall horizontal and vertical turbulence ratio were typically within the range of $v_y'/v_x' \sim 0.3$ to 1.2 and $v_z'/v_x' \sim 0.2$ to 1.1 implying some turbulence anisotropy.

6.2.1 Statistical properties

The skewness and kurtosis of all turbulent velocity components fluctuated significantly. For a finite number of data points, a Gaussian distribution has an expected skewness, $|\mathrm{Sk}| < 4 \times \sqrt{15/\mathrm{N}}$ and kurtosis, $|\mathrm{Ku}| < 4 \times \sqrt{96/\mathrm{N}}$ (Press et al., 1992, Trevethan et al., 2006b), where N is the sample size (herein, N = 10,000). Figure 6-2 shows time series of the skewness for ADV1 sampled at 0.32 m above the bed. The skewness showed some tidal trend in phase with the tidal velocity variation. For the ADV1, the skewness of v_x ranged from -1.45 to 1.35, while v_y ranged from -4.81 to 1.98 and v_z ranged from -0.56 to 0.67. For the three ADVs sampled, over 65% of the skewness values fell within the limit expected of a Gaussian distribution.

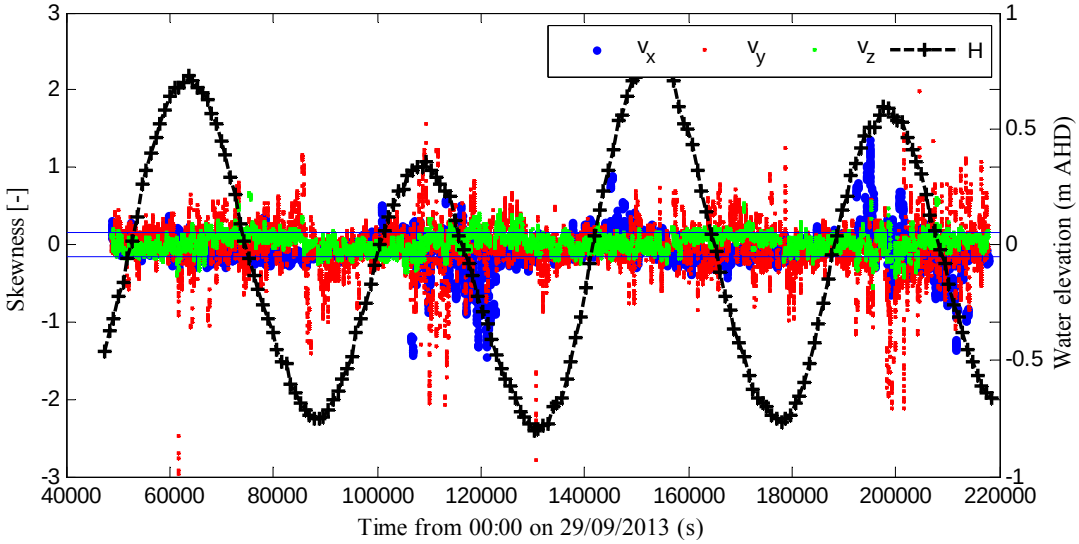

Fig. 6-2 - Skewness and water elevation as a function of time; using ADV1. Sampling volume location: 0.32 m above the bed, 11.06 m from left bank. The two horizontal lines shows the upper and lower limits within which a finite Gaussian distribution is expected.

Figure 6-3 shows the distributions of the skewness of streamwise and vertical velocity with the tidal velocity. The streamwise skewness values were predominantly negative during the ebb tides while the flood tides experienced mixed skewness. On the other hand, the skewness of the vertical turbulent velocity was mainly positive during the ebb. This suggested that the turbulence field close to bed contained eddies generated by ejection type processes during the ebb tides while the flood

tides experienced both ejection and sweep type processes ([24]). However the data suggested that the flood tides generated more eddies associated with high speed sweep against the bed (i.e. $v_x < 0$ & $v_z > 0$) than ejection type process ([25]). The transverse turbulent velocity v_y had the largest values of skewness while v_z skewness values deviated the least from the Gaussian distribution.

Figure 6-4 shows the time variation of the kurtosis for the resulting turbulent field. The kurtoses showed some large deviation from the expected value of a Gaussian distribution. Overall, about 18% of the data had kurtosis within the expected range of a Gaussian distribution while the majority (over 70%) of the kurtosis fell in the range of -0.5 and 2. The high values of kurtosis indicated that 'true' turbulence velocities were peaky and had flat tails compared with a Gaussian distribution. The high values of kurtosis were observed more during the ebb tides than the flood tides with the peaks around high water slack. The transverse turbulent velocity v_y had the largest values of kurtosis while v_z kurtosis values deviated the least from the Gaussian distribution. This was probably caused by secondary flow which generated a larger magnitude of fluctuation in the transverse velocity around zero particularly around slack waters. This could increase the flatness of kurtosis tails, thus, resulting in high kurtosis.

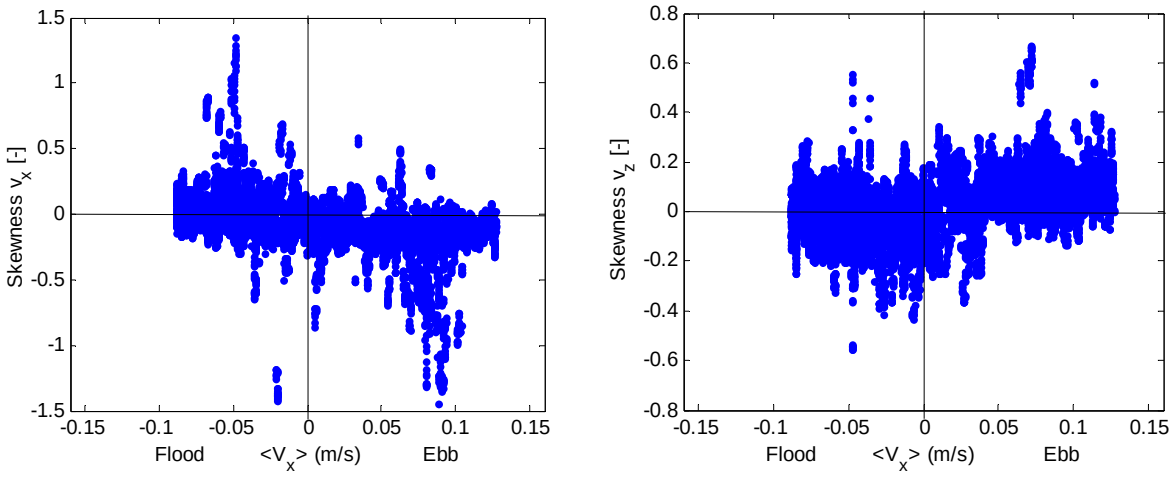

(A) Streamwise velocity skewness (B) Vertical velocity skewness

Fig. 6-3 - Skewness distribution with tidal phase. Sampling volume location: 0.32 m above the bed, 11.06 m from left bank.

[24] A negative skewness in the streamwise velocity is associated with eddies generated from either ejection type processes or from obstruction shedding motion while a positive skewness is associated with high eddies from high speed sweep of the bed (Fox et al., 2005).

[25] $v_x < 0$ & $v_z > 0$ describes an ejection type process while $v_x > 0$ & $v_z < 0$ describes a sweep type process (Nezu and Nakagawa, 1993, Buffin-Bélanger and Roy, 1998)

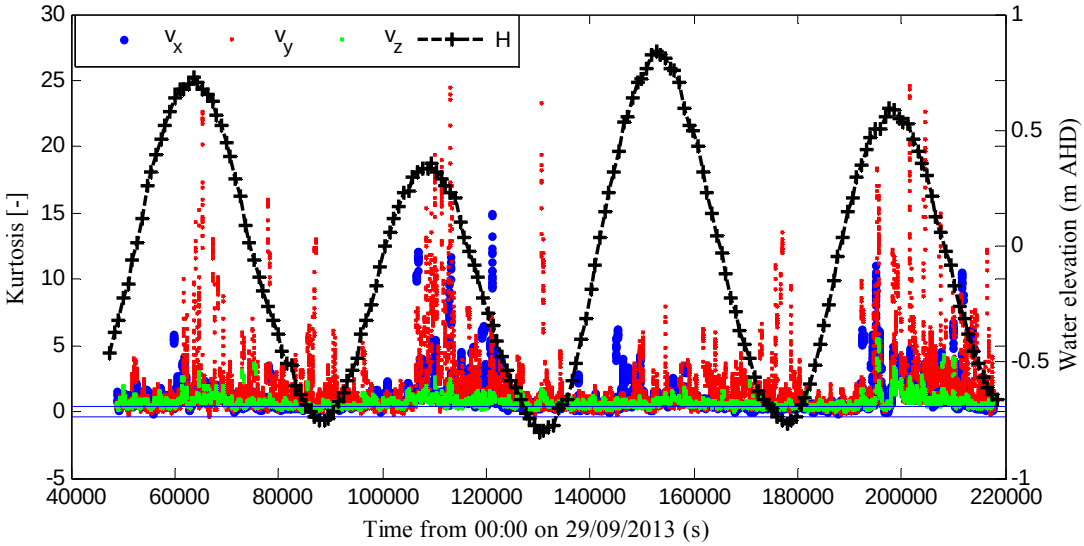

Fig. 6-4 - Kurtosis and water elevation as a function of time; using ADV1. Sampling volume location: 0.32 m above the bed, 11.06 m from left bank. The two horizontal lines show the upper and lower limits within which a finite Gaussian distribution is expected.

Some instance of very high values of kurtosis (up to 30) was observed. Figure 6-5 shows sample portions of the x-component of turbulent velocity time series and the corresponding PDF with a fitted Gaussian distribution. A large deviation from a Gaussian distribution can be seen in Fig. 6-5A. The results showed that the high kurtoses were caused by swift jumps in the turbulent velocity. These events increased the turbulent velocity at a physically plausible acceleration to a large value before decelerating back to the turbulent velocity range with the interval of about 1 s. These events were therefore suspected to be a result of either the motion of marine animals around the sampling volumes of the ADV or intermittency in the turbulence field.

Comments

In a previous study at Eprapah Creek under neap tidal conditions (Study E6) along the same transect (site 2B) (Trevethan et al., 2006b), a comparable distribution of skewness values around a Gaussian distribution were obtained. However, the present maximum and minimum skewness were an order of magnitude higher than those in study E6. Similarly kurtosis values observed herein deviated significantly more from the Gaussian distribution when compared with that of the previous study E6 (Trevethan et al., 2006b). The difference in data processing (e.g. turbulence velocity) possibly contributed to this difference. For example, the slow fluctuations were more isolated into the band-pass data using the triple decomposition method applied in the present study.

The statistical properties of the resulting turbulent field showed some dependence on the distance from the bed. The highest ADV3 sampled at 0.55 m above the bed yielded data that had properties closest to those of a Gaussian distribution.

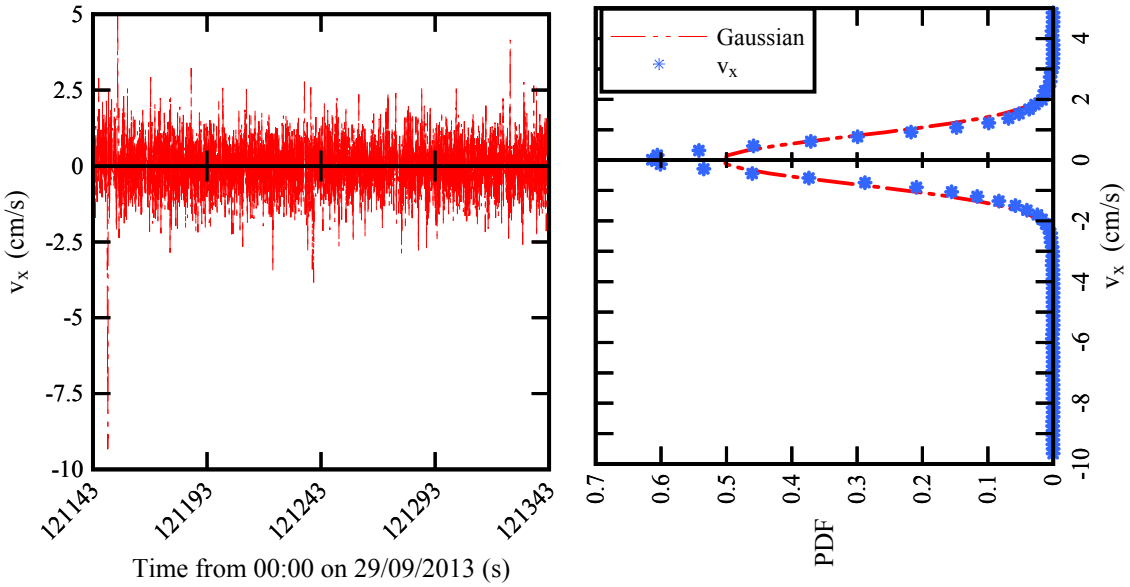

(A) Typical turbulent velocity distribution that resulted in a high kurtosis (Sk= -1.3; Ku = 18)

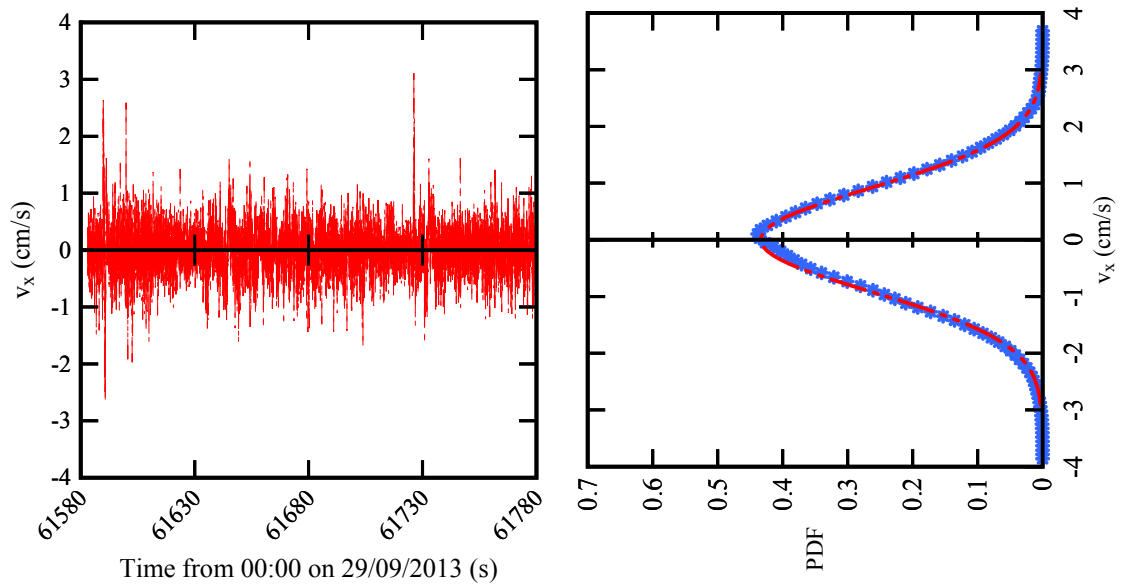

(B) Typical turbulent velocity distribution that resulted in an approximately Gaussian distribution (Sk= -0.07; Ku = -0.072)

Fig. 6-5 - Time series of streamwise velocity variations and resulting PDF with associated skewness and kurtosis.

6.2.2 Time scales

The integral time scale of velocity, T_E is a measure of the longest connection between the turbulent velocity components. The integral time scale varied over the tidal cycle for the x, y and z velocity components. Figure 6-6 shows the T_E for the ADV1 sampled at 0.32 m above the bed. Note the logarithmic scale on the vertical axis in Figure 6-6. All three components of T_E varied with increasing streamwise velocity magnitude. On average, T_E was larger during the flood tide than during the ebb phase of the cycles. For the ADV1 sampled at 0.32 m above the bed, T_{Ey} varied between 0.2 and 0.5 s, T_{Ex} and T_{Ez} both varied between 0.05 and 0.25 s. The plots of integral time scale for other ADV units are presented in Appendix D. The magnitude of T_{Ex} was consistent at the three heights from the bed. However, the magnitude of T_{Ey} and T_{Ez} for the ADV sampled at 0.55 m from the bed differed from the other ADV units (at 0.32 and 0.42 m), on an average by a factor of 2. This disparity might be related to the difference in the instruments.

With the exception of the vertical component of the ADV3 sampled at 0.55 m above the bed, the dimensionless integral time scales were about T_{Ey}/T_{Ex} ~1 to 7 while T_{Ez}/T_{Ex} ~0.8 to 1.6 within the study period. The ADV sampled at 0.55 m above the bed showed T_{Ez}/T_{Ex} up to a factor of 10. The dimensionless integral length scales were consistent with previous studies and also confirmed the anisotropy of the turbulence field (Chanson et al., 2007, Trevethan and Chanson, 2009, Trevethan et al., 2006,2008a).

The dissipation time scale of velocity, τ_E is a measure of the most rapid process in the turbulence field. The dissipation time scales, τ_{Ex}, τ_{Ey}, and τ_{Ez} varied significantly over the tidal cycles without a clear tidal trend. Figure 6-7 shows τ_E for the ADV1 sampled at 0.32 m above the bed (Note the logarithmic scale on the vertical axis.). For the ADV1 unit, τ_{Ex} and τ_{Ez} both varied between 0.00001 and 0.01 s while τ_{Ey} had magnitudes up to 0.1 s. These values are similar in magnitude to previous study in Eprapah Creek reported by Trevethan et al. (2006) where $\tau_E \sim 0.0007 - 0.05$ s during a spring tide and $\tau_E \sim 0.0009 - 0.1$ s during a neap tide. These results suggested that the measured smallest scale processes within the channel were independent of tidal type, phase and large scale flow field. The plots of dissipation time scale for other ADV units are presented in Appendix D. The magnitude of τ_{Ex} was consistent at all three heights from the bed. However the magnitude of τ_{Ey} for the ADV3 located at 0.55 m from the bed differed from the other ADV units (at 0.32 and 0.42 m), on average by an order of magnitude. Similarly, the magnitudes of τ_{Ey} at 0.55 m were on average, an order of magnitude higher than the values at 0.32 m above the bed. This disparity might be related to the difference in the instruments, although the limitations of the instrumentation cannot be ignored.

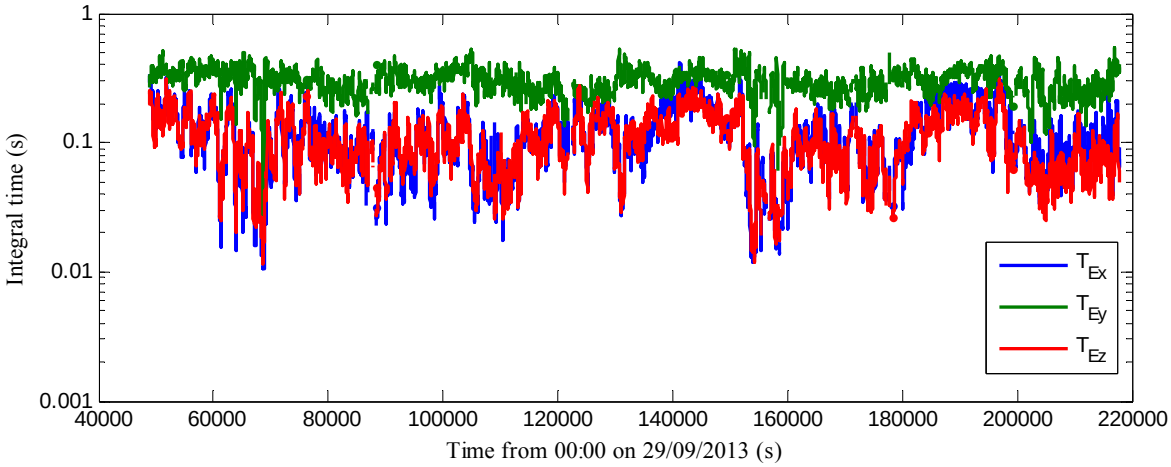

Fig. 6-6 - Time variation of Integral time-scales - using ADV1; sampling volume location: 0.32 m above the bed, 11.06 m from left bank. Calculation based upon 10,000 samples (200 s) taken every 500 samples (10 s) along entire data using the high-pass filtered data.

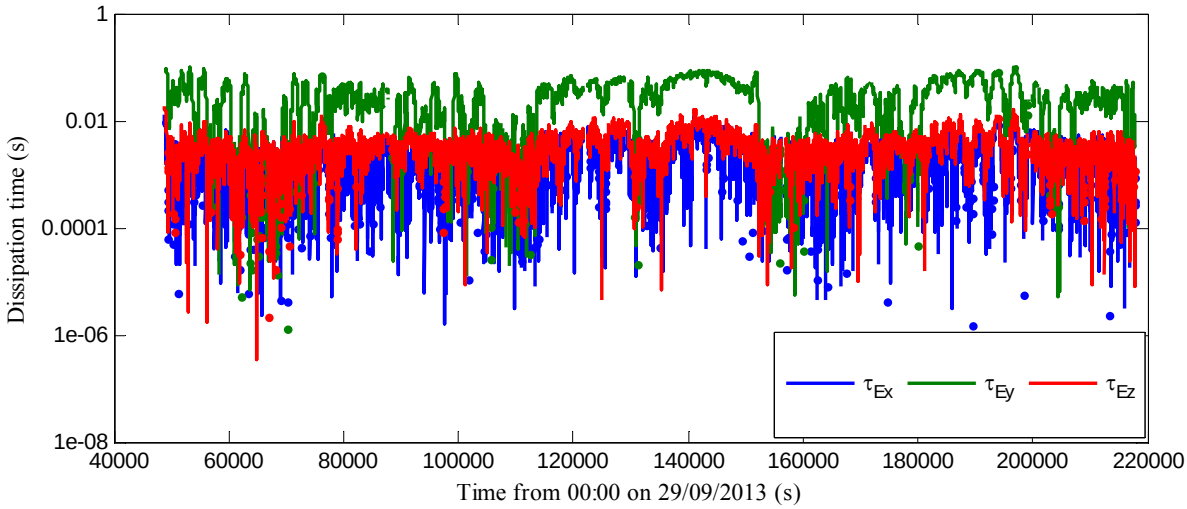

Fig. 6-7 - Time variation of dissipation time-scales - using ADV1; sampling volume location: 0.32 m above the bed, 11.056 m from left bank. Calculation based upon 10,000 samples (200 s) taken every 500 samples (10 s) along entire data using the high-pass filtered data.

Discussion

A comparative study of the time scales was carried out by comparing the data obtained for the present study with that from the previous study E6 (Trevethan et al., 2006b) (Table 1-1) under neap tidal conditions. The study E6 was conducted with the same intrumentation under similar tidal conditions. The data were processed using a double decomposition (DD) technique. Table 6-1 compares the range of values of integral time scales obtained from the present data set using the double decomposition technique and triple decomposition with the previous study E6. For the

double decomposition, an averaging period of 200 s at every 10 s along the data set was used to obtain the turbulent velocities similar to study E6. The integral time scale obtained using double decomposition were on average higher than the values reported by Trevethan et al. (2006) during neap and spring tides by about a factor of two and four, respectively ([26]).

Table 6-1 - Comparison of the integral time scale obtained from turbulence field at Eprapah Creek by application of double decomposition (DD) and triple decomposition (TD) techniques between preset study E14 and previous study E6

Field study	Tidal range (m)	Sampling location from the bed (m)	Instrumentation	Dissipation time scale (s)			Integral time scales (s)		
				τ_{Ex}	τ_{Ey}	τ_{Ez}	T_{Ex}	T_{Ey}	T_{Ez}
(1)	(2)	(3)	(4)	(5)	(6)	(7)	(8)	(9)	(10)
E6 ([+])	1.2	0.4	3D (10 MHz)	0.0007to 0.01	0.0007to 0.01	0.003 to 0.09	0.06 to 1	0.07 to 1	0.6 to 2
		0.2	2D microADV (16 MHz)	0.0009 to 0.02	0.001 to 0.1	--	0.4 to 2	0.7 to 2	--
Present Study ([*])	1.4	0.32	3D microADV (16 MHz)	0.0001 to 0.02	0.001 to 0.18	0.0002 to 0.02	0.19 to 3.71	0.44 to 3.85	0.11 to 2.78
		0.42	2D microADV (16 MHz)	0.0001 to 0.05	0.001 to 0.17	--	0.23 to 3.77	0.38 to 3.87	--
		0.55	3D microADV (16 MHz)	0.0001 to 0.03	0.0001 to 0.03	0.0002 to 0.19	0.22 to 3.73	0.18 to 3.80	0.27 to 3.87
Present Study ([**])	1.4	0.32	3D microADV (16 MHz))	0.0002 to 0.01	0.001 to 0.10	0.0003 to 0.02	0.01 to 0.42	0.03 to 0.54	0.01 to 0.31
		0.42	2D microADV (16 MHz)	0.0002 to 0.02	0.001 to 0.10	--	0.01 to 0.49	0.07 to 0.69	--
		0.55	3D microADV (16 MHz)	0.0001 to 0.01	0.0001 to 0.02	0.0005to 0.12	0.01 to 0.37	0.01 to 0.37	0.05 to 0.66

Notes: ([+]): Field study E6 data set (Trevethan et al, 2006); ([*]): Field study E14 data set processed using double decomposition; ([**]): Field study E14 data set processed using triple decomposition technique; (--): indicates velocity component for which data were not sampled; (DD) : v_x obtained from $v_x = V_x - \overline{V_x}$ with averaging period T = 200 s taken every 10 s along the entire data set; (TD) : v_x obtained as high-pass filtered data of velocity components.

These larger values suggested the presence large scale eddy-like processes such as small scale resonance in the turbulence field which were more prominent during the neap tides than the spring

[26] The difference between integral time scale data obtained during the neap tide E6 and the present study using the same double decomposition settings was not significant in terms of the order of magnitude.

tides. The integral time scales obtained using the triple decomposition technique were lower than the values from study E6 (Trevethan et al., 2006b) by a factor of approximately 8 and an order of magnitude lower than those obtained using the double decomposition technique. The higher integral scales using the double decomposition with period 200 s was indicative of presence of large eddy-like processes (e.g. internal resonance) in the turbulence field. This, at some period hindered the de-correlation of the turbulence velocities after the fixed lag time i.e. $Rij|\tau > 0$.

The dissipation time scale obtained using both techniques with the averaging condition specified were approximately the same values. This confirmed that the dissipation time scale was related to some measurable rapid (i.e. smallest) process within the channel rather than the averaging condition – which defines the integral scales – and therefore depends on the sampling frequency and the sampling volume size of the instruments.

6.2.3 Reynolds stresses and correlation coefficients

The turbulent Reynolds stress tensor varied with times and tides during the field study. A Reynolds stress is basically the net rate of transfer of momentum across a surface in a moving fluid resulting from fluid turbulence. As an illustration, the flux of the x-momentum in the y-direction induces an additional shear stress in the x-direction acting on the surface element normal to the y-direction; this additional stress is called the Reynolds stress or turbulent stress $\rho v_x v_y$ (Chanson, 2009). Figure 6-8 illustrates the variation of the time-averaged normal stress, $\rho\overline{v_x^2}$ as a function of time. $\rho\overline{v_x^2}$ increased with increasing streamwise velocity and peaks occurred around low tides. This suggested a high local turbulent kinetic energy during the low tides. The three normal stresses had average values for the flood and the ebb tides ranging from 0.02 to 0.05 Pa.

The tangential stress, $\rho\overline{v_x v_z}$ exhibited a discernible tidal trend that varied with streamwise velocity. Figure 6-9B shows the time variation of the $\rho\overline{v_x v_z}$ obtained from ADV1 sampled at 0.32 m from the bed. The flood tides exhibited largely positive values of $\rho\overline{v_x v_z}$ while the values during the ebb tides were predominantly negative. The tangential stresses, $\rho\overline{v_x v_y}$ (Fig. 6-9A) and $\rho\overline{v_y v_z}$ (Fig. 6-9C) showed some large magnitude around low tides and during the flood tides but did not show a clear tidal trend. The tangential stresses were an order of magnitude lower than the normal stresses. The tangential stresses were generally larger during the flood tides than the ebb tides. The values of $\rho\overline{v_x v_z}$ for ADV3 sampled at 0.55 m from the bed was on average four times larger than those obtained at 0.32 m ([27]). The average normal and tangential stresses during the field study are summarised in Appendix D.

---

[27] The Reynolds stress tensor data for the three ADV units are presented in Appendix D.

The normalised cross-correlation was obtained between the velocity components of the three ADV units. R_{xz} varied for the ADV sampled at 0.32 m between -0.2 and 0.2 with the peak values corresponding to peak tidal flow. Figure 6-10 shows the variation of R_{xz} with the tidal component of streamwise velocity at 0.55 m and 0.32 m from the bed. R_{xz} showed predominantly positive values during the flood tides and negative values during the ebb tides. The magnitudes of R_{xz} at 0.55 m above the bed were about twice the magnitudes at 0.32 m above the bed. This suggested that R_{xz} decreases towards the bed. Similar correlation distribution toward the bed was also reported for a rough open channel flow (Kironoto and Graf, 1994). The magnitudes of R_{xz} were slightly lower than the values reported previously for study E6 (Trevethan et al., 2006b) at Eprapah Creek based on the double decomposition analysis. For the three ADV units, R_{xy} varied between -0.3 and +0.3 while R_{yz} varied between -0.2 and +0.2 (ADV1 & ADV3) ([28]). R_{xy} showed some tidal trend as it magnitude increased with increasing streamwise velocity, particularly for the ADV2 and ADV3 sampled at 0.42 and 0.55 m above the bed, respectively. However the time series of R_{yz} showed no discernible tidal trend.

The normalised cross-correlation between velocities of different ADV units is presented in Appendix E. The values ranged between -0.1 and 0.1 and were independent of the tidal phase and flow direction.

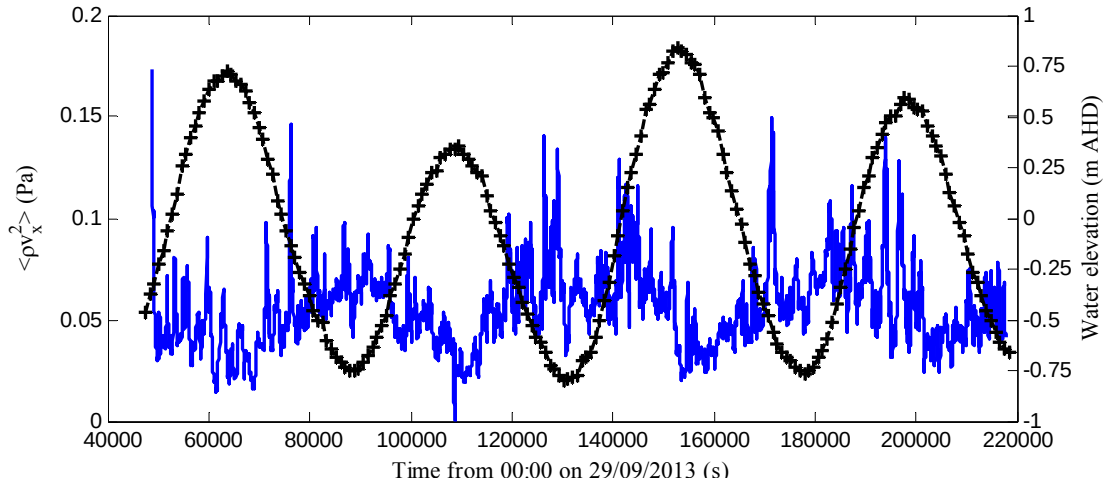

Fig. 6-8 - Time variation of the time-averaged streamwise turbulent normal stress ρv_x^2 - using ADV1; sampling volume location: 0.32 m above the bed, 11.056 m from left bank; – Calculation based upon 10,000 samples (200 s) taken every 500 samples (10 s) along entire data using the high-pass filtered data

[28] See Appendix E

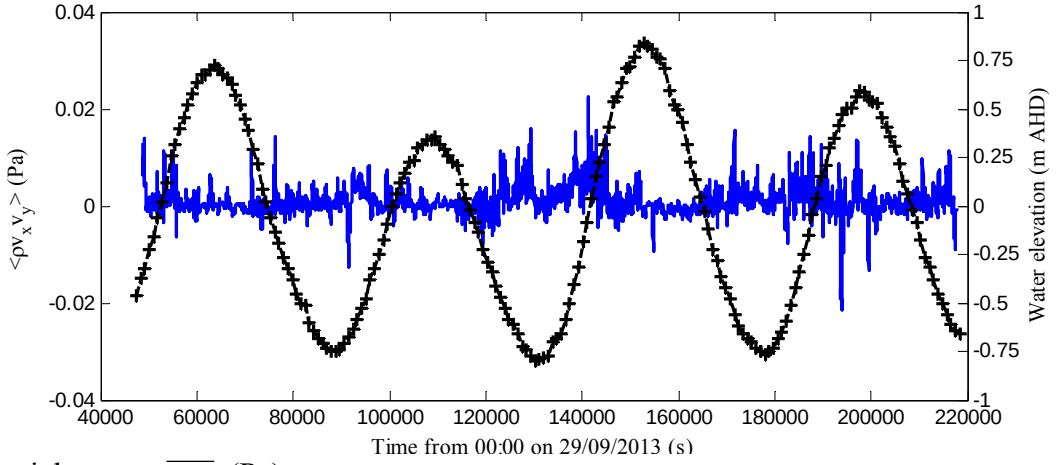

(A) Tangential stress $\overline{\rho v_x v_y}$ (Pa)

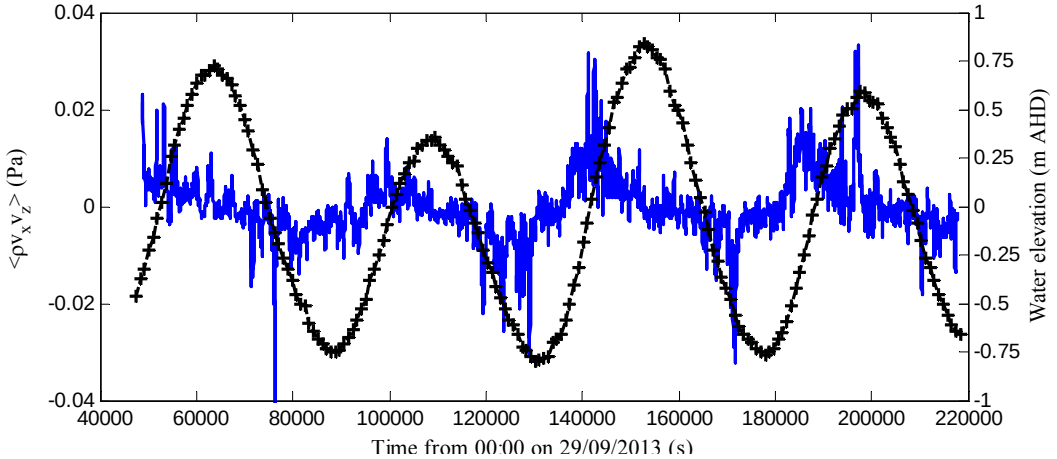

(B) Tangential stress $\overline{\rho v_x v_z}$ (Pa)

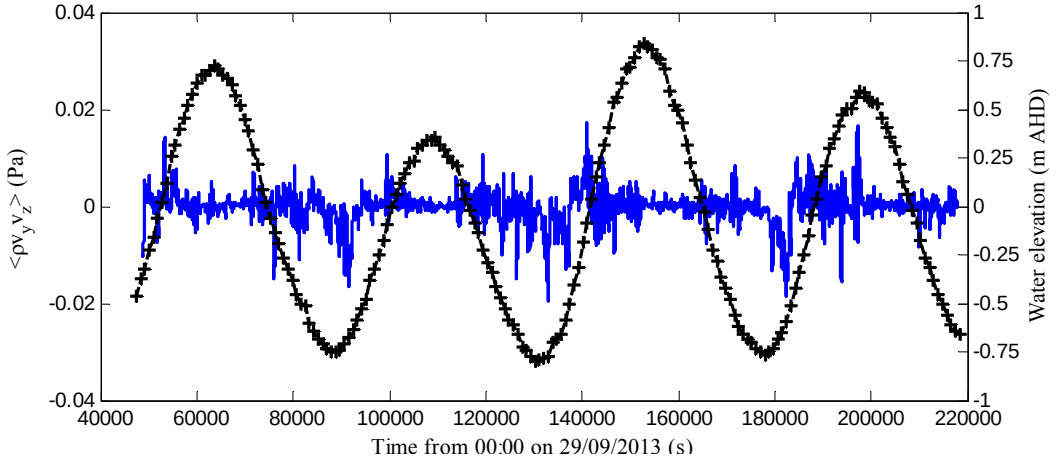

(C) Tangential stress $\overline{\rho v_y v_z}$ (Pa)

Fig. 6-9 - Time variation of the time-averaged streamwise tangential stresses - using ADV1; sampling volume location: 0.32 m above the bed, 11.06 m from left bank. Calculation based upon 10,000 samples (200 s) taken every 500 samples (10 s) along entire data using the high-pass filtered data.

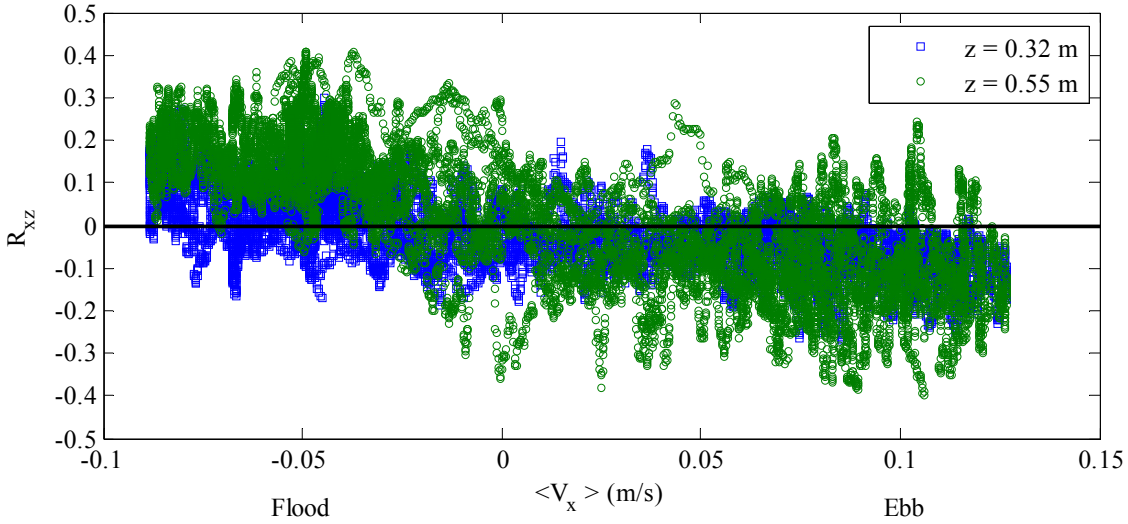

Fig. 6-10 - R_{xz} as a function of tidal streamwise velocity – Calculation based upon 10,000 samples (200 s) taken every 500 samples (10 s) along entire data using the high-pass filtered data

6.3 TURBULENCE COMPARISON BETWEEN MAJOR AND MINOR TIDAL CYCLES

During the field study, two distinct semidiurnal tidal cycles – major and minor cycle – were observed. These two tidal cycles exhibited different periods and amplitudes indicating that some diurnal inequality existed (Fig. 6-11). Herein, some turbulence characteristics were compared as functions of the tidal phase to examine the effects of diurnal inequality on the turbulence properties and the present data were also compared with values reported for studies E5 (under a spring tide) and E6 (under a neap tide). The tidal amplitudes and periods of the two cycles are summarised in Table 6-2.

Field observations showed large variations in turbulence velocity standard deviations through the tidal cycle observed during the field study. The comparisons between the tidal cycles were made in terms of the standard deviations of the turbulent velocities and Reynolds stresses and are presented in polar plots. The magnitudes of the parameter are indicated as a radius from the centre while the angle represents the tidal phase. A flood tide starts (anti-clockwise direction) from the positive x-axis, LT and ends at the high tide HT while the ebb tide begins from HT to the low tide, LT.

Figure 6-12 shows the variation of the standard deviation of velocities (x, y and z) with the tidal phase for the two dissimilar cycles for the ADV sampled at 0.32 m above the bed. The velocity standard deviations (v_x', v_y' and v_z') were of similar magnitudes from the start of the flood tide through the first quadrant. The magnitudes of standard deviations during the mid-flood tide were slightly greater for the major tide than the minor tide. This could be linked with the stronger tidal forcing which induced stronger turbulent sweep against the bed. The ebb phase on the other hand

showed a larger magnitude of velocity standard deviations during the minor tide than the major tides particularly about low tide. The standard deviations were slightly lower than values observed under similar neap tidal condition E6 while those observed under spring tidal condition were larger by up to a factor of 4 (Trevethan et al, 2006).

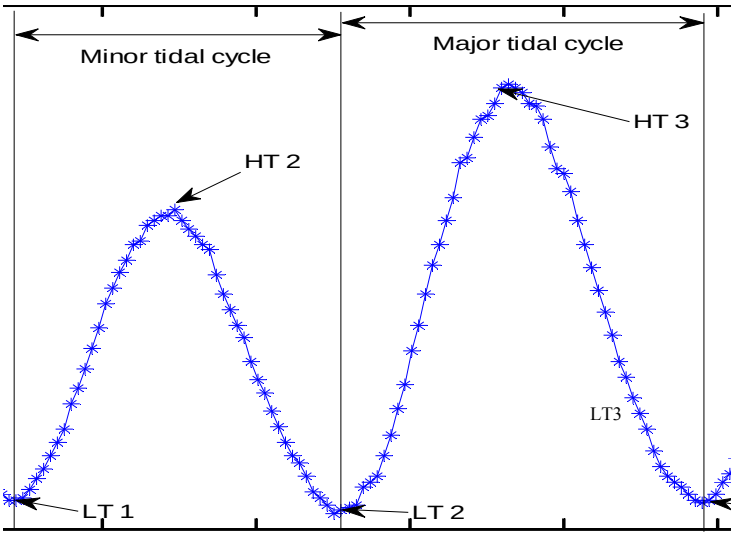

Fig. 6-11 - Time series of water elevation showing two tides with different amplitudes and periods; LT 1 – Low tide 1; HT 2 – High tide 2; LT 2 – Low tide 2; HT 3 – High tide 3; LT 3 – Low tide 3; HT 4 – High tide 4. The periods and amplitudes are provided in Table 6-2.

Table 6-2 Period and average tidal range for two adjacent cycles observed during the field study

Tidal cycle (1)	Time LT – LT (s) (2)	Period (s) (3)			Tidal range (m) (4)
		Flood	Ebb	Total	
Minor	88398 - 130949	20324	22227	42551	0.9
Major	130949 - 177698	22199	24550	46749	1.4

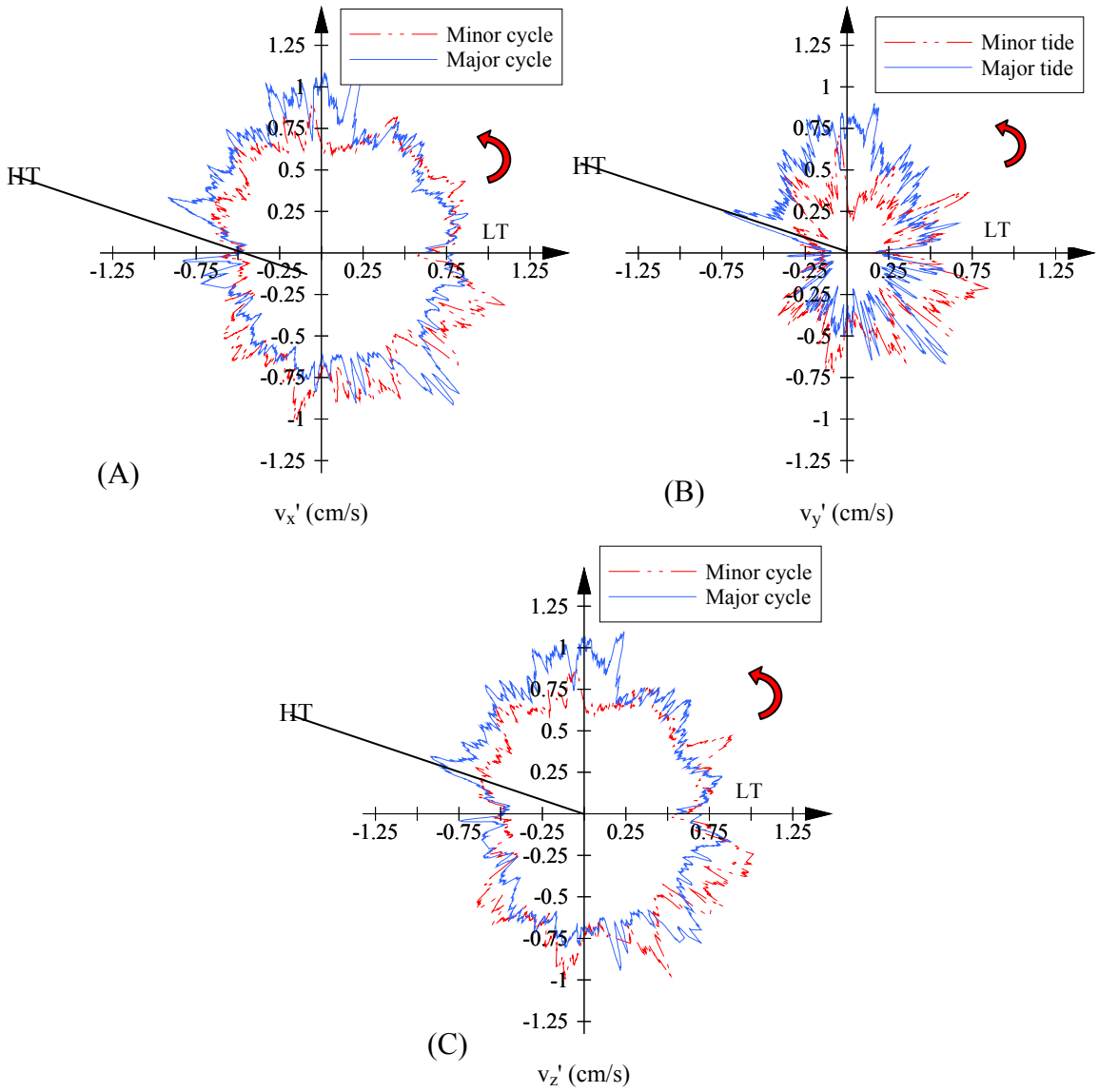

Fig. 6-12 - Standard deviations of turbulent velocities (cm/s) for two dissimilar tidal cycles observed during the field study. (A) Streamwise velocity (B) Transverse Velocity (C) Vertical velocity; using ADV1; sampling volume location: 0.32 m above the bed, 11.056 m from left bank

Figure 6-13 shows the variation in the Reynolds stresses as a function of tidal phase for the dissimilar tidal cycles. The effect observed with the standard deviation was further amplified in the fluctuations of the Reynolds stresses. The magnitudes of Reynolds stresses for the major tide were twice the magnitudes of Reynolds stresses obtained during the minor tides particularly at mid-flood while the reverse was the case for the Reynolds stresses during the ebb phase of the tides. The normal and tangential Reynolds stress values were slightly than those values observed during study E6 and were an order of magnitude lower than those observed during study E5 under a spring tidal condition.

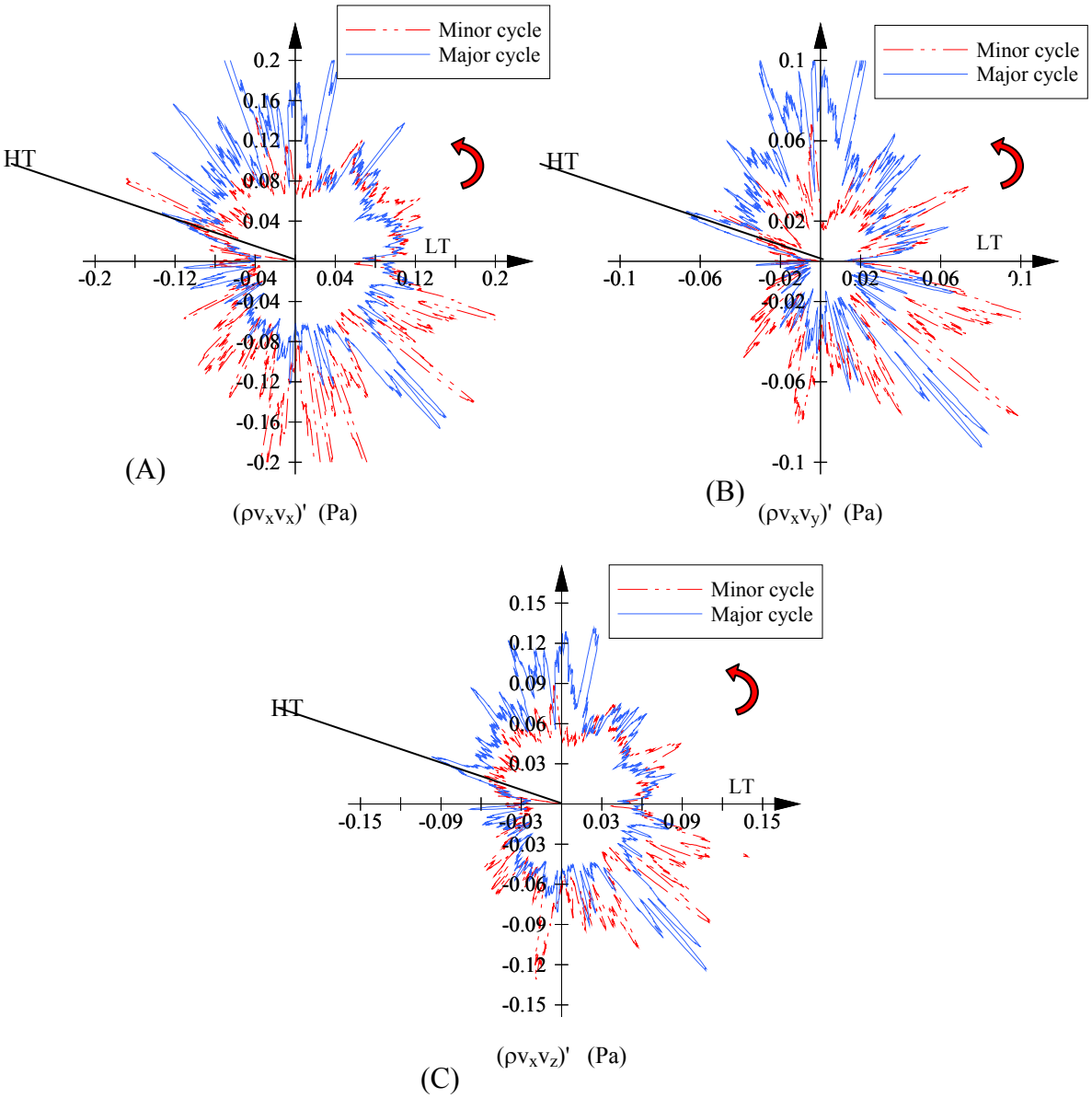

Fig. 6-13 - Standard deviations of Reynolds stresses (Pa) for two dissimilar tidal cycles observed during the field study. (A) Normal stress, $(\rho v_x^2)'$ (B) Tangential stress, $(\rho v_x v_y)'$ (C) Tangential stress, $(\rho v_x v_z)'$; ADV1; sampling volume location: 0.32 m above the bed, 11.056 m from left bank

Discussion

The comparisons of the turbulence properties between the major and minor tides observed during the field study showed quantitative differences. The major tide had higher magnitudes of turbulence velocities and Reynolds stresses than the minor tides during the flood phase while the ebb phase experienced the converse. The slight difference in the values of the standard deviation and Reynold stresses between studies E6 and E14 under similar neap tidal condition was likely a difference in decomposition approach. The large difference in results between E5 and E14 suggests that the neap tides experience less turbulent fluctuations than the spring tides.

7. DISCUSSION AND CONCLUSION

Multi-device measurements of flow fields and physio-chemical properties of a sub-tropical shallow estuary were carried out during a neap tide for a period of 48 hours. During the field study, velocities and water level data were sampled continuously at high frequency (50 Hz) using three ADV units, while ADCP and GPS data were used to obtain mean flow measurement and large scale velocity fluctuations. The study was carried out during a period with no rainfall for the seven preceding days and the freshwater discharge was insignificant. The physiochemical properties fluctuated with the tidal period. The physio-chemical data suggested that the channel was reasonably mixed in terms of temperature, DO, turbidity, and chlorophyll while it was partly stratified in term of pH. The average specific conductivity observed in the channel was in the same range with averaged water conductivity of 49 mS/cm obtained on 2 September 2004, over a full tidal cycle during a drought period (Trevethan et al., 2007b). An unusual aspect of the field observation was the larger streamwise velocity maxima during the ebb tides than the flood tides. This observation was contrary to previous observation within the channel. Visual observations showed the passage of some transient front around high tide slack in the absence of wind effect on the sub-surface layer (See figures in Appendix B).

Multi-device mean flow evaluation

The comparison between the ADCP and the ADV data showed that both devices observed similar time variations in the mean flow field. This sugggested that proper quality-controlled ADCP data could be used to observe large scale variation of flow parameters withina tidal channel. The large sampling volumes of the ADCP would however impair an observation of fine scale flow parameters. The results of GPS-tracked drifter experiments showed that the drifters sampled the sub-surface velocity well and suggested some spatial variation in the transverse velocity distributions within the channel. Unavoidable wind drag on the unsubmerged area of the drifter could modify the velocity measurements. Various forcing factors which include tides and resonances, rough bathymetry, varying transverse shear, and wind played roles in the vertical distribution of velocity within the channel. A unique profile describing the vertical distribution of velocity within the channel could not be identified.

Instantaneous flow field and triple decomposition

The water velocities and water level were highly fluctuating. The fluctuations contained the superimposition of periodic signals with true turbulence and were categorised into tidal, resonance and turbulence fluctuations. A triple decomposition technique was introduced to separate the flow field into the constituents using some characteristic frequencies obtained from a detailed sensitivity

analysis. A vital benefit of the technique is to allow a characterisation of broader temporal scales of fluctuations of high frequency data sampled within a few tidal cycles. For example, the tidal scale fluctuation of velocity and water level was used to obtain the time-lag between the water level and tidal flow within the channel. The result showed that the channel exhibited a mixed type wave with a typical phase-lag between $0.035\pi - 0.116\pi$.

The analysis of events leading to the resonance (slow fluctuation) suggested that resonance could be linked with reflections between landmarks which are both internal and external to the channel. The smallest resonance events observed from the power spectral density of the velocity had a period of ~20 s which corresponds to the wave length of water oscillation between the channel banks. The standard deviations of the slow fluctuation were particularly high at high tides and were observed in form of flow reversals around tide slacks. The amplitude and period of the resonance were significantly high – amplitudes up to 50% of the tidal amplitude and periods > 3,000 s around slack water. The flow reversals were consistent with previous observations at Eprapah Creek. These periodic fluctuations also coincided with the fluctuations of some physio-chemical properties. These large fluctuations are therefore needed to be taken into account in transport modelling of similar shallow water estuarine systems.

Estuarine turbulence characteristics

Upon decomposition of the instantaneous flow field, the statistical analysis of the ensuing 'true' turbulence field was carried out. The mean velocities $\overline{v}_x$, $\overline{v}_y$ and $\overline{v}_z$ for all measured points was practically zero. The standard deviations of velocity components were largest around low tides and showed some clear tidal trend, all being large during the early flood tides. For all ADV units, the horizontal turbulence ratio v'_y/v'_x ranged between 0.5 – 0.9 and decreased towards the bed. The vertical turbulence ratio v'_z/v'_x was on average 1 at z = 0.32 m while v'_z/v'_x was approximately 0.5 for the upper ADV (z = 0.55 m). These results implied some anisotropy of the turbulence field. The results were consistent with previous reported values at Eprapah Creek and were in the range reported in laboratory studies of turbulence. The skewness and kurtosis values for all velocity components varied with streamwise velocity through the observation period. The skewness appeared within the range of -4 and +2. Over 65% of skewness values fell within the range expected of a finite Gaussian distribution. A quadrant analysis of the skewness distribution of the streamwise and vertical turbulent velocity with tidal phase was carried out. The results suggested that the ebb phase turbulence field was predominated by eddies that evolved from ejection type process while that of the flood phase contained mixed eddies with significant amount related to sweep type process. The bulk of the excess kurtosis values (over 70%) fell within the range of -0.5 and +2, slightly deviated from range expected of a normal distribution. Some event of very large

kurtosis (magnitude up to 18) was observed and was possibly linked with intermittency of the turbulence field and marine activities around the ADV probes.

The integral time scales $T_{Ex,}$ T_{Ey} and T_{Ez} ranged between 0.05 and 0.5 s for all the sampled points. The anisotropy of the ensued turbulence field was also confirmed by the integral time scale ratios $T_{Ey}/T_{Ex} \sim 1 - 7$ and $T_{Ez}/T_{Ex} \sim 0.8 - 1.6$ throughout the study period. The integral length scales obtained with the new triple decomposition technique were lower than those obtained with the double decomposition settings used in the past studies while both techniques resulted in integral time scale lower than previously reported in Eprapah Creek. The dissipation time scales which describe the evolution time of the smallest processes in the turbulence field were between 0.0001 and 0.1 s and were independent of tidal phase. These values and observation were consistent with previous observation in Eprapah Creek during the spring and neap tidal condition. The findings showed that dissipation time scale was independent of the tidal cycles and other large scale processes.

The three turbulent normal stresses had time averaged values for the floods and the ebbs ranging from 0.02 to 0.05 Pa while the time-averaged tangential Reynold stresses ranged between -0.02 and 0.02 Pa for all measured points. The normalised cross correlation R_{xz} showed strong relationship with the tidal velocity. The correlation coefficient R_{xz} diminished toward the bed similar to that of laboratory observation reported for turbulence in open channel flow (Kironoto and Graf, 1994).

The instantaneous and tidal flow velocity maxima were higher during the ebb phases than during the flood phases of the tidal cycles. This observation of larger ebb maxima was different from previous observations at Eprapah Creek where larger flood maxima were recorded. In addition, the ebb periods were slightly longer than the flood periods. These observations suggested that the channel was likely ebb-dominated during the study period. Turbulence properties of two semidiurnal tidal cycles with different amplitudes and period were compared. The velocity standard deviations and Reynolds stresses for the flood phase were larger during the flood of the major tide than during those of the minor tides. On the other hand, the velocity standard deviations and Reynolds stresses for the ebb phase were larger for the minor tide than those of the minor tide. The comparative study showed that tidal asymmetry affected the turbulence properties.

Altogether the analysis of the 'true' turbulence field showed some anisotropy and statistical characteristics similar to classical boundary layer results and differed slightly from previous observations in Eprapah Creek, then analysed using a double decomposition technique. The triple decomposition technique described herein allowed the characterisation of broader temporal scale of fluctuations of high frequency data sampled within the durations of few tidal cycles. The study provides the characterisation of ranges of fluctuation required for accurate modelling of shallow water dispersion and mixing in a sub-tropical estuary.

Future research

The present results demonstrated the successful application of the triple decomposition technique to estuarine turbulent data set, to separate the respective contribution of the slow fluctuation and high frequency turbulence. The method should be tested under different tidal and freshwater conditions to test its robustness e.g., during spring tides, during and after a rainstorm. Measurements of suspended sediment concentration data could be further conducted to test differences between flood and ebb tides, reported by Chanson et al. (2007). It is also recommended to conduct detailed investigations other natural systems.

8. ACKNOWLEDGMENTS

The authors thank Professor Satoru Komori (Kyoto University, Japan), Dr Wenxian Lin (James Cook University, Australia) and Dr Adrian McCallum (University of the Sunshine Coast, Australia) for their review and comments that enhanced the report.

The authors acknowledge the support from Dr Michael Holmes and Dr Ian Ramsay and their DSITI (formerly DSITIA) colleagues in providing vertical physiochemical data and, Dr Adrian McCallum in providing additional bathymetric data. They acknowledge the supports received from Dr Badin Gibbes (The University of Queensland), Dr Alistair Grinham (The University of Queensland), Dr Helen Fairweather (University of the Sunshine Coast), Dr Charles Wang (Queensland University of Technology), Dave McIntosh (Queensland University of Technology), Dr Hang Wang (The University of Queensland) in planning, implementing and providing logistics for the field study.

The authors wish to thank all people who participated in the field study, those who assisted with the preparation and data analysis, as well as the Queensland Department of Natural Resources and Mines, Australia for providing access to SunPOZ network for reference station data used for RTK post processing of the high resolution GPS-tracked drifters.

APPENDIX A – LIST OF FIELD PARTICIPANTS

Richard BROWN, Project leader and Supervisor, Queensland University of Technology
Charles WANG, Research fellow, Queensland University of Technology
Dave McINTOSH, Technical Officer, Queensland University of Technology
Tim BODISCO, Research fellow, Queensland University of Technology (Past)
Kabir SUARA, Ph.D candidate, Queensland University of Technology
Lien WILCOX, Technical Officer, Queensland University of Technology
Alex WIMSETT, Project student (graduated), Queensland University of Technology
James KELLY, Project student (graduated), Queensland University of Technology
Matthew RENNIE, Undergrad student, Queensland University of Technology
Callum TYLER, Undergrad student, Queensland University of Technology
Sean McGILL, Project student (graduated), University of the Sunshine Coast

Hubert CHANSON, Project leader and Supervisor, The University of Queensland
Badin GIBBES, Project associate, The University of Queensland
Alistair GRINHAM, Project associate, The University of Queensland
Hang WANG, Research fellow, The University of Queensland
Stewart MATTHEWS, Technical Officer, The University of Queensland
Jason VAN DER GEVEL, Technical Officer, The University of Queensland
Shane WALKER, Technical Officer, The University of Queensland
Simon ALBERT, The University of Queensland

James FELS, QLD DSITIA

Assistance

Helen FAIRWEATHER, Project leader and Supervisor, University of the Sunshine Coast (Pre-field preparation, pre-test of ADV unit and supply of logistics)
Michael HOLMES, Science Leader | Aquatic Ecosystem Health, DSITIA
Ian RAMSAY, Science Leader | Water Assessment & Systems, DSITIA
Fraser REID, Technical Officer, The University of Queensland (Pre-field trip and logistic preparation)

(A) Preparation of the ADV sampling location flood tide (13:02 on 29/09/2013) (Photograph by H. CHANSON) – From left to right: Badin GIBBES, Hubert, CHANSON, Stewart MATTHEWS, Alistair GRINHAM & Richard BROWN; Surveying the channel were David McINTOSH & James KELLY

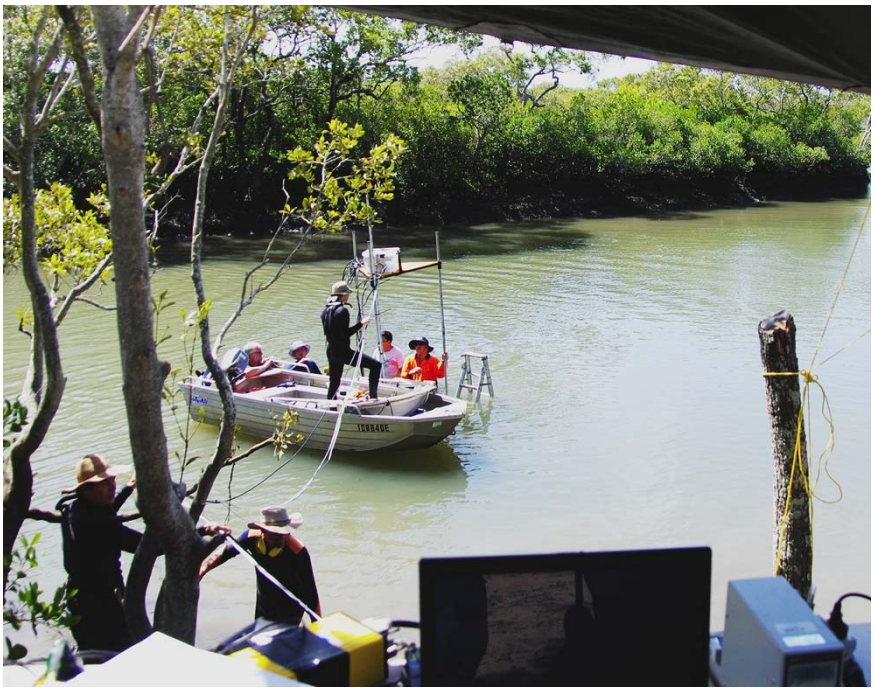

(B) Deployment of the ADV units flood tide (13:26 on 29/09/2013) (Photograph by H. CHANSON) – the same team as identified in (A) joined by Hang WANG in a white T-shirt

(C) Barbecue and kitchen section – left to right: Alex WIMSETT, Richard BROWN, Kabir SUARA, David McINTOSH, Hang WANG, James KELLY, Callum TYLER.

(D) Deployment of UAV – left to right: Charles WANG, Mathew RENNIE and Alex WIMSETT

Fig. A-1 – Photographs of some field participants

APPENDIX B – PHOTOGRAPHS OF FIELD STUDY

(A) Sontek® microADV 16 MHz probes

(B) ADV data acquisition units

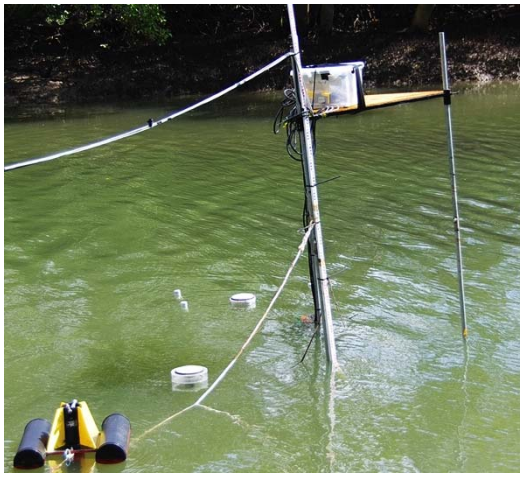

(C) Sub-surface YSI66100 probe & GPS drifters

(D) Teledyne RDI 1200 kHz (ADCP)

(E) Vintage Pro Weather Station

Fig. B-1 - Photographs of devices deployed during the field trip.

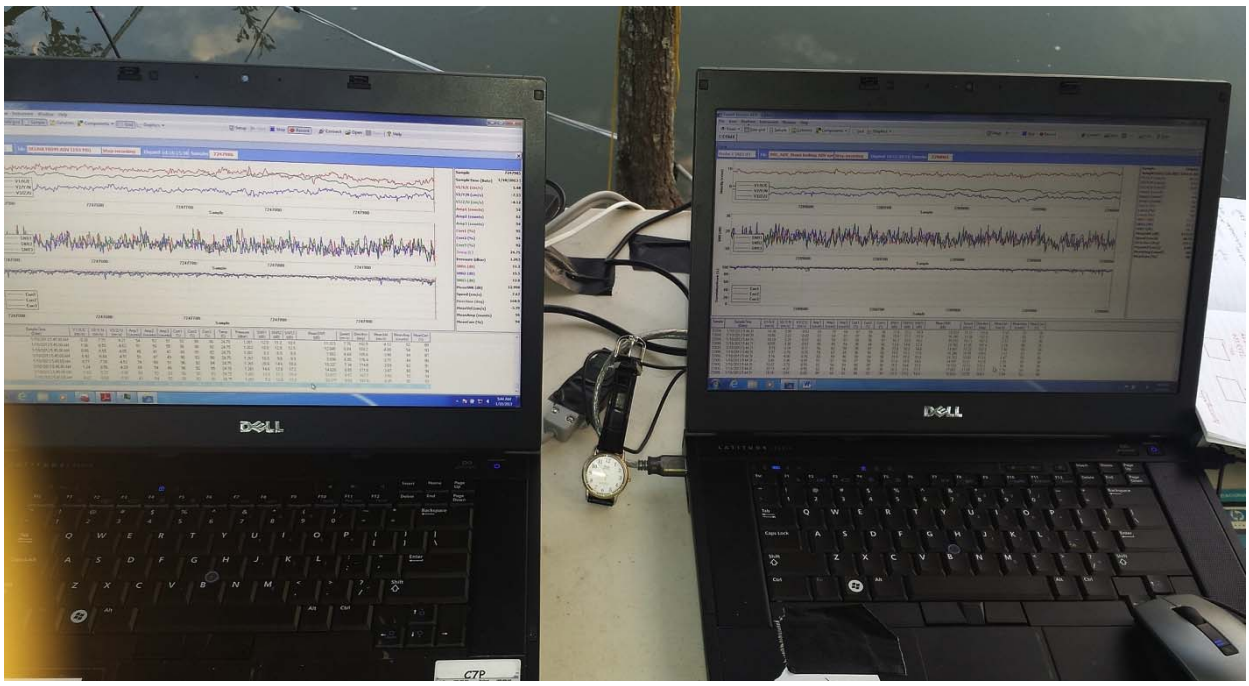

(A) Synchronisation shot between ADV 1, ADV 3 and wrist watch toward the end of the field study

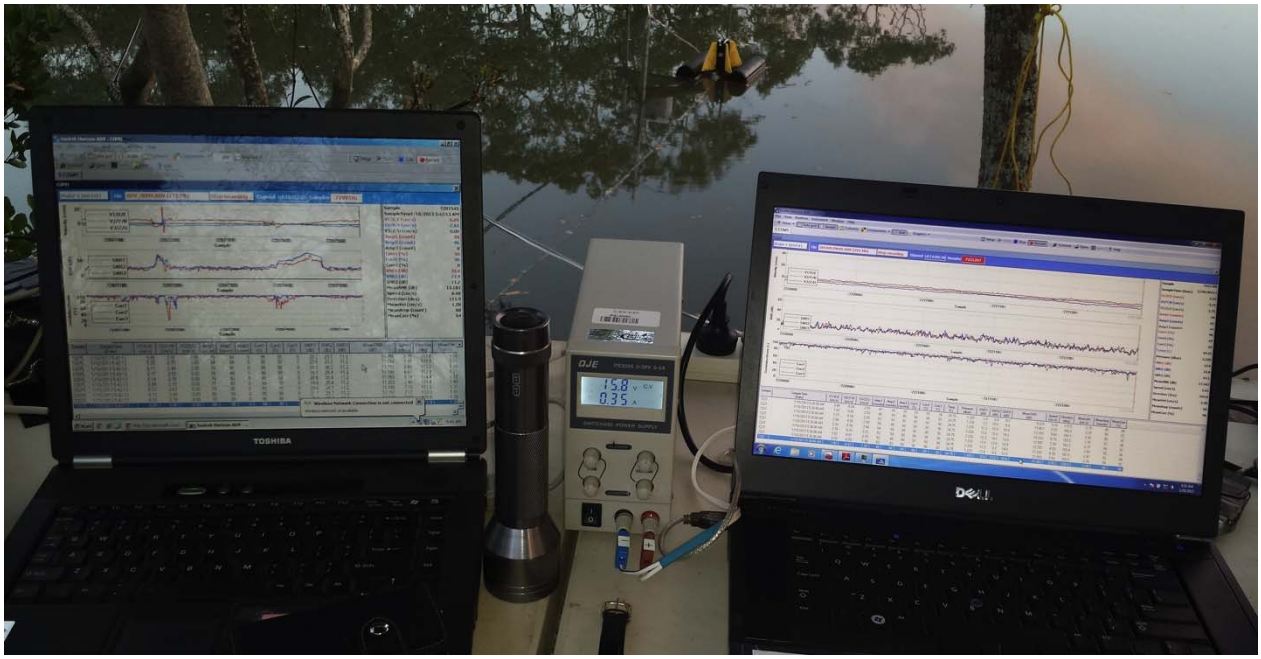

(B) Synchronisation shot between ADV 1, ADV 2 toward the end of the field study

Fig. B-2 - Sample photographs used to estimate the drift of the ADV computer relative to one another and to synchronise the ADV data down to nearest 0.02 s.

(A) Sampling site 2B view from downstream (picture from left bank) during a flood tide at about 13:47 on 29/09/2013. Note the ADV mount at the middle of the channel with YSI6600 mount moored closed to the pole.

(B) View of downstream of site 2B (from a boat) showing stretch of Mangrove muds at the bank during an ebb tide at 10:37 am on 30/09/2013.

Fig. B-3 - Photographs of the sampling site.

Fig. B-4 - Setup of the continuous monitoring station with a computer to an individual ADV probe. From left to right: ADV2, ADV1 and ADV3.

(A) Deployment of high resolution (large capsules) and low resolution (small capsules) GPS-tracked drifters from a boat upstream the ADV sampling location during an ebb tide at 9:39 am on 30/09/2013

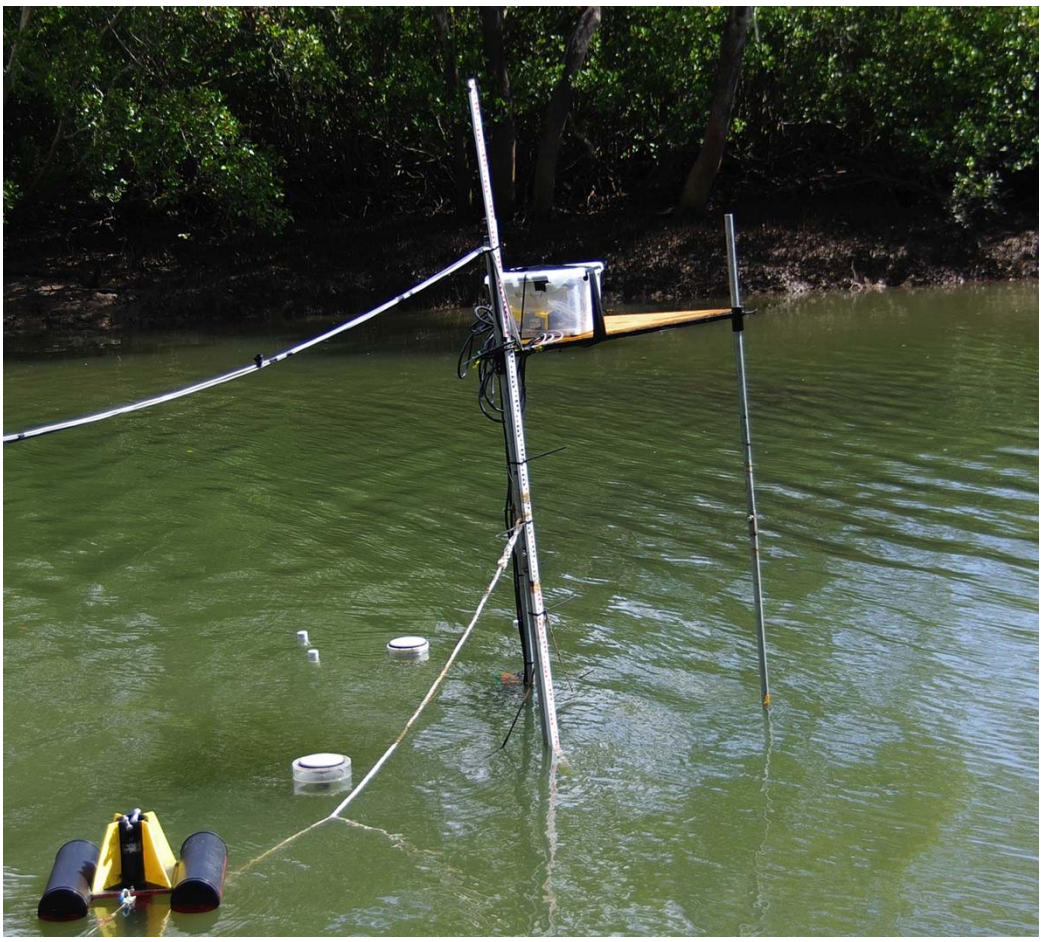

(B) GPS-tracked drifters drifting past the ADVs sampling location about 6 minutes after upstream deployment; Drifters sampled the sub-surface flow while ADVs sampled closer to the bed

(C) GPS-tracked drifters drifting past the ADVs sampling location about 7 minutes after upstream deployment; drifters motion almost independent of one another and initial deployment memory.

Fig. B-5 - Photographs of GPS-tracked drifter experiment during the ebb tide on 30/09/2013.

(A) Sampling location during ebb tide at 10:58 am on 30/09/2013; wind speed of about 1.3 m/s in NNE direction (i.e. blowing downstream the ADV) created energetic subsurface flow across the channel.

(B) Sampling location around high water slack at 5:53 am on 30/09/2013; wind was still and thus, no wind stress on subsurface layer to generate surface waves; ADVs were fully submerged: motion dominated by resonance.

Fig. B-6 - Photographs of sampling location site 2B identifying the combinatory role of wind, current and tidal height on the subsurface layer.

(A) Surface transient front in site 2B at 16:45

(B) Surface transient front in site 2B at 17:01

(C) Surface transient front in site 2B at 17:01 few seconds after (B)

Fig. B-7 - Front passing Site 2B about high tide at 17:00 on 30/09/2013 (147600 s); wind speed was limited to about 0.4 m/s in the NE direction.

APPENDIX C – PHYSIOCHEMICAL PROPERTIES OF EPRAPAH CREEK

C.1 PRESENTATION

During the field study E14 at Eprapah Creek during between 29/09/2013 – 1/10/2013 with neap tidal condition with average tidal range of 1.2 m, two YSI6600 physiochemical probes were deployed at Site 2B (AMTD 2.1 km from the mouth). One probe was deployed next to the bed at 11 m from the left channel around the tripod while the other was mounted about 2 m away from the tripod, next to the free surface. The probes sampled turbidity, temperature, chlorophyll, conductivity, pH, salinity and dissolved oxygen simultaneously and continuously for about 48 hours. Similarly, the DSITIA water quality monitoring group conducted measurement of vertical profile of the physiochemical properties at distance from the mouth of the channel. The locations sampled were River mouth, Site 1 (AMTD 1 km), Site 2 (AMTD 2 km), STP (about AMTD 2.7 km) and Site 3(AMTD 3.1 km). The vertical profiling was carried out at the beginning of ebb during a neap tide on 11 October 2013 with tidal range of 1.5 m.

Figure C-1 shows the photograph of the surface probe mounted on a float close to the ADV setups. Figure C-2 shows the physiochemical parameters of the YSI6600 probes while figured C-3 shows the vertical profiles.

Fig. C-1 - Photographs of the floating mount of the YSI6600 probe.

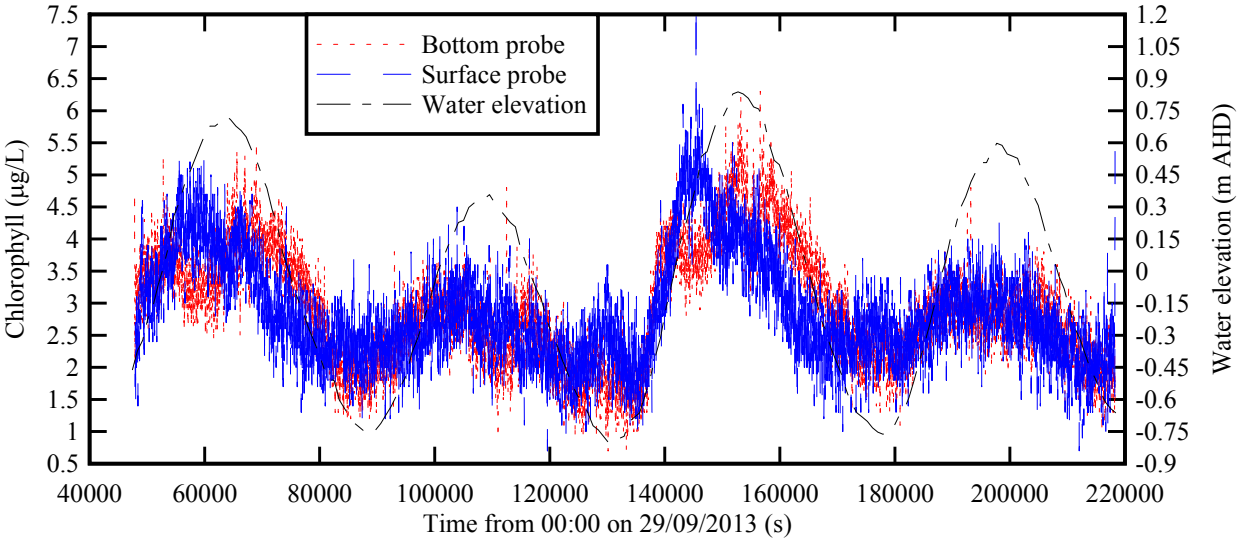

(A) Chlorophyll (µg/L)

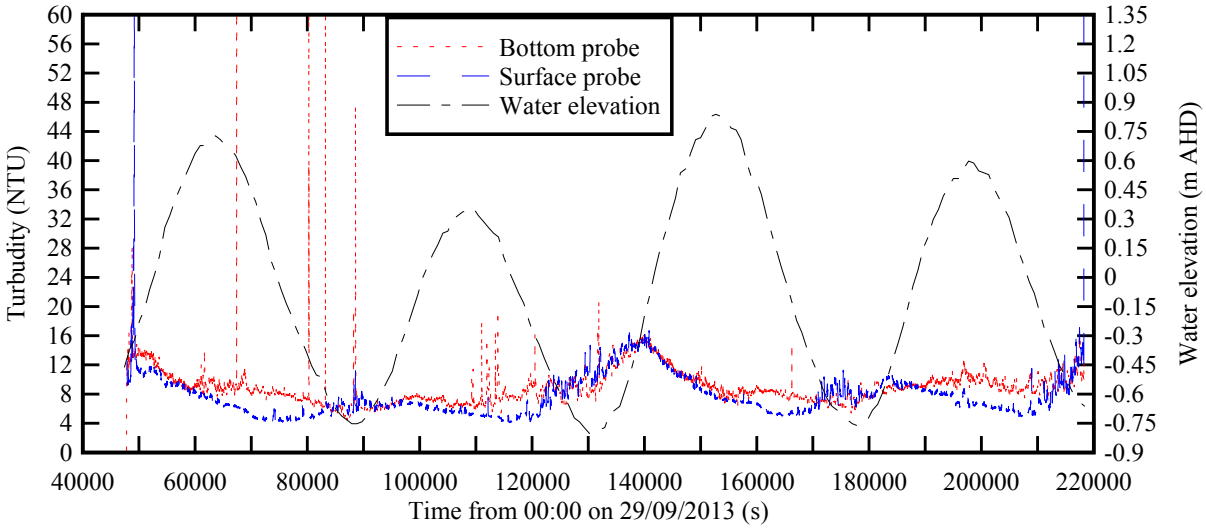

(B)Turbidity (NTU)

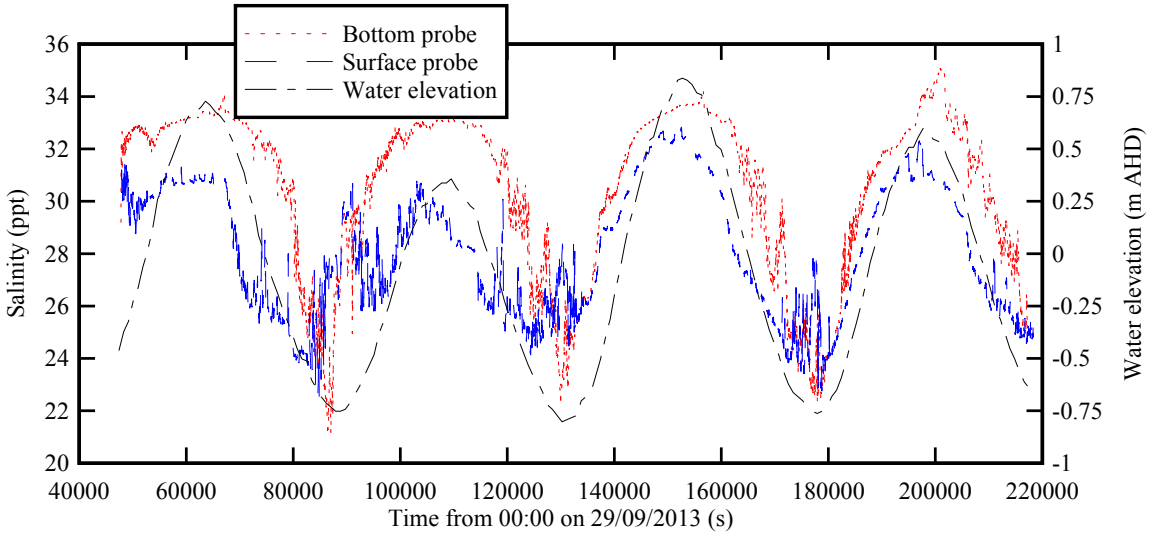

(C) Salinity (ppt)

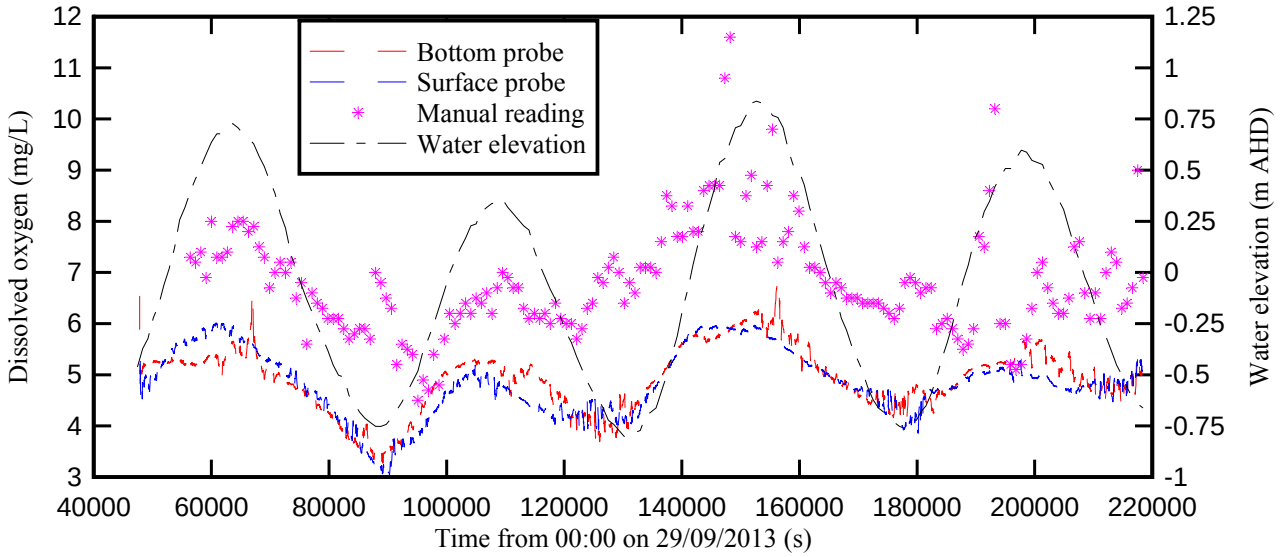

(D) Dissolved oxygen (mg/L)

Fig. C-2 - Chlorophyll, turbidity, salinity and dissolved oxygen as functions of time - Data collected by the YSI6600 units at Site 2B, Eprapah Creek during the study between 29/09/2013 and 01/10/2013.

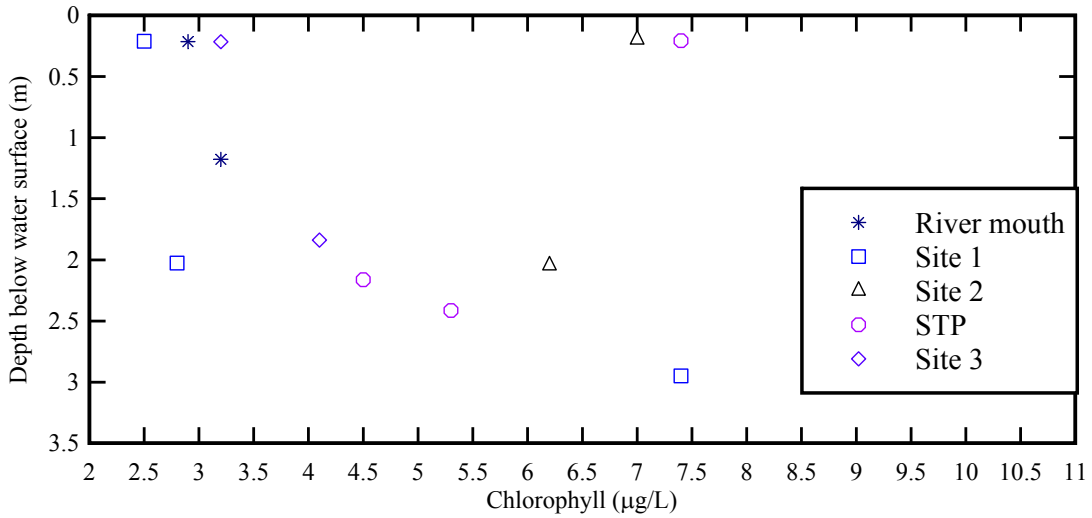

(A) Chlorophyll (µg/L)

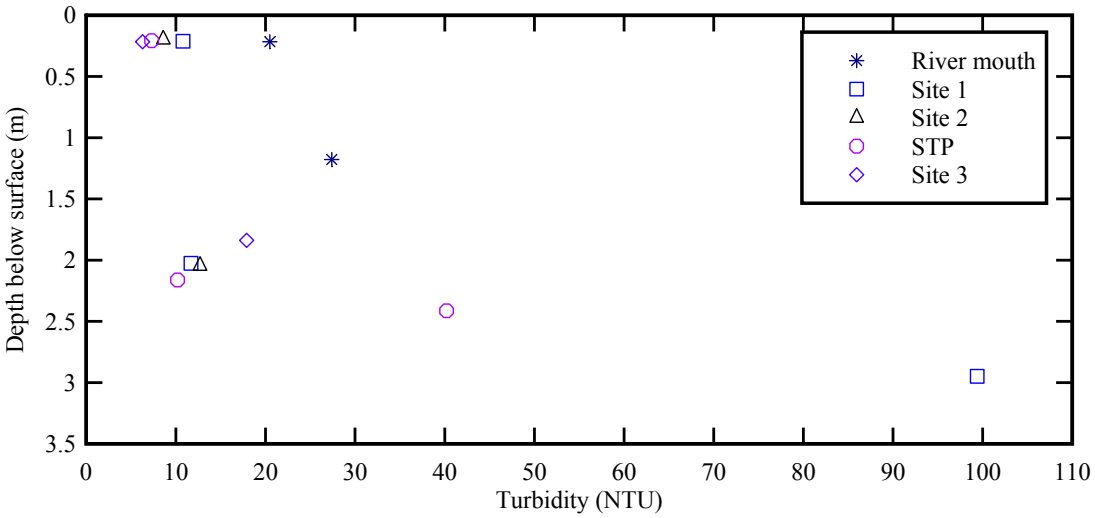

(B) Turbidity (NTU)

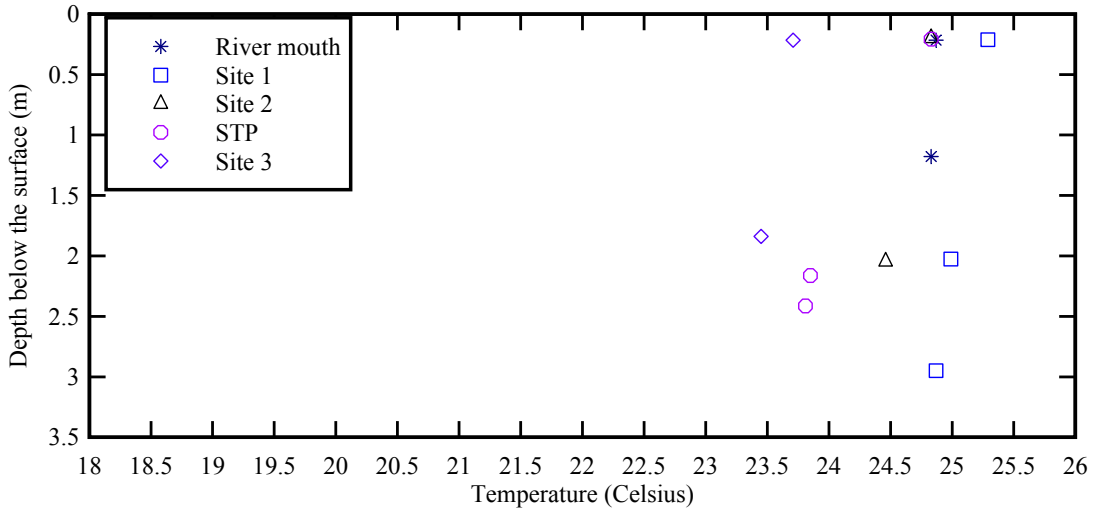

(C) Temperature (Celsius)

Fig. C-3 - Vertical profiles of water properties along Eprapah Creek channel; Data taken on 11 October 2013 at the beginning of the ebb tide. First reading taken at 14:42 (at River mouth) and last reading was taken at 15:09 (at site 3).

APPENDIX D – INSTANTANEOUS FLOW FIELD DATA AND SENSITIVITY ANALYSIS

D.1 PRESENTATION

During the field trip at Eprapah Creek during a neap tidal condition (29/09/2013 – 1/10/2013), the flow fields fluctuated significantly. Three ADV units named ADV1, ADV2 and ADV3 were sampled continuously at 0.32, 0.42 and 0.55 m, respectively above the bed at the rate of 50 Hz. After data quality control, instantaneous flow fields were obtained and are presented herein. The sensitivity analysis for the choice of lower and upper cut off frequencies to separate the flow field into its constituents was completed and presented in this Section. The analysis includes the effect of the lower cut-off frequency on the streamwise velocity components and the effects of the upper cut-off frequency on the turbulence intensities, correlation coefficients and the integral time scale.
Furthermore, the tidal constituents of the streamwise velocity for the 3 sampled locations are presented with respect to tide types. Power spectral analyses of the slow fluctuation (band-pass signal) are also provided herein.

D.2 INSTANTANEOUS DATA

The instantaneous fields of velocity and pressure are highly fluctuating in Eprapah Creek. The measured fields contained the superimposition of periodic fluctuations occurring at many different periods. Herein, the streamwise velocity, V_x is positive downstream (i.e. facing toward the mouth of the creek), the transverse velocity, V_y positive towards the left bank and the vertical velocity, V_z positive upward. These fluctuations can be categorised into tidal, slow and fast fluctuations. The slow fluctuations were pseudo periodic, caused by the reflection of tidal forcing onto certain geographical landmarks.

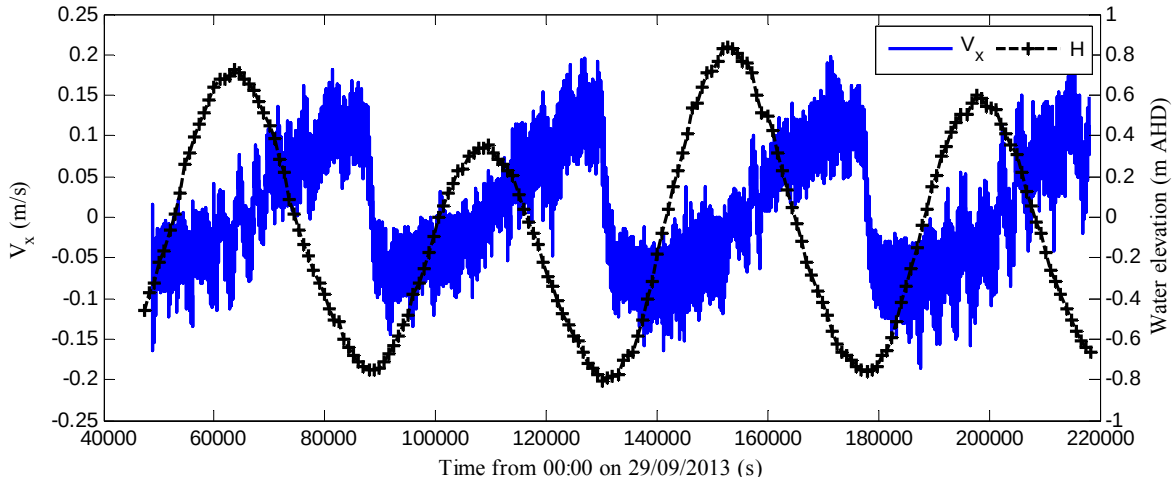

(A) Streamwise velocity, V_x (m/s)

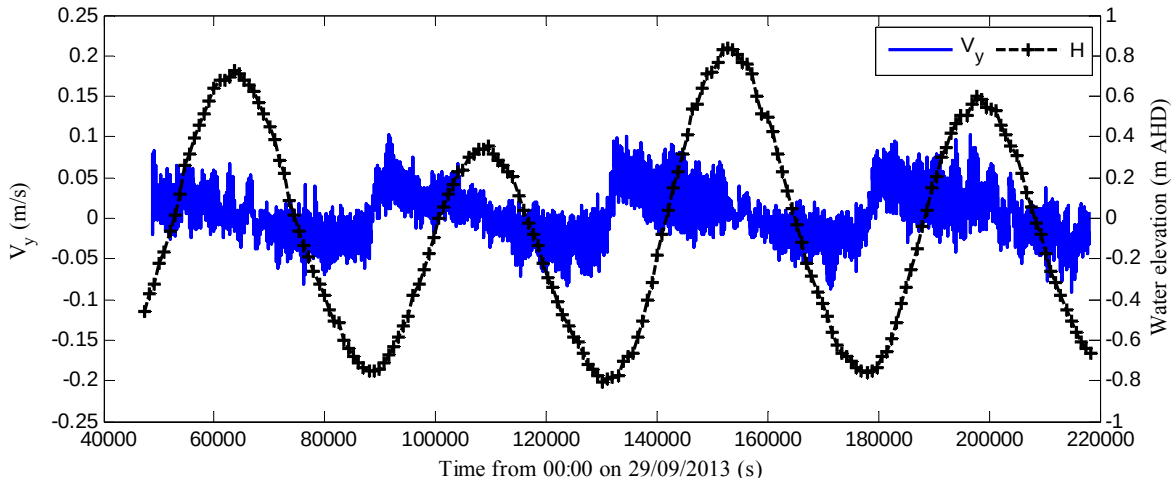

(B) Transverse velocity, V_y (m/s)

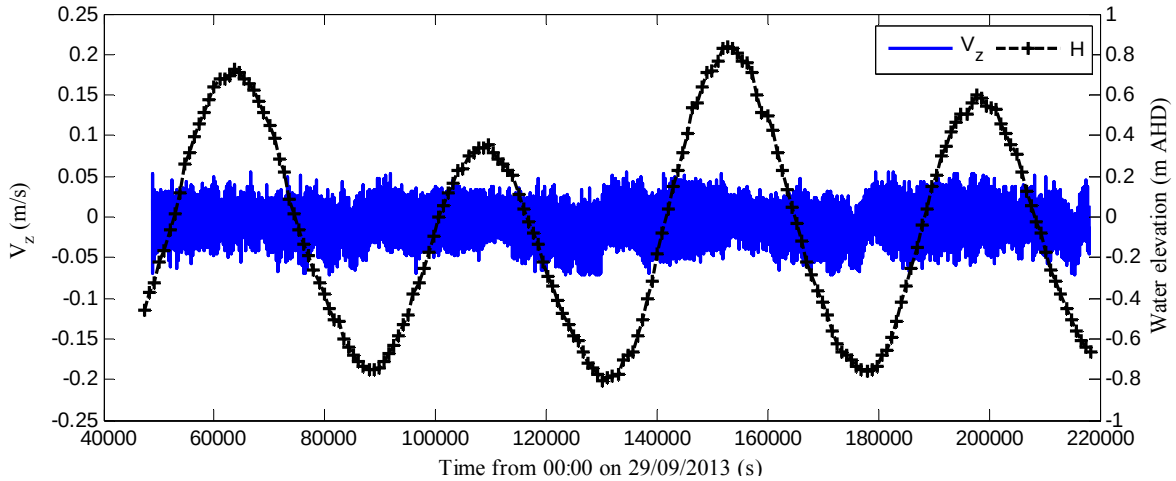

(C) Vertical velocity, V_z (m/s)

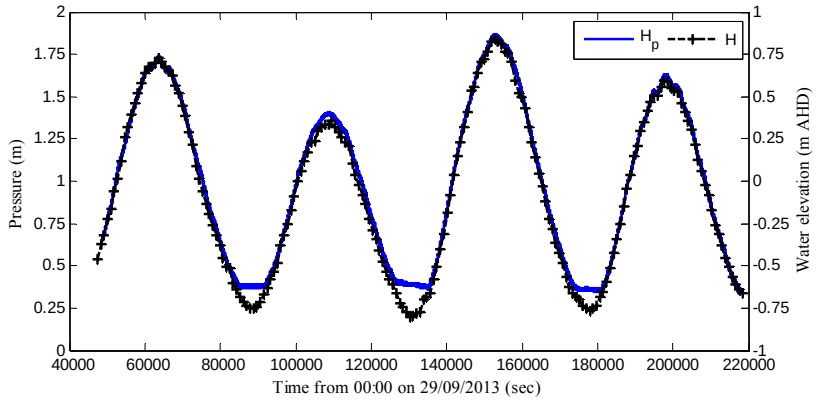

(D) Adjusted pressure measured with ADV1 pressure sensor, H_p (m)

Fig. D-1 - Instantaneous velocity components and water elevation as functions of time. Using 3D microADV A813F (16 MHz), scan rate: 50 Hz, Probe sensor: 0.32 m above the bed, 11.06 m from left bank.

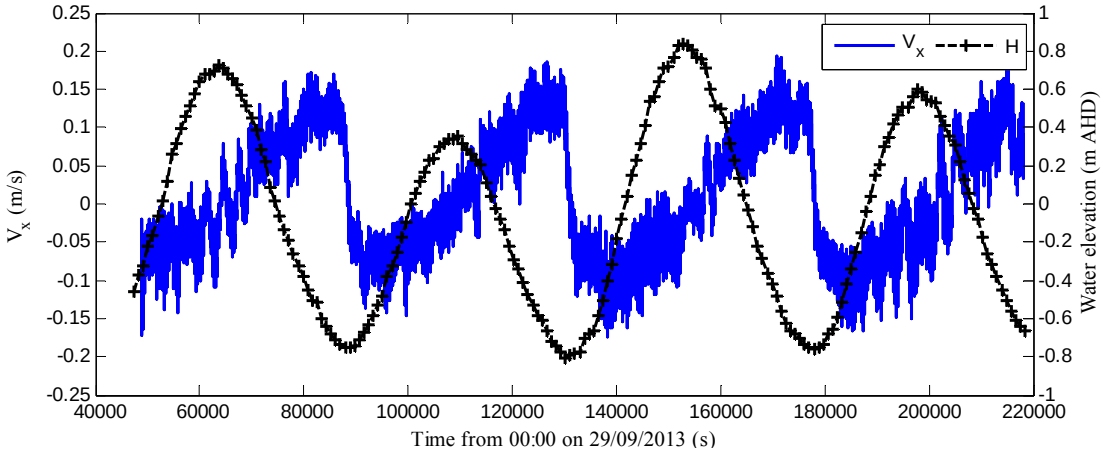

(A) Streamwise velocity, V_x (m/s)

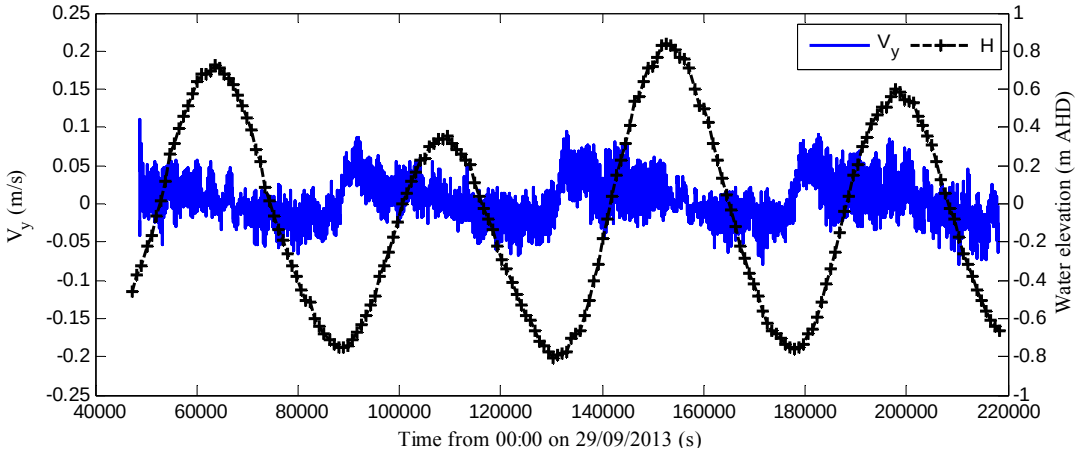

(B) Transverse velocity, V_y (m/s)

Fig. D-2 - Instantaneous velocity components and water elevation as functions of time. Using 2D microADV A641F (16 MHz), scan rate: 50 Hz, Probe sensor: 0.42 m above the bed, 11.04 m from left bank.

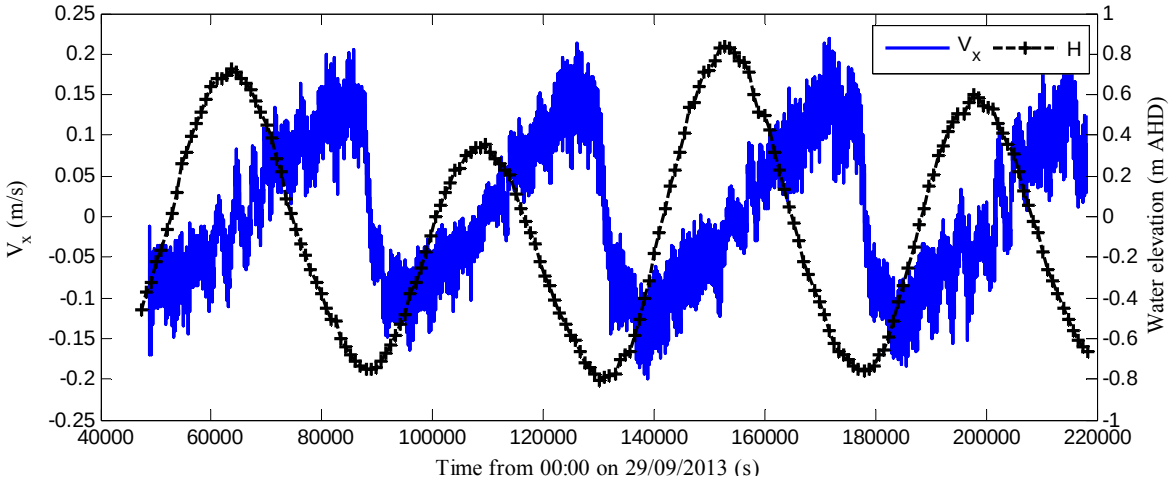

(A) Streamwise velocity, V_x (m/s)

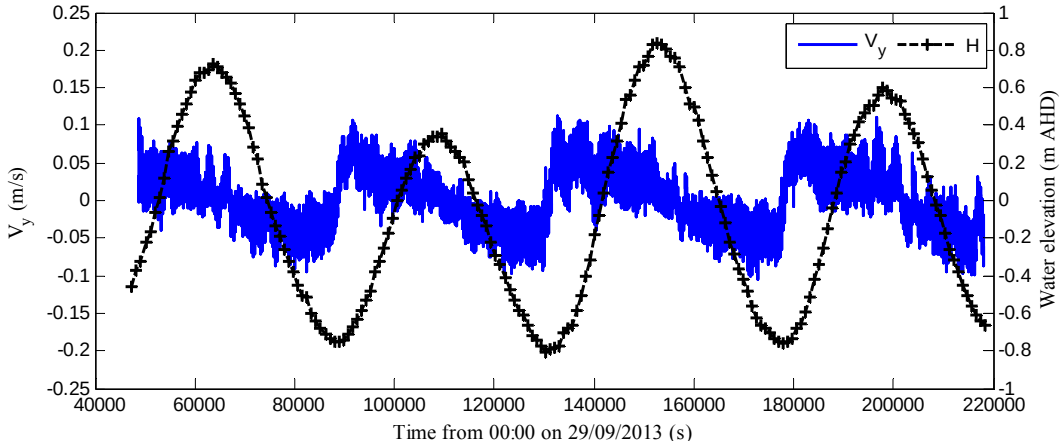

(B) Transverse velocity, V_y (m/s)

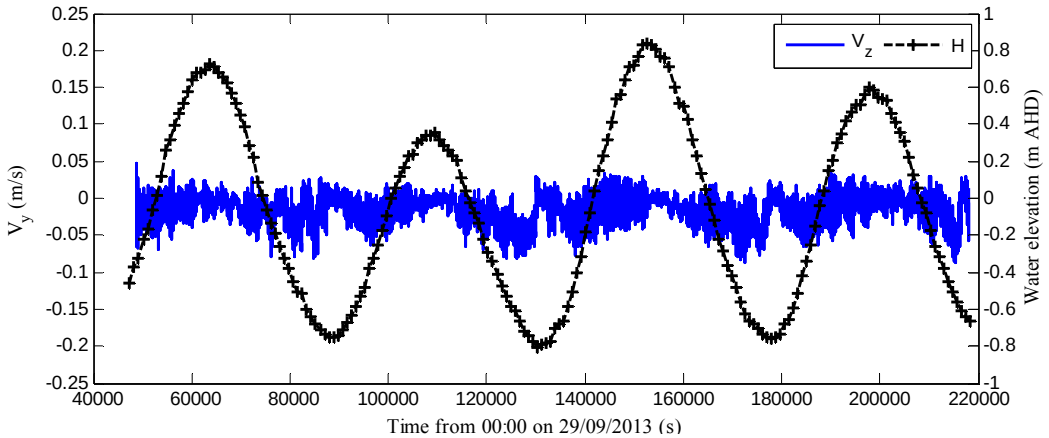

(C) Vertical velocity, V_z (m/s)

Fig. D-3 - Instantaneous velocity components and water elevation as functions of time. Using 3D microADV A843F (16 MHz), scan rate: 50 Hz, Probe sensor: 0.55 m above the bed, 11.05 m from left bank.

D.3 SENSITIVITY ANALYSIS

The decomposition of the instantaneous flow field was performed using a triple decomposition technique discussed in Section 5. The cut-off frequencies were identified by visual observations, power spectra analyses and celerity of water within the channel. Although the flow field in the channel was highly unsteady, the goal was to choose cut-off frequencies that provided physical meanings for the constituents of the decomposed flow fields. Digital filtering technique described in Bendat and Piersol (2011) was applied.

D.3.1 Selection of lower cut-off frequency

Distinctive pseudo-periodic events were observed in the power spectra analyses of instantaneous data of velocity and pressure at low frequency (Fig. D-4). Figures (D-4) to (D-6) show some spectral of velocity and water pressure with smoothed curves highlighting distinctive peaks and troughs in power spectrum of the instantaneous data at frequencies greater than 0.00004 Hz. The peaks could not be confirmed in the smoothed data because of the limited number of data points at this very low frequency. Please note the different vertical axis range for the power spectra density in the figure. The high frequency portions of the spectral density are not shown for clarity. Further analysis was performed around F_{cl} = 0.0001 Hz. Figure D-6 shows that a cut-off frequency higher than 0.0001 Hz introduces some signature of slow fluctuation into the tidal velocity while lower frequency (e.g. F_{cl} = 0.00008 Hz) caused a phase shift around the slack water.

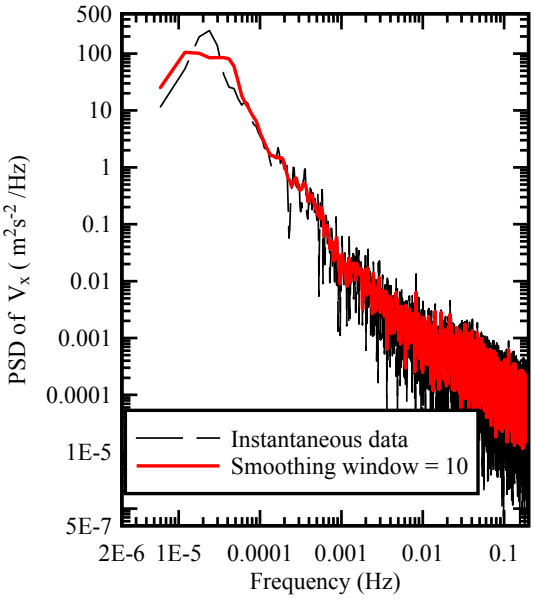

(A) PSD V_x, (m^2s^{-2}/Hz)

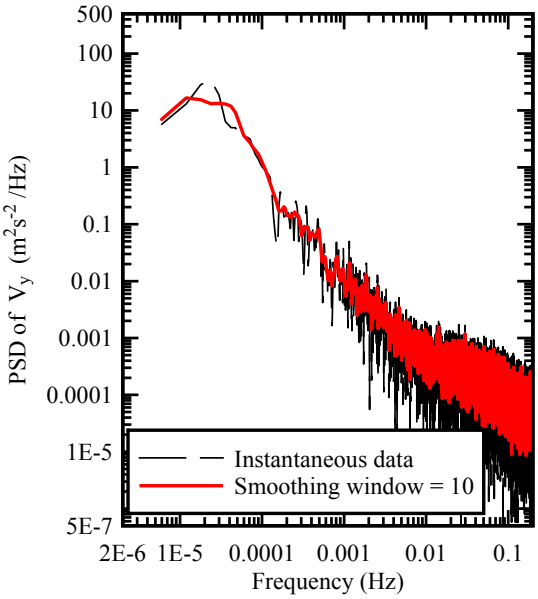

(B) PSD V_y, (m^2s^{-2}/Hz)

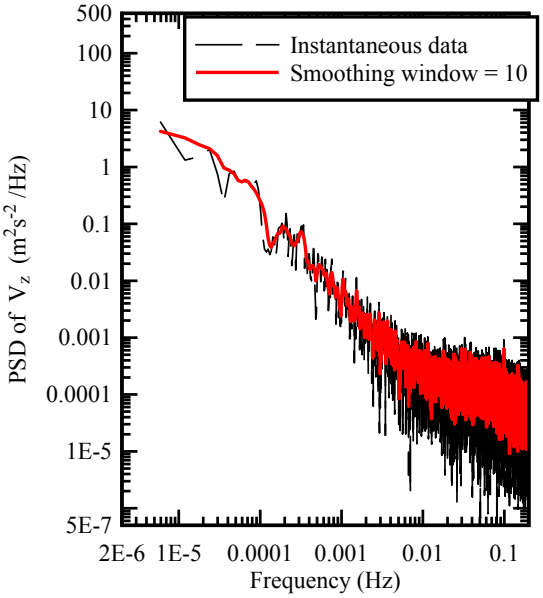

(C) PSD V_z, (m^2s^{-2}/Hz)

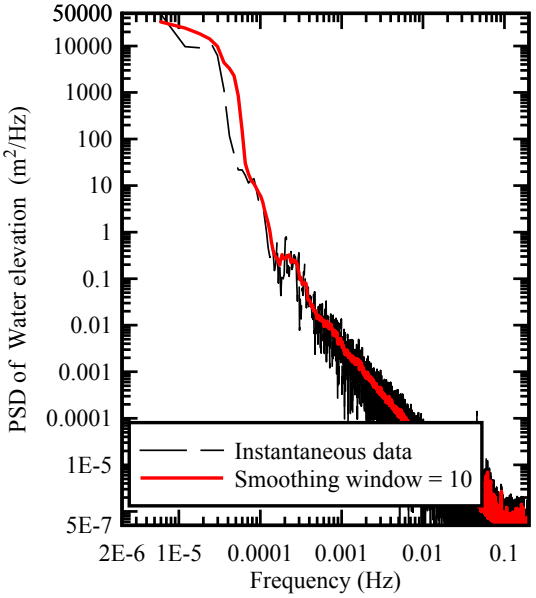

(D) PSD Water elevation, (m^2/Hz)

Fig. D-4 - Spectral analysis of fluctuations of longitudinal velocity V_x, transverse velocity V_y, vertical velocity V_z and water elevation measured using 3D microADV A813F (16 MHz), scan rate: 50 Hz, Probe sensor: 0.32 m above the bed, 11.056 m from left bank.

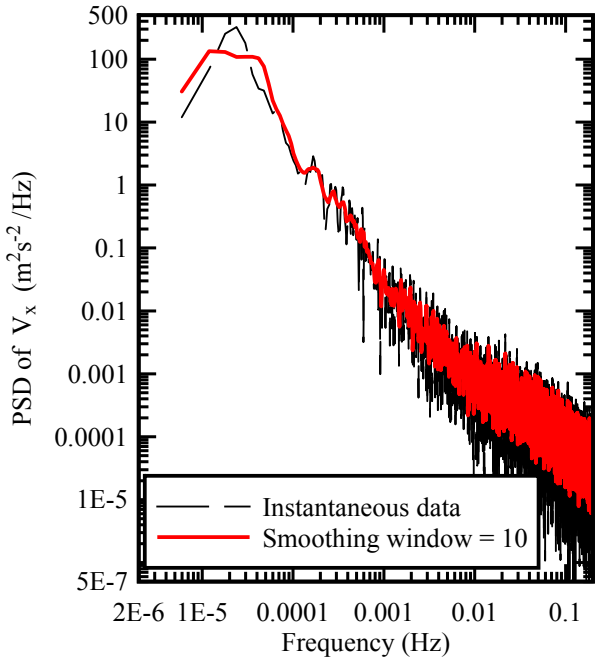

(A) PSD V_x, (m^2s^{-2}/Hz)

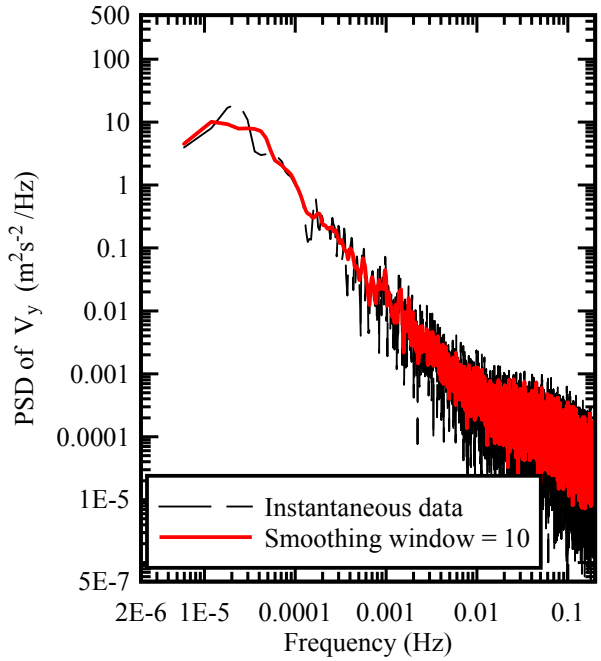

(B) PSD V_y, (m^2s^{-2}/Hz)

Fig. D-5 - Spectral analysis of fluctuations of longitudinal velocity V_x, transverse velocity and V_y using 2D microADV A641F (16 MHz), scan rate: 50 Hz, Probe sensor: 0.42 m above the bed, 11.04 m from left bank

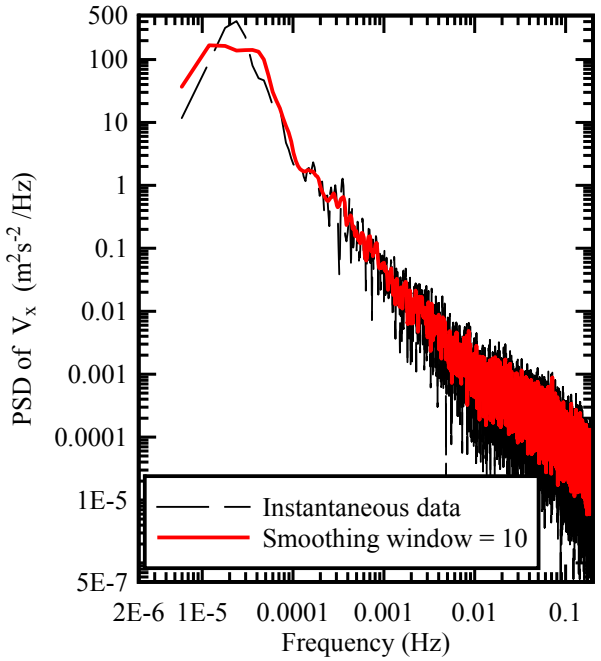

(A) PSD V_x, (m^2s^{-2}/Hz)

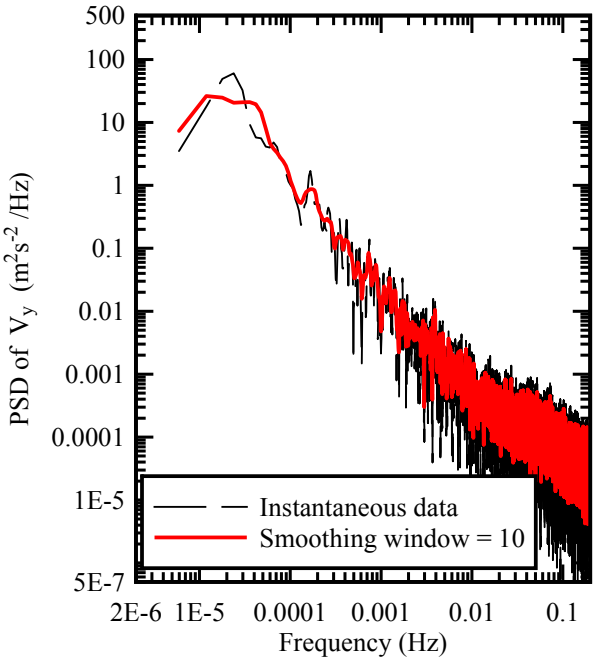

(B) PSD V_y, (m^2s^{-2}/Hz)

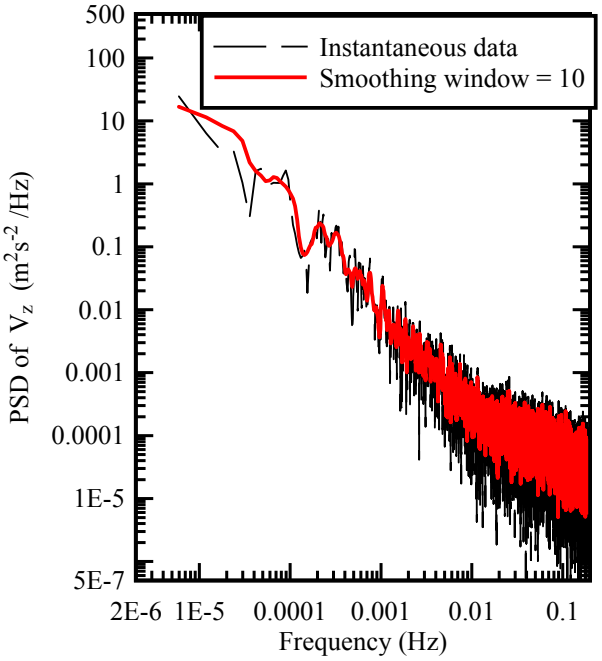

(C) PSD V_z, (m^2s^{-2}/Hz)

Fig. D-6 - Spectral analysis of fluctuations of streamwise velocity V_x, transverse velocity V_y, vertical velocity V_z measured using 3D microADV A843F (16 MHz), scan rate: 50 Hz, Probe sensor: 0.55 m above the bed, 11.05 m from left bank.

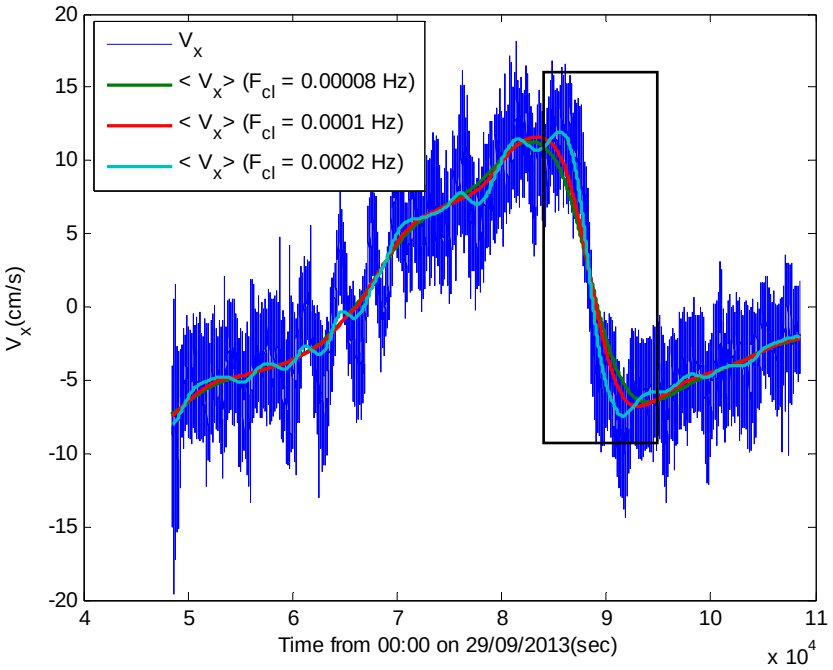

Fig. D-7 - Sensitivity analyis on the effect of the upper cut-off frequency on the approximation of the tidal component of velocity; Streawise velocity of the 3D microADV A813F (16 MHz), scan rate: 50 Hz, Probe sensor: 0.32 m above the bed, 11.056 m from left bank.

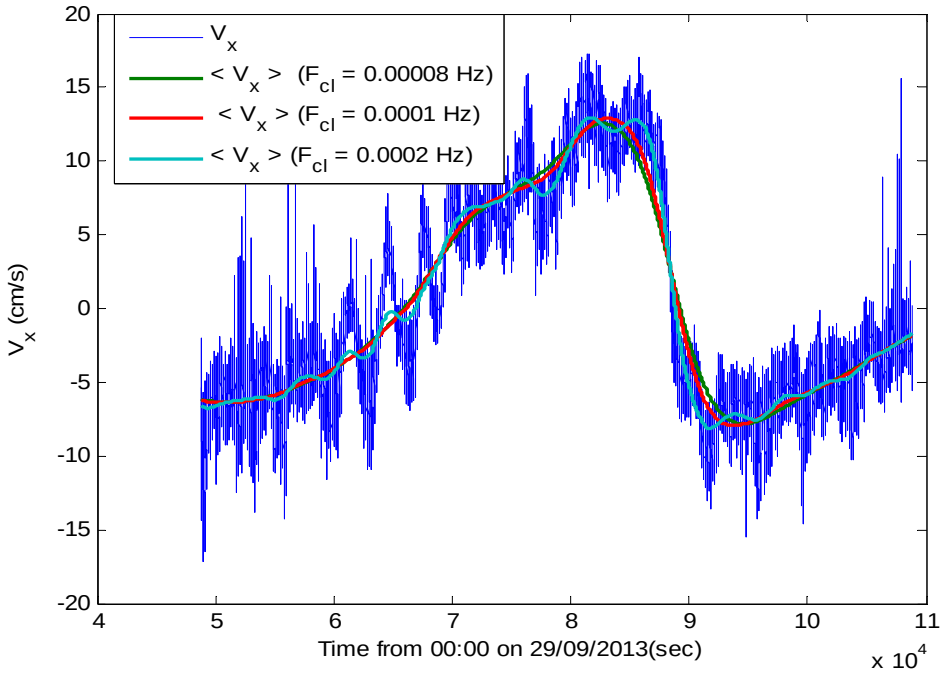

Fig. D-8 - Sensitivity analyis on the effect of the upper cut-off frequency on the approximation of the tidal component of velocity. Streawise velocity of the 2D microADV A641F (16 MHz), scan rate: 50 Hz, Probe sensor: 0.42 m above the bed, 11.042 m from left bank.

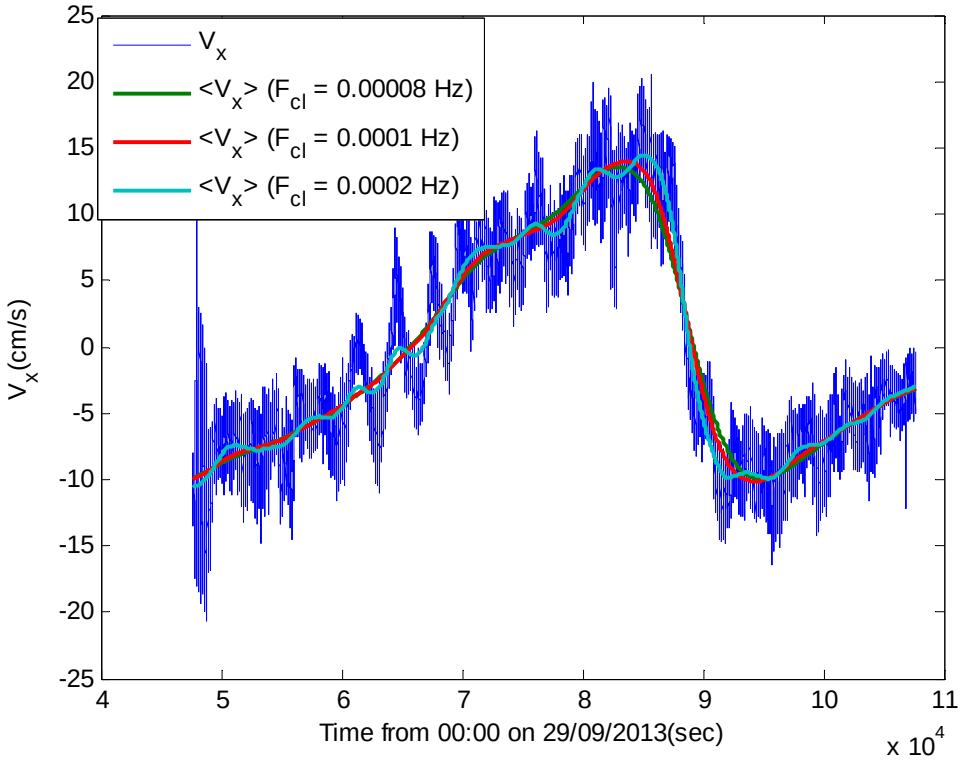

Fig. D-9 - Sensitivity analyis on the effect of the upper cut-off frequency on the approximation of the tidal component of velocity. Streawise velocity of the 3D microADV A843F (16 MHz), scan rate: 50 Hz, Probe sensor: 0.55 m above the bed, 11.05 m from left bank.

D.3.2 ***Selection of upper cut-off frequency***

Effect of upper cut-off frequency on the turbulence ratio

The sensitivity analyses of the effect of the upper cut-off frequency on the horizontal and vertical turbulence ratios at different times during the field study are presented in Figure D-10 to D-12. The turbulence ratios were obtained as ratio of turbulent standard deviations (v_y' and v_z') and the corresponding streamwise component, v_x' (high-pass filtered data). The standard deviations were calculated as the standard based on 10,000 data points (200 s). The horizontal turbulence ratios for ADV1 and ADV2 sampled at 0.32 m and 0.42 m respectively showed large deviations from isotropy as the cut-off frequency s increased, thus a clear cut-off frequency could not be defined based on horizontal turbulence ratio. Turbulence ratios obtained from ADV sampled at 0.55 m showed reduced magnitude behaviour which was dissimilar to what was observed with other ADV. This could be linked with difference in instrumentation. A clear cut-off could not be obtained using the turbulence ratio.

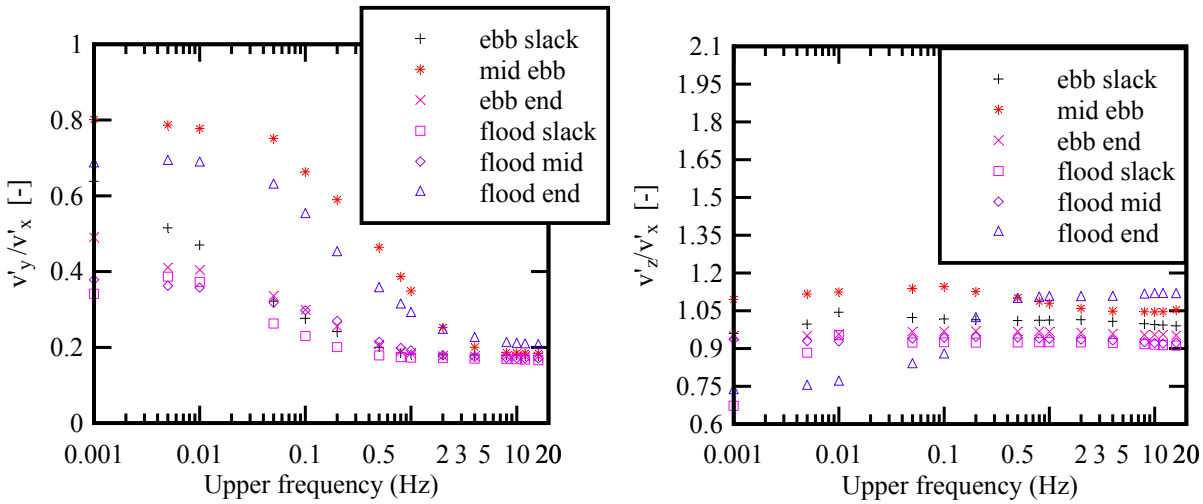

(A) v'_y/v'_x, [-] (B) v'_z/v'_x, [-]

Fig. D-10 - Sensitivity analyses on the effect of cut-off frequency on the turbulence ratios. 3D microADV A813F (16 MHz), scan rate: 50 Hz, Probe sensor: 0.32 m above the bed, 11.056 m from left bank.

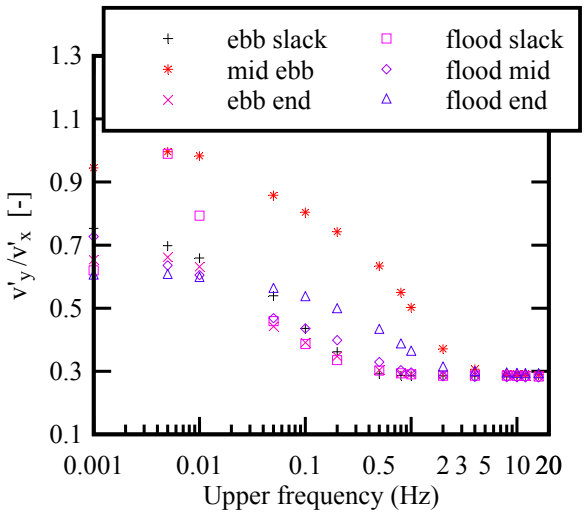

(A) v'_y/v'_x, [-]

Fig. D-11 - Sensitivity analyses on the effect of cut-off frequency on the turbulence ratios. 2D microADV A641F (16 MHz), scan rate: 50 Hz, Probe sensor: 0.42 m above the bed, 11.042 m from left bank.

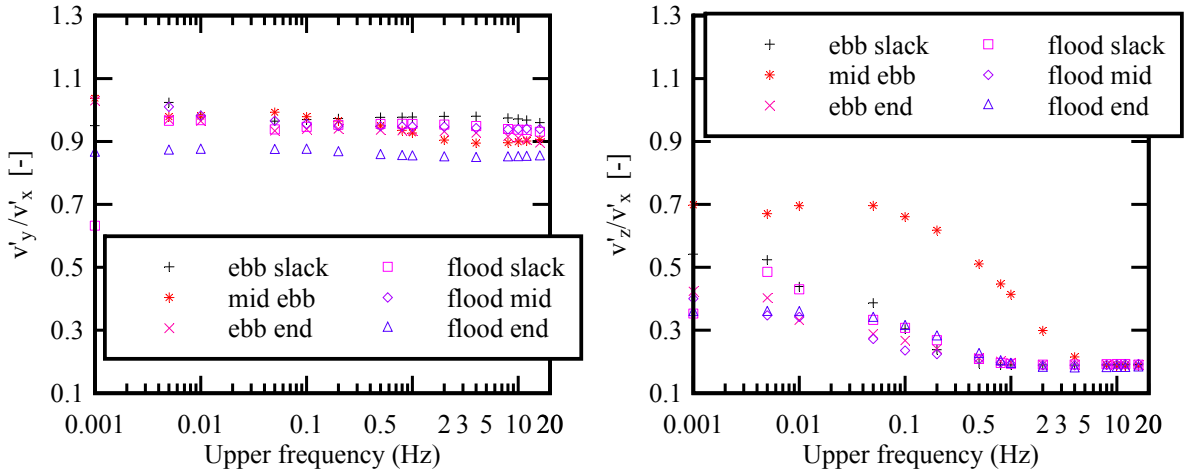

(A) v'_y/v'_x, [-] (B) v'_z/v'_x, [-]

Fig. D-12 - Sensitivity analyses on the effect of cut-off frequency on the turbulence ratios. 3D microADV A843F (16 MHz), scan rate: 50 Hz, Probe sensor: 0.55 m above the bed, 11.05 m from left bank.

Effect of upper cut-off frequency on the Correlation coefficients

The correlation coefficient describes the degree of connections between turbulent velocities. The correlation coefficient is the dimensionless covariance, normalised with the standard deviation of the relevant turbulent velocity component. The sensitivity analyses of the effect of the upper cut-off frequency on the correlation coefficient at different times during the field study are presented in Figure D-13 to D-15. Note the difference in the vertical scales. The correlation coefficients were based on 10,000 data point (high-pass filtered data) taken within the middle of the specified period. R_{xx} had a correlation coefficient of 1 in cut-off frequency independently of the cut-off frequency. The correlation of 1 is expected for R_{xx} because it is equivalent to an autocorrelation with zero time lag. The R_{xy} for the three ADV units approximately approached constant values at frequency between 0.01 Hz and 0.5 Hz. The end of flood tide exhibited some unusual trend in the correlation coefficient variation with the upper cut-off frequency. For example, the correlation coefficient R_{xy} obtained at 0.32 m above the bed jumped from a near constant value of -0.6 to -0.2 while that of ADV2 sampled at 0.42 dropped from -0.1 to -0.4 with the upper cut-off frequency increment between 0.2 and 2 Hz. This prevented the identification of a clear upper cut off frequency based on the longitudinal correlation coefficient. Effect of upper cut-off frequency on R_{yz} and R_{xz} showed some convergence to a frequency independent value for the three ADV at frequencies around 0.2 Hz. This was applicable to all tidal phases studied except end of the flood tide.

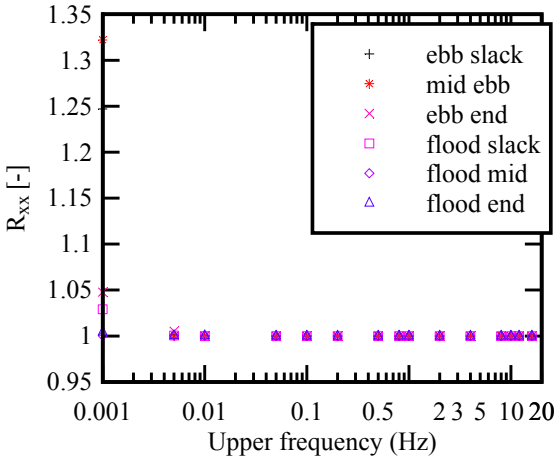

(A) R_{xx}, [-]

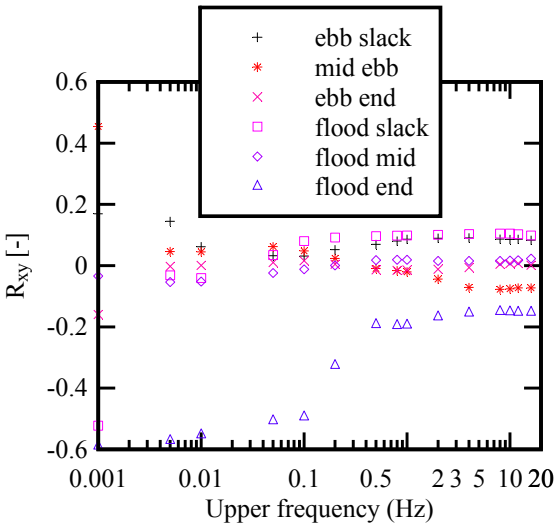

(B) R_{xy}, [-]

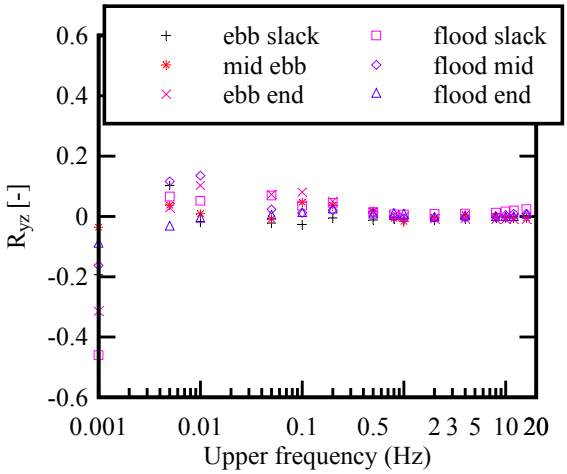

(C) R_{yz}, [-]

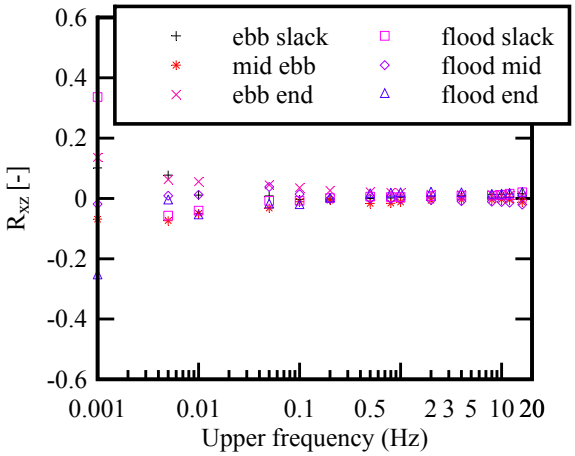

(D) R_{xz}, [-]

Fig. D-13 - Sensitivity analyses on the effect of cut-off frequency on the cross-correlation coefficients between turbulent velocity components. 3D microADV A813F (16 MHz), scan rate: 50 Hz, Probe sensor: 0.32 m above the bed, 11.056 m from left bank.

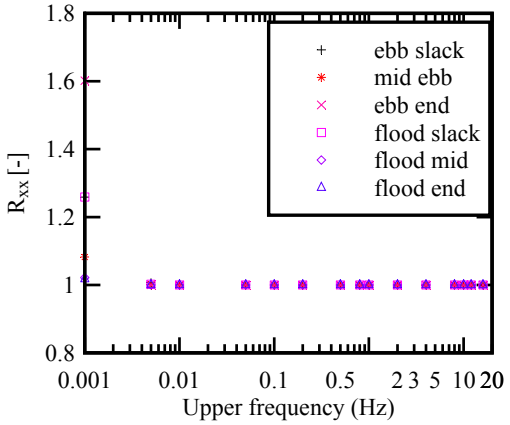

(A) R_{xx}, [-]

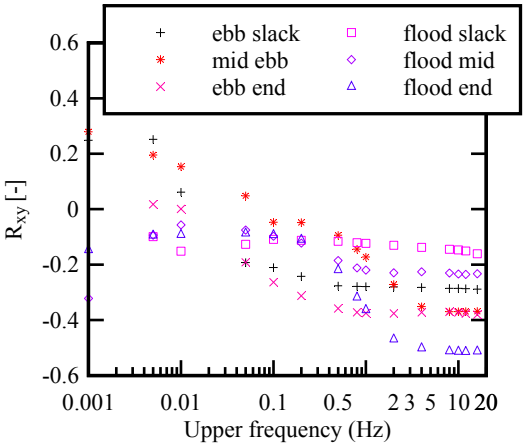

(B) R_{xy}, [-]

Fig. D-14 - Sensitivity analyses on the effect of cut-off frequency on the cross-correlation coefficients between turbulent velocity components. 2D microADV A641F (16 MHz), scan rate: 50 Hz, Probe sensor: 0.42 m above the bed, 11.042 m from left bank.

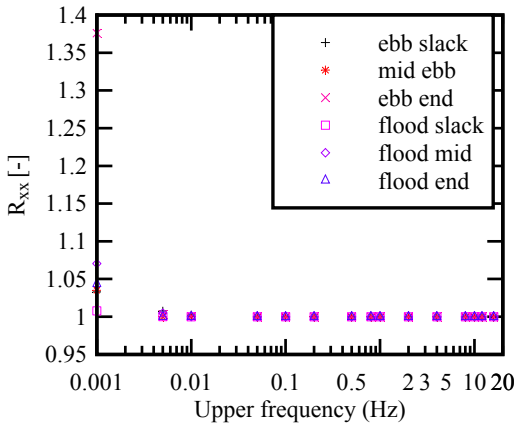

(A) R_{xx}, [-]

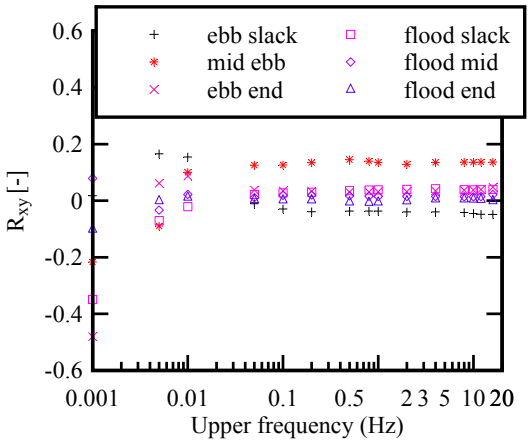

(B) R_{xy}, [-]

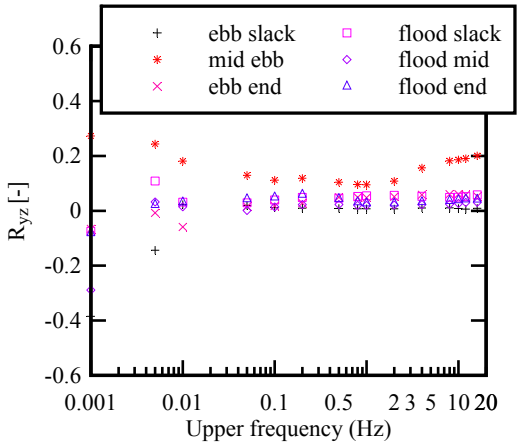

(C) R_{yz}, [-]

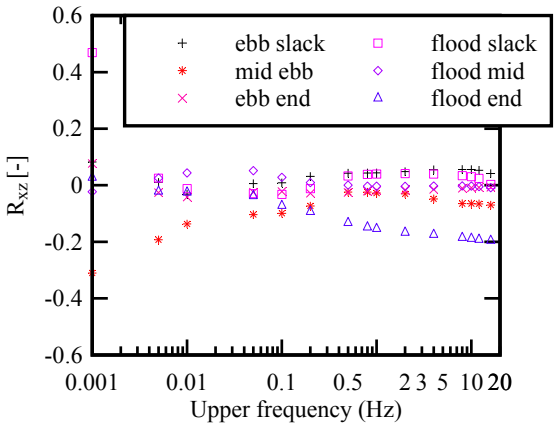

(D) R_{xz}, [-]

Fig. D-15 - Sensitivity analyses on the effect of cut-off frequency on the cross-correlation coefficients between turbulent velocity components. 3D microADV A843F (16 MHz), scan rate: 50 Hz, Probe sensor: 0.55 m above the bed, 11.056 m from left bank.

Effect of upper cut-off frequency on the integral time scale T_{Ex}

The sensitivity analyses of the effect of the upper cut-off frequency on the streamwise integral time scale at different times during the field study are presented in Figure D-17. The normalised autocorrelation function, R describes the evolution of the turbulence field with time. R describes how a turbulence velocity correlates with values at difference times. For example, R_{xx} is defined as:

$$R_{xx}(\tau) = \frac{\overline{v_x(t)v_x(t+\tau)}}{\overline{v_x^2}} \qquad \text{(D-1)}$$

where τ is the time lag. Figure D-16 shows a sample autocorrelation.

The integral time scales were computed from the integral of autocorrelation function R up to the first zero crossing using a 10,000 data points sample (high-pass filtered data) and a fixed lag time of 10 s. The integral time scale for the three ADVs decayed exponentially with increasing upper cut off frequency. This decay indicated that relatively large scale processes were removed with an increase in upper cut-off frequency. However, it is difficult to differentiate between the noise and turbulence at very high frequencies. For an idealised turbulence field, the integral length scale should be independent of tidal phase. Figure D-17 shows that the integral time scales at different tidal phases considered became approximately equal at frequency around 0.1 Hz for all measurement heights. This suggested that a cut-off frequency $\geq$ 0.1 Hz could describe the true turbulence from the observed field data.

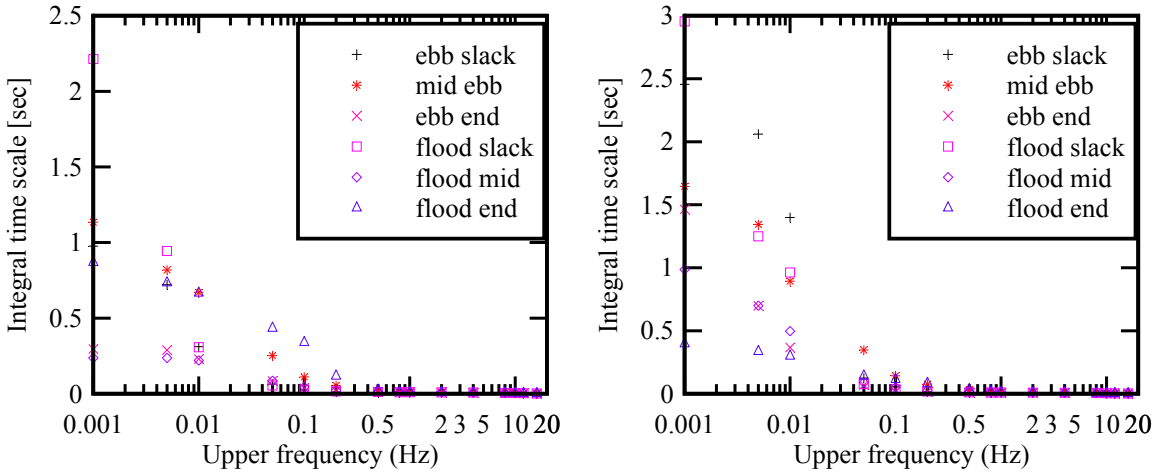

(A) ADV1; 0.32 m above the bed, 11.056 m from left bank (B) ADV2; 0.42 m above the bed, 11.042 m from left bank

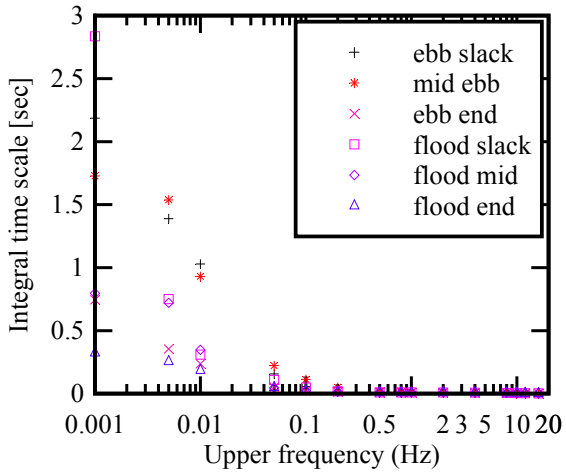

(C) ADV3; 0.55 m above the bed, 11.056 m from left bank

Fig. D-17 - Sensitivity analyses on the effect of cut-off frequency on the Integral time scale.

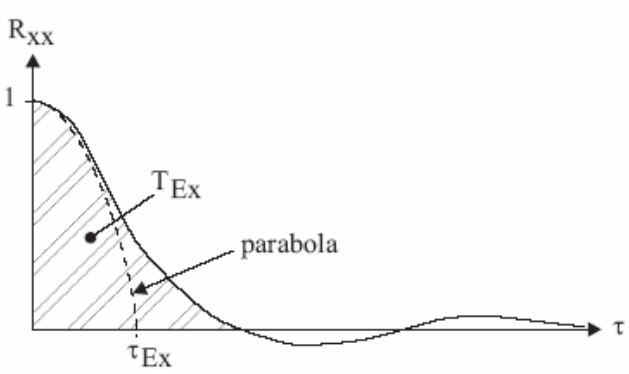

Fig. D-16 - Sketch of typical autocorrelation function of a fluctuating sample as a function of τ.

D.4 TIDAL VELOCITY

Based on power spectral analyses, sensitivity analyses and the physical considerations of the sources of resonance, the cut-off frequencies 0.0001 Hz and 0.1 Hz were respectively chosen as the lower and upper cut-off frequencies for separating the tidal and large scale fluctuation from the true turbulence. The tidal flow field (e.g $<V_x>$) was obtained as the low-pass filtered signal of the instantaneous flow field (e.g. V_x) with a cut off frequency of 0.1 Hz while the true turbulence field (e.g. v_x) was obtained as the high-pass filtered signal of the instantaneous flow field. The slow fluctuation (i.e. Bandpass data), (e.g. $[V_x]$) was obtained by subtracting both the tidal and turbulence signal from the instantaneous data. Figure D-18 illustrates time series of a 200 s long sample of the decomposed data. Note the difference in the vertical axes for the 3 velocity components.

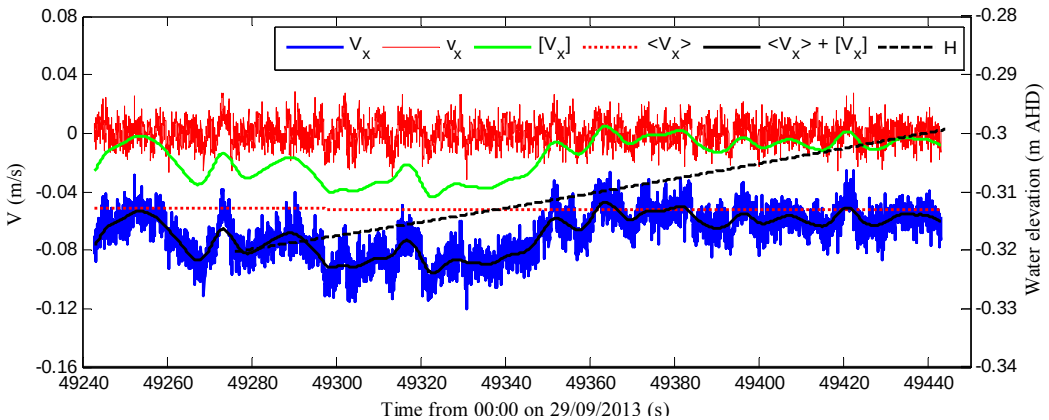

(A) Streamwise velocity (m/s)

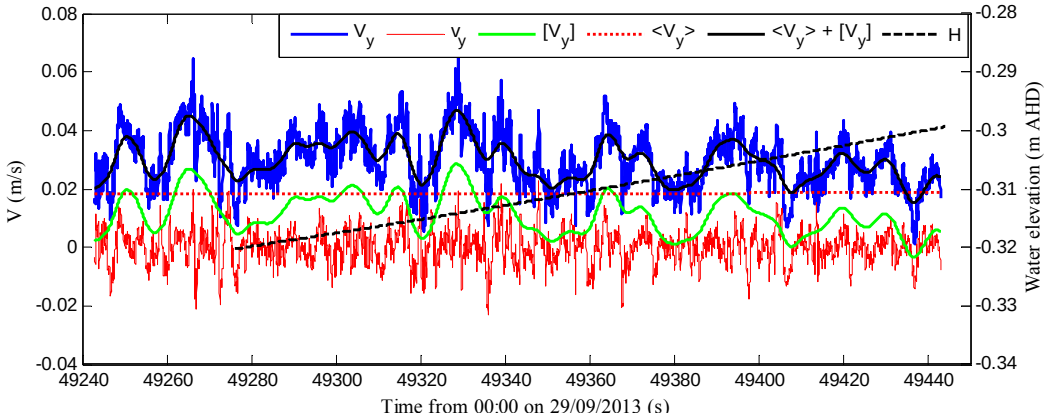

(B) Transverse velocity (m/s)

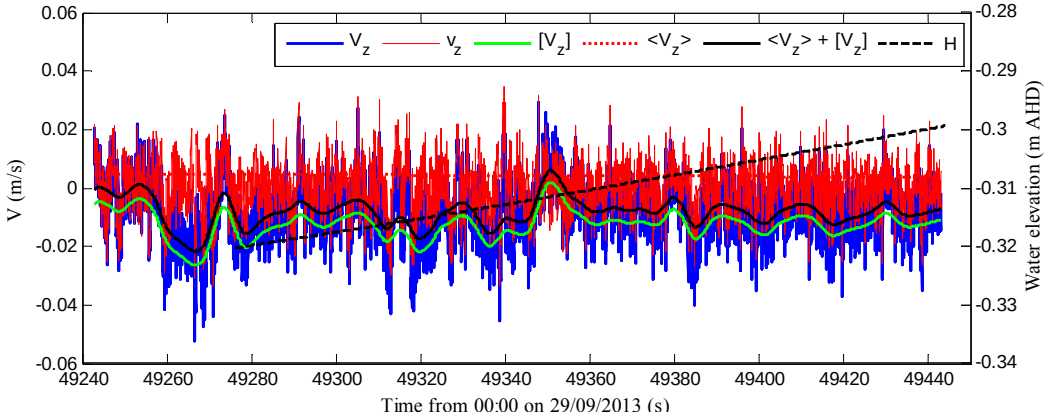

(C)Vertical velocity (m/s)

Fig. D-18 - Time series of velocity components illustrating the results of the triple decomposition on the instantaneous data.

D.4.1 Summary of streamwise tidal components of velocity

This section summarises the streamwise tidal velocity components $<V_x>$ for the ADV units sampled at 0.32 m (ADV1, 3D microADV, 16 MHz), 0.42 m (ADV2, 2D microADV, 16 MHz) and 0.55 m (ADV3, 3D microADV, 16 MHz) above the bed. The data were low-pass filtered from the instantaneous streamwise velocity. Flood and ebb tides were defined based on water levels while streamwise velocities are defined based upon slack, i.e. zero velocity. The high and low tides were defined based on the low-pass filtered water-level. Figure D-19 shows the water levels and definition of the terms used in Table D-1. Table D-1 summarises the maximum and mean values of the streamwise velocity observed for the flood and ebb tides observed during the field work.

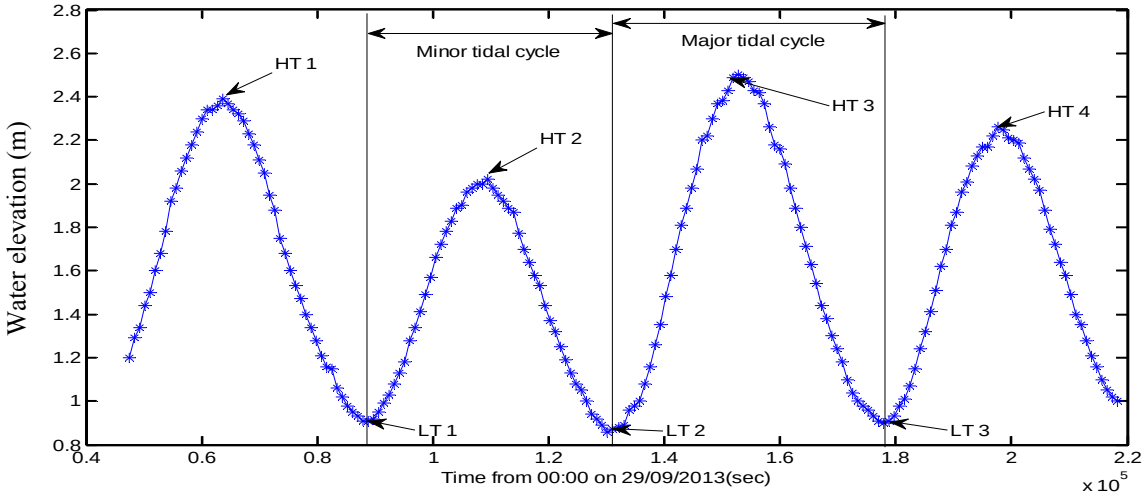

Fig. D-19 Time series of water elevation showing the amplitudes and periods of tides observed during the study. HT 1 – High tide 1; LT 1 – Low tide 1; HT 2 – High tide 2; LT 2 – Low tide 2; HT 3 – High tide 3; LT 3 – Low tide 3; HT 4 – High tide 4.

Table D-1 - Summary of the tidal constituent of the streamwise velocity measured at Eprapah Creek during the field study for ADV1, ADV2 and ADV3 sampled at 0.32 m, 0.42 m and 0.55 m above the bed respectively

Phase (1)	Type (2)	Time HT - LT (s) (3)	Period (s) (4)	Tidal range (m) (5)	ADV Unit (6)	Streamwise tidal velocity (cm/s) (7)	
						Max.	Mean
Ebb 1		66130 - 89043	22,913	1.2	ADV1	11.6	7
		66131 - 89111	22,980		ADV2	12.9	7.8
		65965 - 89154	23,189		ADV3	14	8.4
Flood 1		89043-109498	20,455	0.9	ADV1	6.8	4.2
	Minor	89111 - 109598	20,487		ADV2	7.9	5
		89154 - 109740	20,586		ADV3	10.1	6.2
Ebb 2		109498 - 131596	22,098	0.9	ADV1	12.7	7.2
	Minor	109598- 131690	22,092		ADV2	13.7	8
		109740 -131460	21,720		ADV3	14.7	8.5
Flood 2		131596 - 155631	24,035	1.4	ADV1	8.6	5.8
	Major	131690 - 155550	23,860		ADV2	10.5	6.6
		131460 - 155371	23,911		ADV3	13.5	7.6
Ebb 3		155631 -178631	23,000	1.4	ADV1	12	7.4
	Major	155550 - 178528	22,978		ADV2	13.2	8.1
		155371 - 178482	23,111		ADV3	14.5	8.5
Flood 3		178631 - 202099	23,464	-	ADV1	8.8	5.8
		178528 -201926	23,398		ADV2	10.8	6.5
		178482 - 201984	23,502		ADV3	12.9	7.7

Note: Tidal phase, amplitude and period are measured with respect to water level while streamwise velocities are measured from slack water to slack water.

D.5 SLOW FLUCTUATION POWER SPECTRAL DENSITY

Similar to the power spectral density of the band-pass signal presented in Section 5.5.1 other ADV units showed some characteristic events highlighted by peaks in power spectral density. Figure D-20 shows the spectral analysis of the band-pass horizontal velocity components for ADV placed at z = 0.32 m above the bed. The smoothed curves highlighted some prominent peak in spectral densities corresponding to energetic events. For example, a series of energetic events occurred at a frequency corresponding to period of about 3,400 s. These were observed for both the streamwise velocity and the water level. This period was similar to that of the large period fluctuations observed in the time series of the instantaneous data. The spectral analysis of band-pass velocity components also highlighted other characteristic slow fluctuations with low periods (Fig. D-20). Figures D-21 and D-21 show the spectral analysis of the band-pass longitudinal velocity for ADV units placed at z = 0.42 m and z = 0.55 m respectively from the bed.

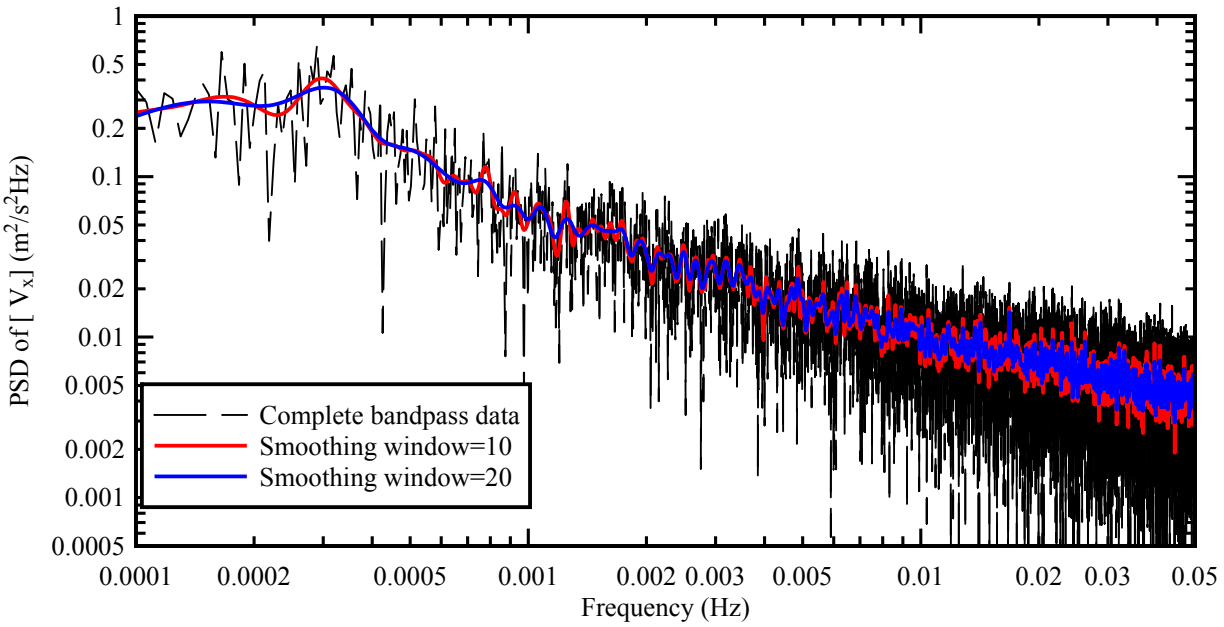

Fig. D-20 - Spectral analysis of fluctuations of longitudinal velocity [V_x] using ADV1. Sampling volume location: 0.32 m above the bed, 11.056 m from left bank.

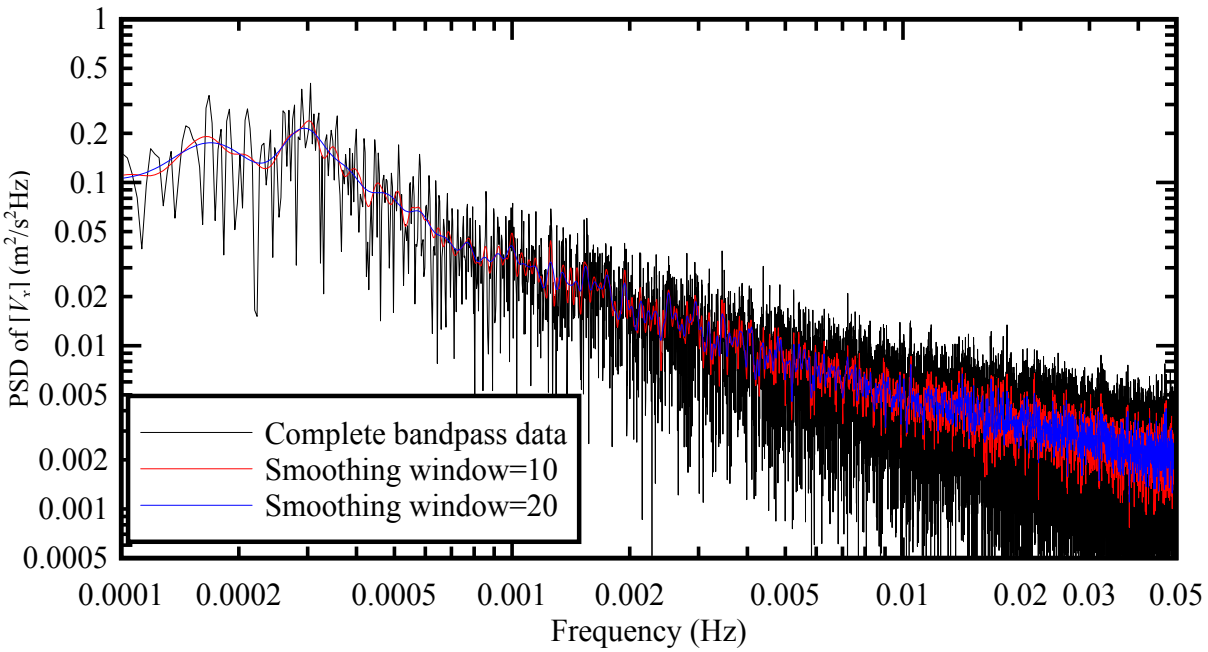

Fig. D-21 - Spectral analysis of fluctuations of longitudinal velocity [V_x] using 2D microADV A641F (16 MHz), scan rate: 50 Hz, Probe sensor: 0.42 m above the bed, 11.042 m from left bank.

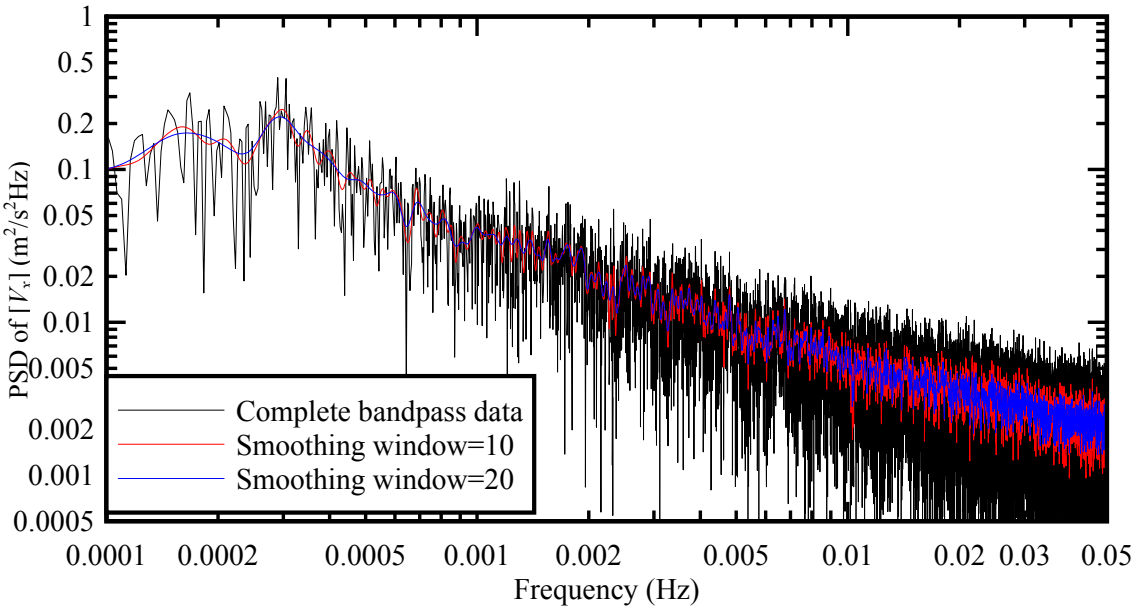

Fig. D-22 - Spectral analysis of fluctuations of longitudinal velocity [V_x] using 3D microADV A843F (16 MHz), scan rate: 50 Hz, Probe sensor: 0.55 m above the bed, 11.05 m from left bank.

APPENDIX E – FIELD DATA AT EPRAPAH CREEK FROM 29/09/2013 TO 1/10/2013

E.1 PRESENTATION

A field study was conducted at Eprapah Creek (Australia) during neap tidal condition between 29 September and 1 October 2013. During the field study three ADV units were sampled at Site 2B that is located 2.1 km upstream of the river mouth. The three ADVs were sampled continuously throughout the field study. Table E-1 shows the information about the ADVs and sampling locations. A triple decomposition technique was applied on the ADV data separating the flow field into the tidal, resonance and true turbulence components using lower and upper cut-off frequency of 0.0001 Hz and 0.1 Hz respectively.

This appendix presents the instantaneous velocities, decomposed velocities, slow fluctuations, standard deviation of fluctuation (slow and fast) and turbulence parameters calculated on the resulting turbulence field.

Table E-1 - Sampling and location information for instruments deployed at Site 2B

Instrument code (1)	Instrument description (2)	Sample location (3)	Sampling frequency (Hz) (4)
ADV1	Sontek 3D-sidelooking microADV A813F (16 MHz)	0.32 m above the bed 11.06 m from the left bank	50
ADV2	Sontek 2D-sidelooking microADV A641F (16 MHz)	0.42 m above the bed 11.04 m from the left bank	50
ADV3	Sontek 3D-downlooking microADV A843F (16 MHz)	0.55 m above the bed 11.05 m from the left bank	50

Notations

R_{ij} Correlation coefficient of Reynolds stress:

$R_{ij} = \frac{\overline{v_i v_j}}{(v_i' v_j')}$; where subscripts i and j represent x,y and z velocities i= j is a normal stress; i≠j is a tangential stress. Subscripts 1,2, and 3 represent the ADV numbers.

T_E Eulerian integral time scale (s);

T_{Ex} Eulerian integral time scale of streamwise velocity (s);

T_{Ey} Eulerian integral time scale of transverse velocity (s);

T_{Ez} Eulerian integral time scale of vertical velocity (s);

V instantaneous velocity (m/s);

V_x instantaneous streamwise velocity (m/s);

V_y instantaneous transverse velocity (m/s);

V_z instantaneous vertical velocity (m/s);

$<V_x>$ tidal component of streamwise velocity (m/s) - low-pass filtered data;

$<V_y>$ tidal component of transverse velocity (m/s) - low-pass filtered data;

$<V_z>$ tidal component of vertical velocity (m/s) - low-pass filtered data;

$[V_x]$ slow fluctuating of component of streamwise velocity (m/s) - band-pass data;

$[V_y]$ slow fluctuating of transverse velocity (m/s) – band-pass data;

$[V_z]$ slow fluctuating of vertical velocity (m/s) – band-pass data;

v_x streamwise turbulence velocity (m/s) – high-pass filtered data;

v_y transverse turbulence velocity (m/s) – high-pass filtered data;

v_z vertical turbulence velocity (m/s) – high-pass filtered data;

$\dot{v_i}$ standard deviation of velocity (m/s); i = x, y or z component;

z elevation of instrument from the bed;

δ small change;

ε wind effect '*Leeway*' [-]

$\rho v_i v_j$ instantaneous Reynolds stress (Pa); i = x, y or z component; j = x, y or z component;

τ lag (s);

τ_E Eulerian dissipation time scale (s);

τ_{Ex} Eulerian dissipation time scale of streamwise velocity (s);

τ_{Ey} Eulerian dissipation time scale of transverse velocity (s);

τ_{Ez} Eulerian integral time scale of vertical velocity (s);

ø diameter;

ζ_{ij} Reynolds stress tensor

Calculation of time scales

The characteristic time scales were calculated from the autocorrelation function of the turbulent velocities. The normalised autocorrelation function, R describes the evolution of the turbulence field with time. R describes how a turbulence velocity correlates with values at difference times. For example, R_{xx} is defined as:

$$R_{xx}(\tau) = \frac{\overline{v_x(t)v_x(t+\tau)}}{\overline{v_x^2}} \qquad \text{(E-1)}$$

where τ is the time lag. The integral time scale is a measure of the correlation time between turbulent velocities. The integral length scale, e.g. T_{Ex} is integral of the autocorrelation function which is obtained herein by numerical integration. The integral of the autocorrelation function is

time dependent and does not approach a constant upper bound. Herein, integration was performed only up to the time of the first zero crossing using a maximum time lag of 10 s ([29]).

The dissipation time scale, also known as Taylor's micro scale is a measure of the most rapid changes that occur in the turbulence velocity. The dissipation time scale, e.g. τ_{Ex} may be estimated from the curvature of the autocorrelation function in the neighbourhood of $\tau = 0$ (Hinze, 1975). For a data sampled every time interval δt, $\tau_{Ex}^{(\delta t)}$ may be described based upon sampling interval δt:

$$\tau_{Ex}^{(\delta t)} = \sqrt{2 \times \frac{\overline{v_x^2}}{\overline{\left(\frac{\delta v_x}{\delta t}\right)^2}}} \qquad \text{(E-2)}$$

The calculation of $\tau_{Ex}^{(\delta t)}$ is repeated for several sampling intervals and may be approximated by a quadratic function (Eqn. E-3) (Fransson et al., 2005, Chanson, 2009):

$$\tau_{Ex}^{(\delta t)} = \tau_{Ex} + a(\delta t) + b(\delta t^2) \qquad \text{(E-3)}$$

That is, τ_{Ex} is the limit of $\tau_{Ex}^{(\delta t)}$ when δt tends to zero.

E-2 ADV DATA

E.2.1 Acoustic Doppler velocimeter, ADV 1 sampled at 0.32 m above the bed

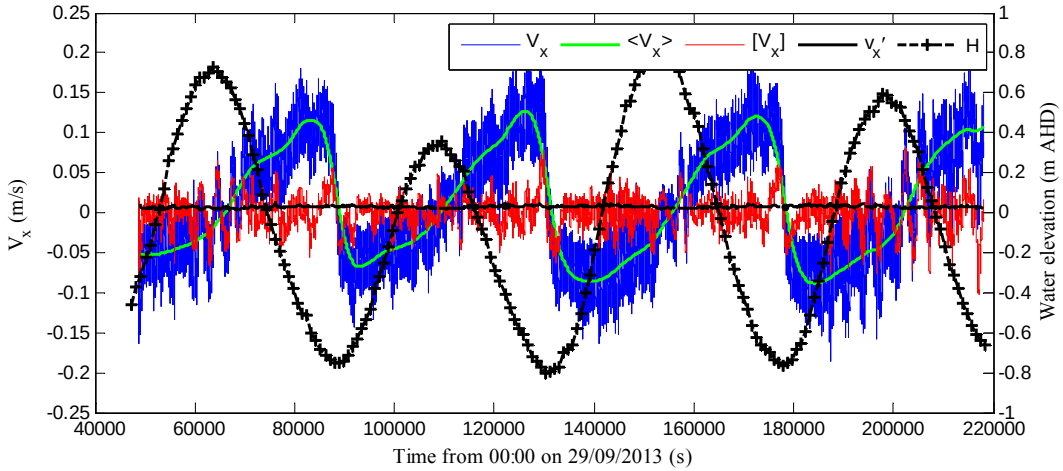

(A) Streamwise velocity

[29] Previous studies in Eprapah Creek reported integral time scales less than 3 s. A fixed time lag of 10 s was chosen to save computation times and to avoid the introduction of large uncorrelated processes.

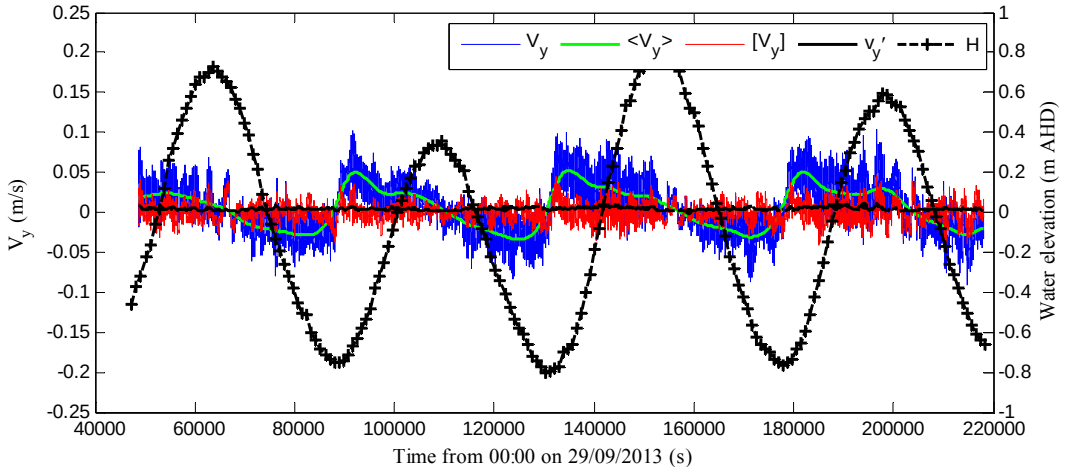

(B) Transverse velocity

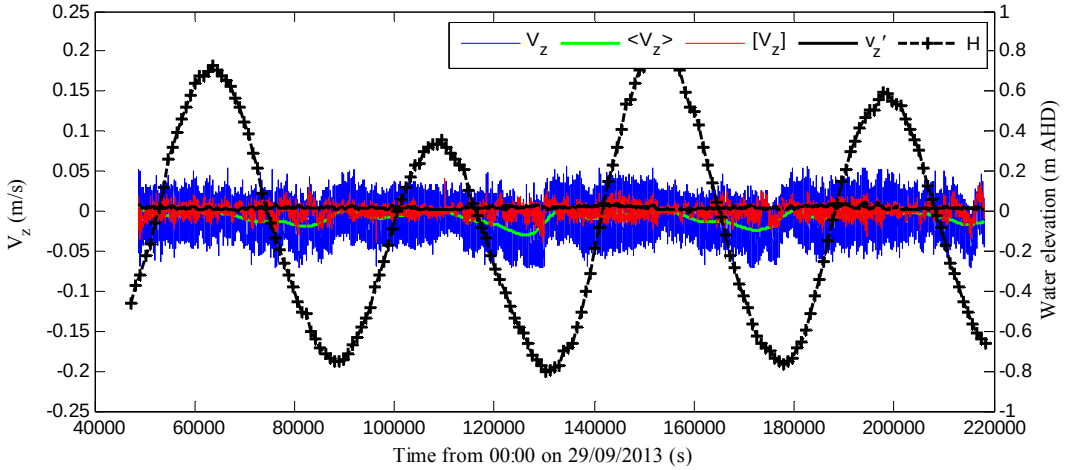

(C) Vertical velocity

Fig. E-1 - Instantaneous and decomposed velocity components as functions of time; using 3D microADV A813F (16 MHz), scan rate: 50 Hz, Probe sensor: 0.32 m above the bed, 11.056 m from left bank.

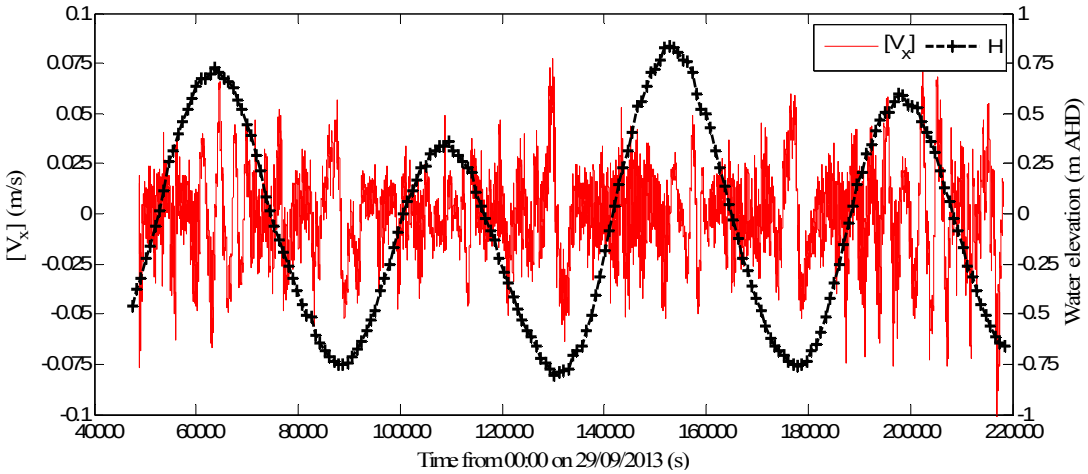

Fig. E-2- Streamwise slow fluctuating velocity as functions of time; using 3D microADV A813F (16 MHz), scan rate: 50 Hz, Probe sensor: 0.32 m above the bed, 11.056 m from left bank

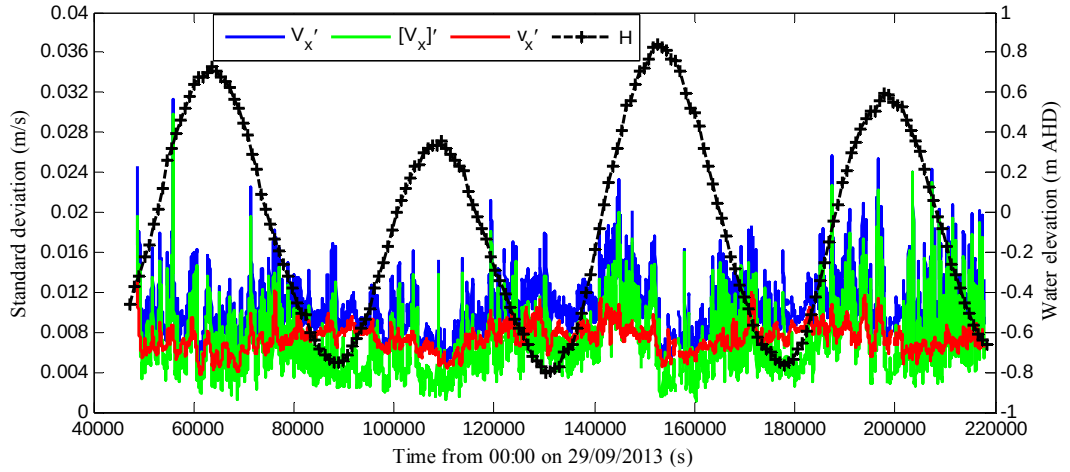

(A) Streamwise velocity standard deviation

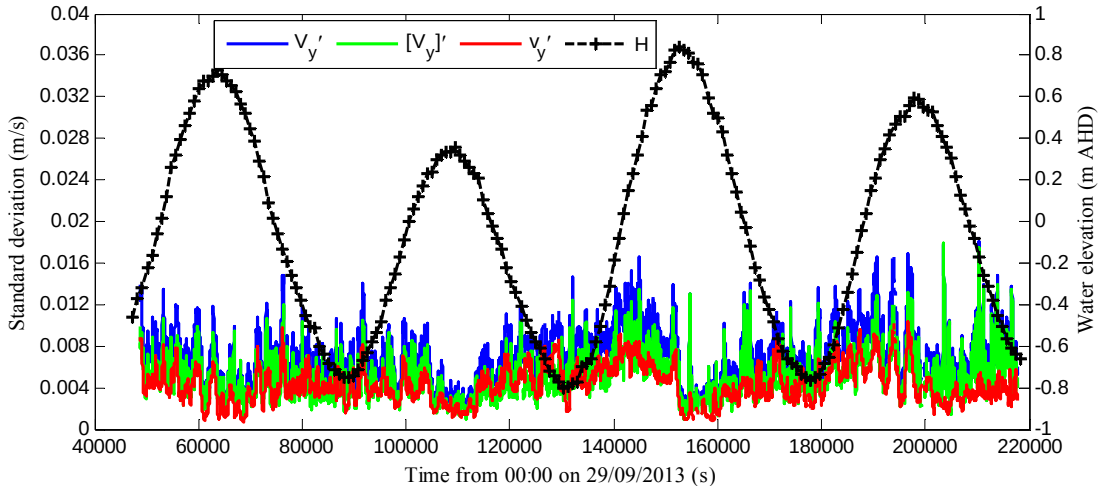

(B) Transverse velocity standard deviation

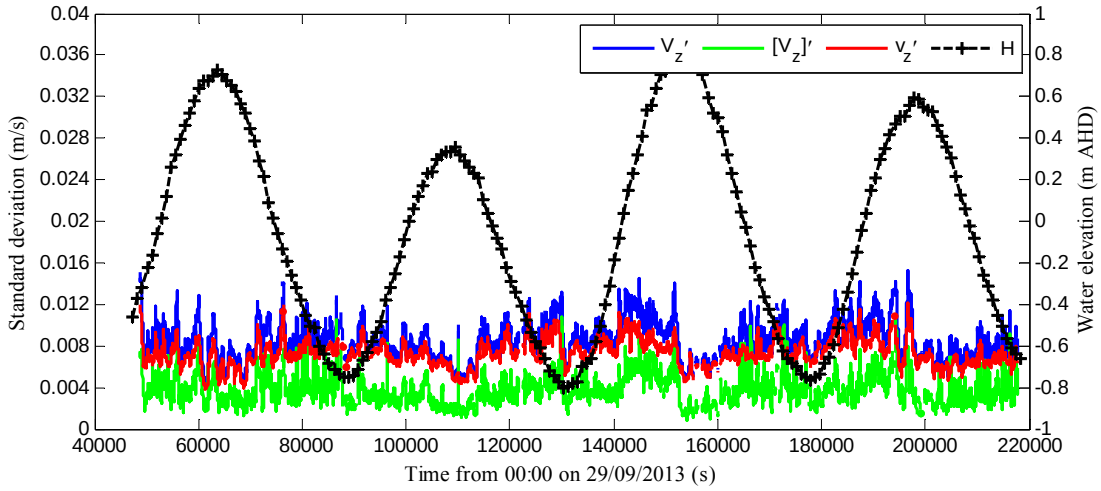

(C) Vertical velocity standard deviation

Fig. E-3 - Standard deviation of velocity fluctuation as functions of time; using 3D microADV A813F (16 MHz), scan rate: 50 Hz, Probe sensor: 0.32 m above the bed, 11.056 m from left bank; Data based on 10,000 samples (200 s) every 10 s along the entire data set

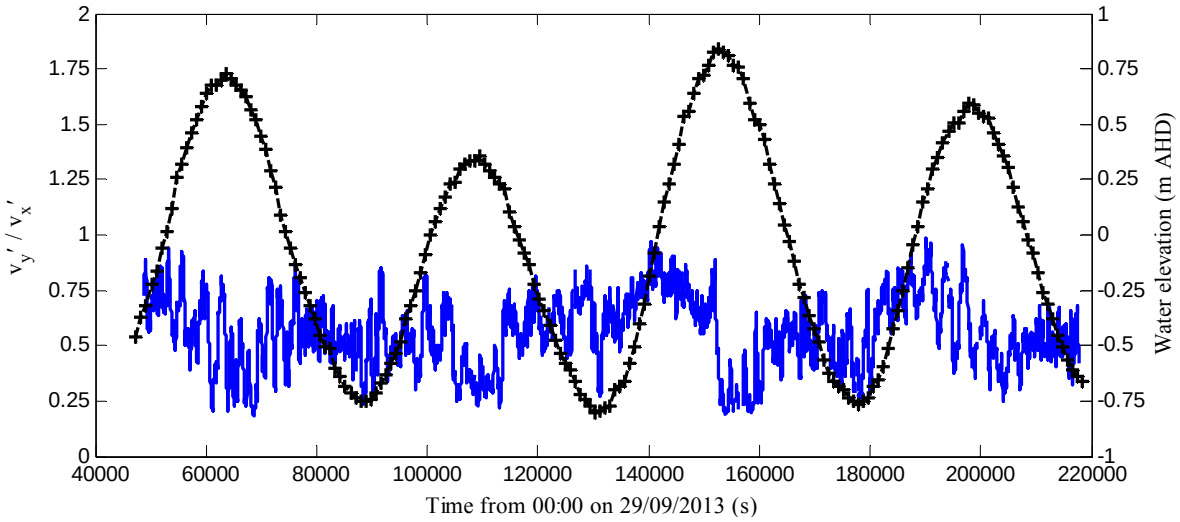

(A) Horizontal turbulence ratio

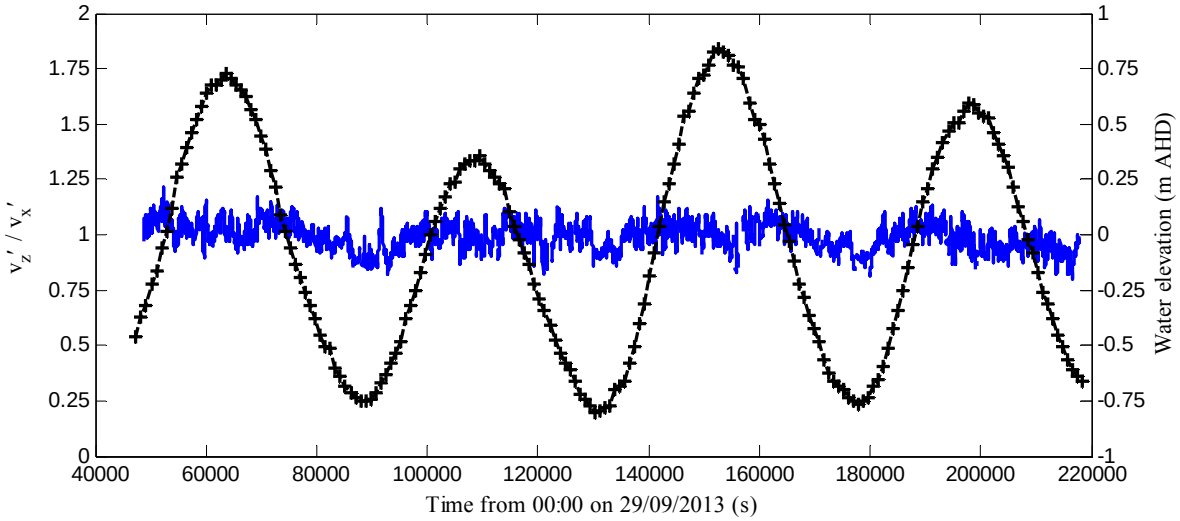

(B) Vertical turbulence ratio

Fig. E-4 - Turbulence intensity as functions of time; using 3D microADV A813F (16 MHz), scan rate: 50 Hz, Probe sensor: 0.32 m above the bed, 11.056 m from left bank; Data based on 10,000 samples (200 s) every 10 s along the entire data set

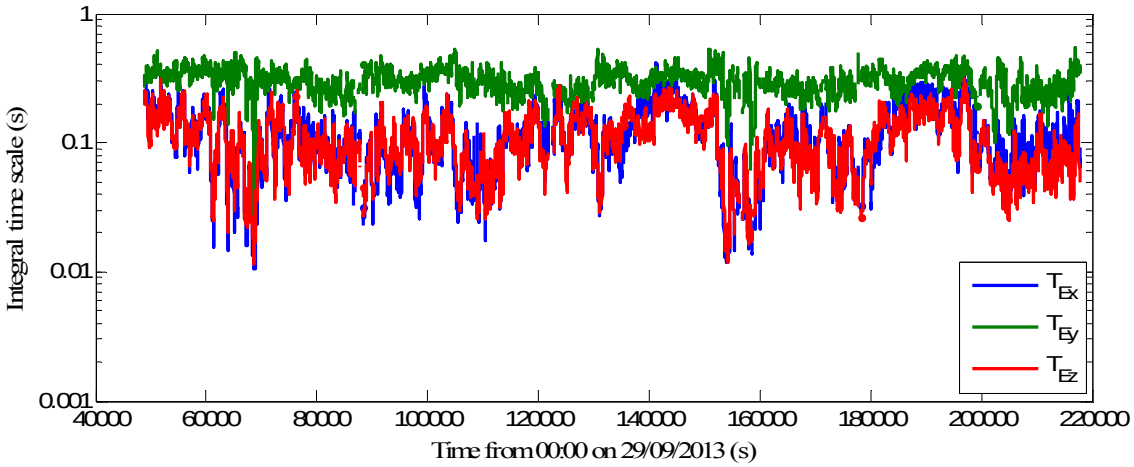

(A) Integral time scale

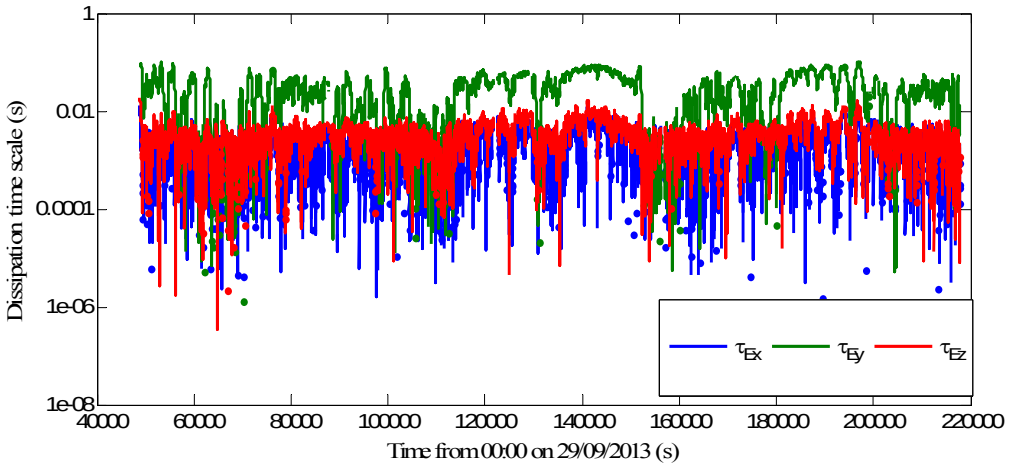

(B) Dissipation time scale

Fig. E-4 - Time scales as functions of time; using 3D microADV A813F (16 MHz), scan rate: 50 Hz, Probe sensor: 0.32 m above the bed, 11.056 m from left bank; Data based on 10,000 samples (200 s) every 10 s along the entire data set

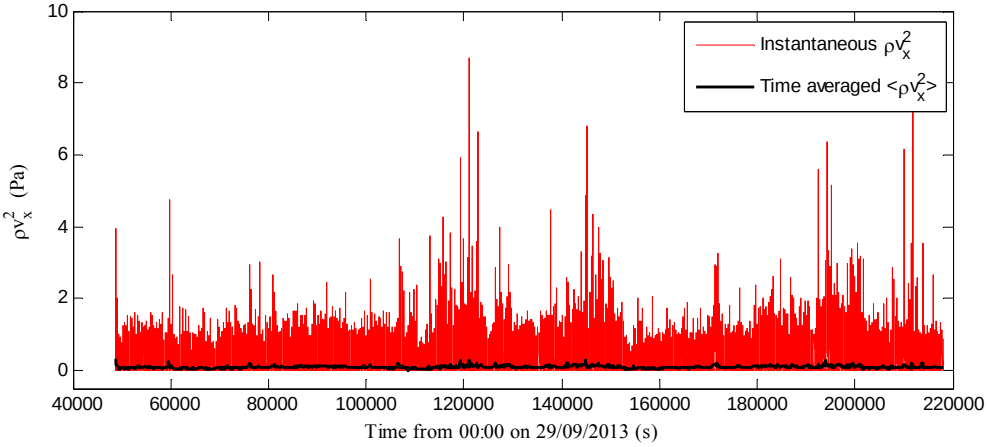

(A) ρv_x^2

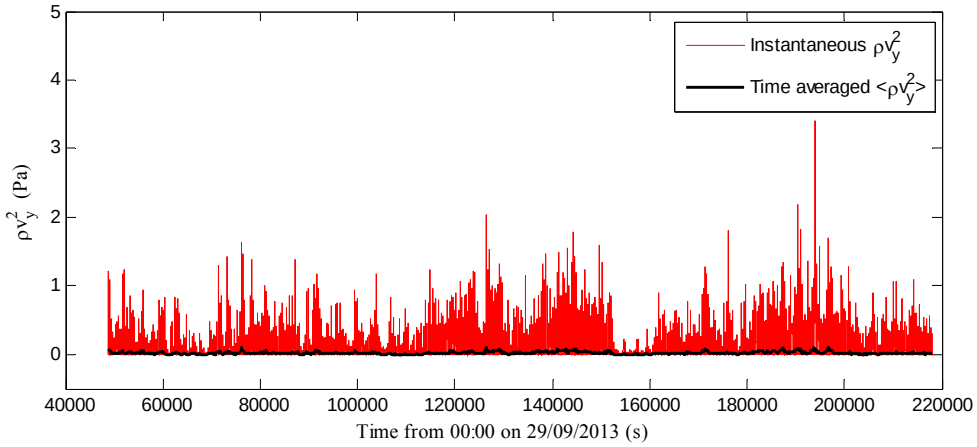

(B) ρv_y^2

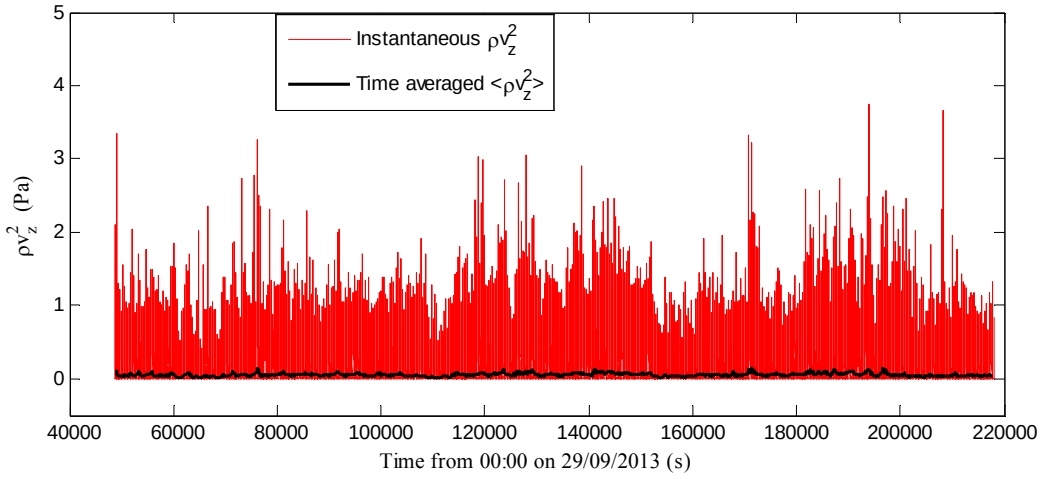

(C) ρv_z^2

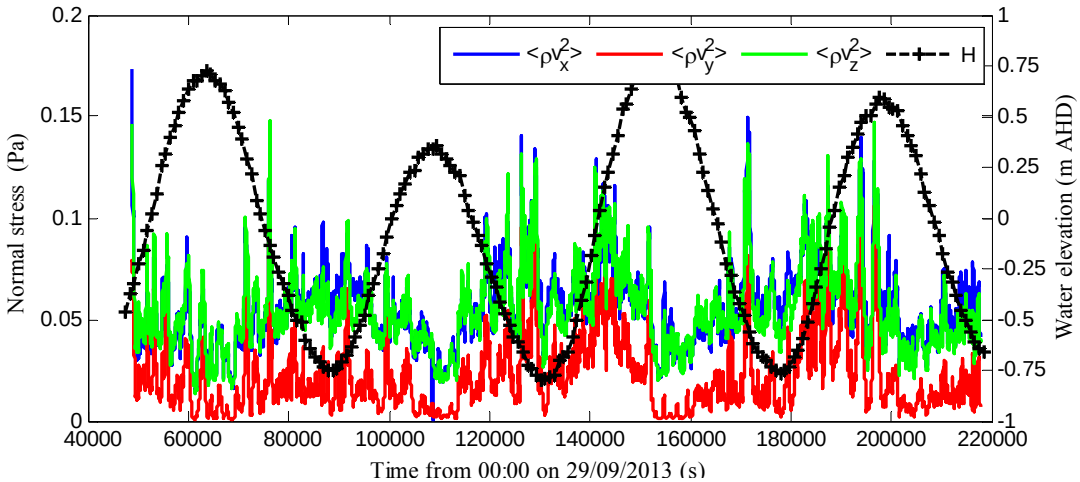

(D) Time-averaged normmal stresses

Fig. E-5 - Instantaneous and time-averaged Normal stresses as functions of time; using 3D microADV A813F (16 MHz), scan rate: 50 Hz, Probe sensor: 0.32 m above the bed, 11.056 m from left bank; Time-averaged based upon 10,000 samples (200 s) every 10 s along the entire data set

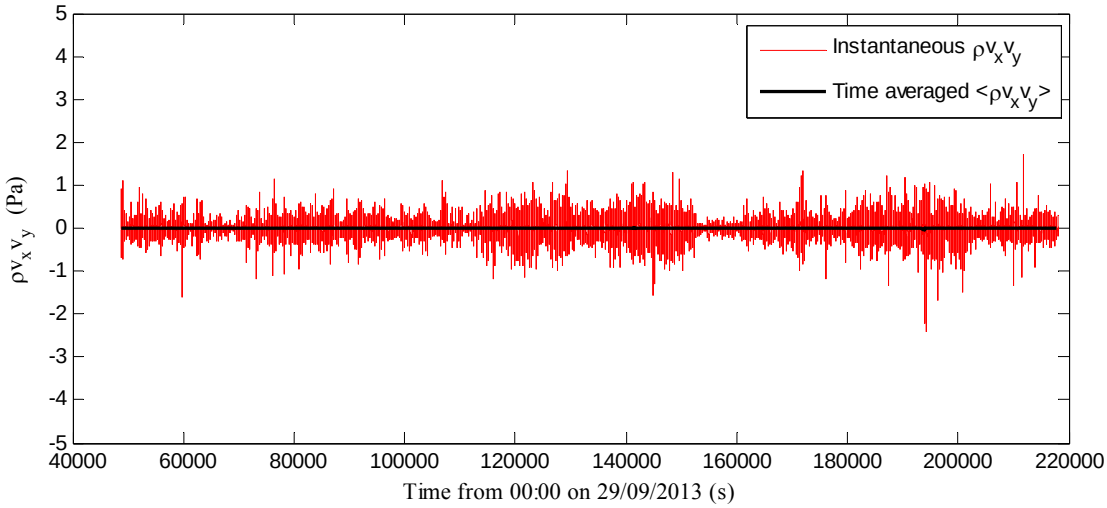

(A) $\rho v_x v_y$

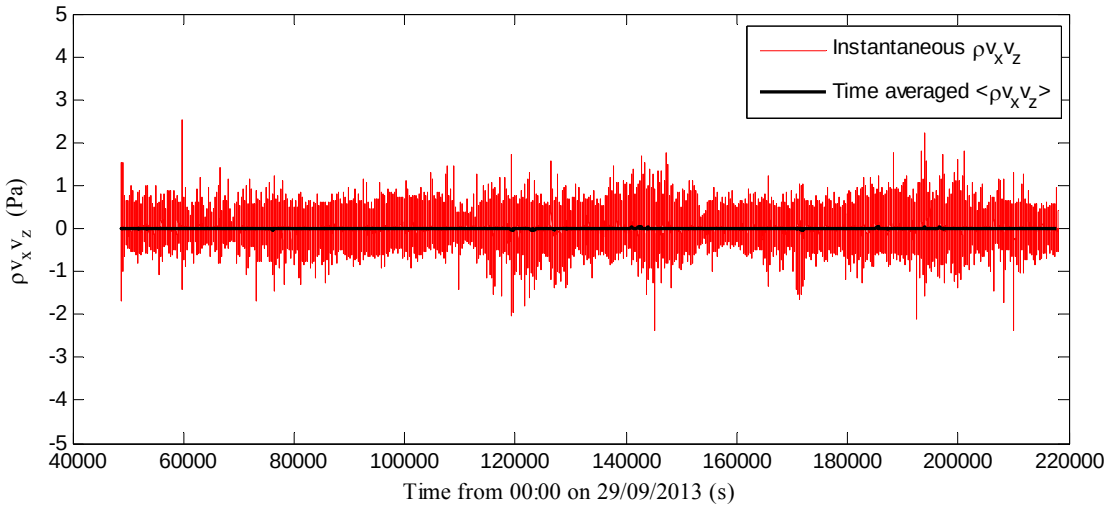

(B) $\rho v_x v_z$

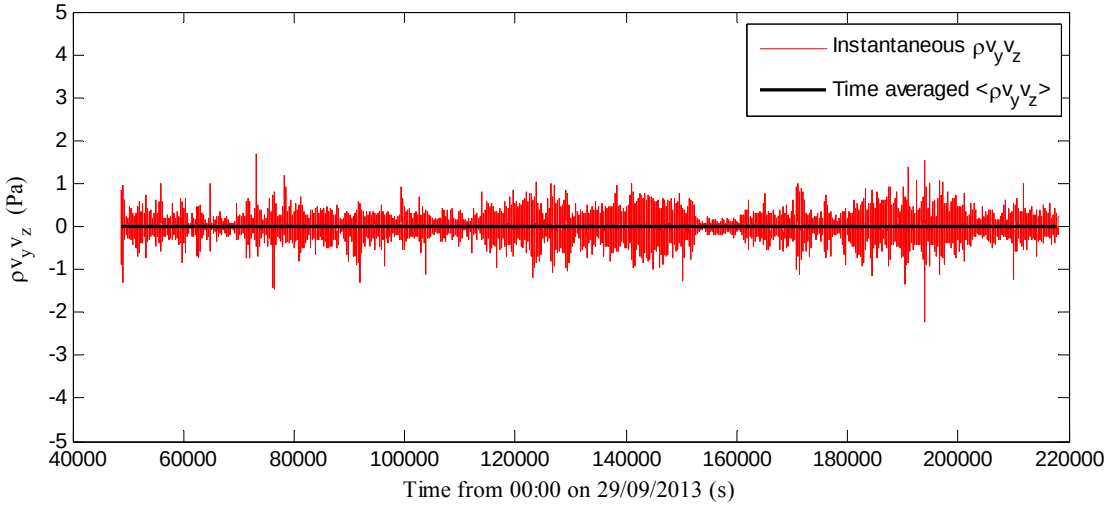

(C) $\rho v_y v_z$

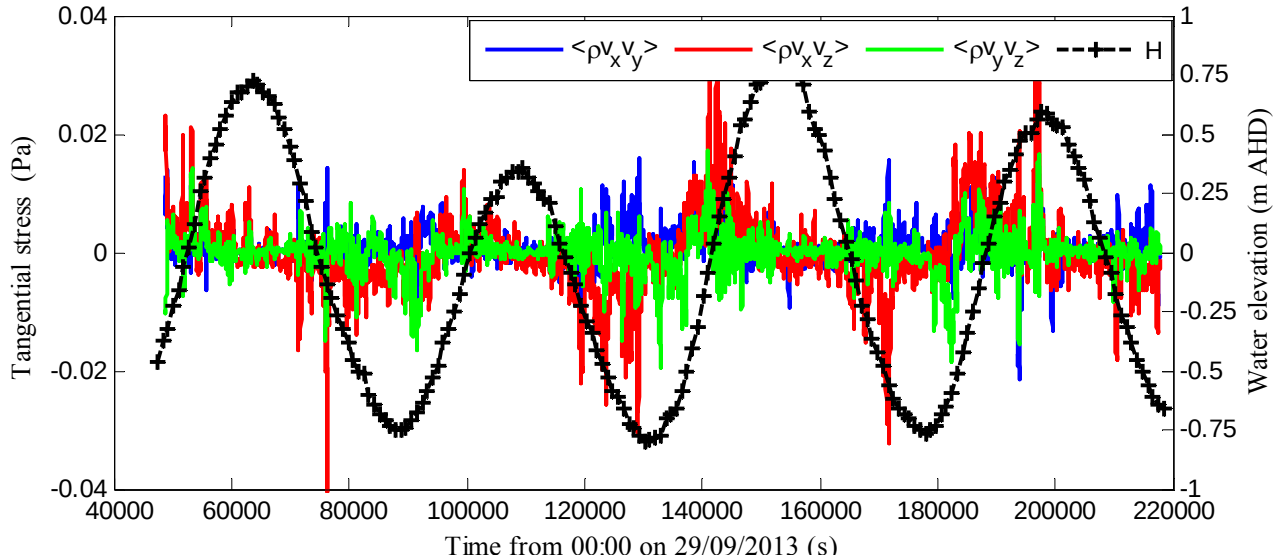

(D) Time-averaged tangential stresses

Fig. E-6 - Instantaneous and time-averaged tangential stresses as functions of time; using 3D microADV A813F (16 MHz), scan rate: 50 Hz, Probe sensor: 0.32 m above the bed, 11.056 m from left bank; Time-averaged based upon 10,000 samples (200 s) every 10 s along the entire data set

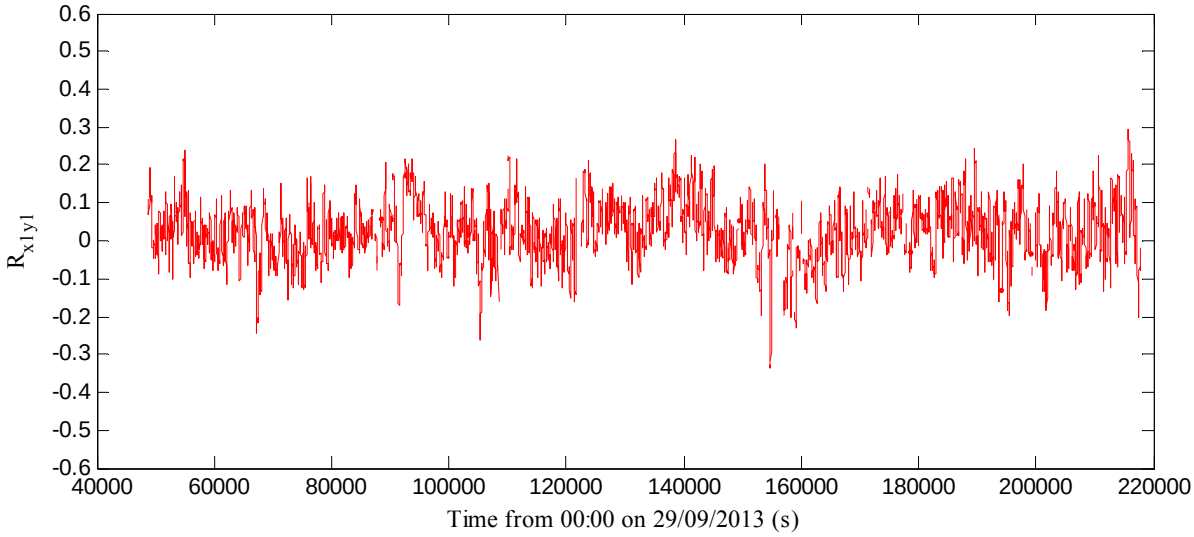

(A) Normal correlation coefficient

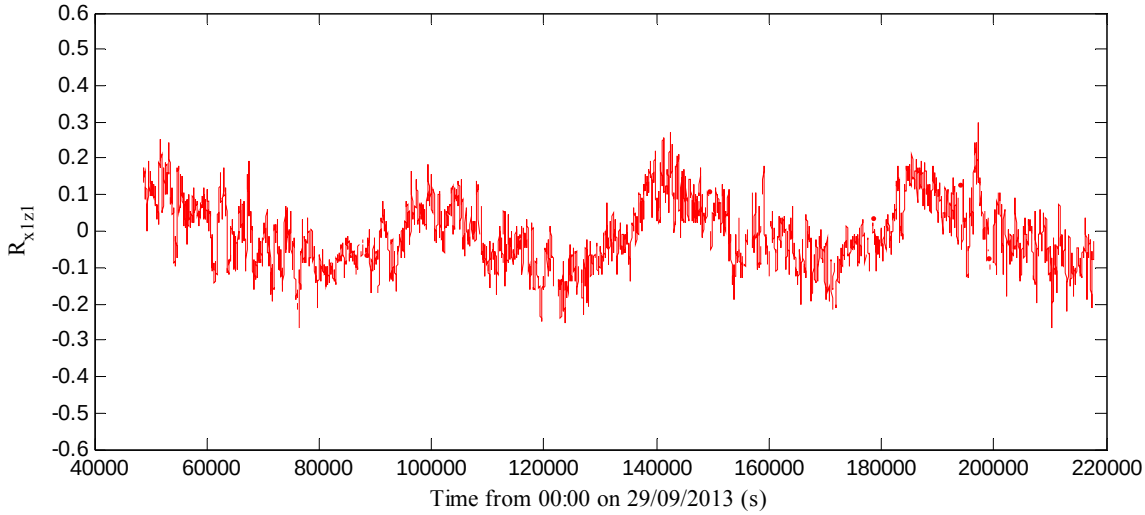

(B) Transverse correlation coefficient

Fig. E-7 - Correlation coefficients as functions of time; using 3D microADV A813F (16 MHz), scan rate: 50 Hz, Probe sensor: 0.32 m above the bed, 11.056 m from left bank; Data based upon 10,000 samples (200 s) every 10 s along the entire data set

E.2.2 Acoustic Doppler velocimeter, ADV 2 sampled at 0.42 m above the bed

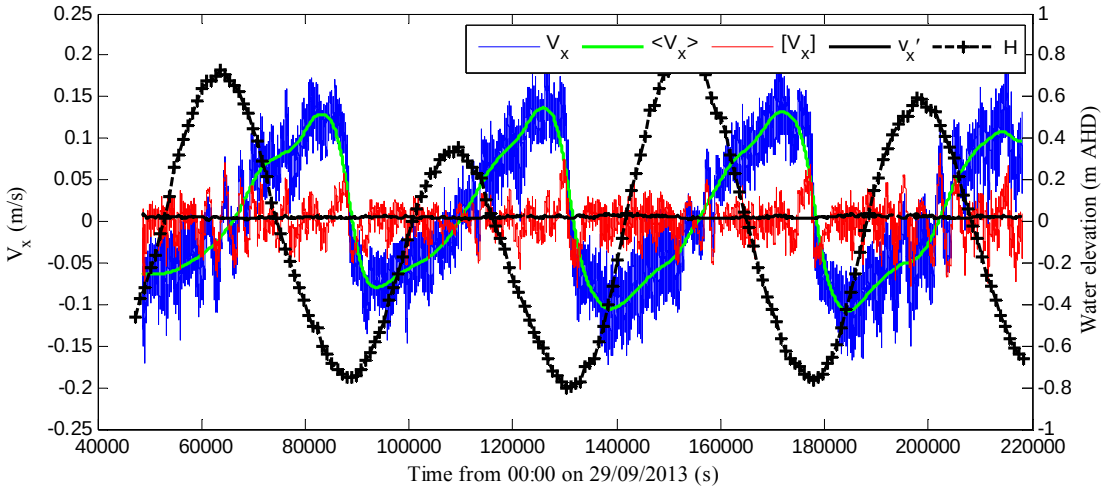

(A) Streamwise velocity

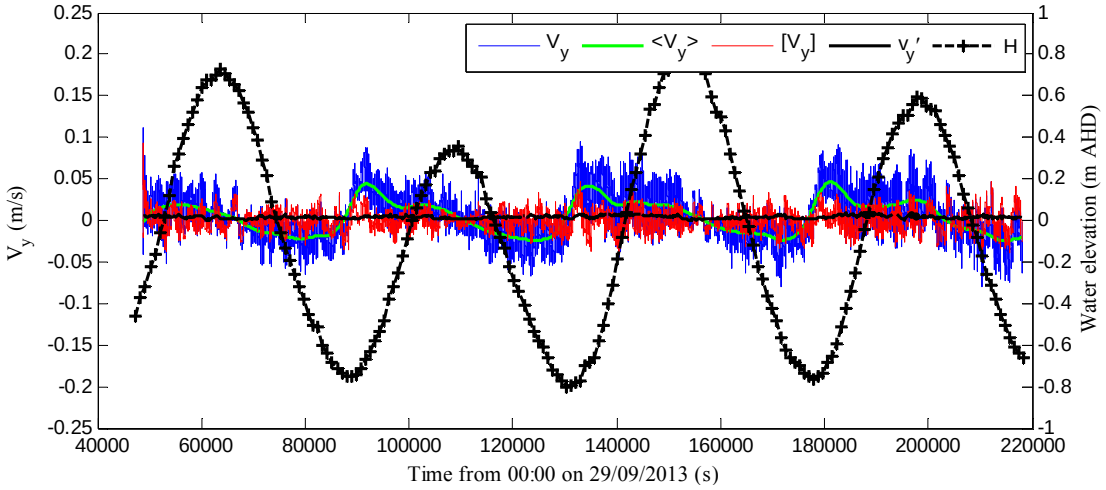

(B) Transverse velocity

Fig. E-8 - Instantaneous and decomposed velocity components as functions of time; using 2D microADV A641F (16 MHz), scan rate: 50 Hz, Probe sensor: 0.42 m above the bed, 11.042 m from left bank

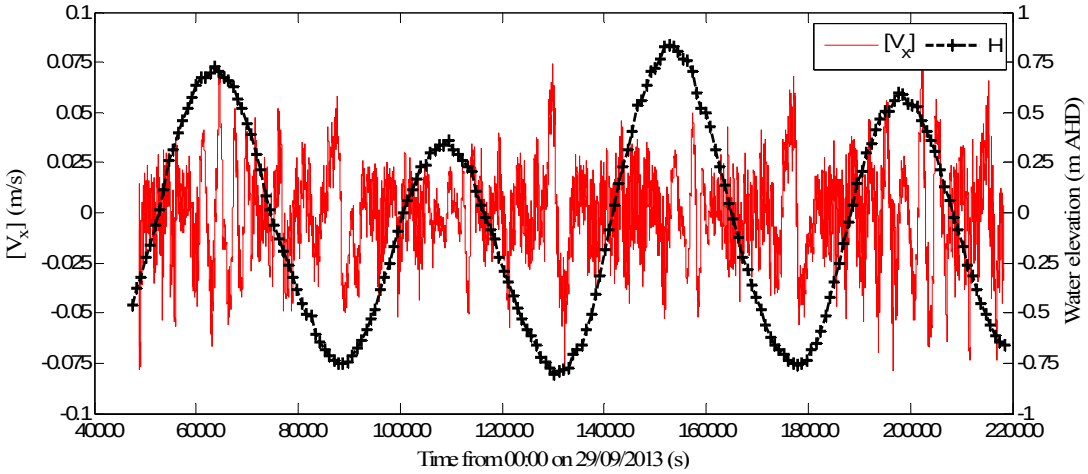

Fig. E-9 - Streamwise slow fluctuating velocity as functions of time; using 2D microADV A641F (16 MHz), scan rate: 50 Hz, Probe sensor: 0.42 m above the bed, 11.042 m from left bank

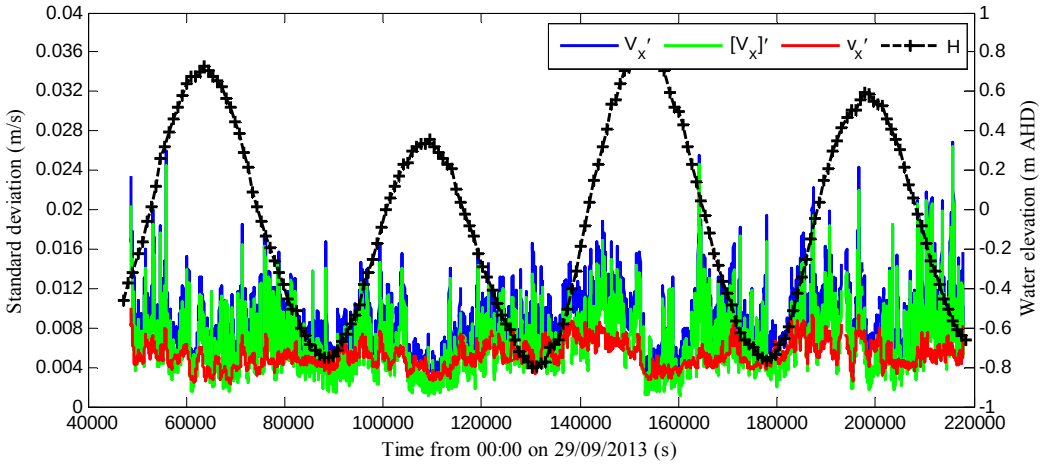

(D) Streamwise velocity standard deviation

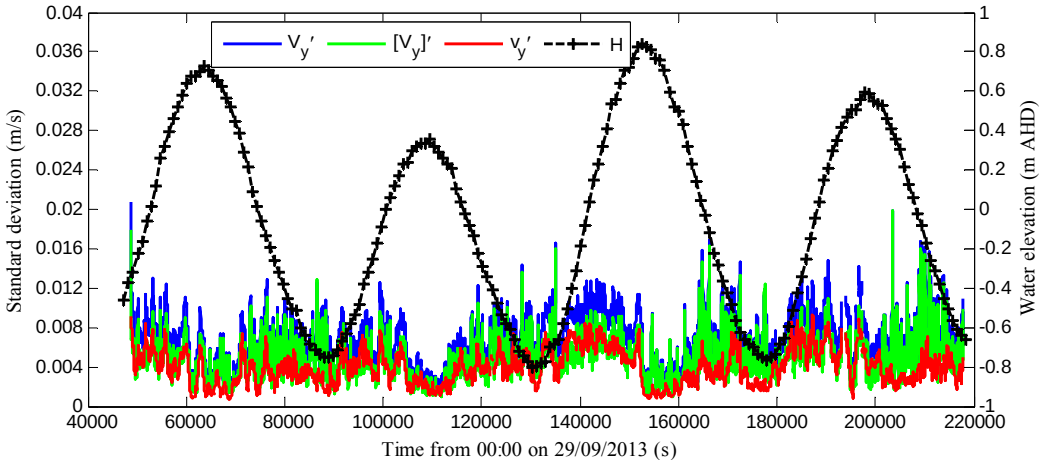

(E) Transverse velocity standard deviation

Fig. E-10 - Standard deviation of velocity fluctuation as functions of time; using 2D microADV A641F (16 MHz), scan rate: 50 Hz, Probe sensor: 0.42 m above the bed, 11.042 m from left bank; Data based on 10,000 samples (200 s) every 10 s along the entire data set

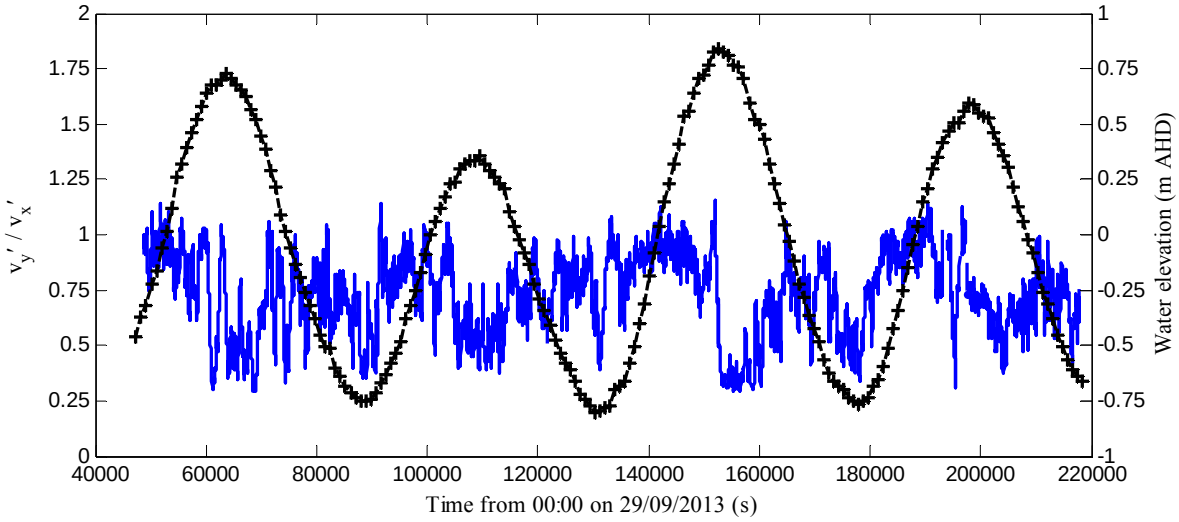

Fig. E-11 - Horizontal turbulence intensity as functions of time; using 2D microADV A641F (16 MHz), scan rate: 50 Hz, Probe sensor: 0.42 m above the bed, 11.042 m from left bank; Data based on 10,000 samples (200 s) every 10 s along the entire data set

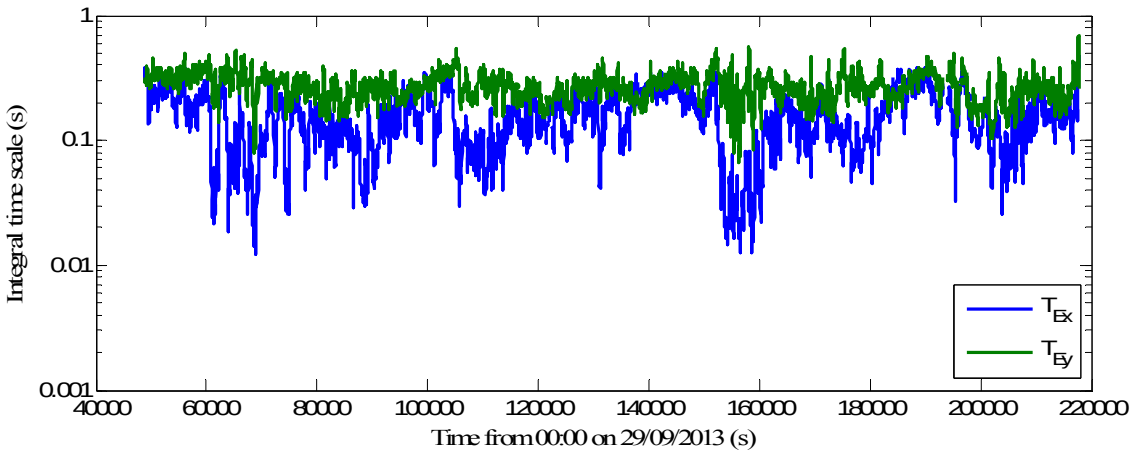

(A) Integral time scale

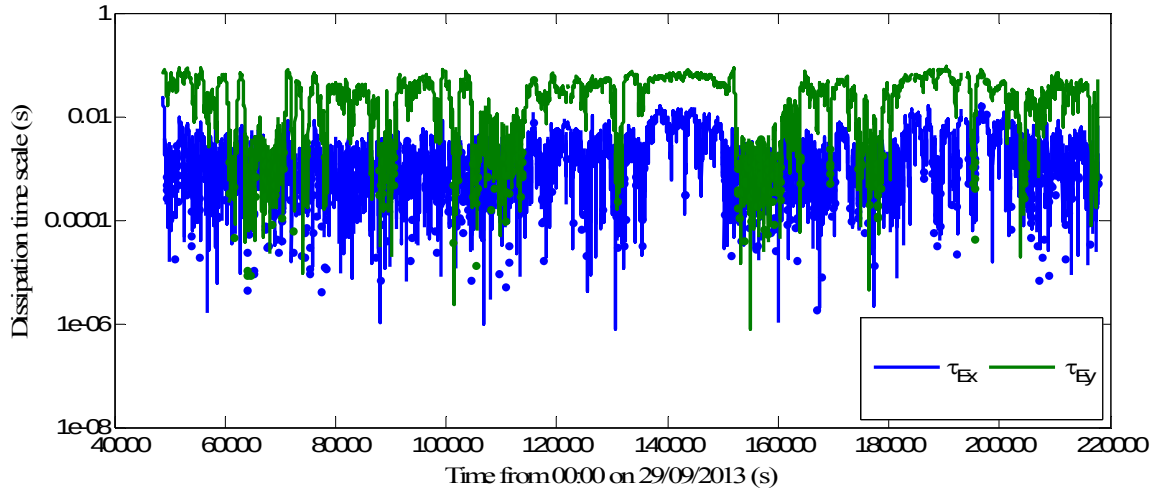

(B) Dissipation time scale

Fig. E-12 - Integral time scale as functions of time; using 2D microADV A641F (16 MHz), scan rate: 50 Hz, Probe sensor: 0.42 m above the bed, 11.042 m from left bank; Data based on 10,000 samples (200 s) every 10 s along the entire data set

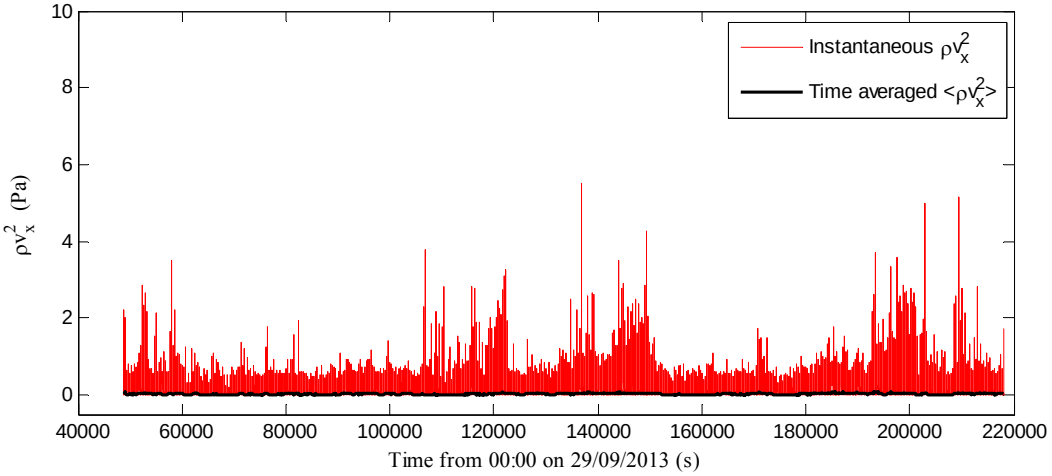

(A) ρv_x^2

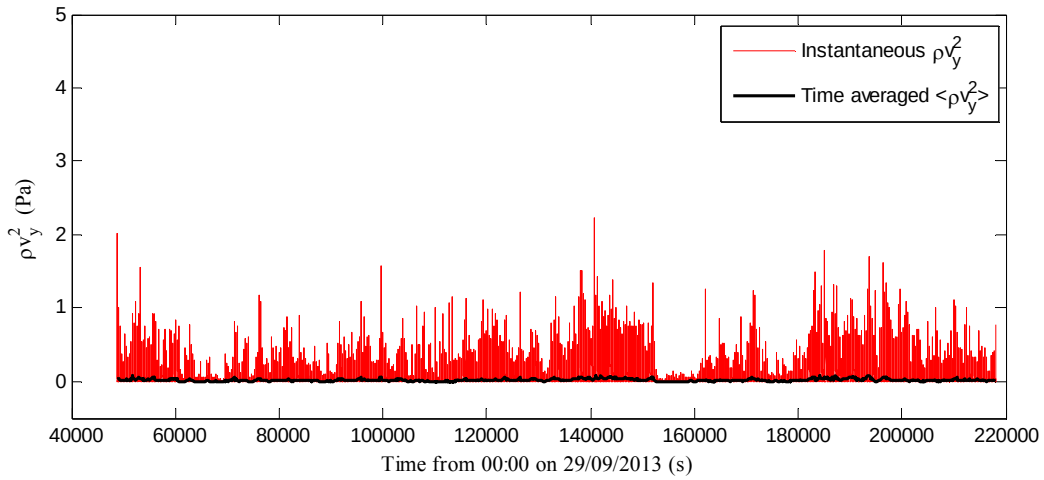

(B) ρv_y^2

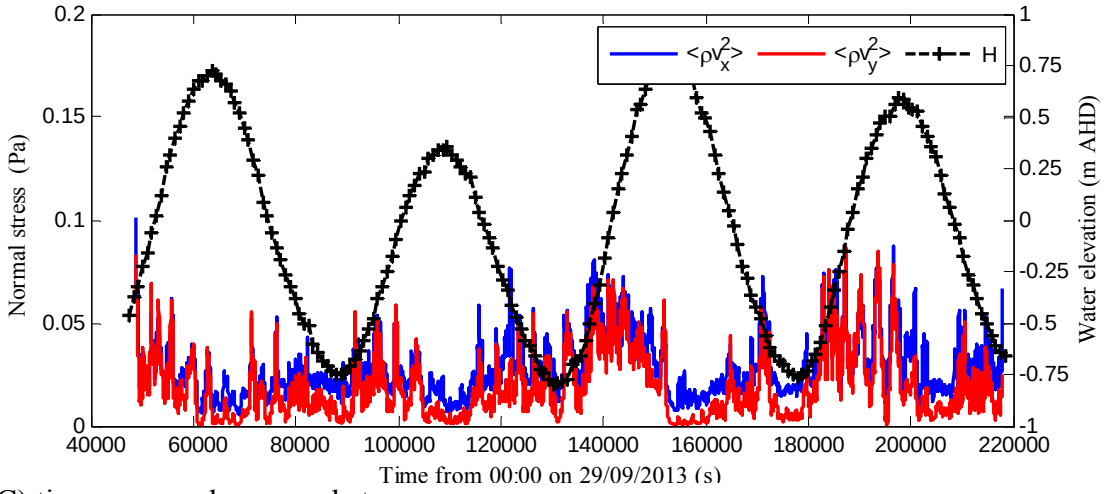

(C) time averaged normmal stresses

Fig. E-13 - Instantaneous and time-averaged Normal stresses as functions of time; using 3D microADV A813F (16 MHz), scan rate: 50 Hz, Probe sensor: 2D microADV A641F (16 MHz), scan rate: 50 Hz, Probe sensor: 0.42 m above the bed, 11.042 m from left bank; Time-averaged based upon 10,000 samples (200 s) every 10 s along the entire data set

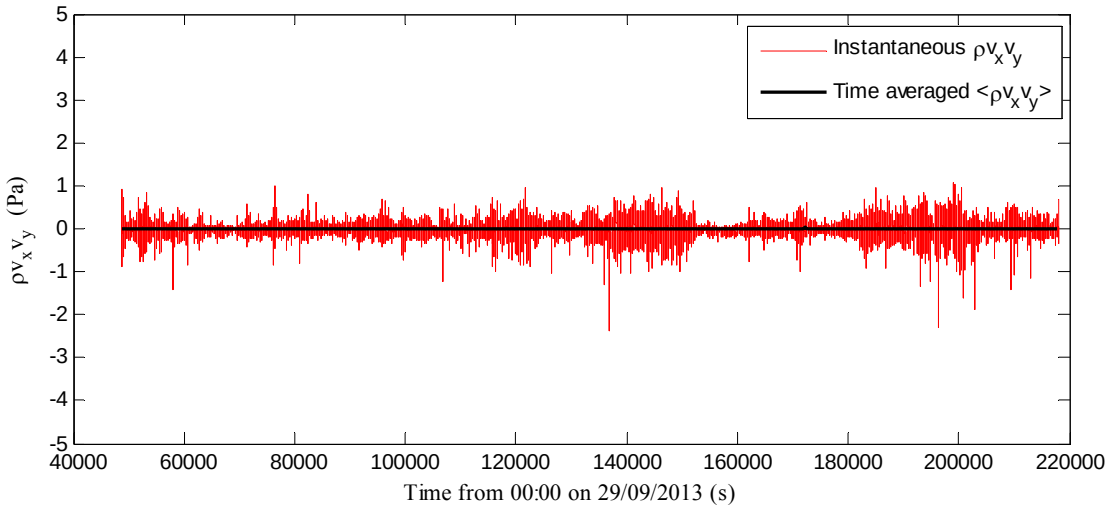

(A) $\rho v_x v_y$

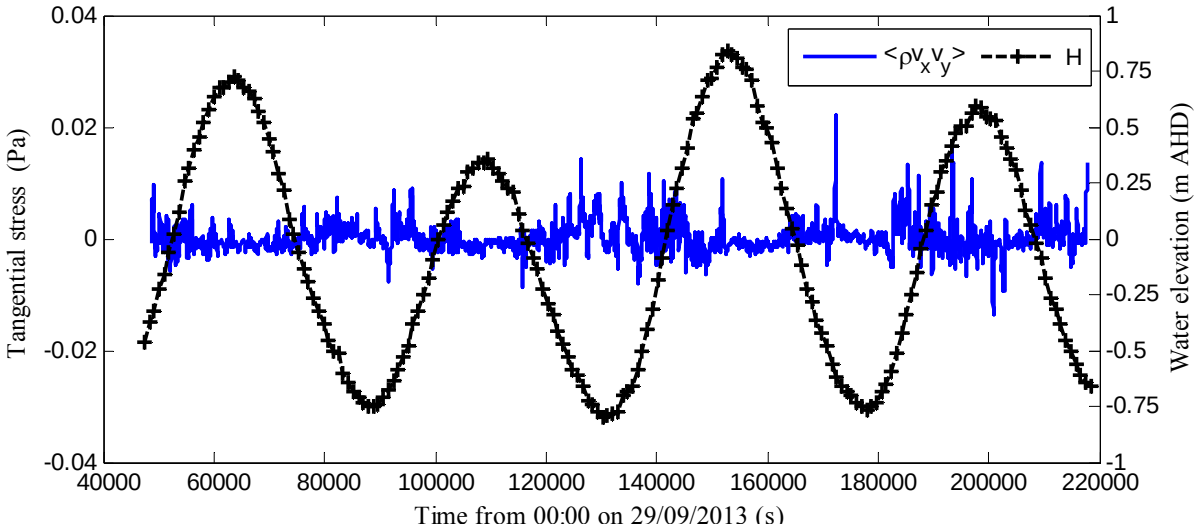

(B) Time-averaged tangential stress

Fig. E-14 - Instantaneous and time-averaged tangential stress as functions of time; using 2D microADV A641F (16 MHz), scan rate: 50 Hz, Probe sensor: 0.42 m above the bed, 11.042 m from left bank; Time-averaged based upon 10,000 samples (200 s) every 10 s along the entire data set

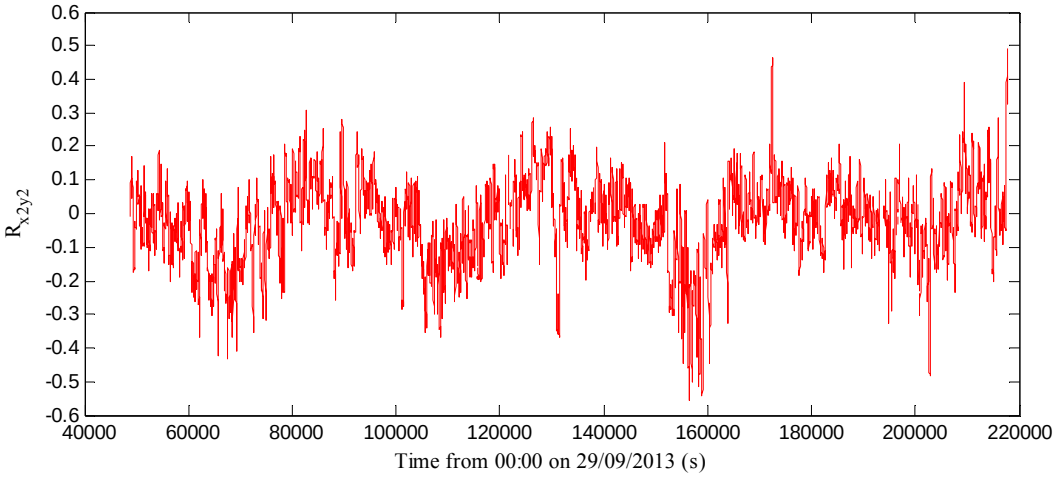

Fig. E-15 - Correlation coefficient, R_{xy} as a function of time; using 2D microADV A641F (16 MHz), scan rate: 50 Hz, Probe sensor: 0.42 m above the bed, 11.042 m from left bank; Data based upon 10,000 samples (200 s) every 10 s along the entire data set

E.2.3 Acoustic Doppler velocimeter, ADV 3 sampled at 0.55 m above the bed

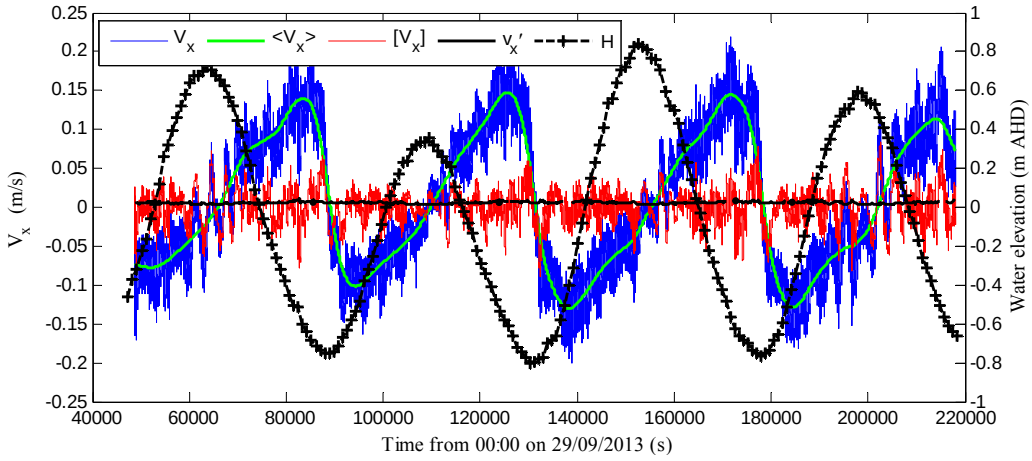

(A) Streamwise velocity

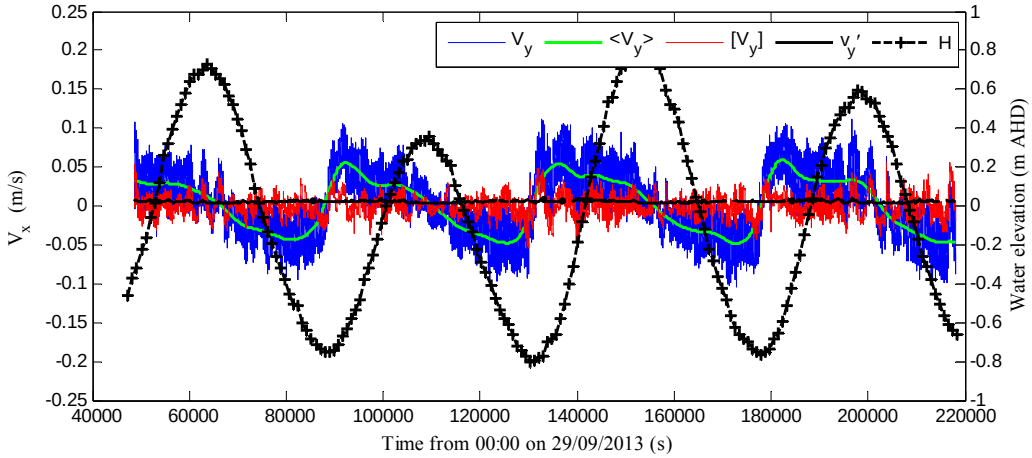

(B) Transverse velocity

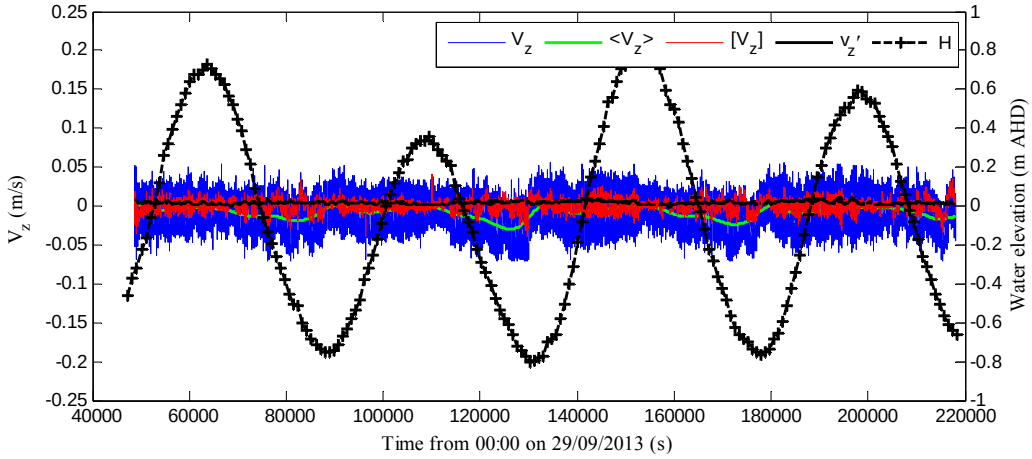

(C) Vertical velocity

Fig. E-16 - Instantaneous and decomposed velocity components as functions of time; using 3D microADV A843F (16 MHz), scan rate: 50 Hz, Probe sensor: 0.55 m above the bed, 11.056 m from left bank

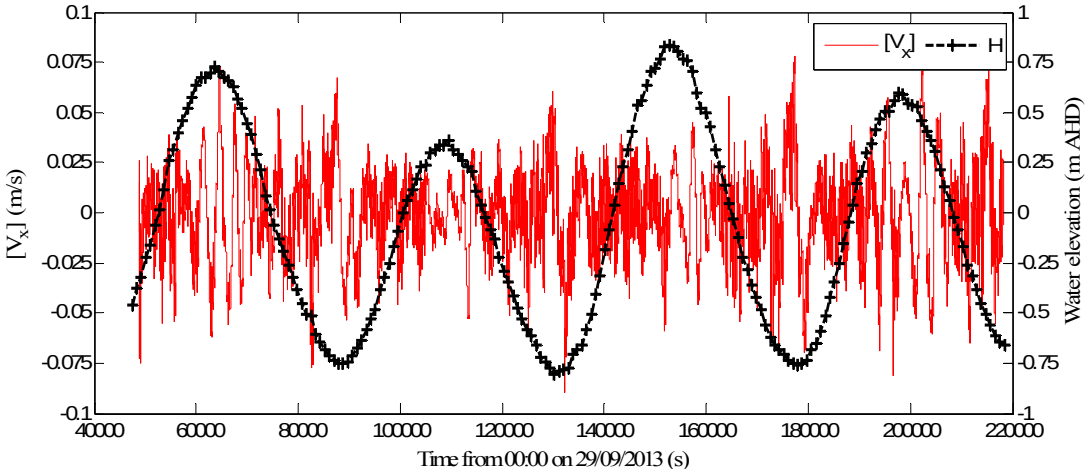

Fig. E-17- Streamwise slow fluctuating velocity as a function of time; using 3D microADV A843F (16 MHz), scan rate: 50 Hz, Probe sensor: 0.55 m above the bed, 11.056 m from left bank

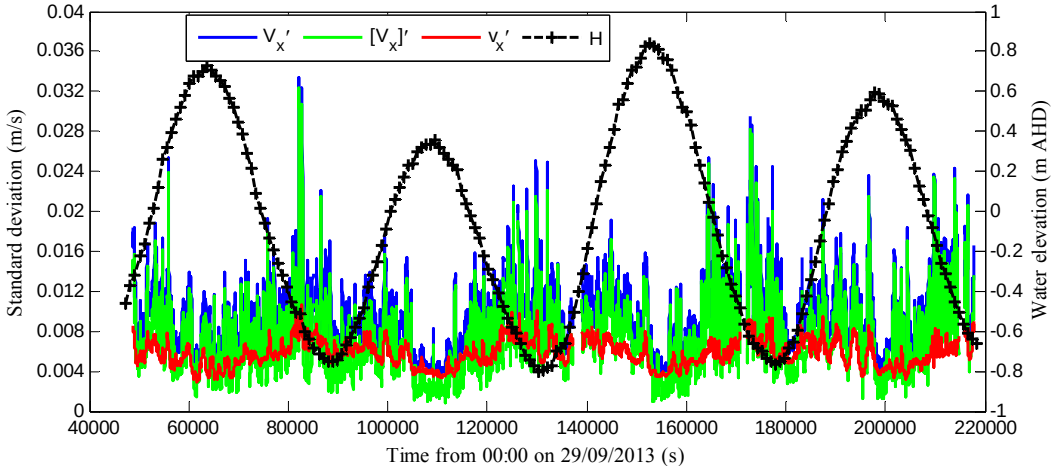

(A) Streamwise velocity standard deviation (m/s)

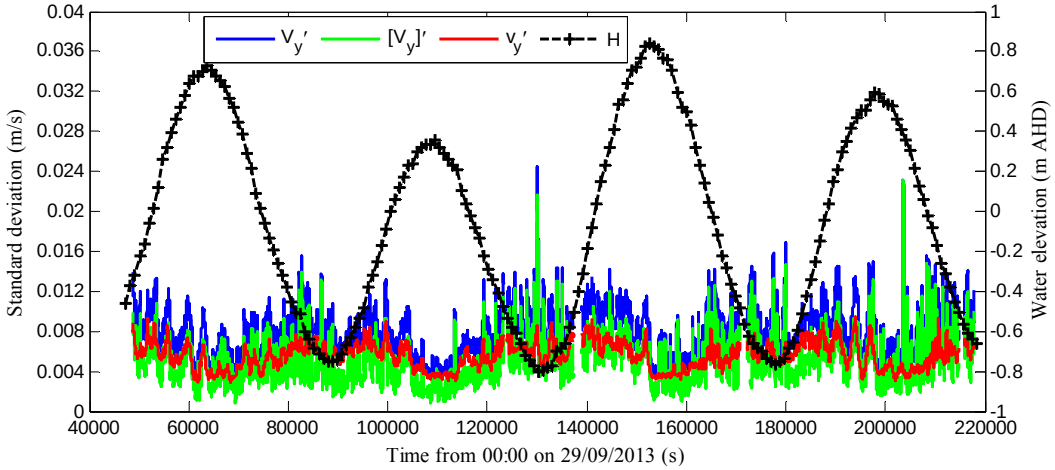

(B) Transverse velocity standard deviation (m/s)

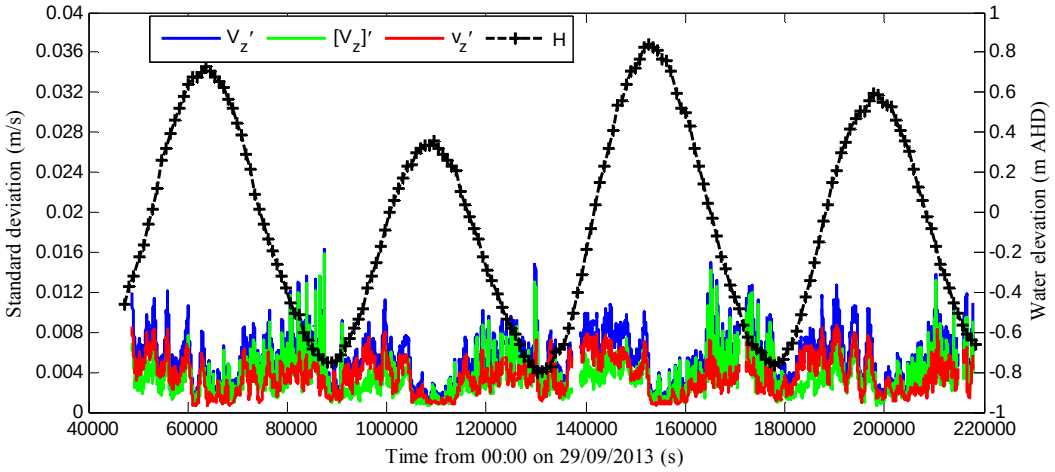

(C) Vertical velocity standard deviation

Fig. E-18 - Standard deviation of velocity fluctuation as functions of time; using 3D microADV A843F (16 MHz), scan rate: 50 Hz, Probe sensor: 0.55 m above the bed, 11.056 m from left bank; Data based on 10,000 samples (200 s) every 10 s along the entire data set

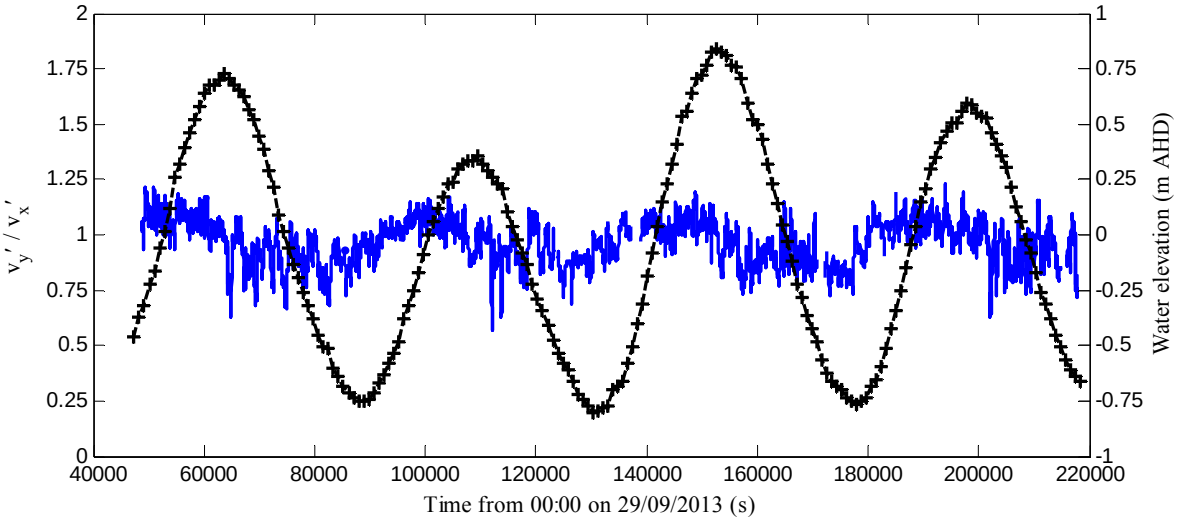

(A) Horizontal turbulence ratio

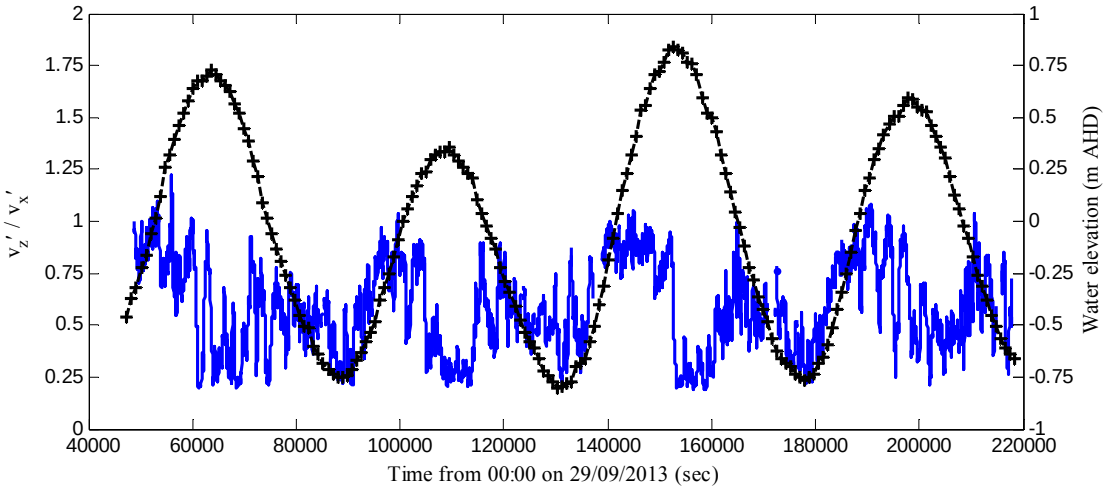

(B) Vertical turbulence ratio

Fig. E-19 - Standard deviation of velocity fluctuation as functions of time; using 3D microADV A843F (16 MHz), scan rate: 50 Hz, Probe sensor: 0.55 m above the bed, 11.056 m from left bank; Data based on 10,000 samples (200 s) every 10 s along the entire data set

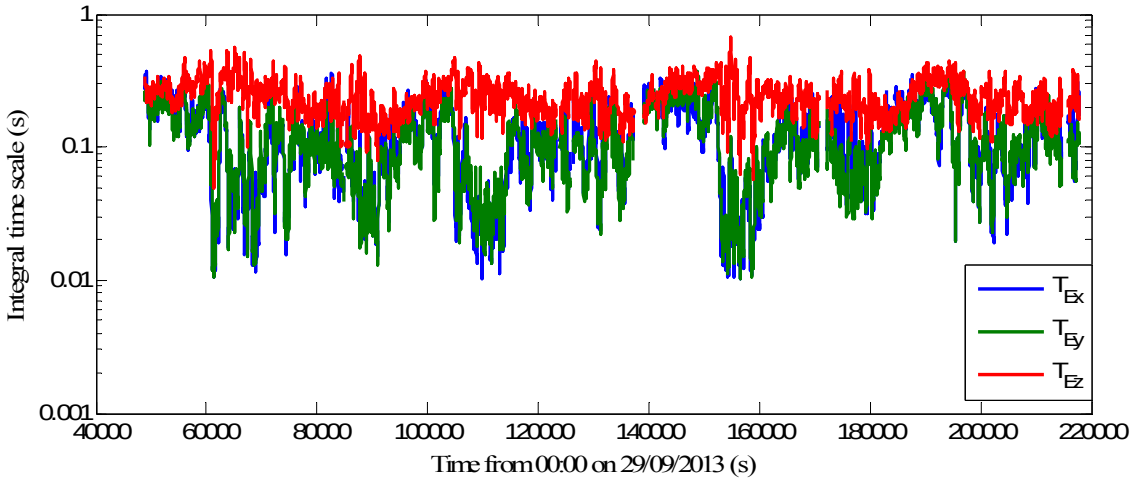

(A) Integral time scales

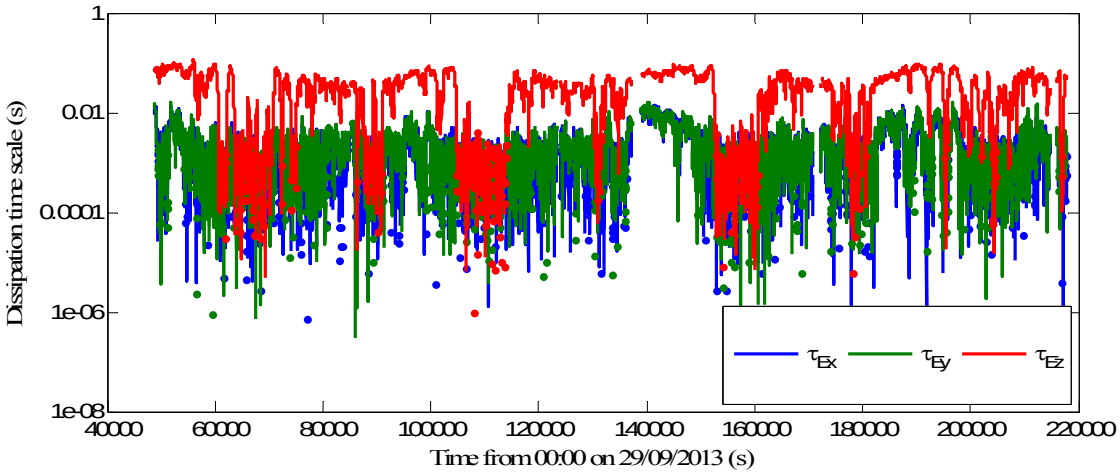

(B) Dissipation time scales

Fig. E-20 - Integral time scale as functions of time; using 3D microADV A843F (16 MHz), scan rate: 50 Hz, Probe sensor: 0.55 m above the bed, 11.056 m from left bank; Data based on 10,000 samples (200 s) every 10 s along the entire data set

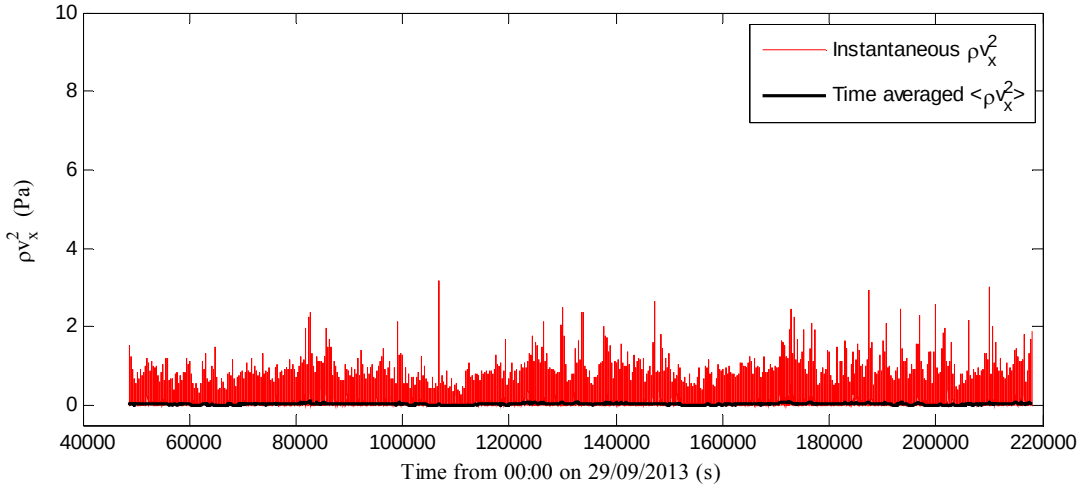

(A) ρvx^2

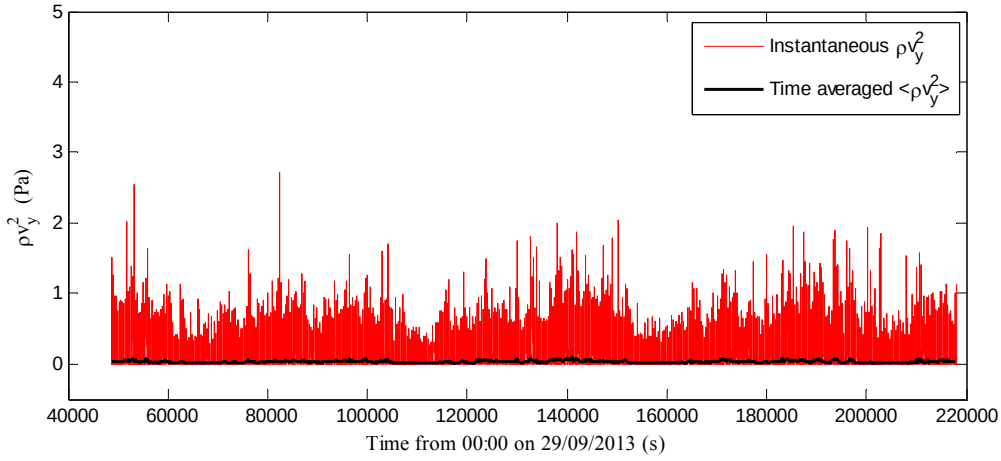

(B) ρvy^2

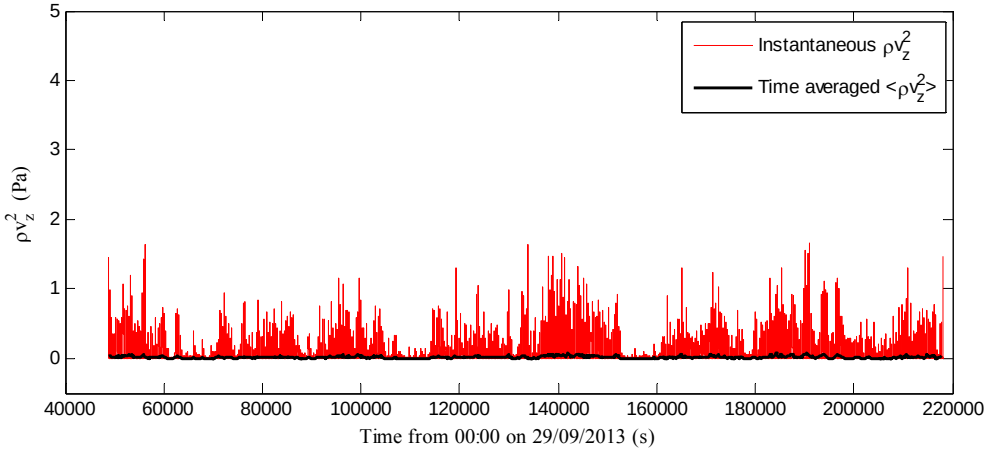

(C) ρv$_z$^{2} (Pa)

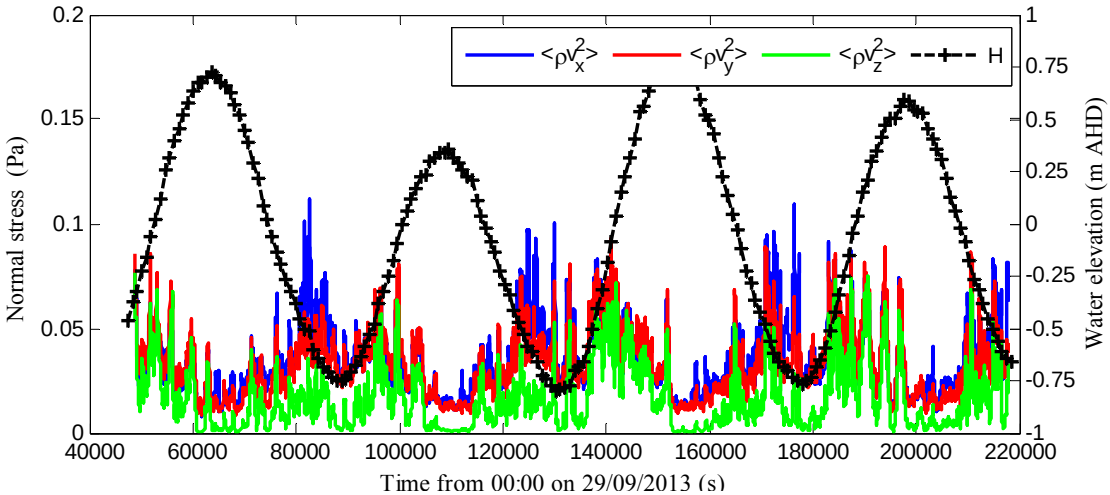

(D) Time-averaged normmal stresses

Fig. E-21 - Instantaneous and time-averaged Normal stresses as functions of time; using 3D microADV A843F (16 MHz), scan rate: 50 Hz, Probe sensor: 0.55 m above the bed, 11.056 m from left bank; Time-averaged based upon 10,000 samples (200 s) every 10 s along the entire data set

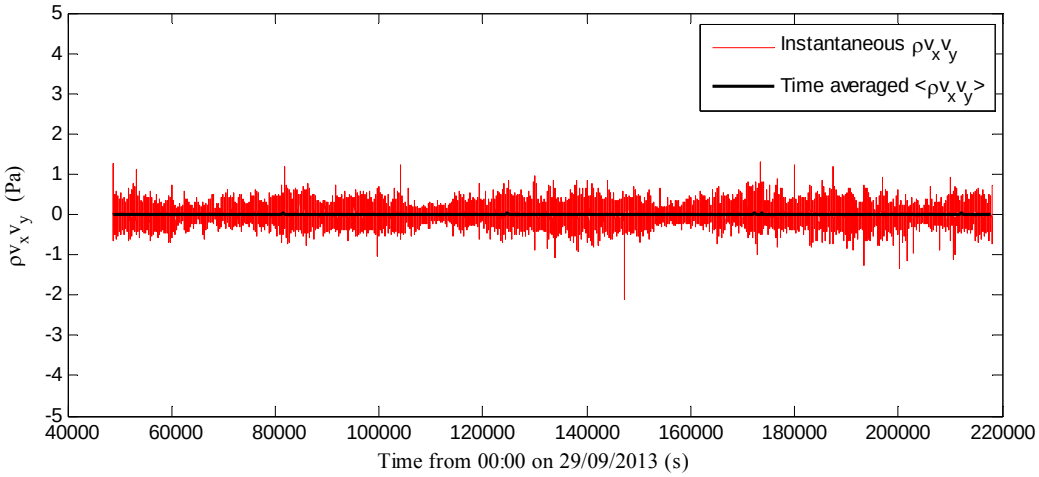

(A) $\rho v_x v_y$

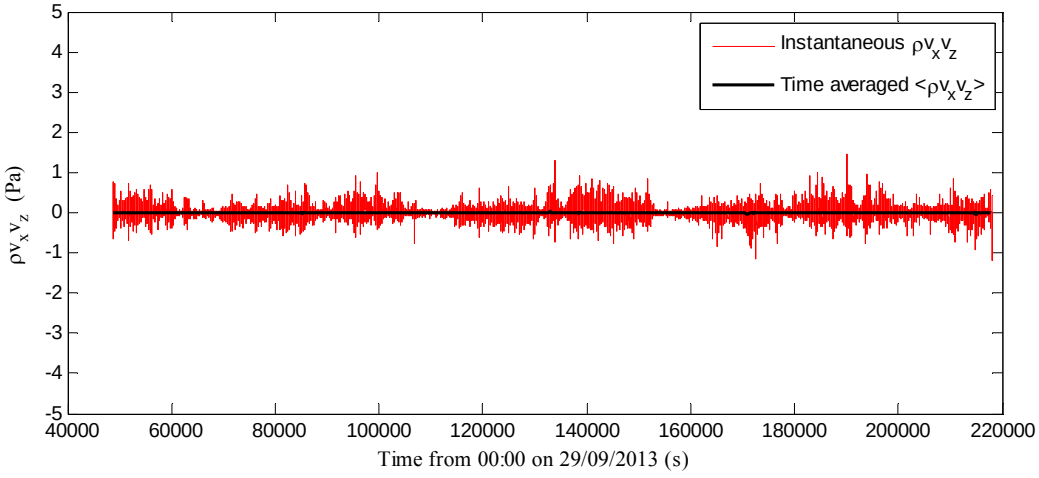

(B) $\rho v_x v_z$

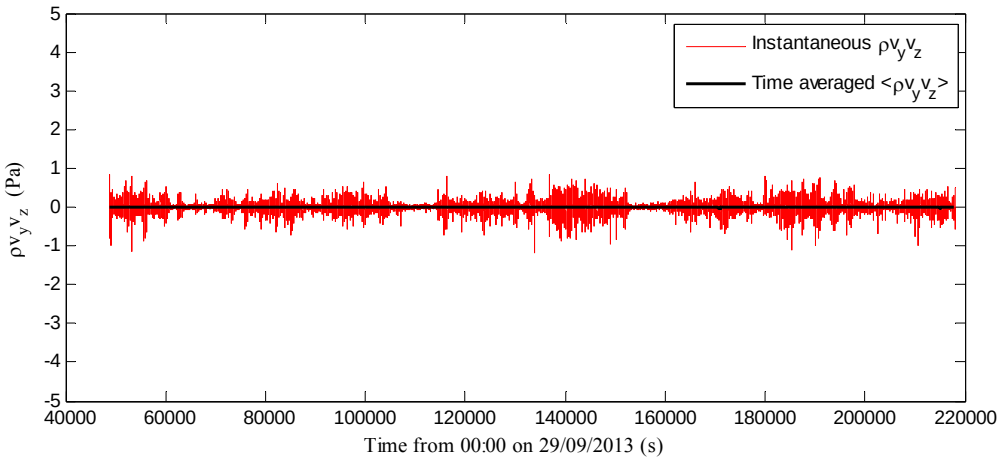

(C) $\rho v_y v_z$

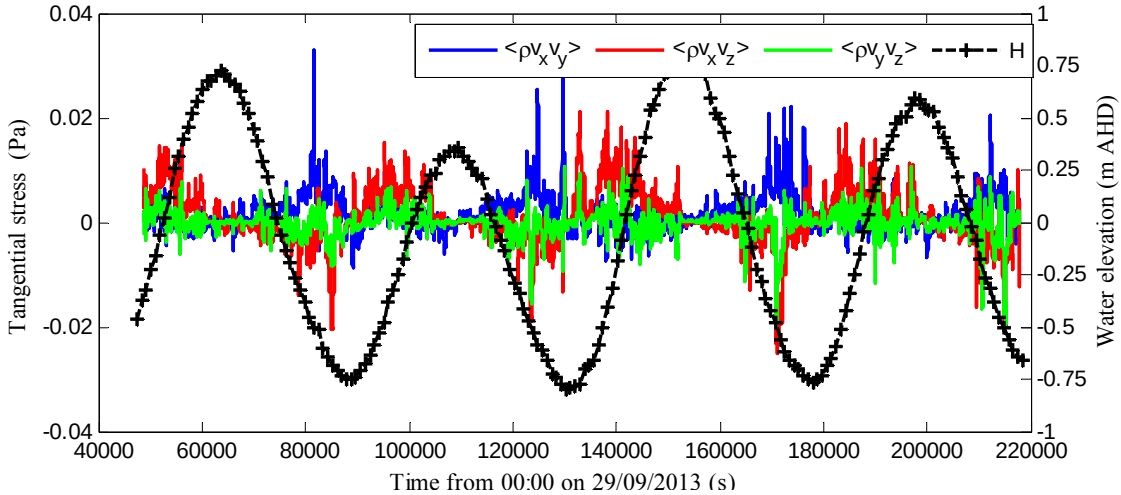

(D) Time-averaged tangential stresses

Fig. E-22 - Instantaneous and time-averaged tangential stresses as functions of time; using 3D microADV A843F (16 MHz), scan rate: 50 Hz, Probe sensor: 0.55 m above the bed, 11.056 m from left bank; Time-averaged based upon 10,000 samples (200 s) every 10 s along the entire data set

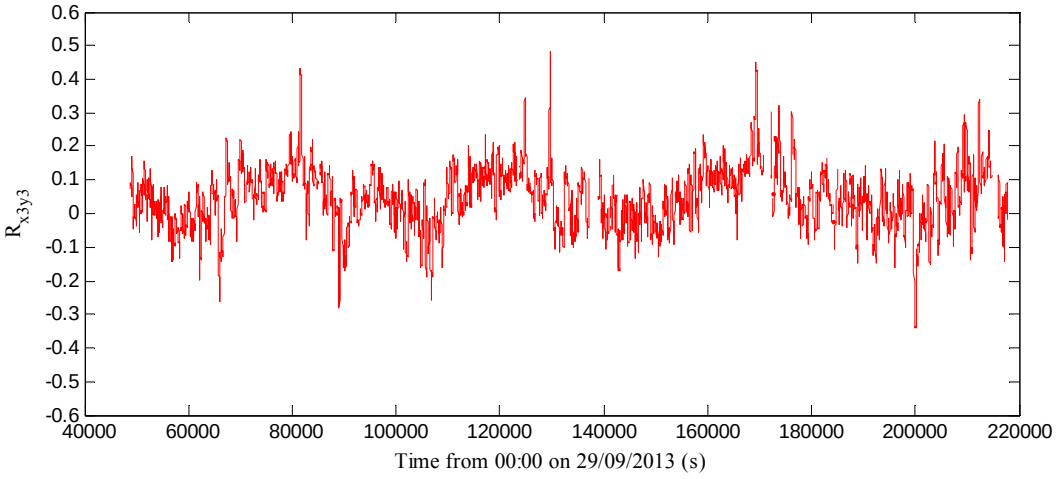

(C) Normal correlation coefficient

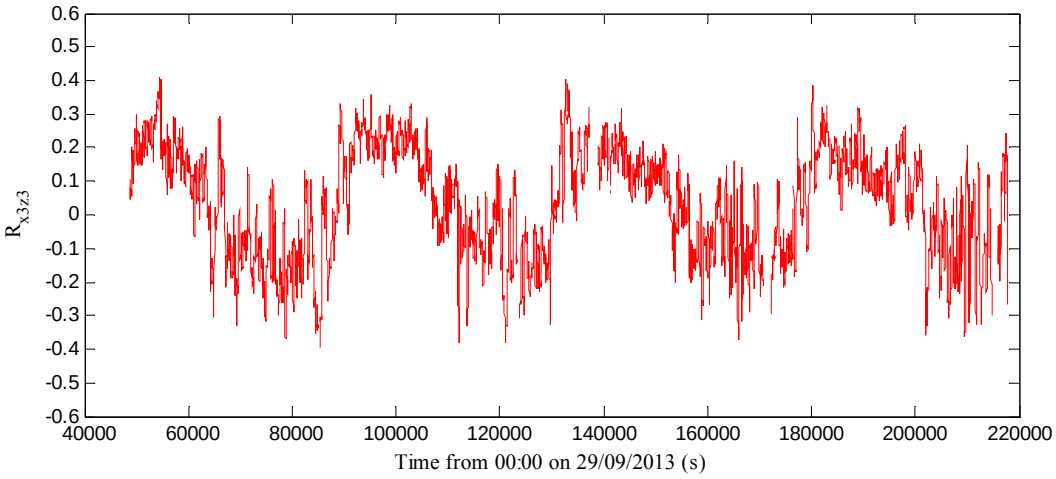

(B) Transverse correlation coefficient

Fig. E-23 - Correlation coefficients as functions of time; using 3D microADV A843F (16 MHz), scan rate: 50 Hz, Probe sensor: 0.55 m above the bed, 11.056 m from left bank; Data based upon 10,000 samples (200 s) every 10 s along the entire data set

E.2.4 Correlation coefficients between Normal stresses between different ADV units

R_{xixj} Correlation coefficient of streamwise turbulent velocity, v between different ADV units:

$$R_{xixj} = \frac{\overline{v_{xi} v_{xj}}}{(v'_{xi} v'_{xj})}$$; where 1,2, and 3 represent the ADV unit number.

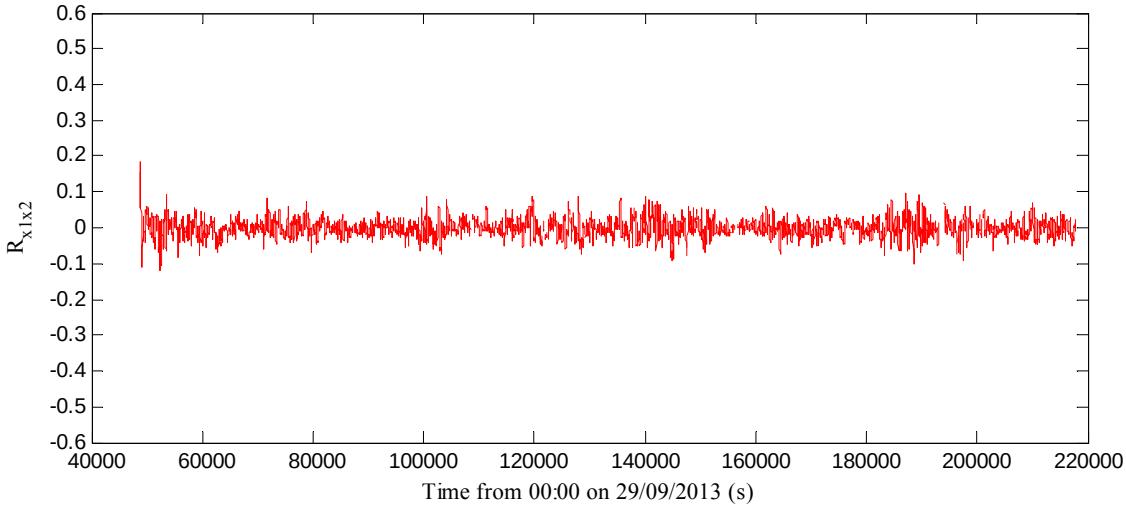

Fig. E-24 - Cross-correlation coefficient R_{xx} between ADV1 and ADV2 as a function of time; Data based upon 10,000 samples (200 s) every 10 s along the entire data set

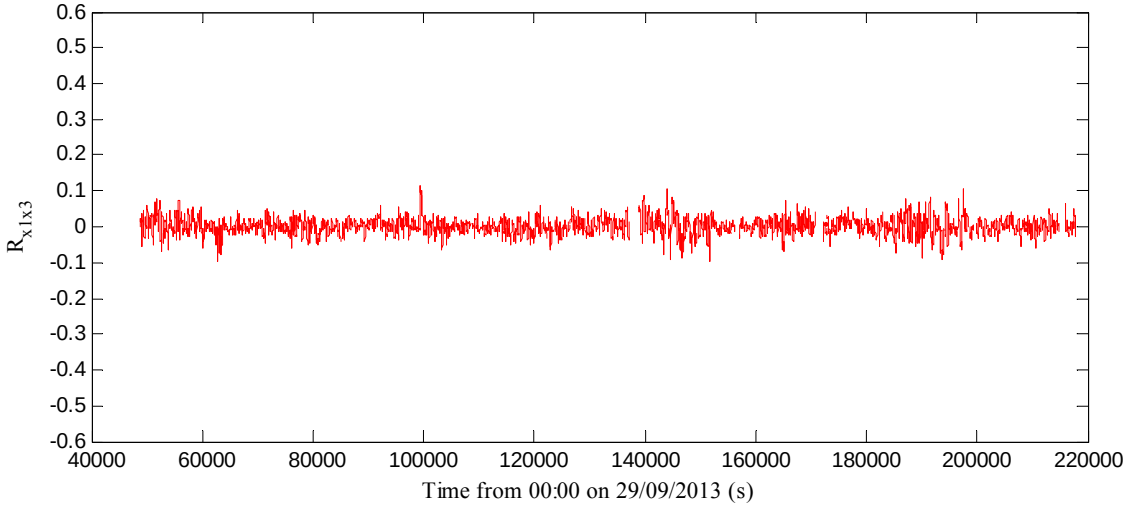

Fig. E-25 - Cross-correlation coefficient R_{xx} btween ADV1 and ADV3 as a function of time; Data based upon 10,000 samples (200 s) every 10 s along the entire data set

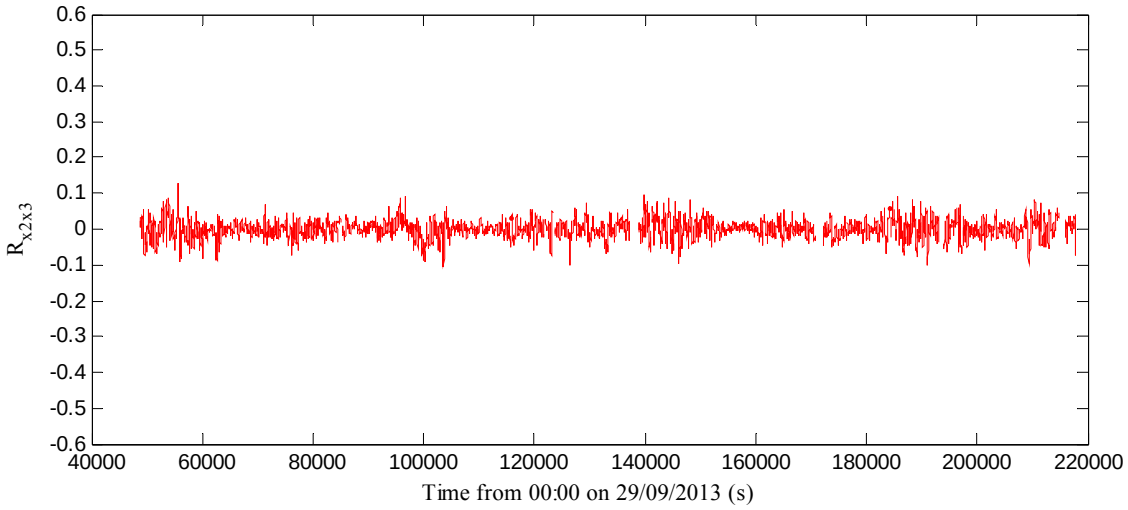

Fig. E-26 - Cross-correlation coefficient R_{xx} btween ADV2 and ADV3 as a function of time; Data based upon 10,000 samples (200 s) every 10 s along the entire data set

E.2.5 Summary of average Reynolds stresses for the flood and ebb tides observed during the field study

Table E-1 - Summary of average Reynolds stresses for the flood and tides during the field trip

Tidal phase (1)	Sampling location (m) (2)	$<\rho v_x v_y>$ (Pa) (3)	$<\rho v_x v_z>$ (Pa) (4)	$<\rho v_y v_z>$ (Pa) (5)	$<\rho v_x^2>$ (Pa) (6)	$<\rho v_y^2>$ (Pa) (7)	$<\rho v_z^2>$ (Pa) (8)
Ebb 1	0.32	0.0003	-0.0037	-0.0002	0.0513	0.0161	0.0511
	0.42	0.0001	--	--	0.0201	0.0103	0.0000
	0.55	0.0032	-0.0022	-0.0006	0.0363	0.0281	0.0103
Ebb 2	0.32	0.0013	-0.0057	-0.0002	0.0569	0.0227	0.0566
	0.42	0.0004	--	--	0.0259	0.0146	--
	0.55	0.0035	-0.0020	-0.0009	0.0370	0.0299	0.0113
Ebb 3	0.32	0.0004	-0.0033	0.0001	0.0505	0.0131	0.0493
	0.42	0.0002	--	--	0.0209	0.0100	0.0000
	0.55	0.0041	-0.0022	-0.0005	0.0369	0.0285	0.0110
Flood 1	0.32	0.0011	0.0004	-0.0006	0.0543	0.0156	0.0511
	0.42	0.0000	--	--	0.0253	0.0164	--
	0.55	0.0004	0.0045	0.0007	0.0327	0.0342	0.0153
Flood 2	0.32	0.0028	0.0047	-0.0005	0.0667	0.0343	0.0669
	0.32	0.0004	--	--	0.0418	0.0336	--
	0.55	0.0001	0.0059	0.0002	0.0420	0.0437	0.0271
Flood 3	0.32	0.0017	0.0056	-0.0005	0.0716	0.0372	0.0715
	0.42	0.0005	--	--	0.0405	0.0334	--
	0.55	0.0013	0.0049	0.0007	0.0392	0.0420	0.0248

Note that flood and ebb tides are defined based on water level.

APPENDIX F – MISCELLANEOUS

F.1 WIND EFFECT ON SURFACE DRIFTER

Herein, we examine the effect of wind on the surface drifter by considering a drifter with a diameter 0.197 m, with only 0.03 m submerged out of the 0.26 m total height. The wind induced slip is calculated using two approaches: 1. using an empirical relation obatined from ocean data and 2. drag force balance on the drifter submerged and unsubmerged surface. The results of both methods are briefly presented below.

Horizontal wind slip from empirical relation

Slip is the horizontal motion of a drifter that differs from the motion of currents ([30]) (Lumpkin and Pazos, 2007). The wind induced drifter U_{slip}, depends on both drifter drag area ratio and wind vector in the vicinity of the measurements. U_{slip}, can be described as:

$$| U_{slip} | = \frac{A}{R} W, \qquad \text{(F-1)}$$

where R is the ratio of drag area (product of drag coefficient and cross-sectional area) of the submerged portion to that of the unsubmerged portion of the drifter, W is the downwind speed in m/s and A = 0.07 (Niiler and Paduan, 1995). Therefore, the slip could be minimised with large R, i.e., minimised unsubmerged area with optimised submerged area. The present drifter configuration results in an estimated wind slip U_{slip} of 0.03 – 0.032 m/s in a downwind of 5 m/s using the simple model in Eqn. F-1. Figure F-1 below shows the distribution of wind slip for various values of downwind speed (0.8 – 10 m/s) and current speed (0.1 – 1 m/s).

[30] Current herein means water current, a terminology borrowed from the field of oceanography as used in the cited literature

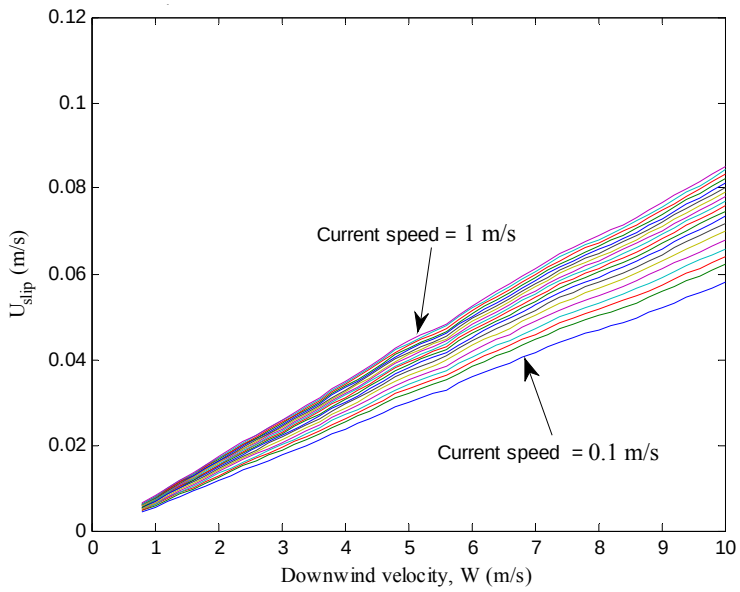

Fig. F-1 - Wind induced slip of the drifter for ranges of downwind and current speeds

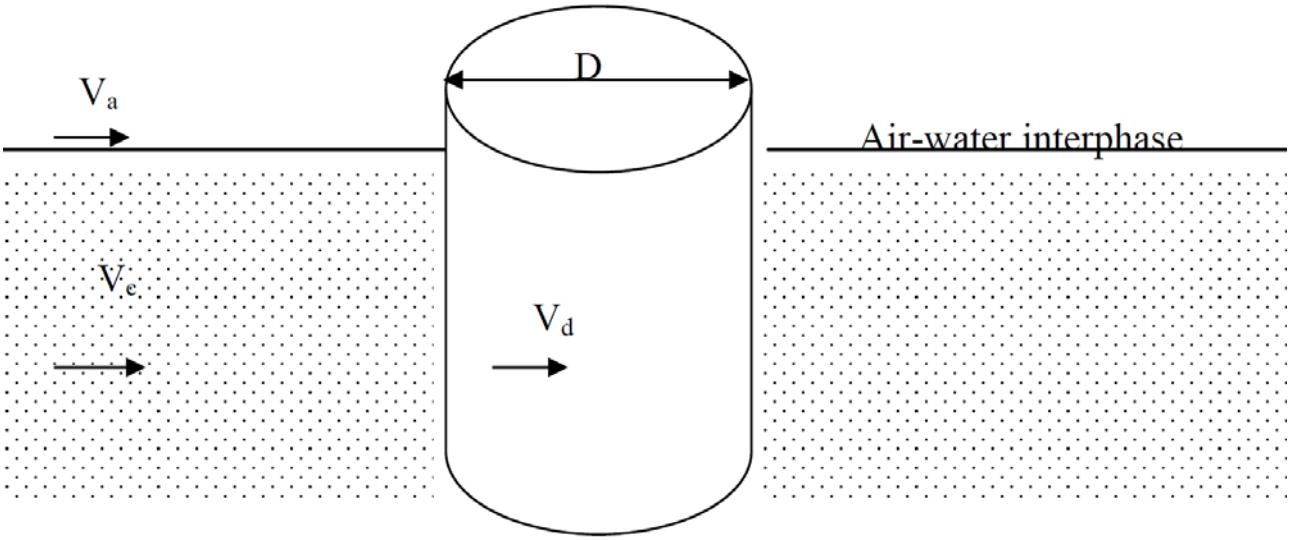

Fig. F-2 - Schematic of drifter design showing the wind and current drags.

Considering the schematics of a drifter above, the total drag is the summation of drag due to the wind on the unsubmerged surface and current on the submerged surface. This could be represented as:

$$\rho_a C_{Da} A_a |V_a - V_d|(V_a - V_d) + \rho_w C_{Dw} A_w |V_c - V_d|(V_c - V_d) = 0 \qquad \text{(F-2)}$$

where ρ is density of fluid in the medium, V is the velocity vector, C_D is coefficient of drag within between the fluid and the cylinder body, A is the normal surface area subscript 'a' denotes the water, subscript 'c' denotes current, and subscript 'd' denotes drifter. Assuming V_a is significantly higher than the V_d, therefore, $V_a - V_d \approx V_a$, (Colin de Verdiere, 1983), we can define the wind coefficient also known as '*Leeway*' ε such that:

$$\varepsilon = \left(\frac{\rho_a C_{Da} A_a}{\rho_w C_{Dw} A_w} \right)^{1/2} \quad \text{(F-3)}$$

$$V_d = V_c + \varepsilon V_a \quad \text{(F-4)}$$

This equation can be simplified by assuming a downwind speed, W which represents the maximum slip on the drifter. Therefore can be described from the second term of Eqn. F- 4 such that:

$$|U_{slip}| = \varepsilon W \quad \text{(F-5)}$$

The present drifter configuration results in an estimated wind slip U_{slip} of 0.04 – 0.05 m/s in a downwind of 5 m/s using Eqn. F-5. Figure 3 below shows the distribution of wind slip for various values of downwind speed (0.8 – 10 m/s) and current speed (0.1 - 1 m/s) using Eqation (F-5).
The empirical relation resulted in smaller wind slip estimates – less than 1% of the downwind speed while the forces balance resulted in wind slip about 1% of the downwind speed. Therefore, wind slip on the present configuration of the drifter was estimated to be around 1% of the downwind speed. Note that the downwind speed results in the maximum wind slip while the upwind speed results in drag of the drifter (i.e., reduced drifter velocity).

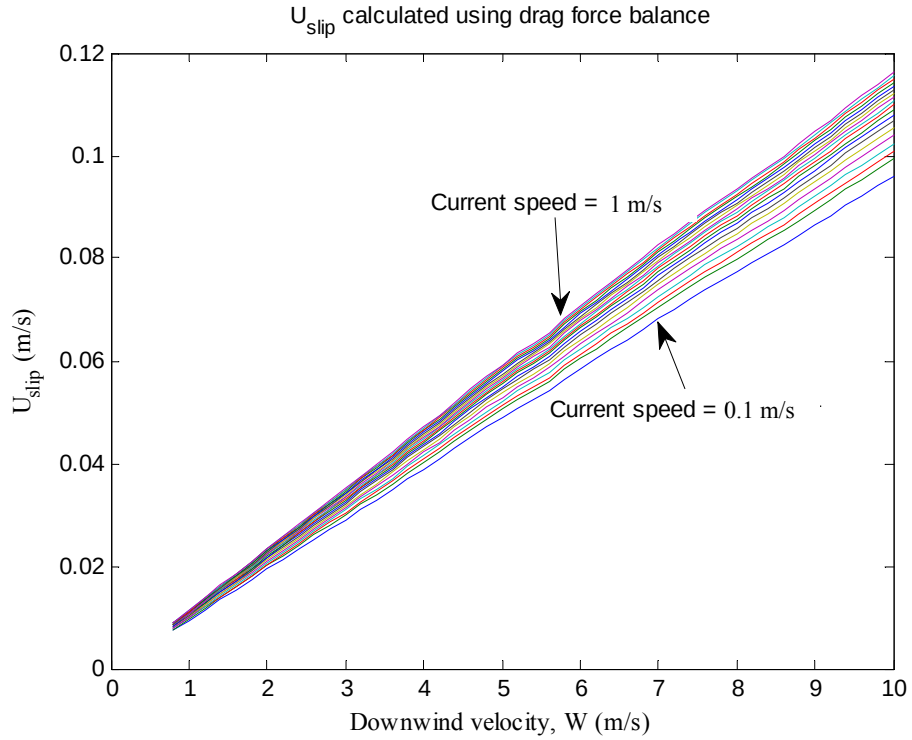

Fig. F-3 - Wind induced slip of the drifter for ranges of downwind and current velocities

F.2 OFF-THE-SHELF LOW RESOLUTION SURFACE DRIFTER

During the field study E14, some cheap off-the-shelf low resolution drifters HOLUX® M241 were deployed alongside the high resolution drifters. The drifter position accuracy is in the order of 2 m. However, the parameters for isolating this error and other inherent errors have not been fully

analysis and thus not documented in this report. Figure F-4 below shows a zoomed up portion of the trajectory of the deployment of the drifter with the high resolution drifter discussed in this report. The plot shows large scatter of the position markers which could result in large velocity fluctuations about the mean velocity. Some analysis is still on-going to estimate parameters for isolating this relative position error and hence understand the applicability of the device and similar low resolution GPS-tracked drifters to shallow water

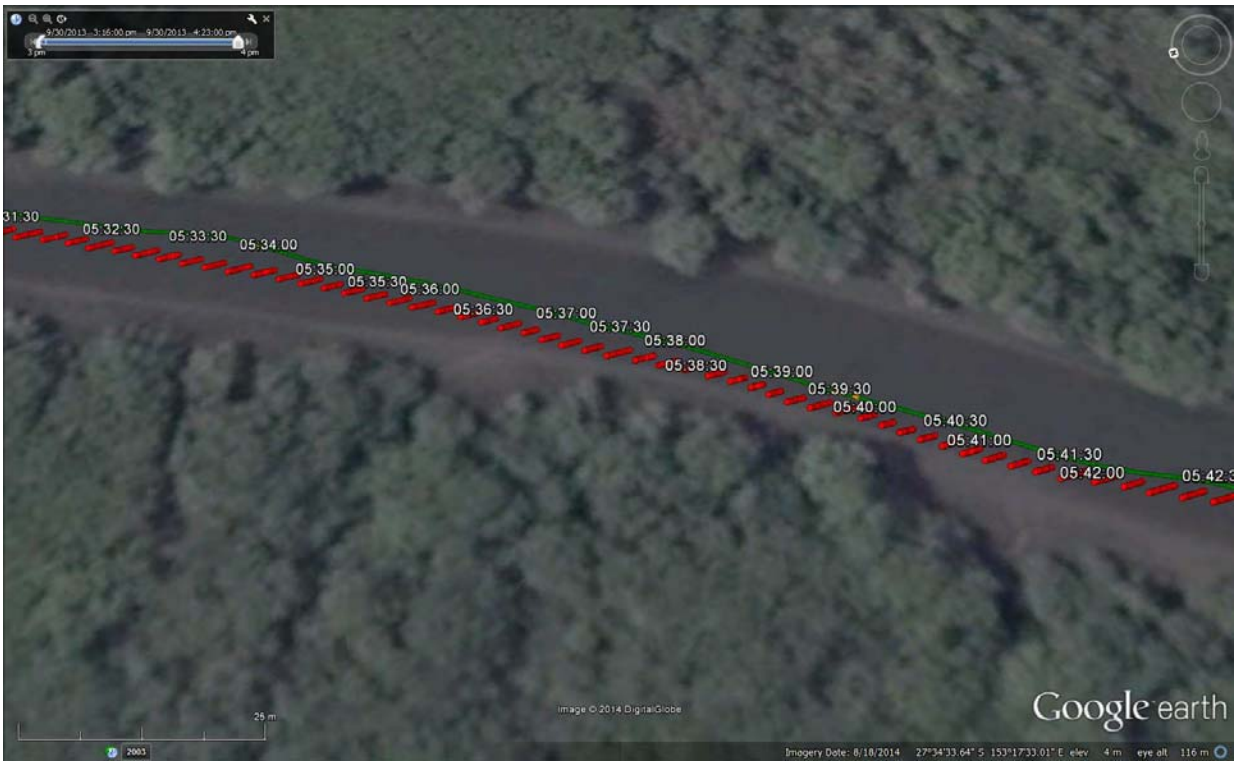

Fig. F-4 - Google Earth Vicinity map of Eprapah Creek; green marker shows trajectory of a high resolution drifter sampled at 10 Hz.; red marker shows trajectory of a low resolution drifter sampled at 1 Hz. The scale is shown in white faint line in the bottom left corner with length equivalent to 29 m. "Eprapah Creek" 153.30^{o}E and -27.567^{o}S. Google Earth 7.1.2.2041. Google Inc. (2013)

REFERENCES

Anzecc, and Armcanz (2000). "Australian and New Zealand Guidelines for Fresh and Marine Water Quality." In: *National Water Quality Management Strategy*, Vol. 1, Paper No. 4, October 2000.

Bendat, J. S., and Piersol, A. G. (2011). "Random data: analysis and measurement procedures." *John Wiley & Sons*, New Jersey, USA, 4th edition.

Brereton, G., and Kodal, A. (1992). "A frequency-domain filtering technique for triple decomposition of unsteady turbulent flow." *Journal of Fluids Engineering*, Vol. 114, pp. 45-51 (DOI: 10.1115/1.2909998).

Brown, R., and Chanson, H. (2012). "Suspended sediment properties and suspended sediment flux estimates in an inundated urban environment during a major flood event." *Water Resources Research*, Vol. 48, W11523, 15 pages (DOI:10.1029/2012WR012381).

Brown, R., and Chanson, H. (2013). "Turbulence and Suspended Sediment Measurements in an Urban Environment during the Brisbane River Flood of January 2011". *Journal of Hydraulic Engineering*, Vol. 139, pp. 244-253 (DOI: 10.1061/(ASCE)HY.1943-7900.0000666).

Buffin-Bélanger, T., and Roy, A. G. (1998). "Effects of a pebble cluster on the turbulent structure of a depth-limited flow in a gravel-bed river." *Geomorphology*, Vol. 25, pp. 249-267 (DOI: 10.1016/S0169-555X(98)00062-2).

Chanson, H. (2004). "Environmental Hydraulics of Open Channel Flows." *Elsevier-Butterworth-Heinemann*, Oxford, UK, 483 pages.

Chanson, H. (2009). "Applied hydrodynamics: an introduction to ideal and real fluid flows." *CRC Press*, AK Leiden, The Netherlands.

Chanson, H. (2008). "Field observations in a small subtropical estuary during and after a rainstorm event." *Estuarine, Coastal and Shelf Science*, Vol. 80, pp. 114-120 (DOI: 10.1016/j.ecss.2008.07.013).

Chanson, H., Brown, R., Ferris, J., Ramsay, I., and Warburton, K. (2005). "Preliminary measurements of turbulence and environmental parameters in a sub-tropical estuary of eastern Australia." *Environmental Fluid Mechanics*, Vol. 5**,** pp. 553-575 (DOI: 10.1007/s10652-005-0928-y).

Chanson, H., Brown, R., and Trevethan, M. (2012). "Turbulence measurements in a small subtropical estuary under king tide conditions." *Environmental Fluid Mechanics*, Vol. 12, pp. 265-289 (DOI: 10.1007/s10652-011-9234-z).

Chanson, H., and Docherty, N. J. (2012). "Turbulent velocity measurements in open channel bores." *European Journal of Mechanics-B/Fluids*, Vol. 32, pp. 52-58 (DOI: 10.1016/j.euromechflu.2011.10.001).

Chanson, H., Takeuchi, M., and Trevethan, M. (2007). "High-Frequency Suspended Sediment Flux Measurement in a Small Estuary." *Proc. of 6th International Conference on Multiphase Flow, ICMF*, Leipzig, Germany, July 9-13, M. Sommerfield Editor, Session 7, Paper No. S7_Mon_C_S7_Mon_C_5, 12 pages (CD-ROM).

Chanson, H., and Trevethan, M. (2010). "Turbulence, turbulent mixing and diffusion in shallow-water estuaries." In: "Atmospheric turbulence, meteorological modeling and aerodynamics." *Nova Science Publishers, New York, NY***,** pp. 167-204.

Chanson, H., Trevethan, M., and Aoki, S.I. (2008). "Acoustic Doppler velocimetry (ADV) in small estuary: Field experience and signal post-processing." *Flow Measurement and Instrumentation,* Vol. 19**,** pp. 307-313 (DOI: 10.1016/j.flowmeasinst.2008.03.003).

Chen, S. N., and Sanford, L. P. (2009). "Axial Wind Effects on Stratification and Longitudinal Salt Transport in an Idealized, Partially Mixed Estuary." *Journal of Physical Oceanography,* Vol. 39**,** pp. 1905-1920 (DOI: 10.1175/2009JPO4016.1).

Davidson, P. A. (2004). "Turbulence: An Introduction for Scientists and Engineers." *Oxford University Press,* New York, USA.

De Verdiere, A. C. (1983). "Lagrangian eddy statistics from surface drifters in the eastern North Atlantic." *Journal of Marine Research,* Vol. 41, pp. 375-398 (DOI: 10.1357/002224083788519713).

Dyer, K. R. (1997). "Estuaries: a physical introduction." *John Wiley and Sons,* Chichester, UK, 2nd edition.

Fischer, H. B. (1976). "Mixing and dispersion in estuaries." *Annual Review of Fluid Mechanics,* Vol 8**,** pp. 107-133 (DOI: 10.1146/annurev.fl.08.010176.000543).

Fischer, H. B., List, E. J., Koh, R. C., Imberger, J., and Brooks, N. H. (1979). "Mixing in inland and coastal waters." *Academic Press,* New York, USA.

Fox, J. F., Papanicolaou, A. N., and Kjos, L. (2005). "Eddy taxonomy methodology around a submerged barb obstacle within a fixed rough bed." *Journal of Engineering Mechanics,* Vol. 131, pp. 1082-1101 (DOI: 10.1061/(ASCE)0733-9399(2005)131:10(1082)).

Fransson, J. H., Matsubara, M., and Alfredsson, P. H. 2005. "Transition induced by free-stream turbulence." *Journal of Fluid Mechanics,* Vol. 527, pp. 1-25 (DOI: 10.1017/S0022112004002770).

González, J. A., Melching, C. S., and Oberg, K. A. (1996). "Analysis of open-channel velocity measurements collected with an acoustic Doppler current profiler." *Proc. 1st International Conference on New/Emerging Concepts for Rivers, RIVERTECH 96,* IWRA, Chicago, USA, 8 pages.

Goring, D. G., and Nikora, V. I. (2002). "Despiking acoustic Doppler velocimeter data." *Journal of Hydraulic Engineering,* Vol. 128, pp. 117-126 (DOI: 10.1061/(ASCE)0733-9429(2002)128:1(117)).

Grass, A. J. (1971). "Structural features of turbulent flow over smooth and rough boundaries." *Journal of Fluid Mechanics,* Vol. 50, pp. 233-255 (DOI: 10.1017/S0022112071002556).

Gunawan, B., Neary, V. S., and McNutt, J. (2011). "ORNL ADCP post-processing guide and MATLAB algorithms for MHK site flow and turbulence analysis." *Report No. ORNL/TML-2011/338,* Office of energy efficiency and renewable energy, Washington D.C., US Department of Energy, Water Power Program, Office of Science and Technical Information, September, 36 pages.

Hinze, J. O. (1975). "Turbulence." *McGraw-Hill*, New York, USA, 2nd edition.

Hussain, A., and Reynolds, W. (1972). "The mechanics of an organized wave in turbulent shear flow. Part 2. Experimental results." *Journal of Fluid Mechanics,* Vol. 54, pp. 241-261 (DOI: 10.1017/S0022112072000667).

Kawanisi, K. (2004). "Structure of turbulent flow in a shallow tidal estuary." *Journal of Hydraulic Engineering*, Vol. 130, pp. 360-370 (DOI: 10.1061/(ASCE)0733-9429(2004)130:4(360)).

Kelly, J. (2014). "GPS Drifter design and testing." *Bachelor Degree Thesis*, Science and Engineering Faculty, Queensland University of Technology.

Kironoto, B., and Graf, W. H. (1994). "Turbulence characteristics in rough uniform open-channel flow." *Proc. of the ICE-Water Maritime and Energy,* Vol. 106, pp. 333-344.

Legleiter, C. J., and Kyriakidis, P. C. (2006). "Forward and inverse transformations between Cartesian and channel-fitted coordinate systems for meandering rivers." *Mathematical Geology*, Vol. 38, pp. 927-958 (DOI: 10.1007/s11004-006-9056-6).

Lumpkin, R., and Pazos, M. (2007). "Measuring surface currents with Surface Velocity Program drifters: the instrument, its data, and some recent results." In: "Lagrangian Analysis and Prediction of Coastal and Ocean Dynamics," *LAPCOD*, A. Griffa et al., Eds., pp. 39-67

MacVean, L. J., and Stacey, M. T. (2011). "Estuarine dispersion from tidal trapping: a new analytical framework." *Estuaries and Coasts,* Vol. 34, pp. 45-59 (DOI: 10.1007/s12237-010-9298-x).

Manwell, J. F., McGowan, J. G., and Rogers, A. L. (2010). "Wind Characteristics and Resources." In: "Wind Energy Explained: Theory, Design and Application", *John Wiley & Sons*, Chichester, UK, 2nd Edition, pp. 23-87 (DOI: 10.1002/9781119994367.ch2).

Nezu, I., and Nakagawa, H. (1993). "Turbulence in open-channel flows." *IAHR Monograph*, IAHR Fluid Mechanics Section. Balkema, Rotterdam, The Netherlands.

Niiler, P. P., and Paduan, J. D. (1995). "Wind-driven motions in the northeast Pacific as measured by Lagrangian drifters." *Journal of Physical Oceanography,* Vol. 25**,** pp. 2819-2830 (DOI: 10.1175/1520-0485(1995)025<2819:WDMITN>2.0.CO;2).

Press, W. H., Teukolsky, S. A., Vetterling, W. T., and Flannery, B. P. (1992). "Numerical recipes in Fortran 77: the art of scientific computing." *Cambridge University Press,* Cambridge, UK, 2nd edition.

Rusello, P. J., Siegel, E., and Alford, M. H. (2011). "High resolution Doppler profiler measurements of turbulence from a profiling body." *Proc. of 10th Working Conference on Current Measurement Technology*, IEEE, OES & CWTM, Monterey, Canada, pp. 259-265 (DOI: 10.1109/CWTM.2011.5759562).

Savenije, H. H. (2006). "Salinity and tides in alluvial estuaries." *Elsevier*, Amsterdam, The Netherlands.

Situ, R., and Brown, R. J. (2013). "Mixing and dispersion of pollutants emitted from an outboard motor." *Marine pollution Bulletin*, Vol. 69, No. 1-2, pp. 19-27 (DOI: 10.1016/j.marpolbul.2012.12.015).

Suara, K., Brown, R., and Chanson, H. (2014a). "Turbulence measurements in a shallow tidal estuary: analysis based on triple decomposition." *Proc. of 19th Australasian Fluid Mechanics Conference*, AFMS, paper 359, 4 pages.

Suara, K., Wang, C., Feng, Y., Brown, R. J., Chanson, H., and Borgas, M. (2014b). "High-Resolution GNSS-Tracked Drifter for Studying Surface Dispersion in Shallow Water." *Journal of Atmospheric and Oceanic Technology*, Vol. 32, Issue 3, pp. 579-590 (DOI: 10.1175/JTECH-D-14-00127.1).

Symonds, D. (2006). "QA/QC Parameters for Acoustic Doppler Current Profilers." *Teledyne RDI Application Note.*

Tamburrino, A., and Gulliver, J. S. (1999). "Large flow structures in a turbulent open channel flow." *Journal of Hydraulic Research,* IAHR, Vol. 37, pp. 363-380 (DOI:10.1080/00221686.1999.9628253).

Tennekes, H., and Lumley, J. L. (1972). "A first course in turbulence." *MIT Press*, Massachussets, USA.

Trevethan, M. (2008). "A Fundamental Study of Turbulence and Turbulent Mixing in a Small Subtropical Estuary." *Ph.D. thesis*, Dept of Civil Engineering, The University of Queensland, 342 pages.

Trevethan, M., and Chanson, H. (2009). "Turbulent mixing in a small estuary: Detailed measurements." *Estuarine, Coastal and Shelf Science,* Vol. 81, pp. 191-200 (DOI: 10.1016/j.ecss.2008.10.020).

Trevethan, M., Chanson, H., and Brown, R. (2006). "Two series of detailed turbulence measurements in a small subtropical estuarine system. Brisbane, Australia." *Report No. CH58/06*, Div.of Civil Engineering, The University of Queensland, Brisbane, Australia, March, 153 pages (ISBN 1864998520).

Trevethan, M., Chanson, H., and Brown, R. (2008a). "Turbulence characteristics of a small subtropical estuary during and after some moderate rainfall." *Estuarine, Coastal and Shelf Science,* Vol. 79, pp. 661-670 (DOI: 10.1016/j.ecss.2008.06.006).

Trevethan, M., Chanson, H., and Brown, R. (2008b). "Turbulent measurements in a small subtropical estuary with semidiurnal tides." *Journal of Hydraulic Engineering,* ASCE, Vol. 134, pp. 1665-1670 (DOI: 10.1061/(ASCE)0733-9429(2008)134:11(1665)).

Trevethan, M., Chanson, H., and Brown, R. J. (2007a). "Turbulence and turbulent flux events in a small subtropical estuary." *Report No. CH65/07,* Div.of Civil Engineering, The University of Queensland, Brisbane, Australia, March, 69 pages (ISBN 9781864998993).

Trevethan, M., Chanson, H., and Takeuchi, M. (2007b). "Continuous high-frequency turbulence and suspended sediment concentration measurements in an upper estuary." *Estuarine, Coastal and Shelf Science,* Vol. 73, pp. 341-350 (DOI: 10.1016/j.ecss.2007.01.014).

Voulgaris, G., and Meyers, S. T. (2004). "Temporal variability of hydrodynamics, sediment concentration and sediment settling velocity in a tidal creek." *Continental Shelf Research*, Vol. 24, pp. 1659-1683 (DOI: 10.1016/j.csr.2004.05.006).

Voulgaris, G., and Throwbridge, J. (1998). "Evaluation of the acoustic Doppler velocimeter (ADV) for turbulence measurements." *Journal of Atmospheric and Oceanic Technology*, Vol. 15, pp. 272-289 (DOI: 10.1175/1520-0426(1998)015<0272:EOTADV>2.0.CO;2).

Walburn, F., Sabbah, H., and Stein, P. (1983). "An experimental evaluation of the use of an ensemble average for the calculation of turbulence in pulsatile flow." *Annals of biomedical engineering*, Vol. 11, pp. 385-399 (DOI: 10.1007/BF02584215).

Internet References

Eprapah Creek catchment	{http://www.redland.qld.gov.au/EnvironmentWaste/Water/Waterways/Pages/OurCatchmentsEprapahCreek.aspx}
Australian Bureau of Meteorology (ABM) 2013	{http://www.bom.gov.au/climate/data/index.shtml?bookmark=200.}

Bibliography

Banner, M.L., and Peirson, W.L. (1998). "Tangential stress beneath wind-driven air–water interfaces." *Journal of Fluid Mechanics*, Vol. 364, pp 115-145.

Brocchini, M., and Peregrine, D.H. (2001). "The dynamics of strong turbulence at free surfaces. Part 1. Description." *Journal of Fluid Mechanics*, Vol. 449, pp. 225-254.

Butler, B., and Burrows, D.W. (2007). "Dissolved Oxygen Guidelines for Freshwater Habitats in Northern Australia." *ACTFR Report No. 07/32*, Department of Environment and Heritage, Canberra, Australia, 51 pages.

Chanson, H. (2014). "Applied Hydrodynamics: An Introduction." *CRC Press*, Taylor & Francis Group, Leiden, The Netherlands, 448 pages & 21 video movies.

Chanson, H., Brown, R., and McIntosh, D. (2014). "Human body stability in floodwaters: the 2011 flood in Brisbane CBD." in "Hydraulic Structures and Society – Engineering Challenges and Extremes", *The University of Queensland*, Brisbane, Australia, Proceedings of the 5th IAHR International Symposium on Hydraulic Structures (ISHS2014), 25-27 June 2014, Brisbane, Australia, H. Chanson and L. Toombes Editors, 9 pages (DOI: 10.14264/uql.2014.48) (ISBN 978-1-74272-115-6).

Chanson, H., Takeuchi, M., and Trevethan, M. (2008). "Using Turbidity and Acoustic Backscatter Intensity as Surrogate Measures of Suspended Sediment Concentration in a Small Sub-Tropical Estuary." *Journal of Environmental Management*, Vol. 88, No. 4, Sept., pp. 1406-1416 (DOI: 10.1016/j.jenvman.2007.07.009).

Chu, C.R., and Jirka, G.H. (2003). "Wind and Stream Flow Induced Reaeration." *Journal of Environmental Engineering*, ASCE, Vol. 129, pp. 1129-1136.

Jirka, G.H., and Ho, A.H.W. (1990). "Measurements of gas concentration fluctuations at water surface." *Journal of Hydraulic Engineering*, ASCE, Vol. 116, No. 6, pp. 835-847.

Trevethan, M., and Aoki, S.I. (2009). "Initial Observations on Relationship between Turbulence and Suspended Sediment Properties in Hamana Lake Japan." *Journal of Coastal Research*, Vol. SI56, pp. 1434-1438.

Trevethan, M., and Chanson, H. (2010). "Turbulence and Turbulent Flux Events in a Small Estuary." *Environmental Fluid Mechanics*, Vol. 10, No. 3, pp. 345-368 (DOI: 10.1007/s10652-009-9134-7).

Wahl, T.L. (2003). "Despiking Acoustic Doppler Velocimeter Data. Discussion." *Jl of Hyd. Engrg.*, ASCE, Vol. 129, No. 6, pp. 484-487.

Zappa, C.J., McGillis, W.R., Raymond, P.A., Edson, J.B., Hintsa, E.J., Zemmelionk, H.J., Dacey, J.W., and Ho, D.T. (2007). "Environmental turbulent mixing controls on air-water gas exchange in marine and aquatic systems." *Geophysical Research Letters*, Vol. 34, L10601, 6 pages, (DOI: 10.1029/2006GL028790).

Bibliographic reference of the Report CH99/15

The Hydraulic Model research report series CH is a refereed publication published by the School of Civil Engineering at the University of Queensland, Brisbane, Australia.

The bibliographic reference of the present report is:

SUARA. K., BROWN, R., and CHANSON, H. (2015). "Turbulence and Mixing in the Environment: Multi-Device Study in a Sub-tropical Estuary." *Hydraulic Model Report No. CH99/15*, School of Civil Engineering, The University of Queensland, Brisbane, Australia, 167 pages (ISBN 978 1 74272 138 5).

The Report CH99/15 is available, in the present form, as a PDF file on the Internet at UQeSpace:

http://espace.library.uq.edu.au/

It is listed at:

http://espace.library.uq.edu.au/list/author_id/193/

HYDRAULIC MODEL RESEARCH REPORT CH

The Hydraulic Model Report CH series is published by the School of Civil Engineering at the University of Queensland. Orders of any reprint(s) of the Hydraulic Model Reports should be addressed to the School Secretary.

School Secretary, School of Civil Engineering, The University of Queensland
Brisbane 4072, Australia - Tel.: (61 7) 3365 3619 - Fax: (61 7) 3365 4599
Url: http://http://www.civil.uq.edu.au// Email: enquiries@civil.uq.edu.au

Report CH	**Unit price**	Quantity	**Total price**
SUARA. K., BROWN, R., and CHANSON, H. (2015). "Turbulence and Mixing in the Environment: Multi-Device Study in a Sub-tropical Estuary." *Hydraulic Model Report No. CH99/15*, School of Civil Engineering, The University of Queensland, Brisbane, Australia, 167 pages (ISBN 978 1 74272 138 5).	AUD$60.00		
LENG, X., and Chanson, H. (2015). "Unsteady Turbulence during the Upstream Propagation of Undular and Breaking Tidal Bores: an Experimental Investigation." *Hydraulic Model Report No. CH98/15*, School of Civil Engineering, The University of Queensland, Brisbane, Australia, 235 pages & 4 video movies (ISBN 978 1 74272 135 4).	AUD$60.00		
ZHANG, G., and CHANSON, H. (2015). "Hydraulics of the Developing Flow Region of Stepped Cascades: an Experimental Investigation." *Hydraulic Model Report No. CH97/15*, School of Civil Engineering, The University of Queensland, Brisbane, Australia, 76 pages (ISBN 978 1 74272 134 7).	AUD$60.00		
LENG, X., and CHANSON, H. (2014). "Turbulent Advances of Breaking Bores: Experimental Observations." *Hydraulic Model Report No. CH96/14*, School of Civil Engineering, The University of Queensland, Brisbane, Australia, 40 pages (ISBN 978 1 74272 130 9).	AUD$40.00		
WANG, H, MURZYN, F., and D., CHANSON, H. (2014). "Pressure, Turbulence and Two-Phase Flow Measurements in Hydraulic Jumps." *Hydraulic Model Report No. CH95/14*, School of Civil Engineering, The University of Queensland, Brisbane, Australia, 154 pages (ISBN 9781742720616 9781742721064).	AUD$60.00		
REUNGOAT, D., CHANSON, H., and KEEVIL, C. (2014). "Turbulence, Sedimentary Processes and Tidal Bore Collision in the Arcins Channel, Garonne River (October 2013)." *Hydraulic Model Report No. CH94/14* School of Civil Engineering, The University of Queensland, Brisbane, Australia, 145 pages (ISBN 9781742721033).	AUD$60.00		
LENG, X., and CHANSON, H. (2014). "Propagation of Negative Surges in Rivers and Estuaries: Unsteady Turbulent Mixing including the Effects of Bed Roughness." *Hydraulic Model Report No. CH93/13*, School of Civil Engineering, The University of Queensland, Brisbane, Australia, 108 pages (ISBN 9781742720944).	AUD$60.00		
WUTHRICH, D., and CHANSON, H. (2014). "Aeration and Energy Dissipation over Stepped Gabion Spillways: a Physical Study." *Hydraulic Model Report No. CH92/13*, School of Civil Engineering, The University of Queensland, Brisbane, Australia, 171 pages and 5 video movies (ISBN 9781742720944).	AUD$60.00		

WANG, H., and CHANSON, H. (2013). "Free-Surface Deformation and Two-Phase Flow Measurements in Hydraulic Jumps". *Hydraulic Model Report No. CH91/13*, School of Civil Engineering, The University of Queensland, Brisbane, Australia, 108 pages (ISBN 9781742720746).	AUD$60.00		
SIMON, B., and CHANSON, H. (2013). "Turbulence Measurements in Tidal Bore-like Positive Surges over a Rough Bed". *Hydraulic Model Report No. CH90/12*, School of Civil Engineering, The University of Queensland, Brisbane, Australia, 176 pages (ISBN 9781742720685).	AUD$60.00		
REUNGOAT, D., CHANSON, H., and CAPLAIN, B. (2012). "Field Measurements in the Tidal Bore of the Garonne River at Arcins (June 2012)." Hydraulic Model Report No. CH89/12, School of Civil Engineering, The University of Queensland, Brisbane, Australia, 121 pages (ISBN 9781742720616).	AUD$60.00		
CHANSON, H., and WANG, H. (2012). "Unsteady Discharge Calibration of a Large V-Notch Weir." *Hydraulic Model Report No. CH88/12*, School of Civil Engineering, The University of Queensland, Brisbane, Australia, 50 pages & 4 movies (ISBN 9781742720579).	AUD$60.00		
FELDER, S., FROMM, C., and CHANSON, H. (2012). "Air Entrainment and Energy Dissipation on a 8.9° Slope Stepped Spillway with Flat and Pooled Steps." *Hydraulic Model Report No. CH86/12*, School of Civil Engineering, The University of Queensland, Brisbane, Australia, 82 pages (ISBN 9781742720531).	AUD$60.00		
FELDER, S., and CHANSON, H. (2012). "Air-Water Flow Measurements in Instationary Free-Surface Flows: a Triple Decomposition Technique." *Hydraulic Model Report No. CH85/12*, School of Civil Engineering, The University of Queensland, Brisbane, Australia, 161 pages (ISBN 9781742720494).	AUD$60.00		
REICHSTETTER, M., and CHANSON, H. (2011). "Physical and Numerical Modelling of Negative Surges in Open Channels." *Hydraulic Model Report No. CH84/11*, School of Civil Engineering, The University of Queensland, Brisbane, Australia, 82 pages (ISBN 9781742720388).	AUD$60.00		
BROWN, R., CHANSON, H., McINTOSH, D., and MADHANI, J. (2011). "Turbulent Velocity and Suspended Sediment Concentration Measurements in an Urban Environment of the Brisbane River Flood Plain at Gardens Point on 12-13 January 2011." *Hydraulic Model Report No. CH83/11*, School of Civil Engineering, The University of Queensland, Brisbane, Australia, 120 pages (ISBN 9781742720272).	AUD$60.00		
CHANSON, H. "The 2010-2011 Floods in Queensland (Australia): Photographic Observations, Comments and Personal Experience." *Hydraulic Model Report No. CH82/11*, School of Civil Engineering, The University of Queensland, Brisbane, Australia, 127 pages (ISBN 9781742720234).	AUD$60.00		
MOUAZE, D., CHANSON, H., and SIMON, B. (2010). "Field Measurements in the Tidal Bore of the Sélune River in the Bay of Mont Saint Michel (September 2010)." *Hydraulic Model Report No. CH81/10*, School of Civil Engineering, The University of Queensland, Brisbane, Australia, 72 pages (ISBN 9781742720210).	AUD$60.00		
JANSSEN, R., and CHANSON, H. (2010). "Hydraulic Structures: Useful Water Harvesting Systems or Relics." *Proceedings of the Third International Junior Researcher and Engineer Workshop on Hydraulic Structures (IJREWHS'10)*, 2-3 May 2010, Edinburgh, Scotland, R. JANSSEN and H. CHANSON (Eds), Hydraulic Model Report CH80/10, School of Civil Engineering, The University of Queensland, Brisbane, Australia, 211 pages (ISBN 9781742720159).	AUD$60.00		
CHANSON, H., LUBIN, P., SIMON, B., and REUNGOAT, D. (2010). "Turbulence and Sediment Processes in the Tidal Bore of the Garonne River: First Observations." *Hydraulic Model Report No. CH79/10*, School of Civil Engineering, The University of Queensland, Brisbane, Australia, 97 pages (ISBN 9781742720104).	AUD$60.00		

CHACHEREAU, Y., and CHANSON, H., (2010). "Free-Surface Turbulent Fluctuations and Air-Water Flow Measurements in Hydraulics Jumps with Small Inflow Froude Numbers." *Hydraulic Model Report No. CH78/10*, School of Civil Engineering, The University of Queensland, Brisbane, Australia, 133 pages (ISBN 9781742720036).	AUD$60.00		
CHANSON, H., BROWN, R., and TREVETHAN, M. (2010). " Turbulence Measurements in a Small Subtropical Estuary under King Tide Conditions." *Hydraulic Model Report No. CH77/10*, School of Civil Engineering, The University of Queensland, Brisbane, Australia, 82 pages (ISBN 9781864999969).	AUD$60.00		
DOCHERTY, N.J., and CHANSON, H. (2010). "Characterisation of Unsteady Turbulence in Breaking Tidal Bores including the Effects of Bed Roughness." *Hydraulic Model Report No. CH76/10*, School of Civil Engineering, The University of Queensland, Brisbane, Australia, 112 pages (ISBN 9781864999884).	AUD$60.00		
CHANSON, H. (2009). "Advective Diffusion of Air Bubbles in Hydraulic Jumps with Large Froude Numbers: an Experimental Study." *Hydraulic Model Report No. CH75/09*, School of Civil Engineering, The University of Queensland, Brisbane, Australia, 89 pages & 3 videos (ISBN 9781864999730).	AUD$60.00		
CHANSON, H. (2009). "An Experimental Study of Tidal Bore Propagation: the Impact of Bridge Piers and Channel Constriction." *Hydraulic Model Report No. CH74/09*, School of Civil Engineering, The University of Queensland, Brisbane, Australia, 110 pages and 5 movies (ISBN 9781864999600).	AUD$60.00		
CHANSON, H. (2008). "Jean-Baptiste Charles Joseph BÉLANGER (1790-1874), the Backwater Equation and the Bélanger Equation." *Hydraulic Model Report No. CH69/08*, Div. of Civil Engineering, The University of Queensland, Brisbane, Australia, 40 pages (ISBN 9781864999211).	AUD$60.00		
GOURLAY, M.R., and HACKER, J. (2008). "Reef-Top Currents in Vicinity of Heron Island Boat Harbour, Great Barrier Reef, Australia: 2. Specific Influences of Tides Meteorological Events and Waves." *Hydraulic Model Report No. CH73/08*, Div. of Civil Engineering, The University of Queensland, Brisbane, Australia, 331 pages (ISBN 9781864999365).	AUD$60.00		
GOURLAY, M.R., and HACKER, J. (2008). "Reef Top Currents in Vicinity of Heron Island Boat Harbour Great Barrier Reef, Australia: 1. Overall influence of Tides, Winds, and Waves." *Hydraulic Model Report CH72/08*, Div. of Civil Engineering, The University of Queensland, Brisbane, Australia, 201 pages (ISBN 9781864999358).	AUD$60.00		
LARRARTE, F., and CHANSON, H. (2008). "Experiences and Challenges in Sewers: Measurements and Hydrodynamics." *Proceedings of the International Meeting on Measurements and Hydraulics of Sewers*, Summer School GEMCEA/LCPC, 19-21 Aug. 2008, Bouguenais, Hydraulic Model Report No. CH70/08, Div. of Civil Engineering, The University of Queensland, Brisbane, Australia (ISBN 9781864999280).	AUD$60.00		
CHANSON, H. (2008). "Photographic Observations of Tidal Bores (Mascarets) in France." *Hydraulic Model Report No. CH71/08*, Div. of Civil Engineering, The University of Queensland, Brisbane, Australia, 104 pages, 1 movie and 2 audio files (ISBN 9781864999303).	AUD$60.00		
CHANSON, H. (2008). "Turbulence in Positive Surges and Tidal Bores. Effects of Bed Roughness and Adverse Bed Slopes." *Hydraulic Model Report No. CH68/08*, Div. of Civil Engineering, The University of Queensland, Brisbane, Australia, 121 pages & 5 movie files (ISBN 9781864999198)	AUD$70.00		

FURUYAMA, S., and CHANSON, H. (2008). "A Numerical Study of Open Channel Flow Hydrodynamics and Turbulence of the Tidal Bore and Dam-Break Flows." *Report No. CH66/08*, Div. of Civil Engineering, The University of Queensland, Brisbane, Australia, May, 88 pages (ISBN 9781864999068).	AUD$60.00		
GUARD, P., MACPHERSON, K., and MOHOUPT, J. (2008). "A Field Investigation into the Groundwater Dynamics of Raine Island." *Report No. CH67/08*, Div. of Civil Engineering, The University of Queensland, Brisbane, Australia, February, 21 pages (ISBN 9781864999075).	AUD$40.00		
FELDER, S., and CHANSON, H. (2008). "Turbulence and Turbulent Length and Time Scales in Skimming Flows on a Stepped Spillway. Dynamic Similarity, Physical Modelling and Scale Effects." *Report No. CH64/07*, Div. of Civil Engineering, The University of Queensland, Brisbane, Australia, March, 217 pages (ISBN 9781864998870).	AUD$60.00		
TREVETHAN, M., CHANSON, H., and BROWN, R.J. (2007). "Turbulence and Turbulent Flux Events in a Small Subtropical Estuary." Report No. CH65/07, Div. of Civil Engineering, The University of Queensland, Brisbane, Australia, November, 67 pages (ISBN 9781864998993)	AUD$60.00		
MURZYN, F., and CHANSON, H. (2007). "Free Surface, Bubbly flow and Turbulence Measurements in Hydraulic Jumps." *Report CH63/07*, Div. of Civil Engineering, The University of Queensland, Brisbane, Australia, August, 116 pages (ISBN 9781864998917).	AUD$60.00		
KUCUKALI, S., and CHANSON, H. (2007). "Turbulence in Hydraulic Jumps: Experimental Measurements." *Report No. CH62/07*, Div. of Civil Engineering, The University of Queensland, Brisbane, Australia, July, 96 pages (ISBN 9781864998825).	AUD$60.00		
CHANSON, H., TAKEUCHI, M, and TREVETHAN, M. (2006). "Using Turbidity and Acoustic Backscatter Intensity as Surrogate Measures of Suspended Sediment Concentration. Application to a Sub-Tropical Estuary (Eprapah Creek)." *Report No. CH60/06*, Div. of Civil Engineering, The University of Queensland, Brisbane, Australia, July, 142 pages (ISBN 1864998628).	AUD$60.00		
CAROSI, G., and CHANSON, H. (2006). "Air-Water Time and Length Scales in Skimming Flows on a Stepped Spillway. Application to the Spray Characterisation." *Report No. CH59/06*, Div. of Civil Engineering, The University of Queensland, Brisbane, Australia, July (ISBN 1864998601).	AUD$60.00		
TREVETHAN, M., CHANSON, H., and BROWN, R. (2006). "Two Series of Detailed Turbulence Measurements in a Small Sub-Tropical Estuarine System." *Report No. CH58/06*, Div. of Civil Engineering, The University of Queensland, Brisbane, Australia, Mar. (ISBN 1864998520).	AUD$60.00		
KOCH, C., and CHANSON, H. (2005). "An Experimental Study of Tidal Bores and Positive Surges: Hydrodynamics and Turbulence of the Bore Front." *Report No. CH56/05*, Dept. of Civil Engineering, The University of Queensland, Brisbane, Australia, July (ISBN 1864998245).	AUD$60.00		
CHANSON, H. (2005). "Applications of the Saint-Venant Equations and Method of Characteristics to the Dam Break Wave Problem." *Report No. CH55/05*, Dept. of Civil Engineering, The University of Queensland, Brisbane, Australia, May (ISBN 1864997966).	AUD$60.00		
CHANSON, H., COUSSOT, P., JARNY, S., and TOQUER, L. (2004). "A Study of Dam Break Wave of Thixotropic Fluid: Bentonite Surges down an Inclined plane." *Report No. CH54/04*, Dept. of Civil Engineering, The University of Queensland, Brisbane, Australia, June, 90 pages (ISBN 1864997710).	AUD$60.00		
CHANSON, H. (2003). "A Hydraulic, Environmental and Ecological Assessment of a Sub-tropical Stream in Eastern Australia: Eprapah Creek, Victoria Point QLD on 4 April 2003." *Report No. CH52/03*, Dept. of Civil Engineering, The University of Queensland, Brisbane, Australia, June, 189 pages (ISBN 1864997044).	AUD$90.00		

CHANSON, H. (2003). "Sudden Flood Release down a Stepped Cascade. Unsteady Air-Water Flow Measurements. Applications to Wave Run-up, Flash Flood and Dam Break Wave." *Report CH51/03*, Dept of Civil Eng., Univ. of Queensland, Brisbane, Australia, 142 pages (ISBN 1864996552).	AUD$60.00		
CHANSON, H,. (2002). "An Experimental Study of Roman Dropshaft Operation : Hydraulics, Two-Phase Flow, Acoustics." *Report CH50/02*, Dept of Civil Eng., Univ. of Queensland, Brisbane, Australia, 99 pages (ISBN 1864996544).	AUD$60.00		
CHANSON, H., and BRATTBERG, T. (1997). "Experimental Investigations of Air Bubble Entrainment in Developing Shear Layers." *Report CH48/97*, Dept. of Civil Engineering, University of Queensland, Australia, Oct., 309 pages (ISBN 0 86776 748 0).	AUD$90.00		
CHANSON, H. (1996). "Some Hydraulic Aspects during Overflow above Inflatable Flexible Membrane Dam." *Report CH47/96*, Dept. of Civil Engineering, University of Queensland, Australia, May, 60 pages (ISBN 0 86776 644 1).	AUD$60.00		
CHANSON, H. (1995). "Flow Characteristics of Undular Hydraulic Jumps. Comparison with Near-Critical Flows." *Report CH45/95*, Dept. of Civil Engineering, University of Queensland, Australia, June, 202 pages (ISBN 0 86776 612 3).	AUD$60.00		
CHANSON, H. (1995). "Air Bubble Entrainment in Free-surface Turbulent Flows. Experimental Investigations." *Report CH46/95*, Dept. of Civil Engineering, University of Queensland, Australia, June, 368 pages (ISBN 0 86776 611 5).	AUD$80.00		
CHANSON, H. (1994). "Hydraulic Design of Stepped Channels and Spillways." *Report CH43/94*, Dept. of Civil Engineering, University of Queensland, Australia, Feb., 169 pages (ISBN 0 86776 560 7).	AUD$60.00		
POSTAGE & HANDLING (per report)	AUD$10.00		
GRAND TOTAL			

OTHER HYDRAULIC RESEARCH REPORTS

Reports/Theses	Unit price	Quantity	Total price
WANG, H. (2014). "Turbulence and Air Entrainment in Hydraulic Jumps." *Ph.D. thesis*, School of Civil Engineering, The University of Queensland, Brisbane, Australia, 341 pages (DOI: 10.14264/uql.2014.542).	AUD$100.00		
KHEZRI, N. (2014). "Modelling Turbulent Mixing and Sediment Process Beneath Tidal Bores: Physical and Numerical Investigations." *Ph.D. thesis*, School of Civil Engineering, The University of Queensland, Brisbane, Australia, 267 pages.	AUD$100.00		
SIMON, B. (2014). "Effects of Tidal Bores on Turbulent Mixing: a Numerical and Physical Study in Positive Surges." *Ph.D. thesis*, School of Civil Engineering, The University of Queensland, Brisbane, Australia, 259 pages (DOI: 10.14264/uql.2014.19).	AUD$100.00		
FELDER, S. (2013). "Air-Water Flow Properties on Stepped Spillways for Embankment Dams: Aeration, Energy Dissipation and Turbulence on Uniform, Non-Uniform and Pooled Stepped Chutes." *Ph.D. thesis*, School of Civil Engineering, The University of Queensland, Brisbane, Australia.	AUD$100.00		

REICHSTETTER, M. (2011). "Hydraulic Modelling of Unsteady Open Channel Flow: Physical and Analytical Validation of Numerical Models of Positive and Negative Surges." *MPhil thesis*, School of Civil Engineering, The University of Queensland, Brisbane, Australia, 112 pages.	AUD$80.00		
TREVETHAN, M. (2008). "A Fundamental Study of Turbulence and Turbulent Mixing in a Small Subtropical Estuary." Ph.D. thesis, Div. of Civil Engineering, The University of Queensland, 342 pages.	AUD$100.00		
GONZALEZ, C.A. (2005). "An Experimental Study of Free-Surface Aeration on Embankment Stepped Chutes." *Ph.D. thesis*, Dept of Civil Engineering, The University of Queensland, Brisbane, Australia, 240 pages.	AUD$80.00		
TOOMBES, L. (2002). "Experimental Study of Air-Water Flow Properties on Low-Gradient Stepped Cascades." *Ph.D. thesis*, Dept of Civil Engineering, The University of Queensland, Brisbane, Australia.	AUD$100.00		
CHANSON, H. (1988). "A Study of Air Entrainment and Aeration Devices on a Spillway Model." *Ph.D. thesis*, University of Canterbury, New Zealand.	AUD$60.00		
POSTAGE & HANDLING (per report)	AUD$10.00		
GRAND TOTAL			

CIVIL ENGINEERING RESEARCH REPORT CE

The Civil Engineering Research Report CE series is published by the School of Civil Engineering at the University of Queensland. Orders of any of the Civil Engineering Research Report CE should be addressed to the School Secretary.

School Secretary, School of Civil Engineering, The University of Queensland
Brisbane 4072, Australia
Tel.: (61 7) 3365 3619 Fax: (61 7) 3365 4599
Url: http://http://www.civil.uq.edu.au// Email: enquiries@civil.uq.edu.au

Recent Research Report CE	Unit price	Quantity	Total price
CALLAGHAN, D.P., NIELSEN, P., and CARTWRIGHT, N. (2006). "Data and Analysis Report: Manihiki and Rakahanga, Northern Cook Islands - For February and October/November 2004 Research Trips." *Research Report CE161*, Division of Civil Engineering, The University of Queensland (ISBN No. 1864998318).	AUD$10.00		
GONZALEZ, C.A., TAKAHASHI, M., and CHANSON, H. (2005). "Effects of Step Roughness in Skimming Flows: an Experimental Study." *Research Report No. CE160*, Dept. of Civil Engineering, The University of Queensland, Brisbane, Australia, July (ISBN 1864998105).	AUD$10.00		

CHANSON, H., and TOOMBES, L. (2001). "Experimental Investigations of Air Entrainment in Transition and Skimming Flows down a Stepped Chute. Application to Embankment Overflow Stepped Spillways." *Research Report No. CE158*, Dept. of Civil Engineering, The University of Queensland, Brisbane, Australia, July, 74 pages (ISBN 1 864995297).	AUD$10.00		
HANDLING (per order)	AUD$10.00		
GRAND TOTAL			

Note: Prices include postages and processing.

PAYMENT INFORMATION

1- VISA Card

Name on the card :	
Visa card number :	
Expiry date :	
Amount :	AUD$ .....

2- Cheque/remittance payable to: THE UNIVERSITY OF QUEENSLAND and crossed "Not Negotiable".

N.B.: For overseas buyers, cheque payable in Australian Dollars drawn on an office in Australia of a bank operating in Australia, payable to: THE UNIVERSITY OF QUEENSLAND and crossed "Not Negotiable".

Orders of any Research Report should be addressed to the School Secretary.

School Secretary, School of Civil Engineering, The University of Queensland

Brisbane 4072, Australia - Tel.: (61 7) 3365 3619 - Fax: (61 7) 3365 4599
Url: http://http://www.civil.uq.edu.au// Email: enquiries@civil.uq.edu.au